



# Università degli Studi di Napoli *Federico II*

DOTTORATO DI RICERCA IN  
**FISICA**

Ciclo- XXXII

Coordinatore: prof. Salvatore Capozziello

## Study of biological interactions between water dispersed 2D-MoS<sub>2</sub> nanosheets and live matter

Settore Scientifico Disciplinare : FIS/07

**Dottorando**  
Manjot Singh

**Tutor**  
Prof. Carlo Altucci

Anni 2017/2020

***“Dedicated to the beloved of beloved ones”***

## **Statement of Originality**

---

I, hereby declare that this thesis has not been submitted as an exercise for a degree at this or any other university and the work carried out in this thesis has been equally and majorly contributed.

I also agree to deposit this thesis in the University's open archive repository.

The contents of this thesis have been successfully carried out with other collaborators and have been duly acknowledged in the acknowledgement section.

---

**Manjot Singh**

## ABSTRACT

---

The unique two dimensional structure and fascinating physicochemical properties of two dimensional materials (2D) have attracted tremendous attention worldwide in disease diagnosis and nano-biomedicine. As an analogue of 2D graphene, transition metal dichalcogenides (TMDs) such as 2D MoS<sub>2</sub>/WS<sub>2</sub> nanosheets have been exploited as representative models in numerous applications ranging from nanoelectronics to the frontiers between nanomedicine and nanotechnology. The intriguing physical and chemical properties of 2D TMDs such as confinement in dimension due to their extreme thinness, stable free standing atomic crystal nanosheets without any substrate, unparalleled surface area to volume ratio, highly biocompatible and flexibility in functionalization with different biological molecules makes them potentially favorable candidate for many biomedical applications.

To get an insight into the biological and environmental fate of these engineered 2D nanosheets, it is very crucial to understand the nano-bio interactions at a prior level. Basically, the biological response to 2D nanomaterials is governed by material-specific behavior which further can be understood by the fundamental physicochemical properties of that material. Generally, three fundamental interaction modes are studied to analyze the biological impact of a given nanomaterial: a) chemical interactions, b) electronic and surface redox reactions and c) very unique physical and mechanical interactions. In general, 2DMs have shown wide range of behaviors with respect to these three modes of interactions at bio-nanosheet interface studies. Among these three modes, physical and mechanical interaction represents a unique way to study the biological response of 2D TMD nanosheets because of their high surface area to volume ratio, surface charge tuning and polarity. To exploit the full potential of 2D TMD nanosheets in biological applications, it is highly required that the given nanomaterial to be highly biocompatible, reproducible in the relevant physiological medium, flexibility in functionalization and with minimum cytotoxicity to the normal cells. In such a case and from the materials perspective, highly versatile, scalable, cost efficient and

green fabrication techniques are required to obtain 2D nanosheets with the desired properties. To accomplish this aim, among various fabrication techniques reported for 2D TMDs such as chemical vapor deposition, electrochemical exfoliation, lithium intercalation, hydrothermal, sol-gel and liquid phase exfoliation, the latter one is the most versatile, scalable and cost effective technique for the production of few-layer nanosheets (1–10 stacked monolayers), with low monolayer content. Particularly in this technique, a careful optimization of exfoliation parameters such as, choice of green solvents, initial concentration of the solution, exfoliation time and controlled centrifugation for size and thickness selection of 2D nanosheets is very crucial to understand their environmental impact and behavior in biological media.

To this aim, my PhD project is focused on the noticeable progress on green and scalable production of MoS<sub>2</sub> nanosheets in water as a pure solvent, having stability up to three weeks or more by carefully optimizing critical exfoliation parameters. Such a long stability time in water, which is a non-trivial result, is crucial to test the impact of 2DMs with biological live matter in its native context, as experiments aimed at these goals may take a few days or even longer to be completed. Thus, we stress that our innovative preparation of naked MoS<sub>2</sub> nanosheets in water solvent represents an essential step ahead for an appropriate characterization of 2DMs – live matter interactions in its natural environment.

Till date, our group has investigated the biological interactions of bare MoS<sub>2</sub> nanosheets with three different kinds of human cells, two tumoral, MCF7 (breast cancer) and U937 (leukemia), and one normal, HaCaT (epithelium), and two different kinds of *Salmonella*- ATCC 14028 and wild type *S.typhimurium*. It is worth noting that while MCF, and HaCaT cells have been already partly investigated with respect to their interactions with MoS<sub>2</sub> nanosheets, U937-MoS<sub>2</sub> interactions are completely unknown so far. Yet, MCF7 (Breast Cancer), Hela (Human Cervical Cancer), PC3 (Human Prostate Cancer), SMCC-7721 (Human Hepatocellular Carcinoma), B16 (Mouse Melanoma) and A549 (Human Lung Carcinoma) as cancer cell lines have been also recently tested as models by other research groups for the interactions between human cells and 2D functionalized

nanomaterials of various composition, there including 2D Black Phosphorus nanosheets, 2D Boron nanosheets, 2D Antimonene quantum dots, 2D Antimonene nanosheets and Tin Sulfide nanosheets. Here, we found a very interesting and novel result from our experiments: the impact of MoS<sub>2</sub> nanoflakes was found to be quite different in normal from cancer cell lines. While the latter cells revealed a significant cytotoxic effect based on a very large increase of cell death, the former were essentially unaffected in this respect and only showed some mechanical damage when morphologically analyzed by SEM microscopy. This cytotoxic effect was also found to be dependent on the concentration and layer number of 2D nanoflakes. In the near future, this preliminary analysis might open up new routes for significant applications of MoS<sub>2</sub> nanosheets as targeted anti-cancer systems. This analysis was further extended to bacteria and viruses. Particularly, we have investigated the mechanical interaction of 2D MoS<sub>2</sub> nanoflakes with two different types of *Salmonella typhimurium* (ATCC 14028 and wild-type) which is a very serious Gram negative facultative anaerobe causing gastroenteritis in humans and in some cases it also results in serious neurological abnormalities with very high mortality rate. SEM analysis performed after the incubation of the complex system revealed significant damage to the bacterial morphology and leakage of intra-cellular components from the bacterial structure. Both of the *salmonella* types when treated with 2D MoS<sub>2</sub> nanosheets, showed that the sharp edges of the nanoflakes can cut and/or damage bacterial membrane leading to an evident bactericidal effect.

Additionally, with a motive to deposit MoS<sub>2</sub> nanosheets onto a patterned or machined substrate, particularly silicon because of its widely explored technological significance and usage in various laser processing techniques, we have first investigated the surface structuring of silicon using femtosecond laser pulses with a broad range of repetition rates (10 Hz – 200 kHz). Careful selection of various experimental conditions results in the formation of surface patterns which paves the way for numerous interesting applications. In view of this, I have introduced some preliminary results of LPE exfoliated MoS<sub>2</sub> nanosheets deposited onto patterned silicon substrate for investigating non-

linear optics of 2D nanosheets based on their thickness and given lateral size, in ongoing projects chapter at the end of this thesis.

Also, enthused from the synergistic impact of 2D MoS<sub>2</sub> nanosheets on *S. typhimurium*, we are currently investigating the potential interaction of the same on two other types of bacteria such as Escherichia coli (*E. coli*) and Staphylococcus aureus (*S. aureus*). In this ongoing research, we have achieved a significant time and concentration dependent damage to bacterial morphology tested at different points. We have also extended our study to analyze the mechanical interaction of water exfoliated 2D MoS<sub>2</sub> nanosheets on a very commonly effected contagious virus, Herpes Simplex Virus (HSV-1), which has shown a good percentage of virus inhibition treated with water exfoliated MoS<sub>2</sub> nanosheets. In fact, further investigations are under study and some of the preliminary results have been added into the ongoing projects chapter of this thesis.

In order to understand the specific mechanism of action of 2D MoS<sub>2</sub> nanosheets on the already tested tumor and normal human cells in this thesis, we have further extended our analysis in another ongoing project to go into deeper insights of 2D MoS<sub>2</sub> nanosheets - live matter interaction using advanced Raman microscopy technique. The cell viability and the subsequent Raman microscopic analysis performed on the MoS<sub>2</sub> nanosheets incubated with the similar human cell lines (MCF-7, U937 and HaCaT) revealed noteworthy results confirming the specific action of MoS<sub>2</sub> nanosheets on tumor cell line (MCF-7 and U937), whereas very little or negligible effect on normal cell line (HaCaT).

## Publications

*\*Research containing equal and major contribution for the desired aim of this thesis and related activities*

- a) Jasneet Kaur, **Manjot Singh\***, Carmela Dell'Aversana, Rosaria Benedetti, Paola Giardina, Manuela Rossi, Mohammadhassan Valadan, Alessandro Vergara, Anna Cutarelli, Angela Michela Immacolata Montone, Lucia Altucci, Federica Corrado, Angela Nebbioso & Carlo Altucci, "Biological interactions of biocompatible and water dispersed MoS<sub>2</sub> nanosheets with bacteria and human cells", *Scientific Reports*, **8**, 16386, (2018), <https://doi.org/10.1038/s41598-018-34679-y>

## Other publications (Research activity not included in this thesis)

- b) E. Allahyari, J. JJ Nivas, G. Avallone, M. Valadan, **M. Singh**, V. Granata, C. Cirillo, A. Vecchione, R. Bruzzese, C. Altucci and S. Amoroso, "Femtosecond laser surface irradiation of silicon in air: pulse repetition rate influence on removal efficiency and surface texture" *Journal of Optics and Laser Technology*, 2020, <https://doi.org/10.1016/j.optlastec.2020.106073>
- c) R. Benedetti, F. Bajardi, S. Capozziello, V. Carafa, M. R. Conte, M. R. Del Sorbo, A. Nebbioso, **M. Singh**, H. G. Stunnenberg, M. Valadan, L. Altucci, and C. Altucci, "Different approaches to understand the interactions between biomolecules", *Analytical Letters*, 2020 <https://doi.org/10.1080/00032719.2020.1716241>
- d) Concetta Imperatore, Mohammadhassan Valadan, Luciana Tartaglione, Marco Persico, Anna Ramunno, Marialuisa Menna, Marcello Casertano, Carmela Dell'Aversano, **Manjot Singh**, Maria Luisa d'Aulizio Garigliota, Francesco Bajardi, Elena Morelli, Caterina Fattorusso \*, Carlo Altucci \*, Michela Varra, "Exploring the photodynamic properties of two antiproliferative benzodiazopyrrole derivatives", *Int. J. Of Mol. Sci.* (2020). <https://doi.org/10.3390/ijms21041246>

## Manuscripts in preparation

- 1) **Manjot Singh**, Mohammadhassan Valadan, Gianluigi Franci, Veronica Folliero, Annalisa Chianese, Lucia Altucci, Massimiliano Galdiero and Carlo Altucci, “ Novel antibacterial and antiviral action of water-dispersed MoS<sub>2</sub>, Graphene and Graphene oxide 2D nanosheets” (*In preparation*)
- 2) **Manjot Singh**, Mohammadhassan Valadan, Carmella Dell Aversana, Angela Capaccio, Guilia Rusciana, Lucia Altucci, Antonio Sasso and Carlo Altucci, “Intriguing mechanism of action of water-dispersed 2D MoS<sub>2</sub> nanoflakes on live-matter by advanced Raman microscopy” (*In preparation*)

## IPSP 2018 Proceedings

- a) Participated in Industrial Problem Solving with Physics (*IPSP 2018*) Edition, held at University of Trento from 16 – 21 July, 2018 and **our team got first prize** in solving the given industrial problem by Lemur Company, Italy.
- b) Z. Bisadi, M. Celli, S.J. A. Lafirenze, C. Puglia, **M. Singh**, C. Vecchi and S. Villa, “Electrostatic charge on extruded silicone elastomer yarns”, (*ISBN 978-88-8443-823-2 Online Version*), 2019.

## International and National Experience

- a) \*Attended **summer school** under the general theme of Graphene Flagship- Graphene study on “*2D materials for environment and energy applications*” at Hindas, Sweden.
- b) \***Oral talk** at European Graphene Forum (EGF) conference in at Venice International University, Italy.  
Title of the talk - “*Exploring the live matter interactions of bacteria and human cells with water exfoliated MoS<sub>2</sub> nanosheets*”.
- c) \***Poster presentation** at Graphene, 2019 conference in Angelicum Centro Congressi, Rome, Italy.

Title of the Poster - *“Biological interactions of bio-compatible and water dispersed MoS<sub>2</sub> nanosheets with bacteria and human cells”*.

## Other Activities

**Referred six research articles of two different international peer reviewed journals- IOP and RSC**

- a) *“Electronic structure and magnetic behaviors of exfoliated MoS<sub>2</sub> nanosheets”* in  
Journal of Physics: Condensed Matter, IOP Publishing.  
Impact Factor- 2.6
- b) *“ Design in silico modelling and functionality theory of folate receptor targeted Rutin encapsulated folic acid conjugated keratin nanoparticles for effective cancer treatment ”* in  
Journal of Biomedical Physics & Engineering Express: IOP publishing  
Impact factor- 1.10
- c) *“Experimental observation of negative grey trion in electron rich WSe<sub>2</sub> monolayer”* in  
Journal of Physics: Condensed Matter, IOP Publishing.  
Impact Factor- 2.6
- d) *“Anti-EGFR antibodies drive 5-fluorouracil gold nanoparticles to colorectal cancer cells in vitro ”* in  
Nanotechnology: IOP Publishing  
Impact Factor- 3.399
- e) *“Tetrahedral photo luminescent manganese(II) halide complexes with 1,3-dimethyl-2-phenyl-1,3-diazaphospholidine-2-oxide as ligand ”* in  
New Journal of Chemistry: RSC Publishing  
Impact Factor- 3.069
- f) *“Strong visible photoluminescence emission of ZnO nanosheets and nanoflowers by a facile hydrothermal route ”* in  
Nanotechnology: IOP Publishing  
Impact Factor- 3.399

*ਵਿਦਿਆ ਵਿਚਾਰੀ ਤਾਂ ਪਰਉਪਕਾਰੀ ॥* (sggs p.356)

*Only that kind of education is worth its name which makes a man a socially useful person, one who spends his life in the service of humanity.*

## **Acknowledgements**

---

My very first impression before starting my PhD journey was not less than a horrible nightmare. But with the consistent support, faith and love from people around transformed this nightmare into a wonderful experience.

First and foremost, I would like to thank my greatest teacher of all: *Waheguru*- the Almighty. I am not capable to do anything but my faith towards Him made me more strong to face the challenges during my PhD journey.

It is truly said that “It’s *not where you are in life; it’s who you have by your side that matters*”. So, for that, I would like to extend my deepest gratitude to my supervisor *Prof. Carlo Altucci*, who has shown a constant support and faith at each single moment of my PhD. I would like to thank him for his kindness and giving me all opportunities to collaborate with different groups, travel for conferences and summer schools abroad which have truly motivated and enriched me to continue in this field and I will be always grateful for that. I truly enjoyed working with him in the past three years, his patience and a good sense of humor are really appreciated. Besides my advisor, I would like to thank *Dr. Jasneet Kaur*, a blessed personality from whom I was able to connect with this PhD opportunity and she was the one who taught me each single scientific aspect and valuable suggestions during my experimental work.

In the course of my research work, I was privileged to work with different collaborators from various backgrounds. At first, I would like to thank my colleague *Mohammadhassan Valadan* for his interesting ideas and criticism towards our experiments and furthermore his artistic skills in Adobe Photoshop were very useful in organizing all images. I would like express my sincere gratitude to *Prof Lucia Altucci* who encouraged and accepted our invitation for a kind and useful collaboration to study the bio-interactions of  $\text{MoS}_2$  with the reported cell lines, provided by them

for my current project. I would like to thank her colleagues- *Carmella Dell' Aversana, Rosaria Benedetti and Angela Nebbioso* (the co-authors) of my PhD project who were the main bio-experiment people; performed bio experiments and their useful analyses. I would also like to thank *Prof Paola Giardina*, who allowed me to work in her chemistry lab and to use the sonicator for my fabrication experiments. I would like to thank *Prof Alesandaro Vergara* for providing us the opportunity to perform Raman experiments and for his valuable suggestions and analyses towards the same. He has been very kind and supportive for each single measurement and always there to guide how to use the Raman spectroscopy tool. I would like to thank *Dr. Federica Corrado* and her colleagues- *Anna Cutarelli, and Angela Michela Immacolata Montone* who gave us the opportunity to collaborate with them to study the antibacterial effect of MoS<sub>2</sub> nanosheets on *Salmonella typhimurium*.

I would like to thank *Prof Manuela Rossi* for her kind cooperation to perform SEM measurements of the samples. Her good sense of humor and very particular observation and expertise in SEM has shown valuable results in understanding the behavior of MoS<sub>2</sub> towards the given cell lines and antibacterial effect. I would also like to thank *Dr. Rocco* for his very kind and recent collaboration for TEM measurements and flexible availability during these ending rush hours of my thesis submission. I would like to thank the technical and administrative staff of the physics department who was very helpful during my conferences and summer school visits.

I must thank the *Italian Education Ministry* for providing me with full funded PhD program which helped me to pursue research in University of Naples Federico II. I must thank my PhD Coordinator *Prof. Salvatore Capozzallo*, for all support and guidance to improve my research and related activities during the coursework. Also, i would like to thank my *external referres* for their valuable suggestions, insightful comments and feedback which have given an improved version of my thesis.

I would like to thank *Prof Salvatore Amoruso, Prof Antonio Sasso, Prof Giulia Rusciano, Prof Massimiliano Galdiero, Gianluigi Franci, Angela Capaccio, Jijil, Elahae, Annalisa and Veronica* for their kind collaboration for the ongoing projects and preliminary results included in this thesis.

The social aspect during my PhD journey has played a key role in motivating me to work very smartly and stress free. I would like to express my sincere gratitude to my all PhD colleagues with whom i have spent these three years in the famous *OG-28 PhD room* and with whom i have learnt many beautiful aspects of italian and napolitan culture. I am really than kful to *Andrea Espoito*,

*Luca, Loris, Mattia, Gianluca, Halima, Daniela* and many more who inculcated the love towards very delicious Italian cuisine, especially the world famous Neapolitan Pizza. The wonderful and useful time spent with these guys have always provided me a sense of belongingness and family atmosphere inside the campus. I would like to thank many of my Indian friends (*Chandan, Ravi, Jaspreet, Satwinder Singh, Midhun, Mritunjaya-Anita Bhabhi, Baabu, Pratibha, Ashwani, Alex, Arjun and Rohit*) for their loving support and memorable weekends as a get together to taste different varieties of Indian cuisine and feeling like home! Iranian friends (*Arash, Elahae, Pegah, Samoney, Zahra*) and South African friends (*Mari and Tanya*) with whom I have learnt new culture and values and interesting time with them to roam around the city. A special thanks to *Mandeep veerji* for their unbiased love and care towards me and their constant help, suggestions and every kind of help being a big brother during my stay in Napoli. He along with his daughter *Ajit* were like a my own family.

I would like to express my gratitude to my *family members* who have been a strong support during these three years of my journey and because of them I was able to stand with all the challenges, happy and sad moments of my life. I wouldn't be where I am today without their concrete faith, support and sacrifice all the way through my university times.

I would like to say a heartfelt thanks to my sisters *Jasleen Kaur* and *Preety Baglat* who have been all the way with me to enhance my morale to work harder and in a smart way. Many thanks for their time and long night contribution in various discussions, fun moments and sometimes watery eyes for each other for our love and blessed moments spent together. It wouldn't have been possible for me to move enthusiastically towards my aim without their help and love.

Last but certainly not least, I am extremely obliged to our PhD secretary *Guido Celentano* and these acknowledgements would not be complete without mentioning his name. He has been our local guardian and I have never seen such a humble person in my life. He was always available for his kind and gentle support for any kind of issue related to accommodation, academic and other documental works. I will always be grateful to him for his selfless service to all foreigners which he still is doing.

## Table of Contents

Declaration

Abstract

Acknowledgements

List of Figures

List of Tables

Acronyms

### *Chapter-1 Introduction*

1.1. Motivation	1
1.2. Research scope and objectives	7
1.3. Organization of thesis	8

### *Chapter-2 Literature framework on 2D TMDs*

2.1. Nanotechnology	16
2.1.1. Nanomaterials	19
2.2. Two dimensional materials (2DMs)	23
2.2.1. 2D transition metal dichalcogenides (2D TMDs)	27
2.2.2. 2D MoS <sub>2</sub>	30
2.2.3. Unique properties of 2D MoS <sub>2</sub>	32
2.2.4. Novel properties of MoS <sub>2</sub> and other TMDs for biomedical applications	33
2.2.5. Fabrication methods of MoS <sub>2</sub> nanosheets	37
2.2.6. Micromechanical exfoliation	39
2.2.7. Chemical vapor deposition (CVD)	42
2.3. Chemical exfoliation approach	
2.3.1. Lithium intercalation	44
2.4. Ultra-sonication assisted exfoliation approach	46
2.4.1. Mechanism of ultra-sonication in a solvent	48
2.4.2. What drives the need for liquid phase exfoliation	50
2.5. Characterization tools	
2.5.1. Introduction	96
2.5.2. UV-visible extinction spectroscopy	97

2.5.3.	Equipment for UV-Visible	102
2.5.4.	Raman spectroscopy	103
2.5.5.	Equipment for Raman spectroscopy	108
2.5.6.	Zeta potential	109
2.5.7.	Equipment for zeta potential	112
2.5.8.	Electron microscopy tool	113
2.5.9.	Basic parts of electron microscopy	113
2.6.	Scanning electron microscopy (SEM)	115
2.6.1.	Equipment for SEM	117
2.7.	Solubility theories	
2.7.1.	General introduction on solubility theory	124
2.7.2.	Thermodynamics of the solution by minimizing the enthalpy of mixing for a stable dispersion	125
2.7.3.	Solubility theory applied to 2D nanosheets in water	128
 <i>Chapter-3 Results and Discussion</i>		
3.1.	Introduction	133
3.1.1.	Preparation of water based MoS <sub>2</sub> dispersions	134
3.1.2.	Characterization results	137
3.1.3.	Yield estimation	140
3.1.4.	UV-Visible extinction spectroscopy	141
3.1.5.	Zeta potential	144
3.1.6.	Raman micro-spectroscopy of MoS <sub>2</sub> nanosheets in absence of cells	145
3.1.7.	SEM of water-dispersed MoS <sub>2</sub> nanosheets	146
3.1.8.	TEM of water based MoS <sub>2</sub> nanosheets	149
3.2.	Experimental details	
3.2.1.	Ultra-sonication technique	151
3.2.2.	Liquid phase exfoliation of MoS <sub>2</sub> nanosheets in water	153
3.2.3.	Research attempts on direct exfoliation of MoS <sub>2</sub> nanosheets in water	154
3.2.4.	Sonicator equipment details	156
3.2.5.	Centrifugation	157
3.2.6.	Centrifuge equipment details	159

3.2.7. Technical characterization details	161
---	-----

## *Chapter-4 Biological interactions result analyses of 2D MoS<sub>2</sub> nanosheets with human cell lines and pathogens*

4.1. Introduction	
4.1.1. General information on the tested human cell lines	172
4.1.2. MCF-7 cell line	173
4.1.3. U937 cell line	174
4.1.4. HaCaT cell line	174
4.2. Cytotoxicity study on different cell lines	
4.2.1. Introduction	175
4.3. Effects of 2D MoS <sub>2</sub> nanosheets on cellular growth	
4.3.1. Cell cycle analyses	176
4.4. Effects of 2D MoS <sub>2</sub> nanosheets on cellular viability	
4.4.1. Cell line culture conditions and preparations	180
4.5. MTT assay on HaCaT and MCF-7 cells pre-incubated with MoS <sub>2</sub> nanosheets	
4.5.1. MTT-cell proliferation assay	184
4.6. Cell morphology by SEM	
4.6.1. Visualization of cell morphology	186
4.7. MoS <sub>2</sub> nanosheets and cells interaction pathways	189
4.8. MoS <sub>2</sub> nanosheets mediated cell death evaluation	
4.8.1. Propidium iodide staining cell death evaluation	191
4.9. Antibacterial effect by naked MoS <sub>2</sub> nanosheets	194
4.10. General information on <i>Salmonella typhimurium</i>	194
4.11. Antibacterial activity: Proliferation test	
4.11.1. Microbial strains, culture conditions and preparations	195
4.12. MTT assay-MTT plots and lab prepared <i>Salmonella typhimurium</i> incubation with 2D MoS <sub>2</sub> nanosheets	
4.12.1. Determination of bacterial viability	198
4.13. SEM of antibacterial effect	
4.13.1. Antibacterial activity: the action mechanism of MoS <sub>2</sub>	199
4.14. Experimental details for human cell lines and bacterial culture	201-204

## *Chapter-5 Conclusion and Future Prospects*

- |                          |     |
|--------------------------|-----|
| 5.1. Conclusions         | 214 |
| 5.2. Some key challenges | 215 |

## *Chapter-6 Ongoing projects*

- |   |     |
|---|-----|
| 6.1. Detailed mechanism analyses of different interaction pathways of water-dispersed 2D MoS <sub>2</sub> nanosheets      | 218 |
| 6.1.1. Experimental procedure   |     |
| 6.1.1.1. Methods  | 220 |
| 6.1.2. Improvement in fabrication protocol by two step exfoliation  | 222 |
| 6.2. Antibacterial and antiviral action of 2D TMDs  | 223 |
| 6.3. Femtosecond laser surface irradiation of silicon substrate in air with special focus on laser pulse repetition rates | 225 |
| 6.4. Conclusions  | 229 |

## List of Figures

**Figure 1.1:** Acme of nanotechnology's potential in various applications where it has shown remarkable results and entry into the commercial market with a variety of products.

**Figure 1.2:** Relevance of nanotechnology in terms of how small it can be exemplified with our day to day stuffs.

**Figure 2.1:** Classification of various nanoparticles based on its size, shape, surface chemistry and type of material which can be exploited in various applications

**Figure 2.2:** Different nanoparticles acting as promising nano-carriers in various biomedical applications

**Figure 2.3:** A horde of potential hands of nanoparticles in nanomedicine field to enhance their potential to a significant level

**Figure 2.4:** Represents the thermal fluctuations in the suspended graphene sheet

**Figure 2.5 :** Family of 2D materials categorized as insulators {members include graphene family, hydrogen boron nitride}; semiconductors {members include transition metal dichalcogenide family-  $\text{MoS}_2$ ,  $\text{WS}_2$  and Group III – VI members-  $\text{InSe}$  and  $\text{GaS}$ }; superconductors {members include  $\text{NbSe}_2$ } and semi metals {members include carbon, silicon, germanium and antimony

**Figure 2.6:** Different biomedical routes making use of fabricated 2D materials in a significant way

**Figure 2.7:** Members of transition metal dichalcogenide family highlighted in the periodic table which can form a number of combinations exhibiting 2D nanosheets morphology with very intriguing properties. Transition metal dichalcogenide structural representation in terms of the

chemical bonds linked with single metal atom and two chalcogen atoms into few atomic structure nanosheet morphology

**Figure 2.8:** Represents the two different structural phases of MoS<sub>2</sub> nanosheets which are a) trigonal prismatic (2H-MoS<sub>2</sub>) a semiconducting form occupies central position in the lattice, whereas in b) is the octahedral arrangement of atoms (1T-MoS<sub>2</sub>) which is metallic in nature

**Figure 2.9:** Different fabrication approaches employed to produce 2D nanosheets with few nanometers of thickness and broad range of lateral sizes of the nanosheets -Top down and bottom up approach to exfoliate 2DMs

**Figure 2.10:** Procedure of micromechanical exfoliation of graphene using scotch tape method and then subsequently depositing it onto a particular substrate

**Figure 2.11:** Steps to grow 2D nanosheets from the precursors followed by nucleation and vapor deposition based controlled growth in a specific pattern, high quality monolayer nanosheets

**Figure 2.12:** Steps to exfoliate 2D MoS<sub>2</sub> nanosheets using lithium intercalation technique

**Figure 2.13:** Procedure for liquid phase exfoliation of 2D nanosheets exfoliated in a suitable solvent/ aqueous surfactant system

**Figure 2.14:** Structural representation of MoS<sub>2</sub> nanoflakes explaining the two different exfoliation mechanisms resulting in separation of bulk crystal into ultrathin 2D nanosheets In one part, inter layer van der Waals forces are broken to isolate the bulk crystal into 2D nanosheets, whereas in another portion fragmentation occurs via breaking of covalent bonds within the bulk

**Figure 2.15:** Schematic of Beer-Lambert law indicating an incident light with intensity  $I_0$ , length of the cuvette with  $l$  and the absorbed light with intensity  $I_1$

**Figure 2.16:** UV-Vis spectrophotometer of Jasco V-530 model with double beam slots for reference and sample used in this thesis

**Figure 2.17:** Schematic of double beam UV-Visible spectrophotometer

**Figure 2.18:** Represents the Energy level diagram of Raman scattering

**Figure 2.19:** Raman microscope used in this thesis

**Figure 2.20:** A) An electrophoretic mobility of the particles measured in a specific cuvette designed for zeta potential with two electrodes which works when an electric field is applied from outside. B) Represents the mobility of different ions in the designed capillary of the cuvette on applying an electric field from outside

**Figure 2.21:** Malvern Zeta sizer nano used in this thesis

**Figure 2.22:** Fundamental scheme of electron-matter interaction when an high energy electron beam hits the surface of the sample and subsequently different signals are received

**Figure 2.23:** Schematic of scanning electron microscope

**Figure 3.1:** Represents the proper setup of sonicator device with an ice-box

**Figure 3.2:** Panel (A-F) represents water-dispersed 2D MoS<sub>2</sub> samples centrifuged at A)160 g, B) 620g, C) 1000g, D) 1400g, E) 2700g and F) 3300g. As the centrifuge speed increases, the color of the supernatant starts to diminish from dark green to light green (A-F).

**Figure 3.3:** Represents the tapered tip (KE-76, 6mm diameter) used for the exfoliation. Particularly, it shows the remaining and un-exfoliated MoS<sub>2</sub> powder cum semi-paste after the exfoliation

**Figure 3.4:** UV-Visible absorbance spectra of water-dispersed MoS<sub>2</sub> nanosheets at centrifuged at different speeds, 620g, 2700g and 3500g for 45 minutes each. Higher centrifuged sample were kept under gravitational storage and at 4°C for three weeks just after the exfoliation. The above graph represents a good stability of water exfoliated samples which is crucial for further studies

**Figure 3.5:** A) UV-Visible extinction spectra of 2D MoS<sub>2</sub> nanosheets dispersion at 620g and 1000g. B) Raman spectra of the two main vibrational modes  $E_{2g}^1$  and  $A_{1g}$  of MoS<sub>2</sub> nanosheets centrifuged at 1000g and 1400g. Raman shift in the region from 380 - 412 cm<sup>-1</sup> range represents MoS<sub>2</sub> nanoflakes in the range from 2-4 layers.

**Figure 3.6:** Pannel (A-D) represents two different scales of SEM obtained for water-exfoliated 2D MoS<sub>2</sub> nanosheets dried under vacuum for 15 minutes and centrifuged dispersion at 2000g. (A) Shows small islands of an ensemble of 2D nanosheets which aggregated on drying. (B-D) shows large and small chunks of 2D MoS<sub>2</sub> nanosheets at 1 μm scale which clearly signifies the ability of water to act as a considerable solvent to exfoliate 2D TMDs for some specific applications where few layer and multi-layer nanosheets are required.

**Figure 3.7:** Pannel (E-H) represents another panel of SEM images at 1 μm scale dried under vacuum for 15 minutes and centrifuged dispersion at 3000g. E) Shows a homogenous distribution of water exfoliated MoS<sub>2</sub> nanosheets over the silicon substrate. F) Shows a peculiar kind of sharp knife type morphology of MoS<sub>2</sub> nanosheets and the surrounding homogenous distribution of small lateral size 2D nanflakes. (G-F) Represents small and large chunks of water exfoliated few layer 2D MoS<sub>2</sub> nanosheets.

**Figure 3.8:** Represents the TEM image of water exfoliated 2D MoS<sub>2</sub> nanosheets at 620 g

**Figure 3.9:** Represents the TEM image of water exfoliated 2D MoS<sub>2</sub> nanosheets at 1400 g.

**Figure 3.10:** Different forces acting on a particle in the given medium

**Figure 3.11:** Eppendorf bench top centrifuge 5804 model used to follow the cascade centrifugation of water exfoliated 2D MoS<sub>2</sub> nanosheets

**Figure 4.1:** Cell cycle analysis. (a) MCF-7, (b) U937 and (c) HaCaT cell lines at different final concentrations of 2D MoS<sub>2</sub> dispersion after 24 h, 48 h and 72 hours from the beginning of the treatment. The cell scattering shows two peaks: G1 (gap 1), the gap between mitosis (nuclear division) and DNA replication, corresponding to cells metabolically active but that do not replicate their DNA and G2 (gap 2) corresponding to cells that grows and synthesize the proteins for mitosis. Between G1 and G2 there is the S phase in which the cells replicate their DNA. The cell death is revealed as percentage of cells in pre-G1 phase; corresponding to a pick of fragmented DNA Error bars indicate standard deviation of triplicate analysis.

**Figure 4.2:** MTT analysis. (a,b) MTT assay performed on U937 cell line with (a) 2000 and (b) 4000 cells at 570 nm absorbance for 24 h and 48 h. (c,d) MTT assay performed on MCF-7 cell line with (c) 2000 and (d) 4000 cells at 570 nm absorbance for 24 h and 48 h. Error bars indicate three independent experiments in (a–d).

**Figure 4.3.** SEM analysis of human cell lines. (a–c) MCF-7 (top, the red arrows indicating the nanoflakes onto the cell), (d–f) U937 (middle, the blue arrows indicating the damaged areas and the red the nanoflakes) and (g–i) HaCaT cells (bottom, the blue arrows indicating the damaged areas and the red the nanoflakes) untreated and treated with MoS<sub>2</sub> dispersion at the indicated concentrations. The N was two at 10 µg/mL and six at 14 µg/mL.

**Figure 4.4.** Interaction pathway for adhesion (MCF-7 and HaCaT cells) and suspension cells (U937) with 2D MoS<sub>2</sub> nanosheets

**Figure 4.5.** Cell death analysis for long duration. (a) Cell Death induced by MoS<sub>2</sub> nanosheets treatment in the same experimental setting of SEM experiment. (b) Cell Death induced by MoS<sub>2</sub> nanosheets treatment with HaCaT cells checked at 24, 48, 72 and 96 h after treatment, in the same

experimental conditions of SEM experiment. Error bars report standard deviation after three independent experiments in (a,b).

**Figure 4.6.** Proliferation test. Two different concentrations of 2D MoS<sub>2</sub> dispersion interacted with *S. typhimurium* represented as (a–f). (a) Positive control of wild-type Salmonella without 2D MoS<sub>2</sub>, (b) incubation at 11.2 µg/mL and (c) at 20 µg/mL; (d–f) Salmonella bacteria grown in the lab (ATCC 14028), (d) positive control without 2D MoS<sub>2</sub>, (e) incubation at 11.2 µg/mL and (f) at 20 µg/mL. All the samples treated with MoS<sub>2</sub> nanoflakes were checked after 4 h from the treatment. (g) MTT plots of 2D MoS<sub>2</sub> dispersion incubated with ATCC 14028 Laboratory Salmonella and (h) wild-type Salmonella at 11.2 µg/mL and 20 µg/mL. The absorbance of the incubation is presented at 450 nm (green) and 490 nm (red) wavelengths. Interaction of 2D MoS<sub>2</sub> nanosheets at 20 µg/mL with average thickness of N = 4.

**Figure 4.7:** (a) Control rod shaped ATCC 14028S. typhimurium (b) fragment of a bacterium cut by a nanosheet evidenced by the red arrow, (c) slight cut at the outer bacterial membrane as shown by red arrow, and (d) leakage of intracellular components of Salmonella bacteria (red arrow) upon interaction with the sharp edges of the 2D MoS<sub>2</sub> nanosheets present nearby (blue arrows).

**Figure 6.1:** Raman imaging of a MCF7 cell exposed to MoS<sub>2</sub> flakes: (a) Bright field image, (b) Comparing of the Raman spectra corresponding to the points indicated in (a), Raman mapping corresponding to the spectral range of (c) 388-415 cm<sup>-1</sup>, (d) 768-800 cm<sup>-1</sup>, (e) 2828-2900 cm<sup>-1</sup> and (f) 2900-3017 cm<sup>-1</sup>. The scale bar is 7 µm.

**Figure 6.2:** (A-B) represents the mechanical damage to the tested bacterium. (A) Shows a clear damage to the circular morphology of *Staphylococcus Aureus* at 100 µg/mL, whereas in (B) a clear mechanical cut on the morphology of *E. Coli* upon interaction is shown with a large MoS<sub>2</sub> nanoflake at 100 µg/mL.

**Figure 6.3:** Panel (A-B) shows a low magnification optical microscope images of only machined silicon substrate at different regions. A) Represents both machined and non-machined surface of the same silicon substrate with dark and light regions, respectively; B) shows a different regions of the patterned silicon substrate with groves and ripples.

**Figure 6.4:** Panel (A-C) shows SEM images of both the machined grooves and ripples on the machined surface and liquid phase exfoliated few layer 2D MoS<sub>2</sub> nanosheets. A) Low resolution microscopic image exhibiting distribution of 2D MoS<sub>2</sub> nanoflakes onto the machined substrate; B) Random distribution of very-few and few layer MoS<sub>2</sub> nanosheets on the patterned silicon substrate and C) shows enlarged at high resolution microscopic image of deposited 2D MoS<sub>2</sub> nanoflakes in between the grooves with irregular morphology and large lateral size of few microns.

## List of Tables

**Table 1:** Mean value of dispersion concentration, number of layers, lateral size and A-exciton wavelength obtained from the optical extinction spectra just after the exfoliation and kept for three weeks of storage based on the metrics.

**Table 2:** Mean value of number of layers and lateral size at the given centrifugal speeds. The given values are obtained from the UV-Visible optical extinction spectra using the metrics as reported by Backes et al.

**Table 3.**  $\zeta$ - Potential values of MoS<sub>2</sub> nanosheets dispersion at different centrifugal forces.

**Table 4.1** Properties of exfoliated MoS<sub>2</sub> nanosheets used in cell cycle progression experiments.

**Table 4.2** Concentration, mean layer number and mean lateral size of exfoliated MoS<sub>2</sub> nanosheets pre-incubated with 3000 HaCaT cells for 24 h and 48 h. Absorbance values at 570 nm after 24 h and 48 h of incubation with nanosheets. Negative control is normalized to absorbance equal to 1.

**Table 4.3:** Concentration, mean layer number and mean lateral size of exfoliated MoS<sub>2</sub> nanosheets pre-incubated with 3000 MCF7 cells for 24 h and 48 h. Absorbance values at 570 nm after 24 h and 48 h of incubation with nanosheets. Negative control is normalized to absorbance equal to 1.

## Acronyms

2D	-	two dimensional
2D TMDs	-	two dimensional dichalcogenides
LPE	-	liquid phase exfoliation
SEM	-	scanning electron microscopy
TEM	-	transmission electron microscopy
2DMs	-	two dimensional materials
HSV-1	-	Herpes Simplex Virus

# CHAPTER- 1

## INTRODUCTION

---

### 1.1 Motivation

The wide vision of nanotechnology has become a research hotspot worldwide because of the application of science at extremely small scale which enables its potential use in many applications<sup>[1,2,3]</sup>. The relevance of nanotechnology with our daily life products can be seen from *Figure 1.1* and *Figure 1.2*. The advancements in nanomaterials design strategies, processing methods and subsequent implementation in consumer market has received considerable attention because of their imperative and intriguing physicochemical properties <sup>[4-7]</sup>. Nanomaterials, in general have received worldwide attention in biological applications because of the ability to tune their physical and chemical properties. The behavior of different nanomaterials with biological environment is usually investigated via different interaction modes such as chemical, surface and mechanical which exhibit the most primitive fundamental phenomenon of this novel research field. Furthermore, these novel interactions strongly affect the biochemical properties of

the corresponding bio-component in contact such as perturbing the cell membrane, membrane stress and the subsequent physical damage. In general, physical or mechanical interactions of different nanomaterials with soft biological structures are investigated by their unique physico-chemical properties such as surface charge, size, morphology, surface area, surface composition, functionalization ability, hydrophobicity, hydrophilicity, biodegradability, bio-compatibility, excellent solubility in the physiological medium, aggregation and agglomeration.

In general, the advancements in nanotechnology and the further studies on the fabrication, functionalization, application and nano-toxicology evaluation of the fabricated nanomaterials has gained increased attention by various research groups. All these studies are possible only after in-depth characterization analyses of the behavior of various nanomaterials with the biological components. So, going back to the historical era, after the successful invention of scanning tunneling microscope in 1981<sup>[1,8]</sup> , zero dimensional Buckminster fullerene in 1985 <sup>[9]</sup> and one dimensional single wall carbon nanotube in 1991<sup>[10]</sup> a significant amount of attention was devoted to the field of nanotechnology. Since then, dozens of Nobel Prizes in various fields of applied sciences has been awarded based on the breakthrough inventions in the field of nanotechnology. Two physicists from University of Manchester earned a Nobel Prize in physics in 2010 by giving a breakthrough invention with the isolation of a new low dimensional nanomaterial, Graphene in 2004 <sup>[11]</sup>, which is a single sheet of carbon atoms. This led to an era of the first truly two dimensional nanomaterial (2D NMs) with new and exciting physics. Since then, very many fascinating classes or categories of 2D materials have been explored and still under investigation which have a plenty of room to be utilized in different areas of applications such as solar cells, gas sensing, catalysis, super capacitors, fuel cells, batteries, biomedical science, live-matter interaction and green and renewable energy sources to name a few.

# EVERYDAY USES OF NANOTECHNOLOGY

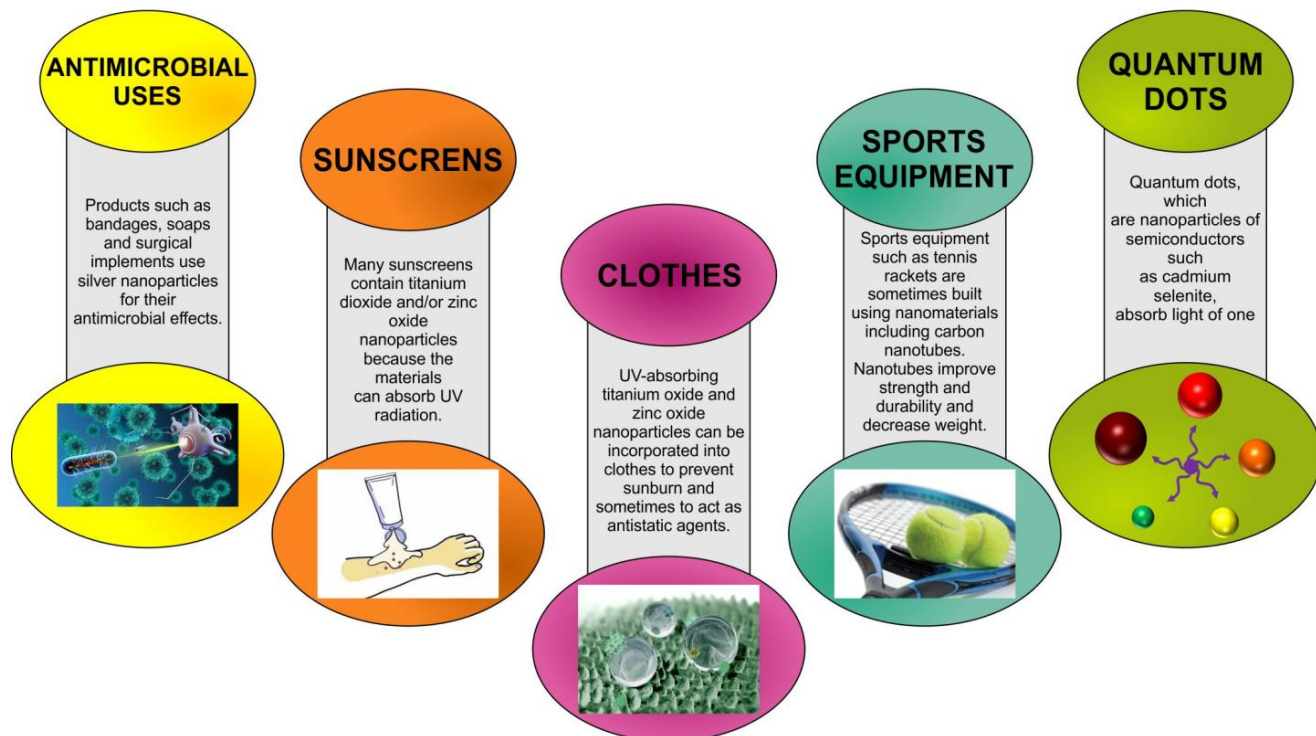
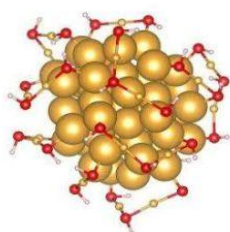


*Figure 1.1:* Acme of nanotechnology's potential in various applications where it has shown remarkable results and entry into the commercial market with a variety of products.

# What is

# NANO TECHNOLOGY

A single **GOLD ATOM** is about a third of a nanometer in diameter.



**A SHEET OF NEWSPAPER**

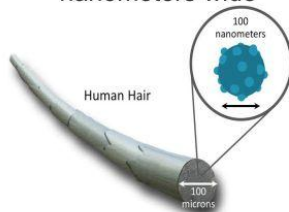
is about 100,000 nanometers thick



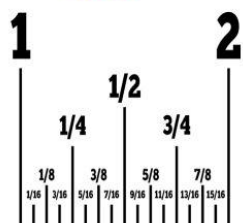
If the diameter of a **MARBLE** was one nanometer, then diameter of the Earth would be about one meter



**A HUMAN HAIR** approximately 80,000 to 100,000 nanometers wide



25,400,000 nanometers in an **INCH**



**HUMAN DNA** is 2.5 nanometers in diameter



One nanometer is about as long as your **FINGERNAIL** grows in one second



**Figure 1.2:** Relevance of nanotechnology in terms of how small it can be exemplified with our day to day stuffs<sup>1</sup>.

<sup>1</sup> The web link for **Figure 1.1** is <https://www.chemeurope.com/en/infographics/296/nanotechnology-day-everyday-uses-of-nanotechnology.html>, <https://nanotechnology.americanchemistry.com/>

The exciting and wide range class of two dimensional nanomaterials (2DMs) has stood up as the main center of attraction in materials chemistry worldwide. Substantial efforts have been put on their novel fabrication routes, in depth characterization analyses and the fundamental electronic, photonic and catalytic behavior [12]. On the other hand, motivations for studying their behavior in biological systems need to be pushed up in order to understand their future biomedical aspect in various related applications. Moreover, the bio-application areas for 2DMs are anticipated to grow at wide scale much in a same way as carbon nanotubes grew far beyond their initial electronics based applications. It is extremely important to study the basic interactions of 2DMs with cells, tissues and other biological components to create a platform for understanding the toxicological fate of the given 2DMs, scientific indulgent in analyzing developmental risks and involuntary human exposure from laboratory scale to scalable fabrication methodologies [13]. In 2DMs, the sheet like morphology with sharp edges and their unique surface chemistry enabled functionalization ability results in autonomous penetration of the 2D nanosheets into the cell membranes followed by lipid extraction and membrane damage [14,15]. For example, the bacterial films formation, bacterial resistance in medical field and various other chronic pathogen related diseases have been under deep investigation to employ the use of potential nanoparticles to act as antibacterial, antiviral and anti-biofilm agents to reduce the damage, cost and other deteriorations in medical science. Two dimensional materials and other nanoparticles have shown a significant potential in dealing with different pathogens at nanoscale, fighting with different morphologies and the subsequent damaging effect [16-23].

The successful utilization of this nanosheet like morphology in biomedical areas largely depends on their green and scalable fabrication route. So, one of the best, reliable and low cost processing

option is the liquid phase exfoliation approach pioneered by Coleman et al in 2008 [24], which has been a subject of extensive research to transfer this fabrication technique from laboratory to industrial scale.

The main aim of my thesis is to study the biological interactions of one of the most explored 2D material after graphene which is MoS<sub>2</sub>, a semiconductor from transition metal dichalcogenide family, with normal and tumor cells along with its antibacterial and antiviral action on different pathogens such as *Salmonella typhimurium* (ATCC 14028 and wild type), *E. coli* and *Staphylococcus aureus*. In view of this, my first approach was to fabricate 2D MoS<sub>2</sub> nanosheets in environmentally benign solvent with a good amount of stability for the desired application. The stability of the nanosheets in green solvents, particularly in water, with or without stabilizers or surfactants, is still a focus of great interest in biomedical science [25-37]. Though, many review articles and research papers have reported the biocompatibility of MoS<sub>2</sub> nanosheets [38-47] but the fabrication protocol and the subsequent physical parameters of 2D nanosheets defines its role with living matter. Water, in general, is considered as a poor solvent for the exfoliation of 2D materials because of the low yield and mismatchment of surface energy parameters with that of the given 2D material. The current thesis work attempts to fabricate 2D MoS<sub>2</sub> nanosheets in de-ionized (DI) water without any surfactant or stabilizer though with less concentration but with a motive to circumvent the use of toxic organic solvents which no doubt can disperse the nanosheets for a long time and at high concentrations. Thanks to the exfoliation parameters which can be tuned to achieve a substantial amount of stability of 2D materials in different solvents including water [48,49]. The successful interaction of these 2D nanosheets with human cells and pathogens gave intriguing results which showed an interesting behavior of 2D

nanosheets with the living matter. It is hoped that this research will form the basis for further study to gain a deeper insight into the mechanism of 2D nanosheets action, particularly with the live matter such as human cells.

## **1.2. Research scope and objectives**

Instead of using any surfactants or stabilizers, we have directly exfoliated MoS<sub>2</sub> bulk powder into 2D nanosheets. No doubt, the yield and concentration achieved in our case after the exfoliation is low as compared to the use of organic solvents which gives long term stability and higher concentration. But on the same hand the use of toxic organic solvents such as N-methyl-2-pyrrolidone (NMP), dimethyl formamide (DMF), dimethyl sulfoxide (DMSO), hexane, butane to name a few have serious health impacts and the post exfoliation steps to remove these solvents are very tedious. Our motive was to study the impact of as exfoliated 2D nanosheets dispersed in pure water with normal HaCaT (epithilium) cell line, MCF7 (breast cancer cell line) and U937 (acute leukemia) cell line. Based on the nature of water dispersed 2D nanosheets, the subsequent impact on each cell line was significant. Furthermore, the nature of cell lines studied has played an important role in studying the interaction of water dispersed 2D nanosheets. Thanks to the flexibility in tuning exfoliation parameters such as initial concentration, amplitude of the probe sonicator, probe tip diameter, type of vessel and output power of the sonicator device. The research scope of the present work has given us a direction in which we tried to understand the mechanism of 2D nanosheets action onto human cells via the presence of calcium and potassium ions into the incubated cell culture media with MoS<sub>2</sub> nanosheets.

### **1.3. Organization of the dissertation**

*In Chapter-1*, I have discussed about the motivation to select my PhD topic based on the appealing demand of nanotechnology in almost all areas of interest. Further I have deliberated the research scope and objectives of my PhD thesis project which covers the mainstream of the present work. Motivated from the intriguing properties of MoS<sub>2</sub> nanosheets and the widely explored member of the transition metal dichalcogenide family, I have chosen it as the main contender to understand the desired application of focus in this thesis. Particularly, to study the scalable fabrication and the subsequent interaction with the live matter, objective of this thesis include the green synthesis route of MoS<sub>2</sub> exfoliation in pure water only.

*In Chapter-2*, initially I have discussed about the significance of nanomaterials in various areas of science which have revolutionized the research and commercial sector worldwide. After then, I have discussed about 2DMs which have recently got a wide-reaching attention. Further, I have explained in detail about 2D TMDs particularly about MoS<sub>2</sub> nanosheets and the main fabrication protocol followed in this thesis which is liquid phase exfoliation (LPE) to understand its live-matter interaction in a significant way. I have discussed about various characterization tools used in this thesis along with the specific model of each tool, such as UV-Visible spectroscopy to measure the absorbance and optical extinction related information of the exfoliated 2D MoS<sub>2</sub> nanosheets. Raman spectroscopy which serves as an important tool to get confirmed information on the number of layers and particularly on the successful exfoliation of the given 2DM. On the other hand, zeta potential gives interesting information on the stability and about the magnitude of surface charge generated after the exfoliation of 2D nanosheets. Another important tool to characterize the exfoliated 2D MoS<sub>2</sub> nanosheets morphology and further to understand its synergistic interaction with the live matter such as various pathogens and human cells, electron

microscopy gives a good option to proceed with. Under this, I have discussed about scanning electron microscope (SEM) which has proven to be very useful in this thesis to understand the morphology and nature of interaction of water exfoliated 2D MoS<sub>2</sub> nanosheets respectively. I have basically discussed solubility theories, though these have not been studied for the water exfoliated 2D nanosheets because the thermodynamics of minimizing the enthalpy of mixing to achieve a stable dispersion works best for those solvents which have well suitable surface energy with that of the given solute. Water, being a poor solvent has high surface energy as compared to that of MoS<sub>2</sub> nanosheets which in consequence cannot be included into the solubility theories. Despite of that to understand the thermodynamics of a stable dispersion it is important to introduce about the crucial solubility parameters reported in general for other solvents and also for the aqueous co-solvent approach.

***In Chapter-3***, I have discussed about the liquid phase exfoliation (LPE) technique employed in this thesis to exfoliate MoS<sub>2</sub> nanosheets keeping in mind the importance of crucial sonication parameters such as nature of solvent, initial concentration, amplitude of the sonicator device, vessel type and time of sonication. After that, post exfoliation steps such as liquid cascade centrifugation (LCC) has been extensively used in this thesis to underline the importance of size selection and the desired concentration for the application of interest for my PhD project. Further, important analysis of the exfoliated samples by UV-Visible spectroscopy, Raman spectroscopy, zeta potential and scanning electron microscopy results have also been discussed.

***In Chapter-4***, I have discussed about the significant live-matter interaction results achieved in this thesis with a motive to exfoliate MoS<sub>2</sub> nanosheets directly in de-ionized water. The evident antibacterial and antiviral effect of MoS<sub>2</sub> nanosheets is confirmed from the statistical tests and microscopy analysis. Further, I have also introduced a separate section for our recently

published work on surface structuring using femtosecond lasers to achieve different surface patterns with a motive to deposit LPE nanosheets specifically onto the machined substrates.

*In Chapter-5*, I have explained the conclusion and future prospects of my thesis project

*In Chapter-6*, I have deliberated about some of our ongoing projects which cover the future outlook of the present work in a number of desired applications. Particularly, the synergistic antibacterial and antiviral effect of MoS<sub>2</sub> nanosheets is under investigation and till date we have achieved valuable results which exemplify the potential of water exfoliated MoS<sub>2</sub> nanosheets to have a significant interaction with different pathogens under study. Additionally, to continue the mainstream study of this thesis which is to understand the mechanism of action of water exfoliated MoS<sub>2</sub> nanosheets on tumor and normal human cell lines, we have employed the use of advanced Raman microscopic analysis to get deeper insights into the interaction of these 2D nanosheets with the cell membrane.

## Bibliography

1. Binnig, G. & Technical, D. Scanning tunneling microscopy: From birth to adolescence. *Rev. Mod. Phys.* **59**, 615-625 (1987).
2. Thiruvengadam, M., Rajakumar, G. & Min, I. Nanotechnology : current uses and future applications in the food industry. *3 Biotech* **8**, 1–13 (2018).
3. H. W. Kroto, J. R. Heath, S. C. O'Brien, R. F. Curl & R. E. Smalley. C<sub>60</sub> : Buckminsterfullerene. *Nature*, **318**, 162-163 (1985).
4. Fajardo, S. *et al.* We are IntechOpen , the world ' s leading publisher of Open Access books Built by scientists , for scientists TOP 1 % . *Intech i*, 13 (2016).
5. Rasmussen, K. *et al.* Physico-chemical properties of manufactured nanomaterials - Characterisation and relevant methods. An outlook based on the OECD Testing Programme. *Regul. Toxicol. Pharmacol.* **92**, 8–28 (2018).
6. Daima, H. K. & Bansal, V. *Influence of Physicochemical Properties of Nanomaterials on Their Antibacterial Applications. Nanotechnology in Diagnosis, Treatment and Prophylaxis of Infectious Diseases* Elsevier Inc. 151-166 (2015).
7. Dykman, L. & Khlebtsov, N. Gold nanoparticles in biomedical applications: Recent advances and perspectives. *Chem. Soc. Rev.* **41**, 2256–2282 (2012).
8. Hamers, R. J., Tromp, R. M. & Welland, M. E. A scanning tunneling microscope for surface science studies. **30**, (1986).
9. H. W. Kroto, J. R. Heath, S. C. O'Brien, R. F. Curl & R. E. Smalley. C<sub>60</sub> : Buckminsterfullerene. *Nature*, **318**, 162-163 (1985).
10. Sumio Iijima. Helical microtubules of graphitic carbon, *Nature*, **354**, 56-58 (1991).
11. Geim, A. Beyond graphene. *Science (80-. )*. **348**, 490–492 (2004).
12. Nicolosi, V., Chhowalla, M., Kanatzidis, M. G., Strano, M. S. & Coleman, J. N. Liquid Exfoliation of Layered Materials. *Science (80-. )*. **340**, 1226419–1226419 (2013).

13. Chen, Y., Tan, C., Zhang, H. & Wang, L. Two-dimensional graphene analogues for biomedical applications. *Chemical Society Reviews* **44**, 2681–2701 (2015).
14. Li, Y. *et al.* Graphene microsheets enter cells through spontaneous membrane penetration at edge asperities and corner sites. *Proc. Natl. Acad. Sci. U. S. A.* **110**, 12295–12300 (2013).
15. Ciclo, X., Dottorato, D. E. L. & Ricerca, D. I. Effects of nanomaterials on biological barriers , fetal and post-natal , and evaluation of epigenetic toxicity. (2015).
16. Zhang, Y. *et al.* 2D Graphdiyne Oxide Serves as a Superior New Generation of Antibacterial Agents. *iScience* **19**, 662–675 (2019).
17. Splendiani, A. *et al.* Emerging photoluminescence in monolayer MoS<sub>2</sub>. *Nano Lett.* **10**, 1271–1275 (2010).
18. Mei, L. *et al.* Two-dimensional nanomaterials beyond graphene for antibacterial applications: current progress and future perspectives. *Theranostics* **10**, 757–781 (2020).
19. Baranwal, A. *et al.* Prospects of nanostructure materials and their composites as antimicrobial agents. *Front. Microbiol.* **9**, (2018).
20. Raghunath, A. & Perumal, E. Metal oxide nanoparticles as antimicrobial agents: a promise for the future. *Int. J. Antimicrob. Agents* **49**, 137–152 (2017).
21. Beyth, N., Hourri-Haddad, Y., Domb, A., Khan, W. & Hazan, R. Alternative antimicrobial approach: Nano-antimicrobial materials. *Evidence-based Complement. Altern. Med.* **2015**, (2015).
22. Shaikh, S. *et al.* Mechanistic Insights into the Antimicrobial Actions of Metallic Nanoparticles and Their Implications for Multidrug Resistance. *Int. J. Mol. Sci.* **20**, 1–15 (2019).
23. Szunerits, S. & Boukherroub, R. Antibacterial activity of graphene-based materials. *J. Mater. Chem. B* **4**, 6892–6912 (2016).

24. Hernandez, Y. *et al.* High-yield production of graphene by liquid-phase exfoliation of graphite. *Nat. Nanotechnol.* **3**, 563–568 (2008).
25. Zeng, G. *et al.* Journal of the Taiwan Institute of Chemical Engineers Surface modification and drug delivery applications of MoS<sub>2</sub> nanosheets with polymers through the combination of mussel inspired chemistry and SET-LRP. *J. Taiwan Inst. Chem. Eng.* **82**, 205–213 (2018).
26. Zheng, K. *et al.* Biosensors and Bioelectronics Graphically encoded suspension array for multiplex immunoassay and quantification of autoimmune biomarkers in patient sera. *Biosens. Bioelectron.* **132**, 47–54 (2019).
27. Dalila, N. R., Arshad, M. K., Gopinath, S. C. B., Norhaimi, W. M. W. & Fathil, M. F. M. Biosensors and Bioelectronics Current and future envision on developing biosensors aided by 2D molybdenum disulfide ( MoS<sub>2</sub> ) productions. *Biosens. Bioelectron.* **132**, 248–264 (2019).
28. Li, X. *et al.* Recent Advances in Synthesis and Biomedical Applications of Two-Dimensional Transition Metal Dichalcogenide Nanosheets. *Small* **13**, 1–28 (2017).
29. Chen, Y., Tan, C., Zhang, H. & Wang, L. Two-dimensional graphene analogues for biomedical applications. *Chem Soc Rev.* **9**, 2681-701 (2015).
30. Al-Ahmady, Z. S., Hadjidemetriou, M., Gubbins, J. & Kostarelos, K. Formation of protein corona in vivo affects drug release from temperature-sensitive liposomes. *J. Control. Release* **276**, 157–167 (2018).
31. Kurapati, R., Kostarelos, K., Prato, M. & Bianco, A. Biomedical Uses for 2D Materials Beyond Graphene: Current Advances and Challenges Ahead. *Adv. Mater.* 6052–6074 (2016).
32. Yousefi, M. *et al.* Anti-bacterial activity of graphene oxide as a new weapon nanomaterial to combat multidrug-resistance bacteria. *Mater. Sci. Eng. C* **74**, 568–581 (2017).
33. Kaur, J. *et al.* Electrostatically driven scalable synthesis of MoS<sub>2</sub>–graphene hybrid films

- assisted by hydrophobins. *RSC Adv.* **7**, 50166–50175 (2017).
34. Castagnola, V. *et al.* Biological recognition of graphene nanoflakes. *Nat. Commun.* **9**, 1–9 (2018).
  35. Kaur, J. *et al.* Green synthesis of luminescent and defect-free bio-nanosheets of MoS<sub>2</sub>: Interfacing twodimensional crystals with hydrophobins. *RSC Adv.* **7**, 22400–22408 (2017).
  36. Zhang, L., Zhao, Y. & Wang, X. Nanoparticle-Mediated Mechanical Destruction of Cell Membranes: A Coarse-Grained Molecular Dynamics Study. *ACS Appl. Mater. Interfaces* **9**, 26665–26673 (2017).
  37. Siepi, M. *et al.* Production of biofunctionalized MoS<sub>2</sub> flakes with rationally modified lysozyme: a biocompatible 2D hybrid material. *2D Mater.* **4**, 35007 (2017).
  38. Liu, T. *et al.* Combined photothermal and photodynamic therapy delivered by PEGylated MoS<sub>2</sub>nanosheets. *Nanoscale* **6**, 11219–11225 (2014).
  39. Zhong, C., Zhao, X., Wang, L., Li, Y. & Zhao, Y. Facile synthesis of biocompatible MoSe<sub>2</sub> nanoparticles for efficient targeted photothermal therapy of human lung cancer. *RSC Adv.* **7**, 7382–7391 (2017).
  40. Biswas, Y., Dule, M. & Mandal, T. K. Poly(ionic liquid)-Promoted Solvent-Borne Efficient Exfoliation of MoS<sub>2</sub>/MoSe<sub>2</sub> Nanosheets for Dual-Responsive Dispersion and Polymer Nanocomposites. *J. Phys. Chem. C* **121**, 4747–4759 (2017).
  41. Yin, W. *et al.* Functionalized Nano-MoS<sub>2</sub> with Peroxidase Catalytic and Near-Infrared Photothermal Activities for Safe and Synergetic Wound Antibacterial Applications. *ACS Nano* **10**, 11000–11011 (2016).
  42. John R.Giudicessi, BA.Michael J.Ackerman., 2013. 基因的改变NIH Public Access. *Bone* **23**, 1–7 (2008).
  43. Feng, W. *et al.* Flower-like PEGylated MoS<sub>2</sub> nanoflakes for near-infrared photothermal

- cancer therapy. *Sci. Rep.* **5**, 1–13 (2015).
44. Chng, E. L. K., Sofer, Z. & Pumera, M. MoS<sub>2</sub> exhibits stronger toxicity with increased exfoliation. *Nanoscale* **6**, 14412–14418 (2014).
  45. Yin, W. *et al.* High-throughput synthesis of single-layer MoS<sub>2</sub> nanosheets as a near-infrared photothermal-triggered drug delivery for effective cancer therapy. *ACS Nano* **8**, 6922–6933 (2014).
  46. Hao, J. *et al.* In Vivo Long-Term Biodistribution, Excretion, and Toxicology of PEGylated Transition-Metal Dichalcogenides MS<sub>2</sub> (M = Mo, W, Ti) Nanosheets. *Adv. Sci.* **4**, (2017).
  47. Zhang, S., Jia, X. & Wang, E. Facile synthesis of optical pH-sensitive molybdenum disulfide quantum dots. *Nanoscale* **8**, 15152–15157 (2016).
  48. QSONICA SONICATORS.pdf.
  49. Processors, U. L. Index.

## **CHAPTER-2**

# **LITERATURE FRAMEWORK ON TWO DIMENSIONAL TRANSITION METAL DICHALCOGENIDES (MoS<sub>2</sub>)**

---

### **2.1. Nanotechnology**

Asking about nanotechnology to a random selection of scientists, engineers, researchers, academicians, industrialists and the common public will give a broad range of replies because the scope and objectives of nanotechnology is actually very vast in itself! For many scientists, it could be nothing new because since ages nanotechnology has been in use by different communities of the society. Moreover, scientists have been working at the nanoscale for decades, through electron microscopy and other evolving techniques. For other groups, it might be very close to a science fiction which now-a days is becoming the reality in many applications such as mini robots into the blood stream to cure deadly diseases, strong defense weapons, renewable energy based automobiles, nano-industries and food technologies to name a few! [<sup>1-4</sup>].

Today's material science can be coined into a single term which is nanotechnology. Basically, it is that field of applied sciences and technology where manipulation of individual atoms and molecules happen at the nanoscale in the range of 1-100 nm. One nanometer is a billionth of a meter, or  $10^{-9}$  of a meter. Depending on the number of dimensions in that range materials can be classified as 0D, 1D, or 2D. It encompasses the concepts of all other fields such as chemistry, physics, mathematics and biology. To understand the impact of nanotechnology, when the bulk material is scaled down to nanoscale, can be seen by the change in its physico-chemical properties at a significant level [5-7]. Nanotechnology can also be defined in terms of “quantum confinement” where, quantum means the atomic nature of the particles and confinement means restriction in the motion of randomly moving electrons in specific energy levels [2,3,8].

Date back to thousands of years ago, Romans were the pioneers of nanotechnology and they used it for eye catching decoration. Roman artisans added tiny nanoparticles of silver and gold in the range of 50 nm to the famous “Glass Chalice” which gave different colors when lit from the front and back side<sup>1</sup>. Actually, it is not the development of our century and what is new about this technology is our ability to understand the nanoscale interactions and manipulation of atoms using different approaches [9].

Even in the 9<sup>th</sup> century, craftsmen in Mesopotamia were oblivious about the use of nanoparticles to create the glittering effect on the pottery. People in actual knew nothing about nanotechnology since ages but they were blindly following traditional recipes to fulfill the need of their profession and to achieve the results with different techniques.

---

<sup>1</sup> [<https://www.smithsonianmag.com/history/this-1600-year-old-goblet-shows-that-the-romans-were-nanotechnology-pioneers-787224/>].

Nanotechnology exists abundantly in nature and in view of that nature gives us classic examples of biological molecular machines such as bacterial flagella which functions at micro and nano scale. Another classic example would be from lotus plant which shows significant water repellence by its leaves giving rise to the famous “Lotus effect”. This effect in principle has conceptualized the idea to develop coatings, paints, fabrics on other surfaces that can be used as self-cleaning objects! <sup>2</sup> A famous science fiction movie “Fantastic Voyage” showed marvels of nanotechnology in 1966 when it was a dream to think of such miniaturization of nanobots/submarines to be used to treat deadly diseases into the bloodstream. In principle, this could be even used to develop targeted drug delivery systems using these nanomachines! [<sup>1,10-13</sup>].

The first scientific approach to understand nanotechnology was made by Faraday when he discovered that going below a certain size gold nanoparticles no longer remain metallic and they change their color as well. The first scientific publication on the use of nanomaterials was printed on CdI<sub>2</sub> nanoparticles in 1922 [<sup>14</sup>] and then on MoS<sub>2</sub> in 1930 [<sup>15</sup>].

Throughout the human history, their exposure to different nanoparticles exists but after the industrial revolution, it has increased dramatically. Richard Zsigmondy, the 1925 Nobel Prize Laureate in chemistry was the first person who explicitly coined the term “nanometer” to characterize particle size and further he also measured the size of gold colloids using microscope. Richard Feynman, the 1965 Nobel Prize Laureate in physics is considered as the “The father of modern Nanotechnology” because during his 1959 American Physical Society

---

<sup>2</sup> [<https://trialx.com/curetalk/2012/10/08/nanotechnology-significance-and-applications-in-the-living-world/>]

meeting at Caltech, United States, he gave a famous lecture entitled, “ There’s plenty of room at the bottom” predicting the possibility of new discoveries and introducing the concept of manipulating matter at atomic level. Since then, his hypotheses have been proven correct and nanotechnology has revolutionized the whole material science in a significant way [16]. A Japanese scientist, Norio Taniguchi was the first person who coined the term ‘nanotechnology’ almost after 15 years of Feynman’s lecture at Caltech, to describe semiconductor process at nanometer scale. This was the era when the prodigies of nanotechnology were evolving and in 1980s Kroto, Smalley and Curl discovered fullerenes which actually started the race of exploration for new materials. Furthermore, this golden era of nanotechnology gave another invention of carbon nanotubes by a Japanese scientist Iijima which actually was a scientific transition from fullerenes and then to today’s Graphene.

### **2.1.1. Nanomaterials**

The extremely small engineered particles whose at least one dimension exists less than or equivalent to 100 nm are nanomaterials. They have significant importance because of their unique physical and chemical properties at the nanoscale which differ considerably from their bulk counterpart of the similar composition. As a result, nanomaterials have now entered into the commercial market from laboratory in terms of their existence in different forms in day to day life. The one reason for which these are very popular in almost all applications is their extremely small size or very high surface to volume ratio which enhances their properties in a dramatic way. **Figure 2.1** represents a general classification of a nanoparticle based on its size, shape, surface chemistry and the type of material employed in various applications. All these categories play a key role in defining its role in a specific application. Because of their significant role in

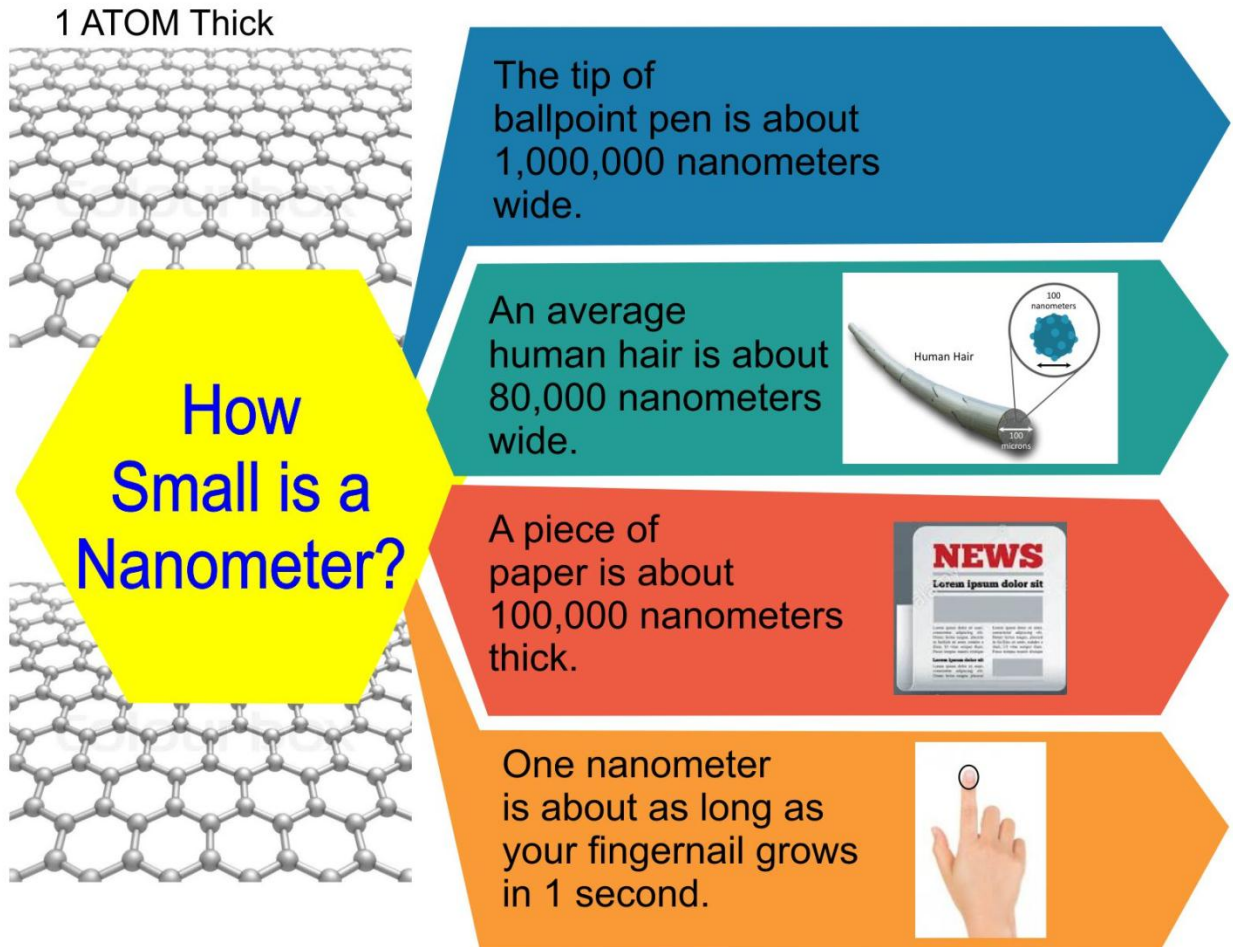


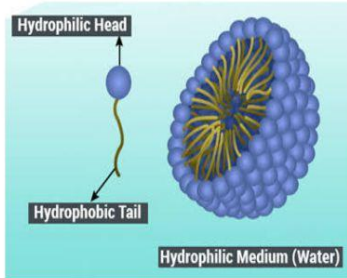
**Figure 2.1:** Classification of various nanoparticles based on its size, shape, surface chemistry and type of material which can be exploited in various applications<sup>3</sup>

numerous application areas, it will not be good to say that nanomaterials are only bound to laboratories rather they have been explored to create materials in nanoforms. For example, nanoform of titanium dioxide is used to implement ‘lotus effect in terms of self-cleaning or its coating onto plastic accessories [17,18]. Thanks not only to the size of nanomaterials but their novel physical and chemical properties by which they can be used to damage and even destroy

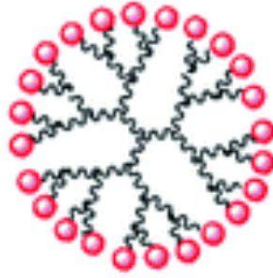
<sup>3</sup> [<http://cnbm.amu.edu.pl/en/nanomaterials>]

# Nano - carriers

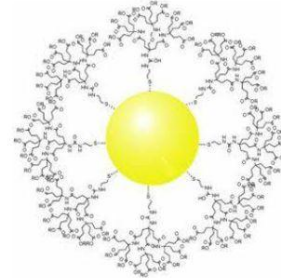
Micelle



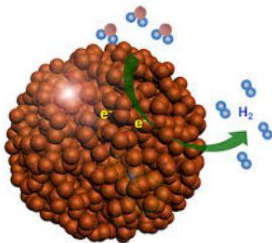
Dendrimer



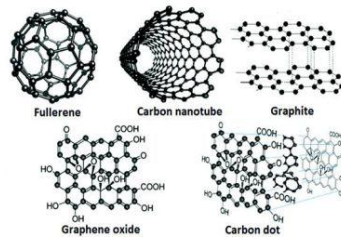
Gold nanoparticle



Porous Silicon nanoparticle



Carbon-based nanomaterials



Liposome

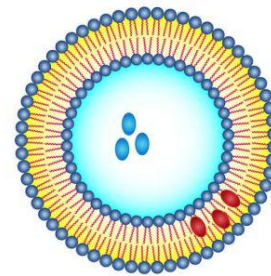


*Figure 2.2: Different nanoparticles acting as promising nano-carriers in various biomedical applications [22].*

the cancer cells from within [19,20]. A huge number of nano morphologies have been reported so far depending on the type of application and as shown in the *Figure 2.2* various morphologies of different nanoparticles such as gold nanoparticle, dendrimers, liposomes and silver nanoparticles to name a few have shown a substantial amount of potential in treating various mortal diseases

such as various types of cancers, antibacterial and antiviral actions, molecular and cellular level interactions<sup>[21,22,23,24]</sup>.

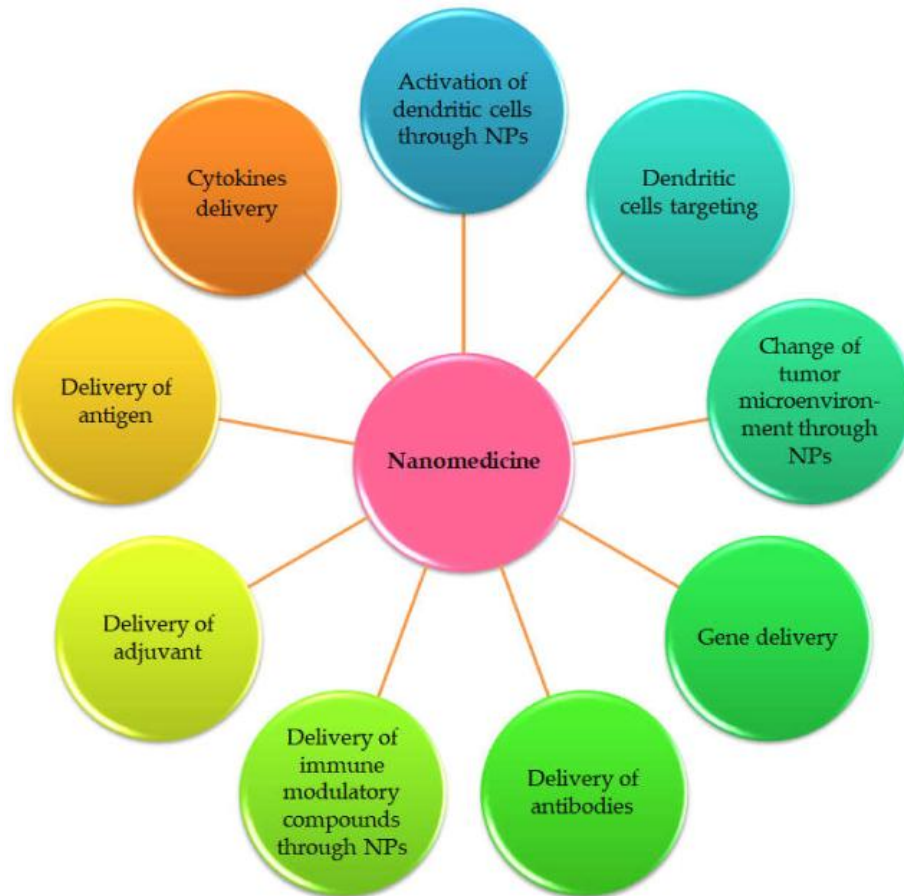


**Figure 2.3:** A horde of potential hands of nanoparticles in nanomedicine field to enhance their potential to a significant level <sup>[25]</sup>.

So, to summarize the potential of various nanoparticles in biomedical science, **Figure 2.3** gives an overview of the different potential hands of nanoparticles in nanomedicine field to revolutionize the field by a significant level.

## 2.2. Two dimensional materials

Particularly, in this section, I will discuss about two dimensional (2D) layered nanomaterials which have given new opportunities to the material scientists throughout the world. For the last 20 years more or less, over a dozen of Nobel Prizes have been awarded for the significant advancements or discoveries in nanotechnology. Among those, one of the Nobel Prize in Physics in 2010 was earned by two physicists from University of Manchester by A. Geim and K. Novoselov for their incredible discovery of the isolation of single graphene layers from the bulk graphite in 2004 [26]. Now, graphene is like a wonder material and undoubtedly the most known and famous among 2D layered materials. Though, the focus of this thesis is not on graphene but it is important to give an introduction because it has opened the doors for a new type of layered nanomaterials, considering the fact that graphene is not the only 2D material known. Dimensionality of a nanomaterial or any material in general, is an important factor which explains the behavior, properties and its applications. And the same is applied to graphene and the other fascinating members of 2D material family which are extremely intriguing in terms of their structure, properties and their use in multiple applications. During late 1930s, it was a theoretical belief that 2D materials could not be exfoliated into layers at non zero temperatures [27]. Even later on, some experiments were performed and the given statement was proven correct and the existence of 2D materials was limited only to academic materials for theoretical studies [28,29]. Then in late 1960s, another report on 2D materials was published based on the explanation that due to thermal fluctuations in the sheet like structure of 2D materials their existence would not be exhibited in the long range order, though in three dimensional space [30].

So, after the successful isolation of graphite into graphene layers in 2004, the leading scientists proved that 2D materials can also exist at finite temperatures [26]. The above depicted **Figure 2.4** was verified by Meyer et al.[31] who experimentally proved that the existence of ripples upon the suspended graphene sheet stabilizes the material and it accounts for the thermal fluctuations which are associated with the thermodynamic stability of the 2D material. Graphene exhibits intriguing and interesting properties such as high electrical and thermal conductivity, high mechanical strength and high mobility because of quantum confinement and anisotropy of the bulk crystal graphite.

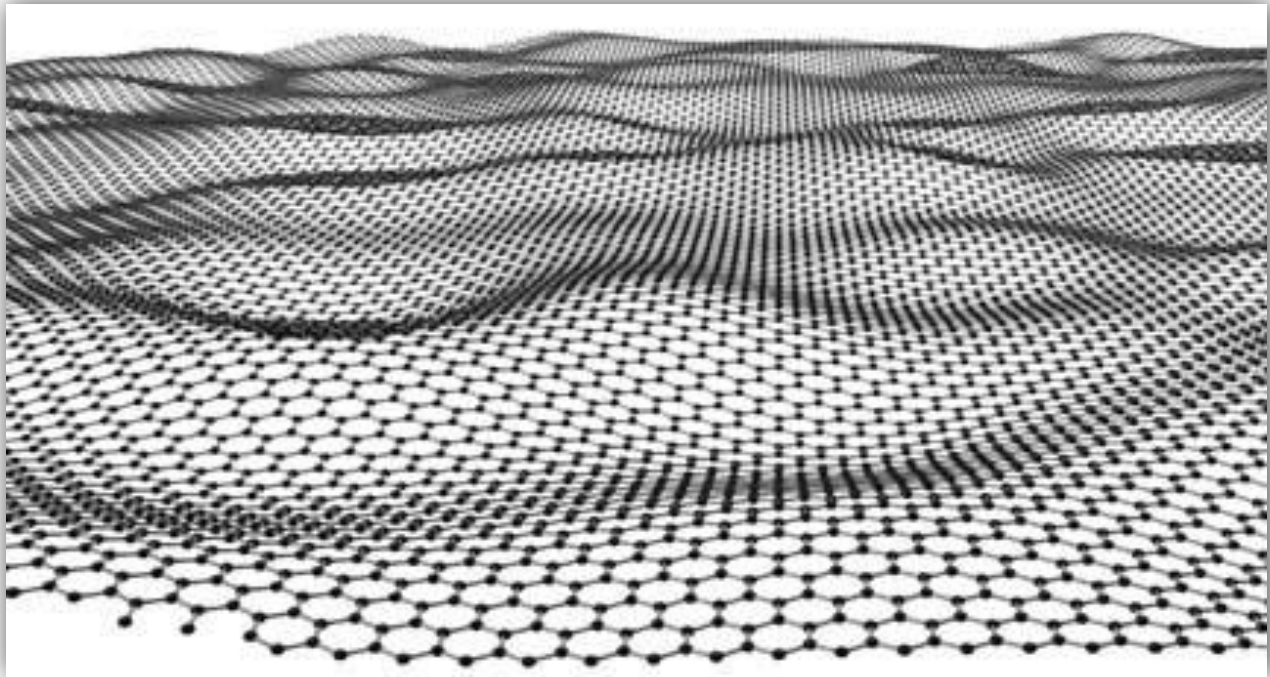


**Figure 2.4:** Represents the thermal fluctuations in the suspended graphene sheet [31].

So, the unprecedented properties of graphene sparked a search for additional 2D materials with their own unique characteristics [32] and this search has attracted a significant attention to dozens

of 2D nanomaterials in recent years including layered double hydroxides (LDHs), transition metal dichalcogenides (TMDs), layered nitrides, transition metal oxides, carbides, carbonitrides (MXenes) and graphene like 2D buckled nanosheets (silicene and germanene) as shown in **Figure 2.5** [<sup>33-36,37</sup>].

In general, 2DMs possess large surface areas combined with outstanding electronic, optical, electrochemical, mechanical and thermal properties that are opening new channels for fundamental scientific research and advanced technological applications [<sup>38,39</sup>] there including sensing, catalysis, energy storage and functional nano composites [<sup>40-42</sup>]. The feature of being some of the thinnest 2D structures among all known materials with very high specific surface area makes them indispensable for applications requiring high levels of surface interactions at the nanoscale i.e. into the frontiers between biology and medicine such as antibacterial activity [<sup>43,44</sup>], biosensors [<sup>45,46</sup>], drug delivery [<sup>47,48</sup>], cancer cell diagnosis and cell imaging [<sup>49</sup>] as shown in **Figure 2.6**. The reason could be attributed for these applications are that 2D nanomaterials are the thinnest materials known which means they exhibit highest specific surface areas of all known materials. These essential characteristics make these materials useful to understand the surface interactions with different moieties. Especially, in different biomedical areas such as in gene sequencing, photothermal therapy and photodynamic therapy, the exceptional surface to volume ratio of these ultrathin layered nanomaterials replaces the already known competitive materials.

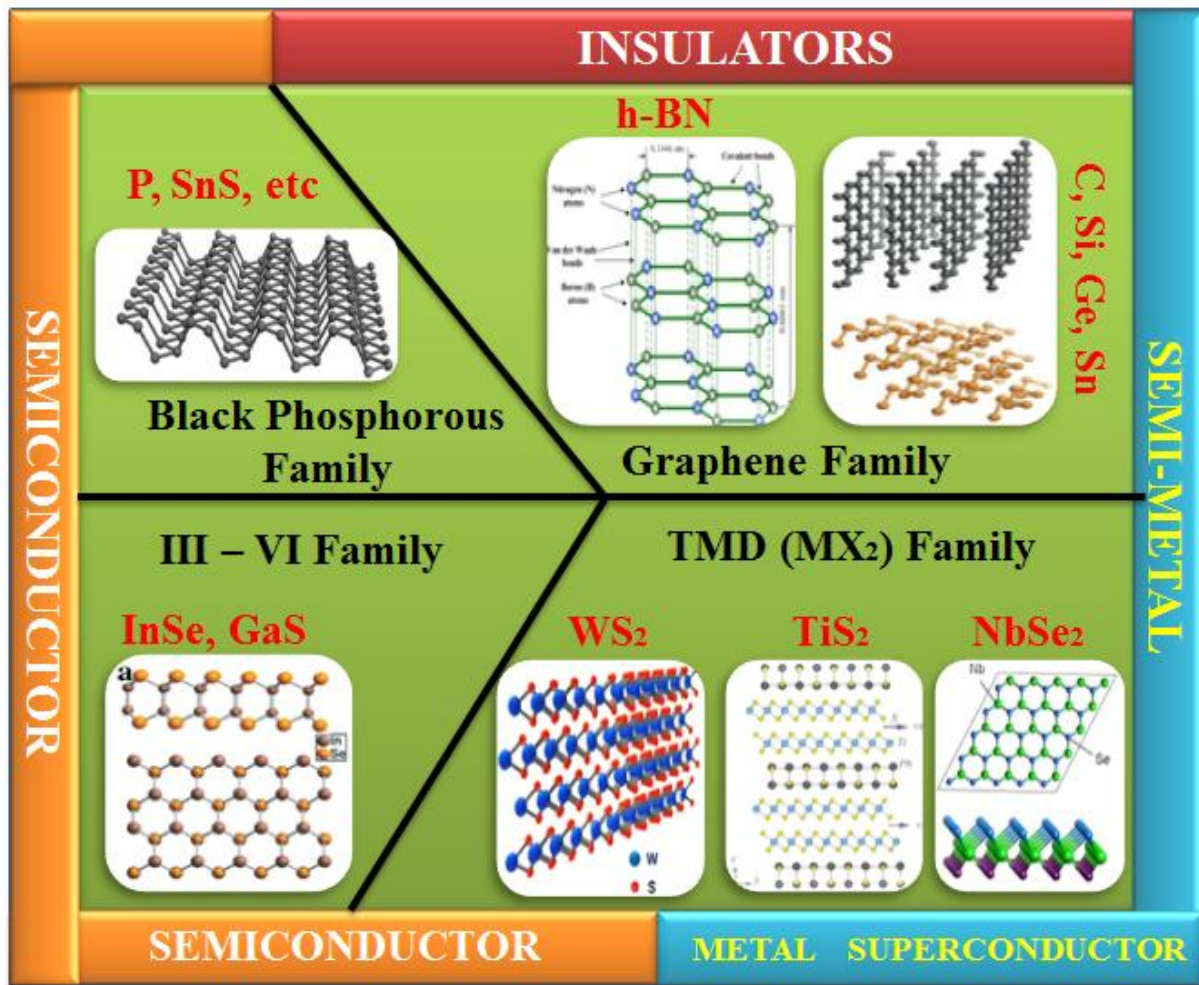


*Figure 2.5 : Family of 2D materials categorized as insulators {members include graphene family, hydrogen boron nitride}; semiconductors {members include transition metal dichalcogenide family-MoS<sub>2</sub>, WS<sub>2</sub> and Group III – VI members- InSe and GaS}; superconductors {members include NbSe<sub>2</sub>} and semi metals {members include carbon, silicon, germanium and antimony} [50].*

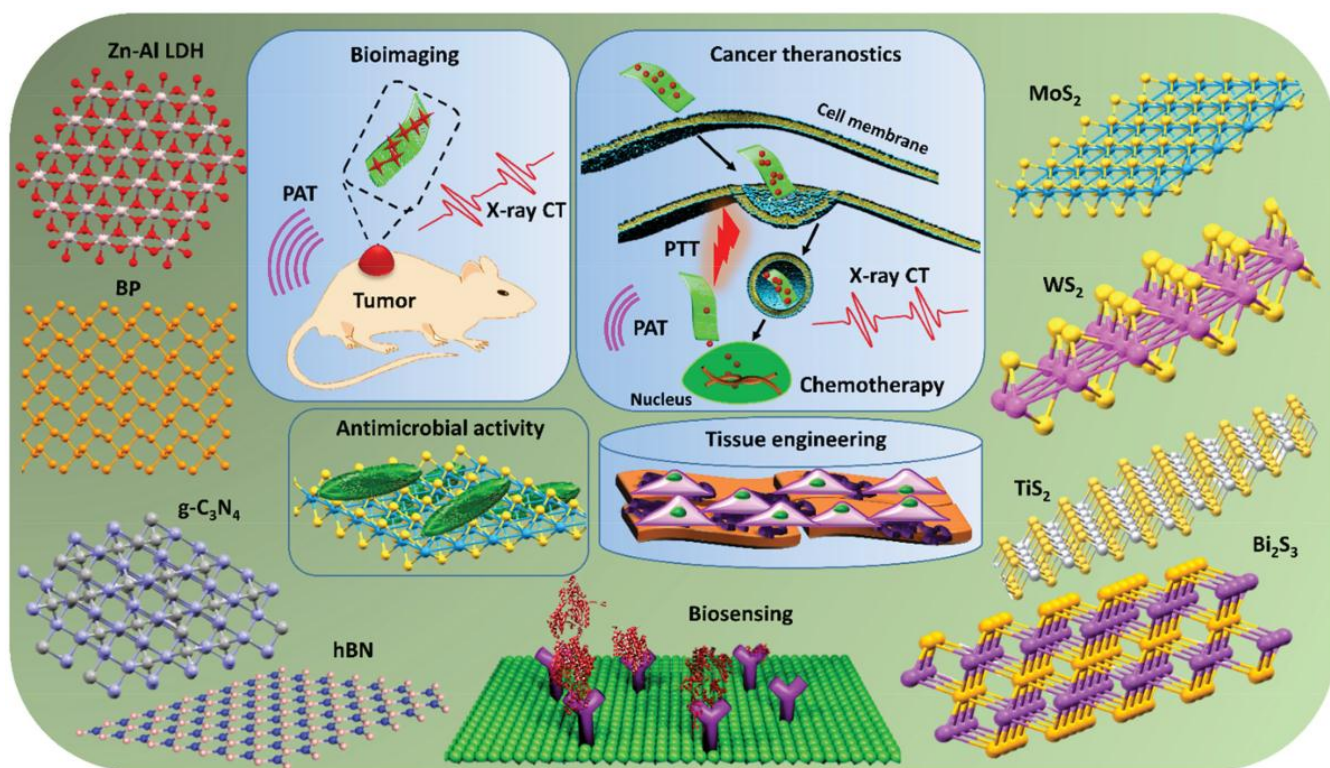
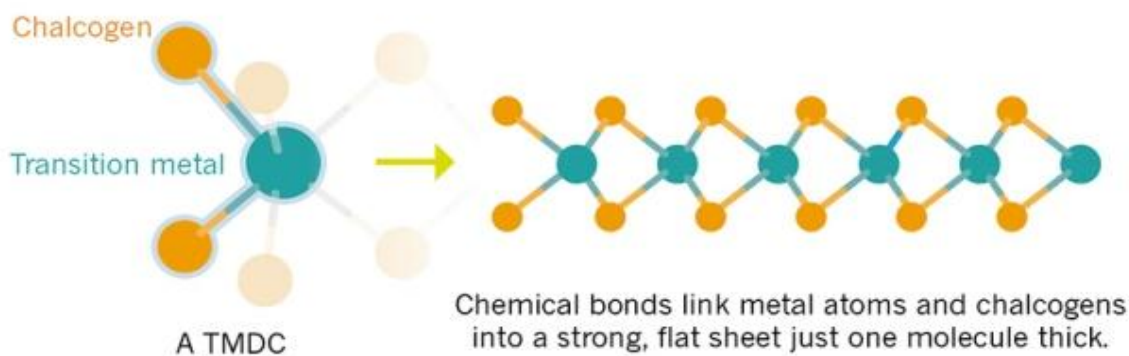


**Figure 2.6:** Different biomedical routes making use of fabricated 2D materials in a significant way [51].

### 2.2.1. Two-dimensional Transition Metal Dichalcogenides

After graphene, the furthestmost explored class of ultrathin 2D nanosheets are those derived from the transition metal dichalcogenide (TMD) families of materials with  $\text{MX}_2$  stoichiometry, where M refers to a transition metal typically from Group 4-7 of the periodic table ( $\text{M} = \text{Mo}, \text{W}, \text{Ti}, \text{Nb}$ ) and X refers to a chalcogen atom such as sulphur (S), selenium (Se) or tellurium (Te). X-M-X form exhibits the typical polymeric form of the TMD in which a plane of transition metal is sandwiched between two planes of chalcogen atoms as shown in **Figure 2.7**. These layers are strongly held together via a covalent bonding and weakly held together with van der Waals forces in bulk form [52,53]. The thickness of each individual single layer of a TMD is 6-7 Å [54]. Approximately, 60 possible configurations of layered TMDs have been identified and reported

covering the full range of electronic behavior from metallic to wide band-gap insulating properties [33,55-57]. The outstanding properties of 2D TMDs could be attributed to the specific geometric structure which differs from Group (4-7) of the periodic table based on their electron arrangement in particular orbitals. X-M-X sandwich form of TMD results in valence satisfied atoms with no reactive sites. Further, machining of the structure by various fabrication protocols results in making the edge or base sites reactive to other compounds. Incongruent electronic states of 2D TMDs is the result of the kind of coordination environment of transition metal and its electronic configuration such as *d*-electron count and the subsequent oxidation state of the metal [33]. Basically, two different coordination geometries of transition metal exists which can be either trigonal prismatic (2H polymorph) or octahedral (1T polymorph) with  $D_{3h}$  and  $D_{3d}$  point group symmetry. In such a case, *d*-electron count of transition metal decides which phase will be thermodynamically stable. Moreover, the same *d*-electron count is also responsible for the electronic and magnetic properties of the given layered material [33,58,59,60,61] with a significant contribution from the chalcogen atom [62]. TMDs from Group 6 of the periodic table such as  $\text{MoS}_2$  and  $\text{WS}_2$  mostly adopt trigonal prismatic geometry with  $d^2$  transition metal center, whereas TMDs from Group 4 of the periodic table exhibits mostly octahedral geometry with  $d^0$  transition metal center.



H																	He	
Li	Be											B	C	N	O	F	Ne	
Na	Mg											Al	Si	P	S	Cl	Ar	
K	Ca	Sc	Ti	V	Cr	Mn	Fe	Co	Ni	Cu	Zn	Ga	Ge	As	Se	Br	Kr	
Rb	Sr	Y	Zr	Nb	Mo	Tc	Ru	Rh	Pd	Ag	Cd	In	Sn	Sb	Te	I	Xe	
Cs	Ba	Ln	Hf	Ta	W	Re	Os	Ir	Pt	Au	Hg	Tl	Pb	Bi	Po	At	Rn	
Fr	Ra	An	Rf	Db	Sg	Bh	Hs	Mt	Ds	Rg								
		La	Ce	Pr	Nd	Pm	Sm	Eu	Gd	Tb	Dy	Ho	Er	Tm	Yb	Lu		
		Ac	Th	Pa	U	Np	Pu	Am	Cm	Bk	Cf	Es	Fm	Md	No	Lr		

**Figure 2.7:** Members of transition metal dichalcogenide family highlighted in the periodic table which can form a number of combinations exhibiting 2D nanosheets morphology with very intriguing properties. Transition metal dichalcogenide structural representation in terms of the chemical bonds linked with single metal atom and two chalcogen atoms into few atomic structure nanosheet morphology [63].

Machining of the bulk crystal to few-layer ultrathin nanosheets results in quantum confinement of the free electrons which in result increases the anisotropy of the given layered material. Because of these confinement and anisotropic effects, the electronic [64–66], optical [67], thermal [61,68], mechanical [69] and structural [54,55,70] properties of the thinned nanosheet material becomes significantly different from the bulk crystal. For example. 2H-TaSe<sub>2</sub> with  $d^1$  metal center is metallic due to partially filled  $dz^2$ , whereas 2H-WSe<sub>2</sub> with  $d^2$  metal center is a semiconductor due to fully occupied  $dz^2$ . Now, in Mo and W having MX<sub>2</sub> elemental formula when exfoliated to single or few layer ultrathin nanosheets produces an indirect to direct band gap semiconductor and significant improvement in their electronic properties with 2H-MoS<sub>2</sub> as semiconductor and 1T-MoS<sub>2</sub> as metallic in nature. Moreover, distinct physical and chemical properties of the machined MX<sub>2</sub> gives intriguing results in electronic [71–73], solar [74,75], energy storage [76,77] and biomedical applications [78,79–92].

### 2.2.2. Two-dimensional molybdenum disulfide (2D-MoS<sub>2</sub>)

In recent years, a major attraction has been devoted to one of the most explored member of TMD family i.e. molybdenum disulfide (MoS<sub>2</sub>) because of its abundance in the earth's crust [93] and geometrically it is easy to exfoliate via various fabrication routes. The proposed applications for MoS<sub>2</sub> are primarily in dry lubricants [93,94–96], catalysts [97, 98,38] and cathodic material for lithium ion batteries [99]. The successful isolation of graphene has opened doors for other materials in various applications. In such a way, fuelled by the expansion in research activities on graphene, arena of applications for MoS<sub>2</sub> has also widened from the conventional ones.

Basically, MoS<sub>2</sub> exists in two different polymorphic forms such as trigonal prismatic (2H-MoS<sub>2</sub>) and octahedral arrangement (1T-MoS<sub>2</sub>) [100–102] as shown in **Figure 2.8**. The bulk crystal of molybdenite consists of hexagonal stacked nanosheets, where each single nanosheet is three

atoms thick. As explained in the previous section that metal atom is sandwiched between two chalcogen sulphur atoms (X-M-X) with monolayer or few layer structures. The intra-layer is covalently bonded with each other, whereas the inter-layer, out of the plane (-X-X-) sulphur atoms are weakly bonded via van der Waals forces.

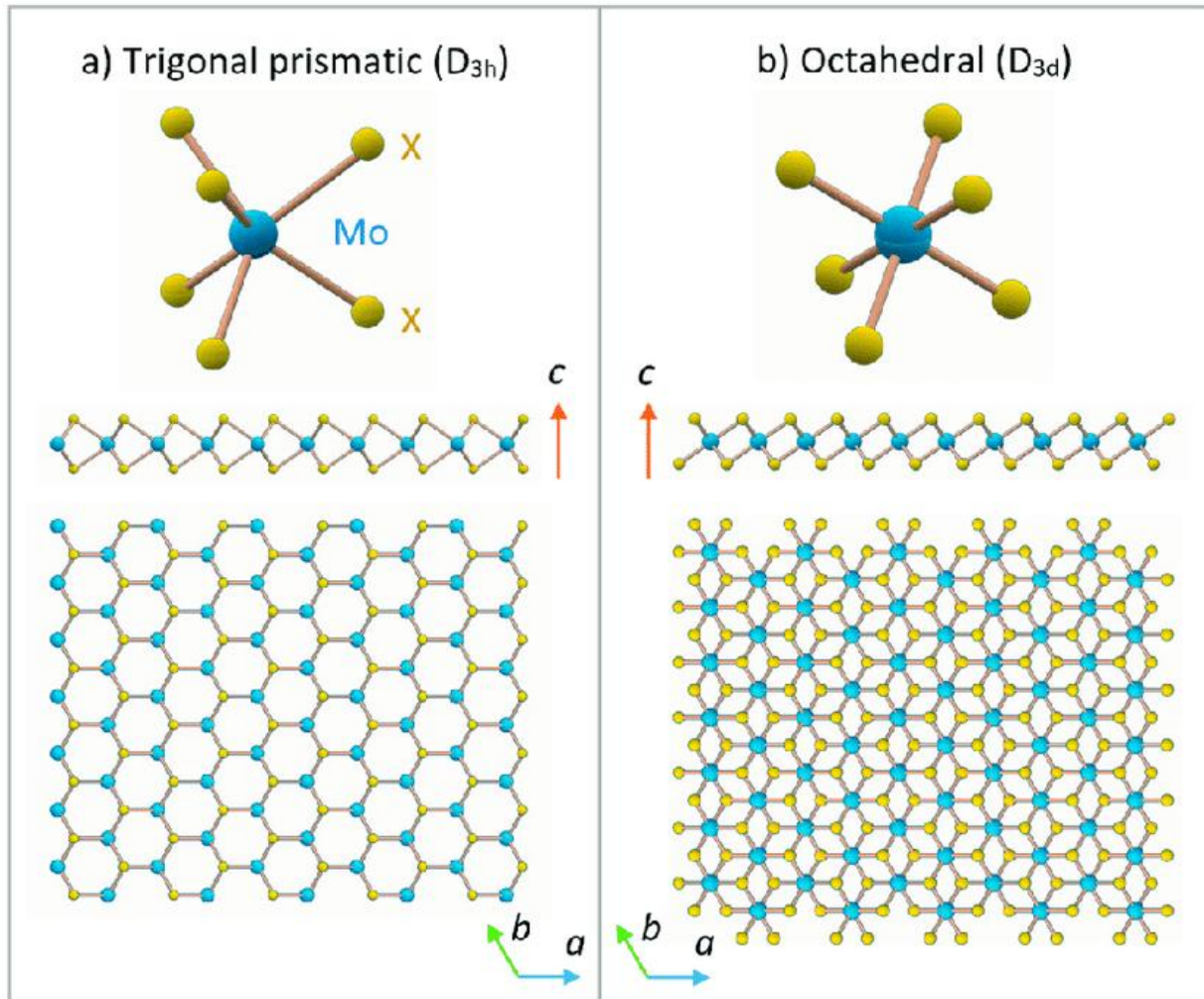


**Figure 2.8:** Represents the two different structural phases of MoS<sub>2</sub> nanosheets which are a) trigonal prismatic (2H-MoS<sub>2</sub>) a semiconducting form occupies central position in the lattice, whereas in b) is the octahedral arrangement of atoms (1T-MoS<sub>2</sub>) which is metallic in nature [103].

2H-MoS<sub>2</sub> is a semiconductor with sizeable band gap, whereas 1T-MoS<sub>2</sub> is metallic in nature. The reason for their different nature of existence could be attributed to the role of *d* electrons filling in specific orbitals. Moreover, 2H-MoS<sub>2</sub> is thermodynamically the stable phase whereas 1T-MoS<sub>2</sub> is metastable [104]. The existence of 1T-MoS<sub>2</sub> metallic state has been reported by several groups by exfoliating 2H-MoS<sub>2</sub> phase using lithium intercalation. So, the disturbance in the MoS<sub>2</sub> lattice by the encapsulation of lithium ions and modification in the d-electron filling of MoS<sub>2</sub> crystal partially. The exact mechanism of this phase transformation from semiconductor to metallic is still not clear and it is very uncertain to give any firm explanation based on only one of the fabrication protocol reported so far [33]. The exfoliated nanosheets generate dangling bonds at the edges and based on the fabrication protocol followed addition of defects results in significant change in the surface chemistry of MoS<sub>2</sub> nanosheets. Moreover, it becomes more useful to play with the surface chemistry of MoS<sub>2</sub> nanosheets for various applications such as hydrogen evolution reaction, catalysis and solar energy [105].

### **2.2.3. Unique properties of MoS<sub>2</sub>**

The reason why MoS<sub>2</sub> has attracted so much attention in the recent years is because of its unique properties which make it a favorable candidate for broad range of applications. The very first unique property which can be observed after the exfoliation of bulk MoS<sub>2</sub> to single layer or few layer ultrathin 2D nanosheets is the increase in energy of the band gap, whereas graphene has zero band gap after exfoliation [106]. Bulk MoS<sub>2</sub> has an indirect band gap with 1.2 eV but after exfoliating the bulk into single layer ultrathin 2D nanosheet, the band gap energy increases to 1.8 – 1.9 eV which is now a direct band gap semiconductor [52,107,107–109,110–112]. The alteration of indirect band gap to direct band gap can be tuned by various fabrication protocols,

functionalization strategies further making MoS<sub>2</sub> an appealing material for advanced electronics applications and for the optimization of electronic devices. Moreover, the increase in energy of the band gap when exfoliated into single layer or bi-layer nanosheets demonstrates the quantum confinement of the electrons which generates a strong photoluminescence and improved optical adsorption ability in the exfoliated material [67,113,114]. On the other hand, 1T-MoS<sub>2</sub>, octahedral arrangement of atoms is metallic in nature and it exhibits photoluminescence after annealing at a certain temperature [115]. As compared to 2H-MoS<sub>2</sub> it is 10<sup>7</sup> times more conductive because of its hydrophilic nature, whereas 2H-MoS<sub>2</sub> is completely hydrophobic [116]. Graphene, in general has Young's modulus of E= 0.8 – 1.0 TPa [117], whereas bulk and suspended MoS<sub>2</sub> nanosheets has Young's modulus of E= 0.24 TPa and 0.33 ± 0.07 TPa, respectively [55,118]. This comparison demonstrates that graphene is the strongest material ever discovered.

#### **2.2.4. Novel properties of MoS<sub>2</sub>/ other TMDs for biomedical applications**

Recently, a horde of nanomaterials such as carbon nanomaterials [119], liposomes [120], metal based nanoparticles [121,122], polymeric nanoparticles [123–125] and quantum dots [126–128] have been designed to overcome the loopholes in biomedical science for the eradication of deadly diseases and for other broad range of biomedical applications. Compared to these nanomaterials, 2D nanomaterials have surpassed them in terms of their exceptional chemical, optical, magnetic and electronic properties. 2D MoS<sub>2</sub> nanosheets have been explored as a promising candidate in the biomedical field because of its exceptional physico-chemical properties [49,129]. The ability to absorb intrinsic near-infrared light, extremely large surface to volume ratio and low toxicity paves a way for this material to be used as a multifunctional nano-platform for different therapeutics and combination assisted therapies for the treatment and diagnosis of cancer and

other diseases. Especially, single layer MoS<sub>2</sub> is a promising candidate for photo thermal therapy agent because of its high absorption in the NIR region (700-1100 nm) and high light to heat conversion efficiency [<sup>130</sup>].

The exceptionally high specific surface area of MoS<sub>2</sub> makes it highly favorable to deliver biomolecules and load various drugs into cells, in bio sensing applications, antibacterial [<sup>131,132</sup>] and tissue engineering [<sup>133,134</sup>]. Subsequently, the ability to functionalize different chemical compounds and the large surface area provides a new paradigm to improve the exfoliation strategies and enhancement in the novel properties for various biomedical areas, especially the bio-interactions, targeted drug delivery with high loading of drug amounts and therapeutic routes [<sup>135</sup>]. MoS<sub>2</sub> and other TMDs have the ability to act as multifunctional 2D nanomaterials at the same time which makes them highly demanding in terms of their fabrication, stability and implementation in a specific application. As a result, various research groups have reported novel multifunctional roles of MoS<sub>2</sub> in gene delivery systems, bio sensing, cellular uptake/internalization, anchoring of DNA, RNA molecules and other organic compounds to name a few! [<sup>136</sup>]. Moreover, MoS<sub>2</sub> is an important trace element, whereas sulfur represents an abundant life element which makes it more desirable for biomedical applications [<sup>137</sup>].

Just to summarize, the above mentioned roles played by MoS<sub>2</sub> and other members of TMD family exhibit a cohort of novel properties which are based on some basic principles to design 2D TMDs for therapeutic applications, bio-interfacing with other molecules, bio-interactions with live matter and tuning of surface properties. Those principles from TMDs properties point of view are as follows:-

#### a) **Versatile and scalable preparation methods.**

The critical requirement for any material to be used in biological systems is its physiological stability. For MoS<sub>2</sub> and other TMDs, liquid phase exfoliation approach and solvothermal fabrication route has proven to be useful and suitable for biological applications [79,101,102,138,139]. Pre-treatment of the bulk crystal or powder, post exfoliation steps, choice of solvent, optimization of different sonication parameters has shown a good amount of yield, monolayer and few layer MoS<sub>2</sub> and other TMDs nanosheets with high biocompatibility [138]. On the other hand, to obtain controlled size, morphology and phases of 2D TMDs nanosheets, solvothermal approach is appropriate which results in the prevention of samples not to get oxidize.

#### b) **Exceptionally large surface area.**

Thanks to the excellent surface chemistry of MoS<sub>2</sub> and other 2D TMD nanosheets which can be tuned according to the type of application, the material is being used for. This multipurpose surface chemistry of MoS<sub>2</sub> nanosheets with large surface area acts as a potential nanoplatform for the integration of different functional moieties, bestowing the obtained nano composite with highly enhanced properties that are useful in number of biomedical studies. This, as a result, turns out to be very useful when these ultrathin nanosheets are utilized for loading different therapeutic agents, acting as a nano drug carrier for cancer treatment [134].

#### c) **Ability to functionalize different moieties**

To understand the fate of these ultrathin 2D nanosheets in biological systems, it is very essential to tune the surface chemistry of these novel materials. Dispersibility, stability and biocompatibility of 2D TMD nanosheets in a particular solvent, surfactant-solvent and stabilizer

can be enhanced by playing with their surface chemistry parameters [<sup>87,116,138,140,141,142</sup>]. By doing so, the properties of 2D TMDs can be engineered to fulfill the requirements for a particular biological application. For example, For targeted drug delivery applications, some targeting moieties such as Hyralaunic acid, Folic acid, specific peptides can be used to assimilate with MoS<sub>2</sub> and other 2D nanosheets, which in further can be used to study their uptake by different cancer cells [<sup>49,143–145</sup>]. These moieties, in addition to their conventional property also enhance the stability of the 2D material in water and other physiological mediums [<sup>90,146</sup>].

#### **d) Low toxicity of MoS<sub>2</sub> and other 2D TMDs**

Cytotoxicity of these materials or nanomaterials in general is an important parameter to be defined very clearly before getting into clinical trials. Toxicity of materials in themselves, is an important step to check its accumulation and retention in the tissues, toxicity with living cells up to a threshold of a certain amount of concentration and toxicity towards their bio-interaction with the outer membrane and inner world of bio-system [<sup>89,147,148</sup>]. It has been already reported that MoS<sub>2</sub> and WS<sub>2</sub> are relatively less toxic than graphene [<sup>149,150,151</sup>] and moreover they are easy to biodegrade and excrete from different routes in, in vivo studies [<sup>152</sup>]. These properties make these ultrathin materials preferable for various biological studies.

#### **e) High absorption in NIR (700-1100 nm) region**

Especially, in cancer diagnostics, photo thermal therapies (PTT), photo acoustic therapies (PAT) and photo dynamic therapy (PDT) are the well-known names to kill the cancer cells and to treat different parts of the body using light and heat at a specific wavelength. These work well in NIR region (700-1100 nm) which is considered as the optical window of bio-tissue. In this specific

region, the scattering and absorbance effect of bio-tissues are minimum that's why excellent photo thermal agents are required which can respond in this optical window and can deeply penetrate into the tissue [<sup>153,154,155</sup>]. In this view, 2D MoS<sub>2</sub> nanosheets have proven to be excellent NIR responsive material and has attracted great attention in recent years to be used as a PTT agent because of its narrow band gap and with its high photo thermal conversion efficiency, it is used to kill cancer cells more efficiently than the conventional gold nanoparticles [<sup>130</sup>]. In general, biocompatibility [<sup>67,156-160</sup>], biosafety [<sup>161-163,164</sup>], low cytotoxicity and high photo thermal conversion efficiency [<sup>165-168,169</sup>] of 2D TMD nanosheets guarantee their potential applications in bioscience and biomedical field .

### **2.2.5. Fabrication methods of MoS<sub>2</sub> nanosheets and other 2D nanomaterials**

Layered materials in general have been explored for decades, whereas the successful isolation of graphite into single layer graphene nanosheets has elicited the research activities on other members of this family due to the intriguing physicochemical properties when exfoliated from bulk to single layer or few layer nanosheets. MoS<sub>2</sub> in bulk form has an indirect band gap of 1.3 eV, whereas when exfoliated to single layer nanosheets, it converts to a direct band gap of 1.8 eV. This transition introduces significant amount of interest in various applications such as catalysis, electronic/optoelectronic devices, energy storage and biomedical science [<sup>158,170,171,33,172,173</sup>]. The advent of these novel properties is the actual driving force which has now attracted great attention and it has been on the forefront of all scientific disciplines including physics, chemistry, material science, medicine and biology. To unravel the mysteries of 2D TMDs, it is very critical to fabricate these materials with controlled size, thickness and optimum concentration (if opting for solution based approaches). Considerable

efforts have been put to synthesize MoS<sub>2</sub> and other 2D TMD nanosheets with controlled size and morphology, modification of laboratory prepared methods to large scale production and with homogenous atomic layers. As the inter-layer structure of MoS<sub>2</sub> nanosheets exhibits strong covalent bonding, whereas the intra-layer structure exhibits weak van der Waals forces which can be broken to obtain single layer or few layer 2D nanosheets with fascinating properties. This has inspired the scientists to separate the bulk crystal into individual layers for many years. At that time, it was unclear about the existence of these individual monolayers but efforts were put to push their thoughts into realization and MoS<sub>2</sub> monolayer was prepared in a same way as graphite by intercalation using tetrabutylammonium (TBA) and water separately between the bulk layers [174,175]. But it was not possible to find out the physical parameters such as thickness/number of layers isolated from the bulk crystal, which at that time was characterized by x-ray diffraction technique [176]. After some years, another group of scientists did some improvement in analyzing the isolated MoS<sub>2</sub> monolayer in a way that they were able to identify that after isolation from the bulk crystal a metastable phase has been created from trigonal prismatic (2H-MoS<sub>2</sub>) to octahedral arrangement (1T-MoS<sub>2</sub>) with different electronic structures and structural distortions [177-179].

Basically, the fabrication strategies for MoS<sub>2</sub> and other 2D TMDs can be divided into two categories as shown in **Figure 2.9**:-

- a) Top-down approach
- b) Bottom-up approach

Every synthesis technique exhibits some merits and demerits which can be dependent on the type of application focused. In top-down approach, larger or bulk materials are removed or exfoliated

to create a 2D nanostructure, whereas in bottom-up approach, self-assembly of nanostructures is carried out from atomic or molecular precursors which are allowed to grow under certain temperature and other growth parameters in a controlled environment [180].

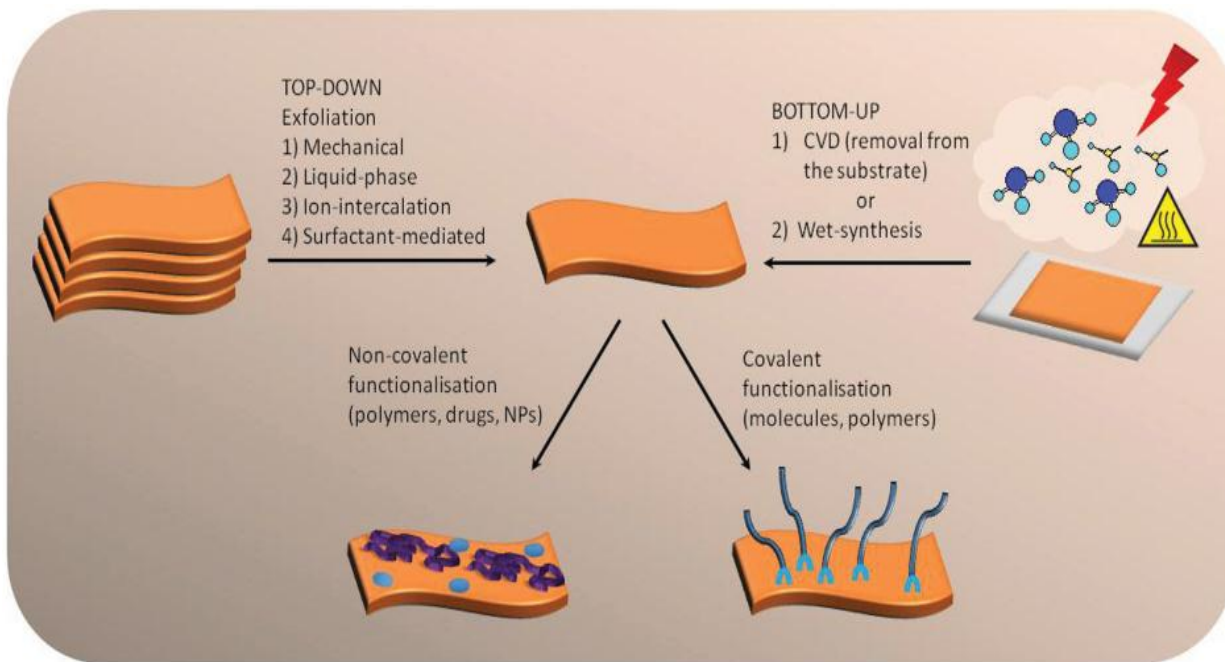


**Figure 2.9:** Different fabrication approaches employed to produce 2D nanosheets with few nanometers of thickness and broad range of lateral sizes of the nanosheets -Top down and bottom up approach to exfoliate 2DMs [51]

### 2.2.6. Micromechanical Exfoliation

The very first isolation of bulk MoS<sub>2</sub> crystals to tens of nanometers thickness nanosheets was reported by Frindt in 1966 which now has become the famous ‘Scotch Tape method’ [176]. In 2004, A. Geim, K. Novoselov and coworkers approached in a more scientific way and improved this micromechanical cleavage method for lamellar crystals with proper assessment of thickness and other properties [26,181]. Basically, any lamellar crystal is placed between the two pieces of a scotch tape and the adhesion between the basal plane of the lamellar crystal and scotch is much

stronger than the weak van der Waals forces between the layers, which results in cleavage of ultrathin layers continuously. Repeating the same process to freshly cleaved nano flakes produces single and few layer 2D nanosheets which after the exfoliation are transferred onto a Si substrate for characterization and on the spot device fabrication as shown in **Figure 2.10**. These two Nobel Prize winner physicists used this technique to isolate graphene from the bulk graphite but a number of other lamellar crystals such as 2D TMDs have also been isolated using the same approach provided the availability of the bulk lamellar crystal of that material [26,102,181,182]. Then, the same physicists reported that rubbing of a lamellar crystal onto a desired solid substrate can also isolate the nanosheets from the parent crystal [181].

To cover the loop holes by one method or the same method, some new techniques, new materials have always been discovered and this is how research works. After six to seven years of the discovery of scotch tape method with proper assessment of the thickness by A. Geim and K. Novoselov, two other scientists found that viscoelastic stamps can also be used to exfoliate other lamellar crystals such as TaSe<sub>2</sub>, MoS<sub>2</sub> and NbSe<sub>2</sub> with the same effect as that of Scotch tape [183,184]. The advantage of this viscoelastic stamp over Scotch tape method is that it does not leave behind the traces of the adhesive bound to the surface of cleaved nanosheets [184]. Further improvement in the micromechanical cleavage was reported with the use of ‘sandpaper’ assisted rubbing of the parent crystal which in result produces friction between the fine grains of the sandpaper to generate shear forces to exfoliate the bulk crystal to thin layered nanosheets with thickness > 100 layers [185].

So, in general, micromechanical exfoliation produces high quality, pure single and few layer nanosheets which are far much better than those produced by any other fabrication method. The best part is that it is facile, cheap and easy to process method which during the exfoliation

reduces the unnecessary cleavage of nanosheets which in results give single layer 2D nanosheets. Simultaneously, the isolated nanosheets can be used for proof-of-concept device fabrication [39,160,186-194] which till date has shown excellent results and that's why most of the researchers prefer to use this technique for device fabrication and optoelectronic applications of other 2D ultrathin nanomaterials [195,196].

Every fabrication technique is associated with some disadvantages as well and so is the case with micromechanical cleavage method. Usually, the amount of 2D TMD nanosheets produced from this technique is very low and more often bi-layer, tri-layer or more nanosheets are isolated which increases the thickness and of no use for practical applications. The morphology of the single layer flakes is irregular which hampers its use for device fabrication because of the lack of assessment and analysis after the exfoliation from bulk crystal. This method in general is not scalable and sometimes it is very time consuming in terms of selection of a particular substrate for the characterization of isolated 2D TMD nanosheets. Especially, biomedicine and other biomedical applications, micromechanical cleavage technique is not favorable because of its low throughput, where these applications demand large amount of solution processed 2D nanosheets.

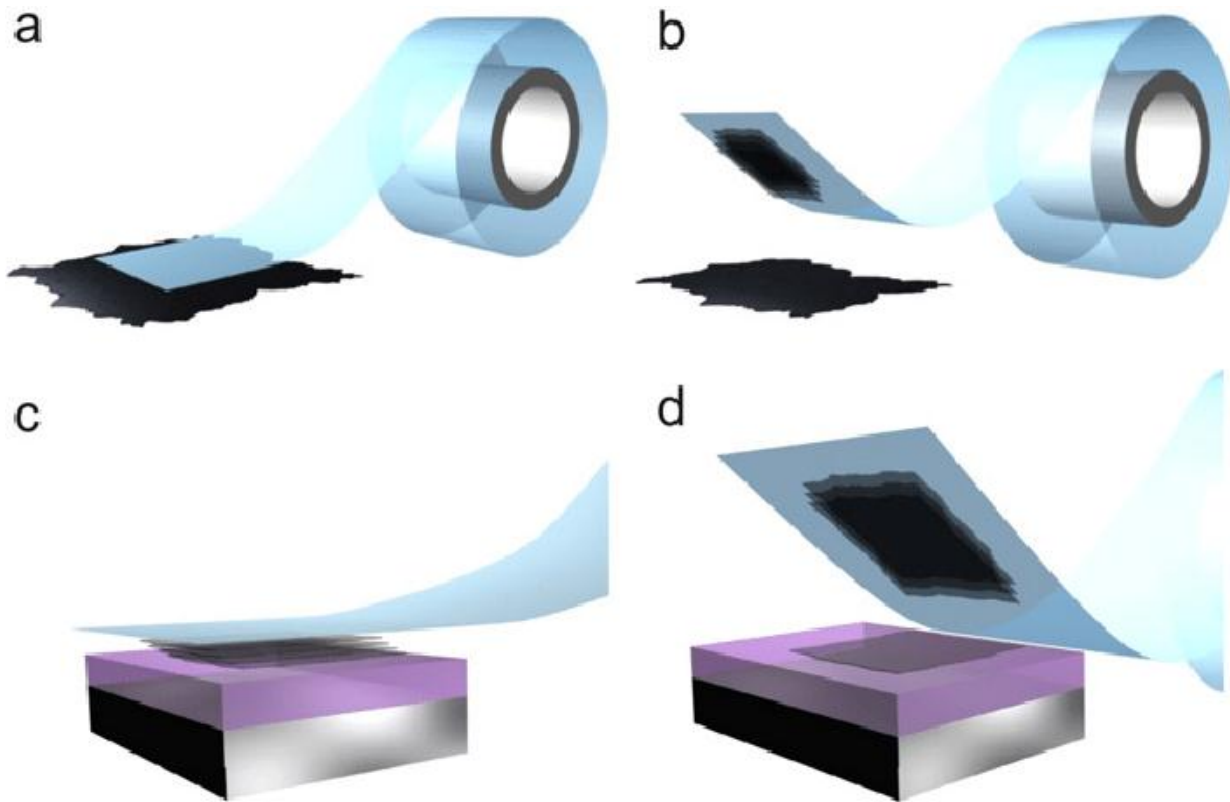


**Figure 2.10:** Procedure of micromechanical exfoliation of graphene using scotch tape method and then subsequently depositing it onto a particular substrate [197]

### 2.2.7. Chemical Vapor Deposition (CVD)

CVD comes under bottom-up technique which is really demanding method for high tech electronics and optoelectronics applications of 2D TMDs. The initial picture of a bottom-up approach is important to understand how CVD works. Basically, initial precursors containing metal and chalcogen are put under a reaction in any phase (solid, liquid or gas) in a controlled environment to produce high quality single layer 2D TMD nanosheets as shown in **Figure 2.11**. The chemistry of this process is robust as the reaction of  $Mn^+$  and  $nX^{2-}$  gives the desired 2D nanomaterial and is same in every case whether the reaction is carried out in solid, liquid or gas phase. The reaction of these energetic ions requires control over the reaction kinetics and growth

of the 2D nanomaterial with proper understanding of the energetics involved in the reaction. One advantage of parent 2D TMD is their high anisotropy which aids in the growth of single layer 2D nanosheets but at the cost of high temperature conditions, long reaction times and high energy process [108,109].

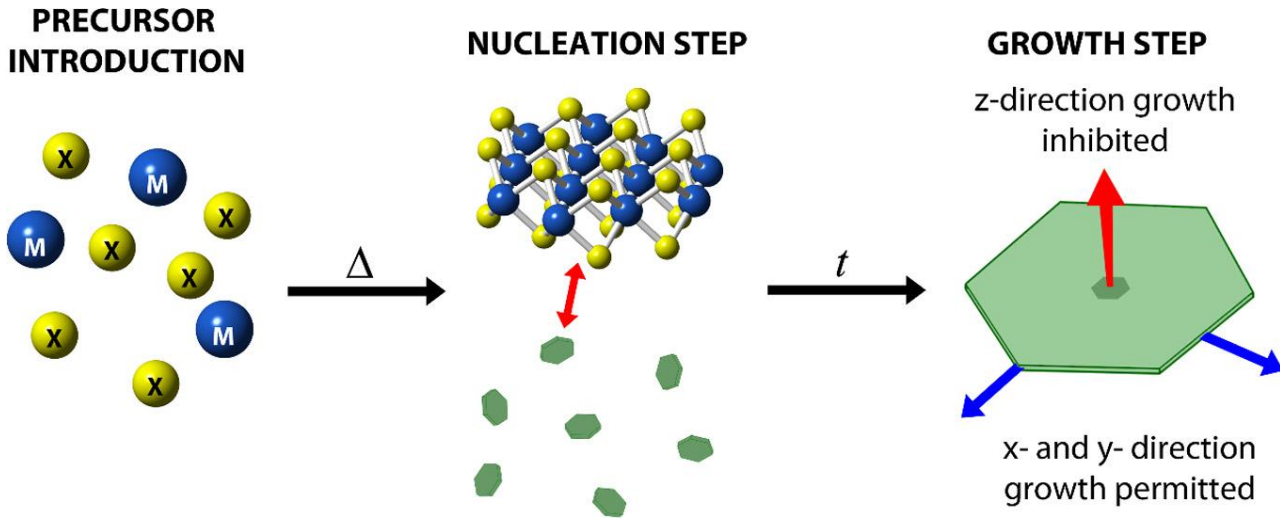


**Figure 2.11:** Steps to grow 2D nanosheets from the precursors followed by nucleation and vapor deposition based controlled growth in a specific pattern, high quality monolayer nanosheets [198].

Typically, single- or few-layer nanosheets can be grown onto substrates in a following way:-

- a) Vaporization of metal and chalcogen atom
- b) Co-deposition of the above onto a desired substrate
- c) Metal film deposition onto a wafer heated with chalcogen source
- d) Transition of metal oxide to metal disulfide by sulfurization process

For example, in case of  $\text{MoS}_2$  and  $\text{WS}_2$  nanosheets it has been reported that growth of both of the materials was performed via the same way but on different substrates, sapphire for  $\text{MoS}_2$  and

SiO<sub>2</sub> for WS<sub>2</sub> [199]. The initial precursor MoO<sub>3</sub> layer is deposited onto a given substrate by thermal deposition and then the obtained product is sulfurized using sulphur gas at high temperature. However, the current method is not scalable and transferrable at industrial level because of harsh reaction conditions such as high vacuum, high temperature, specific substrate and risk in avoiding damage to the grown layers onto the substrate. So, for biomedical applications the current fabrication strategy is not useful as it is more suited for high end electronics applications.

## **2.3. Chemical Exfoliation Approaches**

### **2.3.1. Lithium intercalation technique**

Intercalation approach by name suggests the insertion of some molecules between the layers. Basically, insertion of species in between the TMD layers expands the interlayer distance and weakens the intra layer van der Waals forces which after the aid of ultra-sonication gives high yield and high concentration 2D TMD nanosheets than is possible with any other fabrication method [200]. Usually, the criteria to choose an intercalating specie is based on the reaction of that specie to give gas as by product which subsequently increases the interlayer distance and provides a delamination force to isolate the bulk crystal to single layer or few layer 2D nanosheets. So, direct use of gases, acid intercalation and more commonly lithium is by far the most effective intercalatant to exfoliate 2D TMD nanosheets with promising applications [76,201–204]. Most often 2D TMDs have been approached to exfoliate via lithium intercalation [100,205] to obtain single layer ultrathin 2D nanosheets. The pioneers who first proposed and developed this technique have attracted so much attention in today's era of 2D materials exfoliation for high end applications [175,206–213].

The simple chemistry which is involved in this fabrication technique is implemented in two steps as shown in **Figure 2.12**:-

- a) Firstly, the treatment of bulk MoS<sub>2</sub> or other TMDs with n-butyllithium in an inert gas hexane to yield an intercalated compound with a general formula  $Li_xMX_2$ . In such a case, electron transfer from hexane to bulk TMDs is the driving force which accommodates Li<sup>+</sup> ions between the layers to balance the charge effect [206,212].
- b) Then, the intercalated  $Li_xMX_2$  compound reacts with water followed by ultrasonication which provides an additional mechanical and acoustic energy to exfoliate the bulk lamellar crystal to single layer nanosheets. The metal ion reaction with water gives LiOH and hydrogen gas which acts as a driving force, when it expands and acts as a driving force to peel out the bulk crystal.
- c) So, the production of single layer MoS<sub>2</sub> or other 2D TMD nanosheets can be attributed to the following three parameters involved in this fabrication technique:-
  - 1) Expansion of the interlayer distance and weakening of van der Waals forces upon intercalation.
  - 2) Hydrogen gas a byproduct acts as a driving force to peel out the bulk crystal to single layer nanosheets.
  - 3) Addition of negative charge upon ultrasonication and intercalation results in columbic repulsion of negatively charged nanosheets [214]. This charge transfer changes the phase of MoS<sub>2</sub> from 2H- semiconducting to 1T-metallic which has its

use in applications such as electro-catalytic activities, hydrogen evolution reactions [115,207,208,215–217].

- 4) However, there are certain limitations to this fabrication technique which hampers its use in biomedical applications because of use of harsh chemicals and experimental conditions [100,206,218]. On the other hand, lithiation process proceeds very slowly and most often several days are required to complete the process. The intercalated compounds are unstable in air and they are highly inflammable [219]. So, considering my aim in this thesis, the current technique is not favorable to use and to study the bio-interactions with living matter.

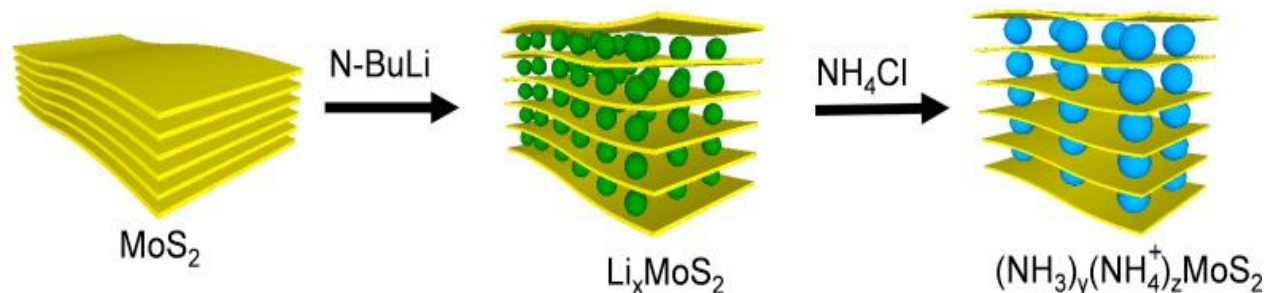


**Figure 2.12:** Steps to exfoliate 2D MoS<sub>2</sub> nanosheets using lithium intercalation technique [220]

## 2.4. Ultra-sonication Assisted Exfoliation Approach

To outwit the above mentioned loopholes in all other fabrication methods, direct exfoliation of layered 2D materials by ultra-sonication in an appropriate solvent appears to be a promising route which subsequently can be used for almost all kinds of applications [101,102,221–230]. The

other fabrication strategies explained in previous sections are not suitable for biomedical applications because of their limitation of processing in harsh environments and use of toxic solvents, chemicals and expensive setup. The best part of ultra-sonication assisted exfoliation technique is that it is versatile, environment friendly, easily scalable and easy to operate. Naturally abundant bulk crystals of layered materials such as graphite, MoS<sub>2</sub>, WS<sub>2</sub> and other innovative members of the 2D family are easy to exfoliate with optimum preparation parameters. The desired lateral size, thickness, concentration and flexible functionalization of the dispersed 2D nanosheets can be facilitated using this approach [231,232]. The intrinsic properties of the exfoliated nanosheets remain preserved provided the non-covalent stabilization feature of this technique.

So, in principle, the energetic agitation produced by the ultra-sonicator device results in the generation of waves which propagate through the given solvent at a fixed value of amplitude and power at a time which generates vibration and cavitation inside the liquid environment [233–235]. The continuous exposure of the sonication induced hydrodynamic forces act as a driving force to break the van der Waals forces of attraction to peel out the bulk crystal into thin 2D nanosheets, followed by centrifugation a post exfoliation step in the technique [101,221]. To make this process scalable, it is vital to efficiently enhance the modes of exfoliation i.e. vibration and cavitation which can be achieved by optimizing different sonication parameters such as using high power sonicator.

### 2.4.1. Mechanism of ultra-sonication in a solvent

Basically, input of strong acoustic and transverse waves generation is the key point which initiates the exfoliation process followed by other parameters as well. High power probe/horn/tip sonicator and more commonly bath sonicator are the two important ultra-sonication devices which have given a significant attention to the material scientists to exfoliate lamellar crystals more easily and within the scope of their lab. In case of high power probe/tip sonicator, the generation and propagation of transverse waves into the given solvent results in two different modes of exfoliation i.e. vibration and cavitation, which acts as a driving force to isolate or peel out the bulk crystal to thin nanosheets, followed by post exfoliation steps. Not only the transverse wave but the combination of compressive wave and tensile stress wave at the interface of the layered crystal aids significantly in peeling out of thin nanosheets from the bulk material [102]. Upon increasing the ultrasonic power, not only the ability of the device to exfoliate enhances considerably but simultaneously the intensity of the cavitation forces becomes more than the vibrational one. In general, cavitation forces carry more energy to exfoliate the layered crystal than the vibrational forces. The use of high input power from a specific horn/probe of the sonicator creates low-high pressure cycles which produce in-situ generation and impulsion of a cavitation bubble within the dispersing medium. Subsequently, this impulsion of a cavitation bubble results in very fast and powerful shockwaves that generates high local pressures and temperatures which is in the range of kPa to MPa and 100s to 1000s °C [234,235]. As soon as the input power is given, the generation of these high-energy cavitation forces from the bubble-collapse mechanism results in shear exfoliation and complete scission of the bulk crystals to 2D nanosheets [233]. Basically, the generation of cavitation forces from the bubble collapse mechanism exfoliates the bulk crystal far more efficiently than the vibrational forces in terms of

higher dispersed concentration but it has some detrimental effects on the lateral dimension of the produced nanosheets [<sup>236–241</sup>].

So, to summarize the above written mechanism ultra-sonication has the potential to produce a horde of novel nanosheets with the desired physical parameters based on the optimization of the initial precursor materials and device settings. The fragmentation, peeling out or complete scission of 2D nanosheets depends upon the cavitation forces formed during the rarefaction cycle of ultrasound waves which forms in-situ cavities or stable but transient microbubbles [<sup>101,102,224,226,242,243</sup>]. Upon continuous provision of high input power from the probe, these microbubbles grow and reach a particular size where they collapse gruffly with an instantaneous generation of high local pressure and temperature. Additionally, with this bubble collapse mechanism, high intensity shock waves are generated which acts as a driving force to exfoliate the bulk crystal to ultrathin poly disperse 2D nanosheets by overcoming the weak van der Waals forces of attraction between the layers. Wherever in the dispersed medium, the absence of cavitation bubbles fragments the nanoflakes because of frictional forces acting on them [<sup>244</sup>]. Whereas, in bath sonication, generation of acoustic waves in particular hot spot regions of the bath sonicator overcome the weak van der Waals forces and exfoliate the layered crystal to thin nanosheets. Other than these, recently developed jet cavitation and high-shear mixing of bulk crystals to ultrathin 2D nanosheets represents another significant phase of exfoliation protocol which gives outstanding yields and concentrations of dispersed nanosheets which can be used in a number of applications such as thin films, composite materials and ink-printing [<sup>236,245</sup>].

One strategy under ultra-sonication approach which has become increasingly popular is the liquid phase exfoliation of layered crystals (LPE). Similar to the concept of ultra-sonication, LPE is applied to a wide range of layered materials in which any layered crystal is immersed into a

suitable solvent or aqueous surfactant solution, which is given a high-energy probe/tip sonication for a certain amount of time, followed by size selective centrifugation steps to achieve the desired 2D nanosheets [<sup>101,221,246,247</sup>]. The thermodynamics of this technique explains that the interaction of liquid-nanosheets interface in a suitable solvent or surfactant solution reduces the net exfoliation energy and subsequently stabilizes it against aggregation effect [<sup>224</sup>]. The high-energy input power device aids in overcoming the weak van der Waals forces, whereas the aqueous surfactant or solvent acts as a stabilizing agent to avoid the re-aggregation of dispersed nanosheets.

#### **2.4.2. What drives the need for liquid phase exfoliation? / Significance of this approach as compared to other techniques**

- ❖ As, explained in the previous section that ultra-sonication is the most easier, scalable, versatile and green approach to exfoliate 2D layered crystals for the desired applications where no pre-treatment, chemical modification using harsh chemicals and toxic environment is not required. Similar is with LPE, which is a straight-forward process and does not even require expensive setup and extraordinary experimental skills, making it viable to the researchers worldwide.
- ❖ Coleman and co-workers are the pioneers who revealed the initial physics and thermodynamics of this technique by exfoliating graphite in a wisely chosen solvent [<sup>221</sup>].
- ❖ It is one of the most versatile, scalable and cost effective fabrication technique among the other synthesis methods to exfoliate 2D nanomaterials [<sup>248,249</sup>].

- ❖ Usually, to prepare the hetero-structures and nano-composites lengthy and tedious experimental techniques are followed but LPE offers a very simple and feasible approach by simply mixing dispersions with dissimilar constituents. Two different materials with different properties and structures can form a composite or nano-composite using this technique.
- ❖ Versatility of this approach not only covers the lamellar crystals in 2D form such as graphite, 2D TMDs, hexagonal boron nitride and black phosphorous but also to more bizarre structures such as layered oxides  $\text{MoO}_2$  [250],  $\text{MoO}_3$  [251], Group III-VI semiconductors  $\text{GaS}$  [252],  $\text{InSe}$  [253],  $\text{SnS}$  [254], layered silicates [255] (talc or mica), layered hydroxides ( $\text{Ni(OH)}_2$  [256],  $\text{Co(OH)}_2$  [257]) just to name a few!
- ❖ As compared to other techniques, it produces extremely high concentrations exceeding the range of 1g/l and even more, which can be used for industrial based implementation of this method. The produced dispersions are quite stable and can be avoided against aggregation by using suitable solvents and aqueous surfactant solutions [224].
- ❖ The flexibility in producing single layer and few layer 2D nanosheets of varied bulk layered crystals and a broad range of lateral size distribution differs from material to material. For example, mean of the size distribution of  $\text{MoS}_2$  and  $\text{WS}_2$  nanosheets is considerable smaller than those of graphite and black phosphorous.
- ❖ The best part of this method is that the exfoliated dispersions can be processed into thin films and nanostructured materials using inkjet printing [258,259], spray deposition [260] and freeze-drying [261] which further can be used in broad range of applications.

**To briefly define the procedure of LPE** so as to get the insight of how it works, following steps are as shown in *Figure 2.13*:-

- a) As the bulk layered crystals have a strong covalent bonding between the layers but weak van der Waals forces between the adjacent layers so, to break or to overcome these weak forces of attraction, high energy power is imparted directly into the dispersed medium.
- b) This, in result generates strong vibration and cavitation forces which act as a driving force to break the bulk crystals into thin layers.
- c) Now the peeled or isolated sheets need to be dispersed and quite stable for practical implementations of these exfoliated dispersions. For this, suitable solvents, aqueous surfactant solutions or stabilizers are required which will be selected on the basis of thermodynamics and solubility theory of the dispersions.
- d) The wisely selected solvent or aqueous surfactant or stabilizer will play a dual role, one, they will minimize the net exfoliation energy and simultaneously they will adsorb to the surface of exfoliated nanosheets to avoid the re-aggregation in the same medium.
- e) The as exfoliated nanosheets are poly disperse in nature, means they exhibit varying sizes and thicknesses in the same dispersion. These final dispersions are not appropriate for various practical applications such as (printed optoelectronics, inkjet printing, hydrogen evolution reactions and electrochemical devices) because of low monolayer content [<sup>262-265</sup>]. So, to unveil the full potential of as exfoliated nanosheets, the foremost important step in LPE is ‘size selection’ by centrifuging the dispersions with specific centrifuge parameters.

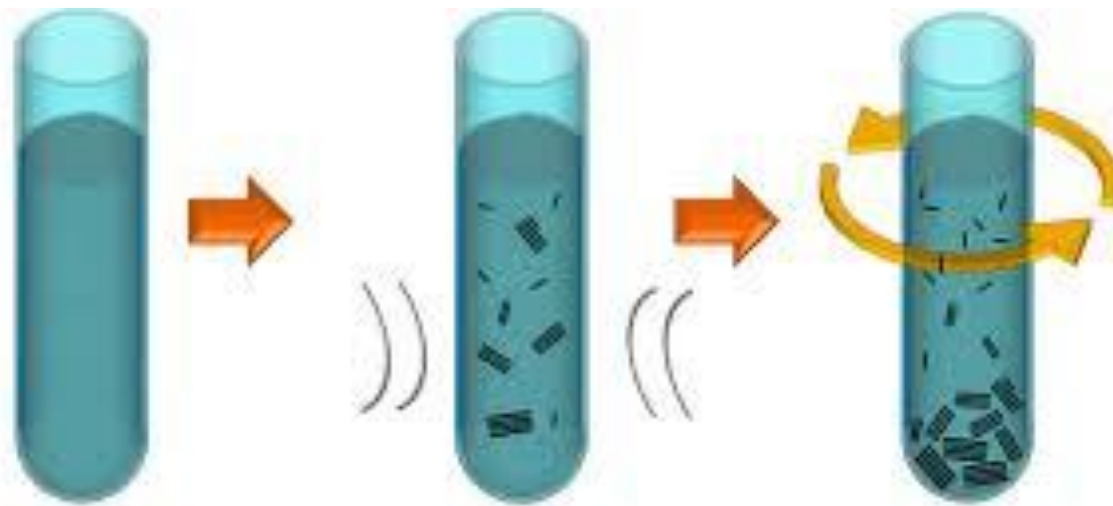


**Figure 2.13:** Procedure for liquid phase exfoliation of 2D nanosheets exfoliated in a suitable solvent/ aqueous surfactant system

The interesting physics behind the LPE process requires the monitoring and analysis of each single step to explore its potential in different areas of applications. The properties of the dispersed nanosheets can be attributed to a number of pre and post exfoliation parameters which are fundamental to comprehend the role played by each in the successful exfoliation of 2D nanosheets. In the last five to six years, a number of studies have been reported on the effect of ultrasound physics and sonication parameters such as initial bulk concentration, kind of solvent or aqueous surfactant or polymer solution, processing time and volume on the exfoliation efficiency of 2D layered TMDs [<sup>127,239–241,266–271,272</sup>].

To understand the effect of all the sonication parameters in detail along with reference to the work done by different research groups worldwide in this field, I have listed and explained each parameter one by one. LPE can be performed using tip/probe sonicator with specified output power, bath sonicator, house -hold kitchen blender, rotor stator mixer for shear exfoliation, jet

cavitation and micro fluidization. The experiments for this thesis have solely been performed using tip sonicator. In the following section I will try to explain the influence of ultrasound physics on the exfoliation of MoS<sub>2</sub> and other layered materials.

### **1) Influence of ultrasound physics on the exfoliation process**

Generally, ultrasound represents the sound waves whose frequencies exceeds the upper limit of audible sound but when these same frequencies interact with solid materials the scenario becomes complicated but interesting as well. K. S. Suslick et al. and others have explained very nicely the physics behind the ultrasonic waves propagation and its interaction with inorganic particles [273–277]. As explained already in the previous sections that the intensity of the ultrasound irradiation and the subsequent generation of acoustic waves into the dispersed medium produce low and high pressure cycles. Depending on the given frequency of the sonicator device, these cycles create cavitation and bubble formation which upon continuous irradiation grow, pulsate and collapse with each other generating strong shock waves. These shock waves act as a driving force in isolating and peeling out of the bulk crystal to ultra-thin 2D nanosheets [239,240,268,273–277]. These conditions disparagingly affect the lateral size, thickness and final concentration of the dispersed MoS<sub>2</sub> and other layered nanosheets. So, this ultrasound physics breaks down the weak van der Waals forces of attraction which leads to the delamination of bulk layers and it also breaks strong covalent bonding between the layers which fragments the bulk into nano dimensions as seen from the *Figure 2.14*.

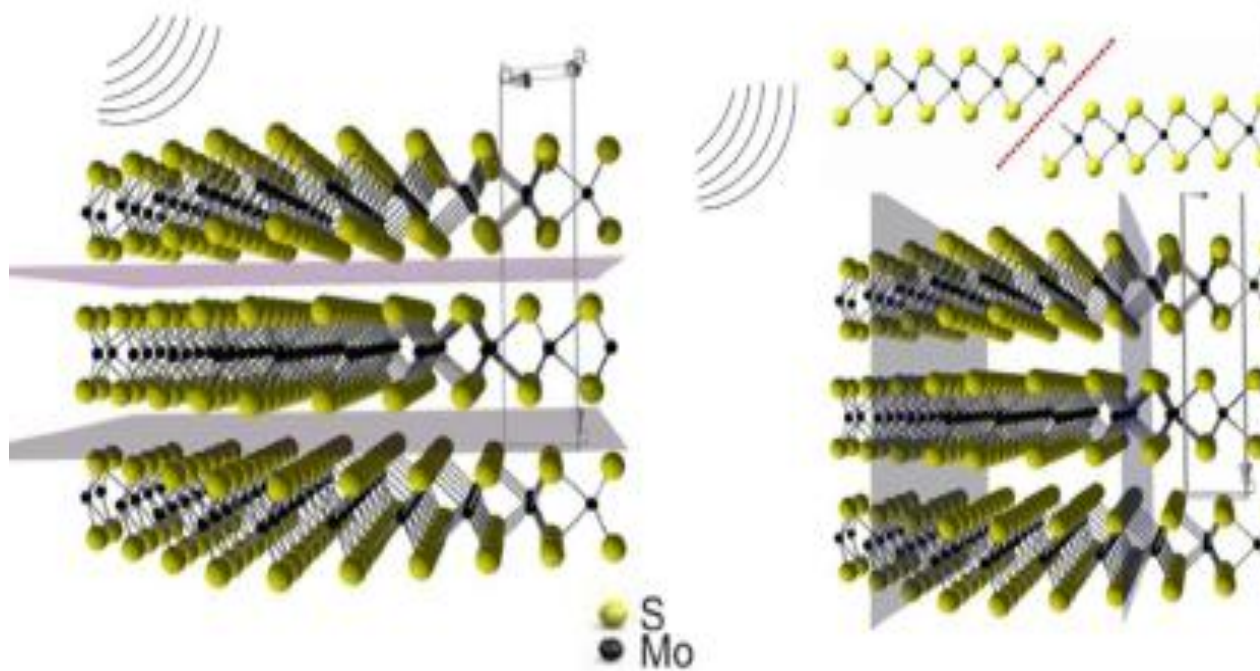


**Figure 2.14:** Structural representation of MoS<sub>2</sub> nanoflakes explaining the two different exfoliation mechanisms resulting in separation of bulk crystal into ultrathin 2D nanosheets. In one part, inter layer van der Waals forces are broken to isolate the bulk crystal into 2D nanosheets, whereas in another portion fragmentation occurs via breaking of covalent bonds within the bulk [278]

Now, at this point the important sonication parameters which play a key role in the successful exfoliation of 2D MoS<sub>2</sub> and other layered nanosheets are shape of the tip or sonotrode, pressure and temperature during the exfoliation, cooling system, ultrasound intensity, density of the solvent used, depth of the sonotrode immersed into the same medium, amplitude of the device and frequency of the sonicator [267–269]. Variation in these parameters drastically affects the reproducibility in the results obtained. Especially, for biomedical applications, irreproducibility

in the results can create serious discrepancies between the analyses and the subsequent bio-interaction study with layered materials. On the other hand, though, bath sonicators gives good yield but it is very complicated to repeat the experiment with the same conditions, position of exfoliation tube in the bath, level of water and so on to get similar results [266]. In such a case, tip sonicators gives accuracy in the results when the focus of the study is to analyze the properties of the exfoliated nanosheets for a number of practical applications such as biomedical science, optoelectronics, thin films and hydrogen evolution reaction to name a few! There are some other reports where the authors have utilized both bath and tip sonicators to achieve hetero-dimensional nanostructures such as MoS<sub>2</sub> quantum dots lying onto MoS<sub>2</sub> nanosheets [127].

Noteworthy decrease in the lateral size of the exfoliated nanosheets, increase in the dispersed concentration up to a certain level and no change in the thickness of the as obtained product can be seen by increasing the power of the tip sonicator from 350 W to 500 W [241]. Using aqueous surfactant solution to exfoliate MoS<sub>2</sub> / WS<sub>2</sub> nanosheets, a study reported an expected upsurge in the concentration with increasing ultrasound power [269]. It was also reported that upon increasing the ultrasound power up to a certain value, the concentration started to fall but the area of nanosheets became slightly larger [240]. The reason for the above explanation was explained on the basis of two different types of cavitation such as non-inertial and inertial cavitation in which the authors have categorized both of the effects on the basis of different sonication powers. This subsequently results in large and small lateral size 2D nanosheets.

Apart from the above mentioned points, the depth of tip immersion into the exfoliation tube plays an important role in the generation of cavitation inside the dispersing medium. The most effective probe depth to achieve non-inertial cavitation is 0.5 cm from the bottom of the tube. In result, additional shear force is generated which peels out the bulk material to thin nanosheets

[<sup>270</sup>]. Even in the device manuals it is clearly mentioned that immersing the tip above or below the threshold value will not exfoliate the given material and would give damaging results. This could even damage the bottom part of tip, if in case high power and continuous mode sonicator is used for a long duration.

## **2) Impact of the nature of the solvent**

The very first question that comes into the mind before designing for any set of experiments related to LPE of 2D nanomaterials is the choice of the solvent and on what basis? It is widely considered that the birth of LPE took place when the first report on the exfoliation of graphite using a wisely chosen solvent was published by Coleman and co-workers in 2008 [<sup>221</sup>]. So, the selection of a solvent depends strongly on the material, purpose of its production and the principles of the thermodynamic solutions. This has been nicely shown in series of research articles by the pioneers of this fabrication technique [<sup>101,246,279,280</sup>]. Some other research groups have also explained the choice of solvent for an effective exfoliation of large number of layered materials [<sup>281–283,284</sup>]. Wisely choosing a solvent result in effective exfoliation of the given layered 2D material which can be ascribed in the following steps:-

- Solvent should be able to impart the high end acoustic energy from the sonotrode tip [<sup>239</sup>].
- Appropriate solvent with the correct parameters in a sense to intercalate into the layered material and to minimize the net exfoliation energy between the dispersing medium and inter-layer forces of the bulk crystal [<sup>101,246</sup>].
- Solvent should be able to avoid the aggregation of the nanosheets by steric repulsion based on the molecular size of the solvent [<sup>238,285</sup>].

In general, a huge amount of work has been devoted to understand the criteria for an appropriate choice of solvents to exfoliate 2D nanosheets to explain their significant enhancement in the efficiency of exfoliation. In most of the works cited above, majority of the research groups have formulated different solubility theories to estimate the exfoliating ability of the solvents towards layered 2D materials. In order to minimize the net exfoliation energy, quantitative characteristics of the desired solvent and that of layered material should have similar values of surface energy which is considered as a solubility parameter for the solvent. As reported in some literature works that a well suitable solvent will have a common value of surface tension ( $\sigma$ ) around  $40 \text{ mJ}\cdot\text{m}^{-2}$ , corresponding to surface energy ( $\gamma$ ) value around  $70 \text{ mJ}\cdot\text{m}^{-2}$  [<sup>101,246,283</sup>]. The concept of an appropriate solubility parameter to choose an effective solvent works as first screening of the solvents. Till date, both for  $\text{MoS}_2$  and  $\text{WS}_2$  nanosheets, the best solvents which have given highest yield and highest concentration are N-vinyl-pyrrolidinone, DMSO, N-dodecyl-pyrrolidone, cyclohexyl-pyrrolidinone, dimethyl-imidazolidinone and DMF [<sup>246,283</sup>]. A significant contribution on investigating the matching solubility parameters for a broad range of solvents has been reported by various research groups which theoretically and experimentally reveals the importance of a solvent properties in efficiently exfoliating wide number of layered 2D materials [<sup>101,102,239,281,286</sup>].

The criteria and theoretical calculations made to choose an effective solvent was suited best for those organic solvents which by nature are highly toxic, expensive and exhibit high boiling points. The physical and chemical properties of such solvents often complicate the post exfoliation steps when there is a need to evaporate the solvent for thin films or other applications. Recently, these so called preferred solvents have been placed on the candidate list

of ‘Substances of Very High Concern’ (SVHC) [287] by the European Union<sup>4</sup> under the [Regulation (EC) no. 1907/2006] and in USA [as well because NMP and DMF presents severe health risks and reproductive toxicants [221,288].

To circumvent these serious issues, various research groups have made successful attempts by exfoliating 2D MoS<sub>2</sub>/WS<sub>2</sub> and other layered materials in low boiling point solvents such as ethanol, acetone, water, tetra hydrofuran (THF), isopropanol, methanol etc. The applicability of the solubility theories have also been reported for water-alcohol [281–283,289], water-acetone [282] and water-IPA [290] mixtures. Particularly, in such solvents molecule size of the solvent is crucial in imparting efficient energy to the material upon continuous ultrasound irradiation.

### **3) Influence of sonication power and type**

As widely adopted and easily accessible, two different types of ultrasonic devices are available- bath sonicator and probe/tip sonicator. Other sonication devices such as household kitchen blender [248], wet jet milling device [291], ball milling [292–294], fluid dynamics in a hydrodynamic apparatus [295–297] and rotor stator mixer [245,298] have also been reported for efficient exfoliation of layered materials at both industrial and laboratory scale. It has been reported that high energy tip sonicator produces high quality 2D nanosheets exhibiting appealing concentrations and a good amount of yield as compared to a bath sonicator. It is even much better than a bath sonicator in terms of processing time as it can disperse high concentration dispersions in shorter times in the range of ~1 g/L in <24 h for initial bulk material concentrations of 30–50 g/L [101,238,299]. The reason as explained above that the introduction of cavitation and vibration forces from the dispersing medium generates cavities or micro-bubbles which in result produces strong

---

<sup>4</sup> European Chemicals Agency (ECHA) candidate list of Substances of Very High Concern (SVHC). Available from:<http://echa.europa.eu/candidate-list-table> (accessed 10-01-2017)

acoustic shockwaves with high speed jets and high local temperature and pressure. This all is imparted to the bulk layered crystal which acts as a driving force to peel out the bulk lamellar crystal to ultrathin 2D nanosheets. Some authors have studied the impact of different ultrasonic powers of a probe sonicator on concentration and morphology of MoS<sub>2</sub> nanosheets exfoliated in NMP. They observed that the optimal power within the same dispersion which can effectively exfoliate MoS<sub>2</sub> nanosheets in NMP was in between 250-320 W [<sup>240</sup>]. Below this, the cavitation effect is very less which in result produces less exfoliation energy to exfoliate the layered crystal. Going above 320 W, high concentration of cavities in the same medium suppresses the cavitation forces which actually work as a shielding barrier for the nanosheets. But at high power, lateral size and thickness decreases significantly whereas at low power sonication, large lateral size flakes are obtained [<sup>241</sup>].

In general, the above cited exfoliation methods should be adopted based on the layered material chosen. Graphite, for example can be exfoliated using all of the above methods but other layered materials could have different properties and criteria to be ready for exfoliation using these methods. 2D TMDs have significant applications in high tech optoelectronics, thin films, hydrogen evolution reaction and various biomedical areas where thin and large nanosheets are required and in such a case high energy tip sonication will meet the desired outcome rather than bath sonication. So, investigation of different exfoliation methods is very essential to test the potential of new layered materials to exfoliate. Both bath sonication and tip sonication have different potentials to exfoliate lamellar crystals based on their mechanical setup. The former one exhibits a bath containing de-ionized water up to a certain level where a glass vial containing the layered material is immersed into it at a fixed position where the strong ultrasonic vibrations

travels through the bath and vial positioned and acts as a driving force to peel out the bulk crystal to thin nanosheets by. It is usually a time consuming method and less reproducible method which gives large lateral size with single or few layer nanosheets exhibiting an optimum amount of concentration [<sup>221,238,247,285,300</sup>]. Whereas, the latter exhibits a high energy sonotrode or tip which is immersed into the dispersing medium up to a certain depth and upon ultrasonic irradiation the cavitation physics isolates the bulk crystal to high quality, high concentration and poly disperse 2D nanosheets with high reproducibility [<sup>101,251</sup>]. It is combined with different varieties of probe shapes, sizes and device controllers for other functions such as amplitude setting, frequency setting and pulse ON-OFF modes for long terms effective usage of this tip sonicator.

#### **4) Impact of sonication time on the efficiency of exfoliation**

Sonication time has a great influence on the desired outcomes from the exfoliation of 2D TMDs and other layered materials. Linear relationship between the final concentration and sonication time has been reported in a number of research articles but up to a certain point after which the final concentration tends to start decreasing because of the inhibition of cavitation bubbles after a saturation point. Prolonged sonication leads to more extensive scission and fragmentation of 2D nanosheets which in result decreases both the thickness and lateral size of the exfoliated nanosheets. Coleman and co-workers have investigated widely the effect of sonication time on the exfoliation efficiency and subsequently on the product parameters [<sup>246,279</sup>]. Even using bath sonicator for prolonged hours of sonication, an optimum relation between the concentration and lateral size has been observed which marks an important point to control the sonication time for the desired product parameters, though with high concentrations. Recently, Piers Turner et al. have reported a controlled sonication route for graphene nanosheets with flake size control using

advanced cavitation physics based metrology device via LPE. They have achieved 18% yield after three hours of controlled sonication under a controlled temperature and other parameters by which they controlled inertial cavitation dose which resulted in consistent ultra-sonication throughout the time [301].

### **5) Influence of surfactants/stabilizers on the efficiency of exfoliation**

Generally, surfactants or stabilizers act as a solid support for not only 2D materials but other nanomaterials in a given dispersant to enhance the stabilization, to avoid the aggregation and to increase the interaction of dispersed nanoparticles with the surrounding medium with optimally high concentrations. So is the case with graphite, 2D TMDs and other layered materials. The use of surfactants/stabilizers during the exfoliation have stretched the impact of given 2D material in various applications making them environmentally safe and reducing the cost as well [302].

Basically, the role of a surfactant can be summarized in two steps:-

- a) It aids in modifying the surface tension of a given solvent to augment the solubility and stability of the exfoliated nanosheets [303].
- b) A given surfactant also adsorbs onto the surface of exfoliated nanosheets which in result intensify the repulsive forces between the layers and impedes the aggregation in the dispersing medium [304,305].

There have been a numerous reports in the literature which embrace the selection of a suitable surfactant or stabilizer in aqueous based dispersions and in low-boiling point solvents for producing a good amount (high yield), appreciable concentrations, optimum lateral size and thickness of 2D TMDs [69,247,302,305–311,312,313]. This process can even be applied to scale up the

LPE process for various industrial applications [302]. Some authors have also tested the continuous supply of the surfactants during the exfoliation which resulted in improved yield and concentration of the final product [313]. Apart from the benefits of adding surfactants, there are some demerits as well. It becomes very annoying to remove the surfactant/ stabilizer completely from the nanosheets surface for further processing and characterization analysis. This, in results deteriorates the properties of the exfoliated nanosheets and retreating their novel potential in the desired application. Strategies to remove the surfactant completely from the surface of nanosheets are extremely time consuming and furthermore it also leads to the aggregation of exfoliated nanosheets which again hampers their potential in practical applications. Nonetheless, it is not possible to remove the surfactants/stabilizers completely, some residues still remain there.

#### **6) Effective size selection process**

The major obstruction of liquid phase exfoliated 2D nanosheets dispersions is its tendency to give broad range of lateral size and thicknesses dispersals in the range of few nanometers to micrometers and number of layers attribute to less than 30 and specifically aqueous surfactant exfoliated MoS<sub>2</sub> nanosheets attributes to a lateral size in the range between 50 nm – 500 nm and number of layers between 1-10 [275,314]. So this poly-disperse nature of exfoliated 2D nanosheets hampers its use in various applications such as catalysis, printed optoelectronic devices, 2D material based environment friendly inks where monolayer nanosheets are highly required for the best performance in commercial applications [315–317] and it accounts for a critical issue because the properties of the exfoliated nanosheets are highly dependent on their physical parameters obtained. In such a case, it becomes difficult to unveil the potential of these

exfoliated nanosheets in particular areas of interest. Therefore, post exfoliation size selection step by centrifugation is very crucial to achieve monolayer enriched 2D nanosheets or in general size selection based on the desired application. The conventional homogenous centrifugation steps attributed to poor control on size and thickness of the exfoliated nanosheets because the dispersions were usually separated using one step low centrifugal force, resulting in the separation of un-exfoliated material in the sediment and thus supernatant used for further characterization [<sup>101,221,224,247</sup>].

Usually, centrifugal speed and time are key parameters which separate the exfoliated nanosheets based on their lateral size and thickness. This further depends on the viscosity of the solvent. Low centrifugal speed at the starting will give both large and small nanosheets whereas; higher centrifugal speed will isolate thinner/smaller nanosheets for the desired applications. On the other hand, density gradient based ultracentrifugation technique is solely based to separate the nanosheets based on their thickness. Moreover, it is actually very complex technique, giving low yield nanosheets and limited to polymer stabilized dispersions [<sup>318</sup>].

So, to circumvent the above issues, Claudia Backes et al. [<sup>319</sup>] has developed a scalable, high yield and efficient centrifugation based technique called as liquid cascade centrifugation (LCC), which is performed in a cascade with increasing centrifugation acceleration, allowing the dispersed nanosheets to be separated by lateral size and thickness in a controlled way. Various cascades can be designed according to the desired application. Basically, based on the Claudia Backes et al's demonstration of this process, it is a multistep process whereby each cascade is opted with higher centrifugal speed than the preceding step. Except the first step, after each step sediment of the centrifuged dispersion is retained and the supernatant is subjected to next higher centrifugal speed. Each retained sediment contains nanosheets with a range of lateral size trapped

between the two centrifuge steps with different speeds and this sediment can be re-dispersed into the similar fresh solvent/aqueous surfactant solution with a mild sonication to achieve the desired concentration of a nanosheet. Depending on the desired final concentration, there is also flexibility in choosing the re-dispersed concentration of fresh solvent/aqueous surfactant solution. Complete removal of the supernatant, long centrifugation time (say for 2 hours) to achieve a pellet like sediment at the bottom of the tube or vial and subsequently the filling height of the dispersions are some of the crucial factors to keep in mind while following LCC. A number of 2D TMDs such as MoS<sub>2</sub>, WS<sub>2</sub>, layered hydroxides, sulphides and other members of the 2D material family have been subjected to LCC with very interesting size and monolayer enriched thickness selections [<sup>252,256,319,320</sup>]. The LCC obtained nanosheets are enriched with significant spectral properties with high monolayer content and specific size selected 2D nanosheets, in result of which the same group has derived some metrics to get in-situ information of average number of layers, concentration and lateral size of nanosheets by UV-Vis spectroscopy. This technique now has been adopted widely by a number of research groups working with LPE to get size and thickness selected desired nanosheets of various layered materials with some adjustments based on the density of the material and density and viscosity of the dispersing medium.

So, in general, LCC is very flexible, versatile, scalable and universally applicable technique to get size selected 2D nanosheets. The best part of this technique is that it gives high yield, controlled way to get the desired concentration of a particular size selected dispersion and completely no wastage of the material during centrifugation process. For the post exfoliation steps in this thesis, we have employed LCC to tune the final concentration and other physical

parameters of exfoliated MoS<sub>2</sub> nanosheets to understand the interaction of these nanosheets with live matter.

## Bibliography

1. Article, R., Goyal, R. & Kumar, S. Nanotechnology: A novel approach towards cancer treatment. **1**, 84–96 (2014).
2. Subedi, S. K. An introduction to nanotechnology and its implications. 78–81 (1985).
3. Hersam, M. C. Nanotechnology research directions for societal needs in 2020 : summary of international study. 897–919 (2020).
4. Iavicoli, I., Leso, V., Ricciardi, W., Hodson, L. L. & Hoover, M. D. Opportunities and challenges of nanotechnology in the green economy. 1–11 (2014).
5. Gupta, S. R. N. Advances in Molecular Nanotechnology from Premodern to Modern Era. **2**, 99–106 (2014).
6. Black, G. Nanotechnology in the developing world. 41–50 (2005).
7. Advanced, O. F. © I A E M E NANOMATERIALS AND NANOTECHNOLOGY : FUTURE. 41–47 (2014).
8. Neikov, O. D. & Yefimov, N. A. *Nanopowders. Handbook of Non-Ferrous Metal Powders* (Elsevier Ltd., 2019). doi:10.1016/B978-0-08-100543-9.00009-9
9. Nasrollahzadeh, M., Sajadi, S. M. & Sajjadi, M. *Applications of Nanotechnology in Daily Life. An Introduction to Green Nanotechnology* **28**, (Elsevier Ltd., 2019).
10. Nikalje, A. P. Nanotechnology and its Applications in Medicine. **5**, 81–89 (2015).
11. Steichen, S. D., Caldorera-moore, M. & Peppas, N. A. European Journal of Pharmaceutical Sciences A review of current nanoparticle and targeting moieties for the delivery of cancer therapeutics. *Eur. J. Pharm. Sci.* **48**, 416–427 (2013).
12. Sahoo, S. K., Parveen, S. & Panda, J. J. The present and future of nanotechnology in human health care. **3**, 20–31 (2007).
13. Misra, R., Acharya, S. & Sahoo, S. K. Cancer nanotechnology: application of nanotechnology in cancer therapy. *Drug Discov. Today* **15**, 842–850 (2010).

14. Photographs, S. The crystal structure of cadmium iodide. **1**, 3–7 (1922).
15. Splendiani, A. *et al.* Emerging photoluminescence in monolayer MoS<sub>2</sub>. *Nano Lett.* **10**, 1271–1275 (2010).
16. Hulla, J. E., Sahu, S. C. & Hayes, A. W. Nanotechnology : History and future. **34**, 1318–1321 (2015).
17. Samal, S. S., Jeyaraman, P., Vishwakarma, V. & Samal, S. S. Sonochemical Coating of Ag-TiO<sub>2</sub> Nanoparticles on Textile Fabrics for Stain Repellency and Self-Cleaning- The Indian Scenario : A Review. **9**, 519–525 (2010).
18. Zhang, X. *et al.* Superhydrophobic TiO<sub>2</sub> Surfaces : Preparation , Photocatalytic Wettability Conversion , and Superhydrophobic - Superhydrophilic Patterning. 14521–14529 (2007). doi:10.1021/jp0744432
19. Asghari, F., Khademi, R. & Ranjbar, F. E. Application of Nanotechnology in Targeting of Cancer Stem Cells : A Review. **12**, 227–239 (2019).
20. Liu, Y. *et al.* Molybdenum disulfide/graphene oxide nanocomposites show favorable lung targeting and enhanced drug loading/tumor-killing efficacy with improved biocompatibility. *NPG Asia Mater.* **10**, e458 (2018).
21. Gentile, A., Ruffino, F. & Grimaldi, M. G. Complex-Morphology Metal-Based Nanostructures : Fabrication , Characterization , and Applications. (2016). doi:10.3390/nano6060110
22. Shi, X. & Tian, F. Multiscale Modeling and Simulation of Nano-Carriers Delivery through Biological Barriers — A Review. (2018). doi:10.1002/adts.201800105
23. Panahi, Y. *et al.* Recent advances on liposomal nanoparticles: synthesis, characterization and biomedical applications. *Artif. Cells, Nanomedicine Biotechnol.* **45**, 788–799 (2017).
24. Zhang, X. F., Liu, Z. G., Shen, W. & Gurunathan, S. Silver nanoparticles: Synthesis, characterization, properties, applications, and therapeutic approaches. *Int. J. Mol. Sci.* **17**, (2016).

25. Liu, J., Chen, Q., Feng, L. & Liu, Z. Nanomedicine for tumor microenvironment modulation and cancer treatment enhancement. *Nano Today* **21**, 55–73 (2018).
26. Raimond, J. M., Brune, M., Compton, Q., Martini, F. De & Monroe, C. Electric Field Effect in Atomically Thin Carbon Films. **306**, 666–670 (2004).
27. De, N. 'i. h. p. **3**, 177–222 (1935).
28. Search, H., Journals, C., Contact, A., Iopscience, M. & Address, I. P. Nucleation and growth of thin films. **399**, (1984).
29. Zinke-allmang, M., Feldman, L. C. & Grabow, M. H. Clustering on surfaces. *Phys. Rev. Lett.* **20**, 4762 (1979).
30. Meyer, J. C. *et al.* The structure of suspended graphene sheets. **446**, (2007).
31. Chimene, D., Alge, D. L. & Gaharwar, A. K. Two-Dimensional Nanomaterials for Biomedical Applications: Emerging Trends and Future Prospects. *Adv. Mater.* **27**, 7261–7284 (2015).
32. Chhowalla, M. *et al.* The chemistry of two-dimensional layered transition metal dichalcogenide nanosheets. *Nat. Chem.* **5**, 263–275 (2013).
33. Osada, M. & Sasaki, T. Two-Dimensional Dielectric Nanosheets : Novel Nanoelectronics From Nanocrystal Building Blocks. 210–228 (2012). doi:10.1002/adma.201103241
34. Golberg, D. *et al.* Boron Nitride Nanotubes and. **4**, 2979–2993 (2010).
35. Koski, K. J. *et al.* The New Skinny in Two-Dimensional. 3739–3743 (2013). doi:10.1021/nm4022422
36. Naguib, M., Mochalin, V. N., Barsoum, M. W. & Gogotsi, Y. 25th Anniversary Article : MXenes : A New Family of Two-Dimensional Materials. 992–1005 (2013). doi:10.1002/adma.201304138
37. Li, Y. *et al.* MoS<sub>2</sub> nanoparticles grown on graphene: An advanced catalyst for the hydrogen evolution reaction. *J. Am. Chem. Soc.* **133**, 7296–7299 (2011).

39. Radisavljevic, B., Radenovic, A., Brivio, J., Giacometti, V. & Kis, A. Single-layer MoS<sub>2</sub> transistors. *Nat. Nanotechnol.* **6**, 147–150 (2011).
40. Wang, T., Chen, S., Pang, H., Xue, H. & Yu, Y. MoS<sub>2</sub>-Based Nanocomposites for Electrochemical Energy Storage. (2017). doi:10.1002/advs.201600289
41. Arora, Y., Shah, A. P., Battu, S., Maliakkal, C. B. & Haram, S. Nanostructured MoS<sub>2</sub> / BiVO<sub>4</sub> Composites for Energy Storage Applications. 1–7 (2016). doi:10.1038/srep36294
42. He, Z. & Que, W. Molybdenum disulfide nanomaterials: Structures, properties, synthesis and recent progress on hydrogen evolution reaction. *Appl. Mater. Today* **3**, 23–56 (2016).
43. Gurunathan, S., Han, J. W., Dayem, A. A., Eppakayala, V. & Kim, J. H. Oxidative stress-mediated antibacterial activity of graphene oxide and reduced graphene oxide in *Pseudomonas aeruginosa*. *Int J Nanomed* **7**, 5901–5914 (2012).
44. Huang, X. *et al.* Nanoscale functionalization of transition metal. 17193–17198 (2017). doi:10.1039/c7nr06807g
45. Hu, Y., Huang, Y., Tan, C., Zhang, X. & Lu, Q. MATERIALS CHEMISTRY Two-dimensional transition metal dichalcogenide nanomaterials for biosensing applications. 24–36 (2017). doi:10.1039/c6qm00195e
46. Kalantar-zadeh, K. & Ou, J. Z. Biosensors Based on Two-Dimensional MoS<sub>2</sub>. (2016). doi:10.1021/acssensors.5b00142
47. Lim, C., Garaj, S. & Leong, D. T. Directing Assembly and Disassembly of 2D MoS<sub>2</sub> Nanosheets with DNA for Drug Delivery. (2017). doi:10.1021/acsami.7b02529
48. Liu, Y. & Liu, J. Nanoscale. 13187–13194 (2017). doi:10.1039/c7nr04199c
49. Liu, T. *et al.* Drug Delivery with PEGylated MoS<sub>2</sub> Nano-sheets for Combined Photothermal and Chemotherapy of Cancer. *Adv. Mater.* **26**, 3433–3440 (2014).
50. Lv, R. *et al.* Two-dimensional transition metal dichalcogenides: Clusters, ribbons, sheets and more. *Nano Today* **10**, 559–592 (2015).

51. Kurapati, R., Kostarelos, K., Prato, M. & Bianco, A. Biomedical Uses for 2D Materials Beyond Graphene: Current Advances and Challenges Ahead. *Adv. Mater.* 6052–6074 (2016). doi:10.1002/adma.201506306
52. Nanoscale, C. Nanoscale Atomically thin layers of MoS<sub>2</sub> via a two step thermal. 461–466 (2012). doi:10.1039/c1nr10803d
53. Huang, Y., Guo, J., Kang, Y., Ai, Y. & Li, C. M. Two dimensional atomically thin MoS<sub>2</sub> nanosheets and their sensing applications. *Nanoscale* **7**, 19358–19376 (2015).
54. Bertolazzi, S., Brivio, J. & Kis, A. Stretching and Breaking of Ultrathin. 9703–9709 (2011). doi:10.1021/nn203879f
55. Castellanos-gomez, A., Poot, M., Steele, G. A. & Zant, H. S. J. Van Der. Elastic Properties of Freely Suspended MoS<sub>2</sub> Nanosheets. 772–775 (2012). doi:10.1002/adma.201103965
56. Yao, W. Electronic structures and theoretical modelling of two-dimensional group-VIB transition metal dichalcogenides. **44**, (2015).
57. Darancet, P., Millis, A. J. & Marianetti, C. A. Three-dimensional metallic and two-dimensional insulating behavior in octahedral tantalum dichalcogenides. **45134**, 2–6 (2014).
58. Ke, Q. & Wang, J. Graphene-based materials for supercapacitor electrodes – A review. *J. Mater.* **2**, 37–54 (2016).
59. Wang, H., Feng, H. & Li, J. Graphene and Graphene-like Layered Transition Metal Dichalcogenides in Energy Conversion and Storage. 1–17 (2014). doi:10.1002/sml.201303711
60. Heine, T. Transition metal chalcogenides: Ultrathin inorganic materials with tunable electronic properties. *Acc. Chem. Res.* **48**, 65–72 (2015).
61. Peimyoo, N. *et al.* Thermal conductivity determination of suspended mono- and bilayer WS<sub>2</sub> by Raman spectroscopy. **3**, 1–12 (2014).

62. Taylor, P., Wilson, J. A. & Yoffe, A. D. Advances in Physics The transition metal dichalcogenides discussion and interpretation of the observed optical , electrical and structural properties. 37–41 (2006). doi:10.1080/00018736900101307
63. Gibney, E. 2D or not 2D. *Nature* **522**, 274–276 (2015).
64. Mak, K. F., Lee, C., Hone, J., Shan, J. & Heinz, T. F. Atomically thin MoS<sub>2</sub>: A new direct-gap semiconductor. *Phys. Rev. Lett.* **105**, 2–5 (2010).
65. Tongay, S. *et al.* Thermally Driven Crossover from Indirect toward Direct Bandgap in 2D Semiconductors: MoSe<sub>2</sub> versus MoS<sub>2</sub>. (2012). doi:10.1021/nl302584w
66. Thin, A. Evolution of Electronic Structure in. 791–797 (2013). doi:10.1021/nn305275h
67. Splendiani, A. *et al.* Emerging Photoluminescence in Monolayer. 1271–1275 (2010). doi:10.1021/nl903868w
68. Sahoo, S., Gaur, A. P. S., Ahmadi, M. & Katiyar, R. S. Temperature-Dependent Raman Studies and Thermal Conductivity of Few-Layer MoS<sub>2</sub>. (2013). doi:10.1021/jp402509w
69. Online, V. A., Kim, S., Wie, J. J., Mahmood, Q. & Park, H. S. Nanoscale Anomalous nano-inclusion effects of 2D MoS<sub>2</sub> and WS<sub>2</sub> nanosheets on the mechanical stiffness of polymer nanocomposites †. 7430–7435 (2014). doi:10.1039/c4nr01208a
70. May, P. *et al.* Reinforcement of metal with liquid-exfoliated inorganic nano-platelets Reinforcement of metal with liquid-exfoliated inorganic nano-platelets. **163106**, 1–5 (2014).
71. Lee, S. & Zhong, Z. Nanoscale Nanoelectronic circuits based on two-dimensional. 13283–13300 (2014). doi:10.1039/c4nr03670k
72. Two-dimensional, S. *et al.* Emerging Device Applications for. 1102–1120 (2014). doi:10.1021/nn500064s
73. Ganatra, R. & Zhang, Q. Few-layer MoS<sub>2</sub>: A promising layered semiconductor. *ACS Nano* **8**, 4074–4099 (2014).

74. Wi, S. *et al.* Enhancement of Photovoltaic Response in Multilayer MoS<sub>2</sub> Induced by Plasma Doping. 5270–5281 (2014). doi:10.1021/nn5013429
75. Article, R. Chem Soc Rev. 2986–3017 (2013). doi:10.1039/c2cs35310e
76. Stephenson, T., Li, Z. & Mitlin, D. Environmental Science. 209–231 (2014). doi:10.1039/c3ee42591f
77. Sen, U. K., Johari, P., Basu, S., Nayak, C. & Mitra, S. An experimental and computational study to molybdenum disulfide †. 10243–10254 (2014). doi:10.1039/c4nr02480j
78. Chen, Y., Tan, C., Zhang, H. & Wang, L. Two-dimensional graphene analogues for biomedical applications. *Chemical Society Reviews* (2015). doi:10.1039/c4cs00300d
79. Lv, R. *et al.* Transition Metal Dichalcogenides and Beyond : Synthesis , Properties , and Applications of Single- and Few-Layer Nanosheets Published as part of the Accounts of Chemical Research special issue ‘ 2D Nanomaterials beyond Graphene ’ . (2015). doi:10.1021/ar5002846
80. Kaur, J. *et al.* Green synthesis of luminescent and defect-free bio-nanosheets of MoS<sub>2</sub>: Interfacing twodimensional crystals with hydrophobins. *RSC Adv.* **7**, 22400–22408 (2017).
81. Kaur, J. *et al.* Electrostatically driven scalable synthesis of MoS<sub>2</sub>–graphene hybrid films assisted by hydrophobins. *RSC Adv.* **7**, 50166–50175 (2017).
82. Zhang, L., Zhao, Y. & Wang, X. Nanoparticle-Mediated Mechanical Destruction of Cell Membranes: A Coarse-Grained Molecular Dynamics Study. *ACS Appl. Mater. Interfaces* **9**, 26665–26673 (2017).
83. Liu, T. & Liu, Z. 2D MoS<sub>2</sub> Nanostructures for Biomedical Applications. *Adv. Healthc. Mater.* **1701158**, 1701158 (2017).
84. McManus, D. *et al.* Water-based and biocompatible 2D crystal inks for all-inkjet-printed heterostructures. *Nat. Nanotechnol.* **12**, 343–350 (2017).
85. Siepi, M. *et al.* Production of biofunctionalized MoS<sub>2</sub> flakes with rationally modified

- lysozyme: a biocompatible 2D hybrid material. *2D Mater.* **4**, 35007 (2017).
86. Li, X. *et al.* Recent Advances in Synthesis and Biomedical Applications of Two-Dimensional Transition Metal Dichalcogenide Nanosheets. *Small* **13**, 1–28 (2017).
  87. Li, Z. & Wong, S. L. Functionalization of 2D transition metal dichalcogenides for biomedical applications. *Mater. Sci. Eng. C* **70**, 1095–1106 (2017).
  88. Zhang, S. H. & Wang, L. As featured in : Chem Soc Rev biomedical applications. (2015). doi:10.1039/c4cs00300d
  89. Shah, P., Narayanan, T. N., Li, C.-Z. & Alwarappan, S. Probing the biocompatibility of MoS<sub>2</sub> nanosheets by cytotoxicity assay and electrical impedance spectroscopy. *Nanotechnology* **26**, 315102 (2015).
  90. Nanobiotechnol, J. *et al.* Functionalized - MoS<sub>2</sub> - erlotinib produces hyperthermia under NIR. *J. Nanobiotechnology* 1–15 (2019). doi:10.1186/s12951-019-0508-9
  91. Tang, K. *et al.* Molybdenum disulfide (MoS<sub>2</sub>) nanosheets vertically coated on titanium for disinfection in the dark. *Arab. J. Chem.* (2018). doi:10.1016/j.arabjc.2017.12.013
  92. Senapati, S. *et al.* Engineered Cellular Uptake and Controlled Drug Delivery Using Two Dimensional Nanoparticle and Polymer for Cancer Treatment. *Mol. Pharm.* **15**, 679–694 (2018).
  93. Wang, Q. H., Kalantar-Zadeh, K., Kis, A., Coleman, J. N. & Strano, M. S. Electronics and optoelectronics of two-dimensional transition metal dichalcogenides. *Nature Nanotechnology* (2012). doi:10.1038/nnano.2012.193
  94. Domínguez-meister, S., Cristina, T., Brizuela, M. & Sánchez-lópez, J. C. Solid lubricant behavior of MoS<sub>2</sub> and WSe<sub>2</sub> -based nanocomposite coatings. 122–133 (2017). doi:10.1080/14686996.2016.1275784
  95. Mechanisms, F. & Films, M. D. Lubrication and Failure Mechanisms of Molybdenum Disulfide Films Effect of Atmosphere Lubrication and Failure Mechanisms I - Effect of Atmosphere. (2020).

96. Vazirisereshk, M. R., Martini, A., Strubbe, D. A. & Baykara, M. Z. Solid Lubrication with MoS<sub>2</sub>: A Review. (2019).
97. Han, S. A., Bhatia, R. & Kim, S. Synthesis, properties and potential applications of two-dimensional transition metal dichalcogenides. ??? (2015). doi:10.1186/s40580-015-0048-4
98. Louwen, J. N., Frenken, J. W. M. & Groot, I. M. N. hydrodesulfurization catalyst. *Nat. Commun.* 1–8 doi:10.1038/s41467-019-10526-0
99. Rao, C. N. R., Maitra, U. & Waghmare, U. V. Extraordinary attributes of 2-dimensional MoS<sub>2</sub> nanosheets. **609**, 172–183 (2014).
100. Zheng, J. *et al.* High yield exfoliation of two-dimensional chalcogenides using sodium naphthalenide. *Nat. Commun.* 1–7 (2014). doi:10.1038/ncomms3995
101. Coleman, J. N. *et al.* Two-Dimensional Nanosheets Produced by Liquid Exfoliation of Layered Materials. *Science (80-. )*. **331**, 568–571 (2011).
102. Nicolosi, V., Chhowalla, M., Kanatzidis, M. G., Strano, M. S. & Coleman, J. N. Liquid Exfoliation of Layered Materials. *Science (80-. )*. **340**, 1226419–1226419 (2013).
103. Zappa, D. Molybdenum dichalcogenides for environmental chemical sensing. *Materials (Basel)*. **10**, 1–22 (2017).
104. Benavente, E., Ana, M. A. S., Mendiza, F. & Gonza, G. Intercalation chemistry of molybdenum disulfide. **224**, 87–109 (2002).
105. Jaramillo, T. F.; Jorgensen, K. P.; Bonde, J.; Nielsen, J. H.;Horch, S.; Chorkendorff, I. Identification of Active Edge Sites for Electrochemical H<sub>2</sub> Evolution from MoS<sub>2</sub> Nanocatalysts. *Science* 2007, 317, 100–102.pdf.
106. Singh, V., Joung, D., Zhai, L. & Das, S. Progress in Materials Science Graphene based materials: Past, present and future. *Prog. Mater. Sci.* **56**, 1178–1271 (2011).
107. Large-Area Atomically Thin MoS<sub>2</sub> Nanosheets Prepared Using Electrochemical Exfoliation. (2014).

108. Zhan, Y., Liu, Z., Najmaei, S., Ajayan, P. M. & Lou, J. Large-Area Vapor-Phase Growth and Characterization of MoS<sub>2</sub> Atomic Layers on a SiO<sub>2</sub> Substrate. 966–971 (2012). doi:10.1002/sml.201102654
109. Lee, Y. *et al.* Synthesis of Large-Area MoS<sub>2</sub> Atomic Layers with Chemical Vapor Deposition. 2320–2325 (2012). doi:10.1002/adma.201104798
110. Kolobov, A. V. *Springer Series in Materials Science 239 Two-Dimensional Dichalcogenides.*
111. Kc, S., Longo, R. C., Addou, R., Wallace, R. M. & Cho, K. Impact of intrinsic atomic defects on the electronic structure of MoS<sub>2</sub> monolayers. doi:10.1088/0957-4484/25/37/375703
112. Zhou, L., He, B., Yang, Y. & He, Y. Facile approach to surface functionalized MoS<sub>2</sub> nanosheets. 32570–32578 (2014). doi:10.1039/c4ra04682j
113. Nan, H. *et al.* Strong Photoluminescence Enhancement of MoS<sub>2</sub> through Defect Engineering and Oxygen Bonding. 5738–5745 (2014). doi:10.1021/nn500532f
114. Liu, D. *et al.* Sulfur vacancies in monolayer MoS<sub>2</sub> and its electrical contacts Sulfur vacancies in monolayer MoS<sub>2</sub> and its electrical contacts. **183113**, (2014).
115. Eda, G. *et al.* Photoluminescence from chemically exfoliated MoS<sub>2</sub>. *Nano Lett.* **11**, 5111–5116 (2011).
116. Voiry, D. *et al.* Covalent functionalization of monolayered transition metal dichalcogenides by phase engineering. *Nat. Chem.* **7**, 45–49 (2014).
117. Lee, C., Wei, X., Kysar, J. W. & Hone, J. of Monolayer Graphene. **321**, 385–389 (2008).
118. Feldman, L. ELASTIC CONSTANTS OF 2H-MoTe<sub>2</sub> and 2H-NbSe<sub>2</sub> EXTRACTED FROM MEASURED DISPERSION CURVES AND LINEAR COMPRESSIBILITIES. **37**, (1976).
119. Anderson, T., Hu, R., Yang, C., Yoon, H. S. & Yong, K. Biomaterials Science. 1244–1253 (2014). doi:10.1039/c4bm00019f

120. Schwendener, R. A. CHAPTER 9 Liposomes in Biology and Medicine. (2007).
121. Luo, Y., Chang, L. W. & Lin, P. Metal-Based Nanoparticles and the Immune System : Activation , Inflammation , and Potential Applications. **2015**, (2015).
122. Baran, J. Applications of Noble Metal-Based Nanoparticles in Medicine a. (2018). doi:10.3390/ijms19124031
123. Parveen, S. & Sahoo, S. K. Polymeric nanoparticles for cancer therapy. **2330**, (2008).
124. Houdaihed, L., Evans, J. C. & Allen, C. Overcoming the Road Blocks : Advancement of Block Copolymer Micelles for Cancer Therapy in the Clinic. (2017). doi:10.1021/acs.molpharmaceut.7b00188
125. Vogus, D. R. *et al.* A hyaluronic acid conjugate engineered to synergistically and sequentially deliver gemcitabine and doxorubicin to treat triple negative breast cancer. *J. Control. Release* **267**, 191–202 (2017).
126. Wu, C. *et al.* Biomaterials Highly efficient cascading synergy of cancer photo-immunotherapy enabled by engineered graphene quantum dots / photosensitizer / CpG oligonucleotides hybrid nanotheranostics. *Biomaterials* **205**, 106–119 (2019).
127. Nanosheets, E. M., Gopalakrishnan, D., Damien, D. & Shaijumon, M. M. MoS<sub>2</sub> Quantum Dot-Interspersed. 5297–5303 (2014). doi:10.1021/nn501479e
128. Chen, M.-L., Liu, J.-W., Hu, B., Chen, M.-L. & Wang, J.-H. Conjugation of quantum dots with graphene for fluorescence imaging of live cells. *Analyst* **136**, 4277 (2011).
129. Wang, S. *et al.* Biomaterials Biocompatible PEGylated MoS<sub>2</sub> nanosheets : Controllable bottom-up synthesis and highly efficient photothermal regression of tumor. *Biomaterials* **39**, 206–217 (2015).
130. Chou, S. S., Kim, J. & Foley, B. M. NIH Public Access. **52**, 4160–4164 (2014).
131. Yin, W. *et al.* Functionalized Nano-MoS<sub>2</sub> with Peroxidase Catalytic and Near-Infrared Photothermal Activities for Safe and Synergetic Wound Antibacterial Applications. *ACS Nano* **10**, 11000–11011 (2016).

132. Kaur, J. *et al.* Biological interactions of biocompatible and water-dispersed MoS<sub>2</sub> nanosheets with bacteria and human cells. 1–15 (2018). doi:10.1038/s41598-018-34679-y
133. Wang, X. *et al.* ORIGINAL ARTICLE A 3D-printed scaffold with MoS<sub>2</sub> nanosheets for tumor therapy and tissue regeneration. (2017). doi:10.1038/am.2017.47
134. Manuscript, A. & Biodegradable, T. N.-R. NIH Public Access. **14**, 900–909 (2014).
135. Yin, W. *et al.* High-throughput synthesis of single-layer MoS<sub>2</sub> nanosheets as a near-infrared photothermal-triggered drug delivery for effective cancer therapy. *ACS Nano* **8**, 6922–6933 (2014).
136. Kim, J., Kim, H. & Kim, W. J. Single-Layered MoS<sub>2</sub> – PEI – PEG Nanocomposite-Mediated Gene Delivery Controlled by Photo and Redox Stimuli. 1184–1192 (2016). doi:10.1002/sml.201501655
137. Chen, Y., Wang, L. & Shi, J. Nano Today Two-dimensional non-carbonaceous materials-enabled efficient photothermal cancer therapy. **11**, 292–308 (2016).
138. Kalantar-zadeh, K. *et al.* Two-Dimensional Transition Metal Dichalcogenides in Biosystems. 5086–5099 (2015). doi:10.1002/adfm.201500891
139. Rao, C. N. R., Matte, H. S. S. R. & Maitra, U. Graphene Analogues of Inorganic Layered Materials *Angewandte*. 2–27 (2013). doi:10.1002/anie.201301548
140. Chen, X. & McDonald, A. R. Functionalization of Two-Dimensional Transition-Metal Dichalcogenides. 5738–5746 (2016). doi:10.1002/adma.201505345
141. Presolski, S. & Pumera, M. Covalent functionalization of MoS<sub>2</sub>. **19**, 140–145 (2016).
142. Yan, L., Zhao, F., Li, S. & Zhao, Y. Low-toxic and safe nanomaterials by surface-chemical design , carbon nanotubes , fullerenes , metallofullerenes , and graphenes. (2011). doi:10.1039/c0nr00647e
143. Liu, X. *et al.* CuS nanocomposites as a difunctional nanoplatform for targeted chemophotothermal therapy of cancer cells †. 5358–5367 (2014). doi:10.1039/c4tb00919c

144. Shen, H., Zhang, L., Liu, M. & Zhang, Z. Biomedical applications of graphene. *Theranostics* **2**, 283–294 (2012).
145. Sun, T. *et al.* Engineered Nanoparticles for Drug Delivery in Cancer Therapy *Angewandte*. 12320–12364 (2014). doi:10.1002/anie.201403036
146. Chen, Y., Tan, C., Zhang, H. & Wang, L. Two-dimensional graphene analogues for biomedical applications. *Chemical Society Reviews* **44**, 2681–2701 (2015).
147. Wang, L. *et al.* Use of Synchrotron Radiation- Analytical Techniques To Reveal Chemical Origin of Silver-Nanoparticle. 6532–6547 (2015). doi:10.1021/acsnano.5b02483
148. Wang, L. *et al.* Revealing the Binding Structure of the Protein Corona on Gold Nanorods Using Synchrotron Radiation-Based Techniques : Understanding the Reduced Damage in Cell Membranes. (2013). doi:10.1021/ja406924v
149. Teo, W. Z., Chng, E. L. K., Sofer, Z. & Pumera, M. Cytotoxicity of exfoliated transition-metal dichalcogenides (MoS<sub>2</sub>, WS<sub>2</sub>, and WSe<sub>2</sub>) is lower than that of graphene and its analogues. *Chem. - A Eur. J.* **20**, 9627–9632 (2014).
150. Liu, T. *et al.* Ultra-small MoS<sub>2</sub> nanodots with rapid body clearance for photothermal cancer therapy. **9**, 3003–3017 (2016).
151. Appel, J. H. *et al.* Low Cytotoxicity and Genotoxicity of Two-Dimensional MoS<sub>2</sub> and WS<sub>2</sub>. (2016). doi:10.1021/acsbiomaterials.5b00467
152. Mo, M. S. M. *et al.* In Vivo Long-Term Biodistribution , Excretion , and Toxicology of PEGylated Transition-Metal Dichalcogenides. **2**, (2017).
153. Chen, Z., Sun, W., Butt, H. & Wu, S. Upconverting-Nanoparticle-Assisted Photochemistry Induced by Low-Intensity Near-Infrared Light : How Low Can We Go? 9165–9170 (2015). doi:10.1002/chem.201500108
154. P. Reineck, A. Francis, A. Orth, D. W. M. Lau, R. D. V. Nixon-Luke, I. Das Rastogi, W. A. W. Razali, N. M. Cordina, L. M. Parker, V. K. A. Sreenivasan, L. J. Brown and B. C. Gibson, *Adv. Opt. Mater.*, 2016, 4, 1549–1557.pdf.

155. Ahmad, I., Ahmed, S., Anwar, Z., Sheraz, M. A. & Sikorski, M. Photostability and Photostabilization of Drugs and Drug Products. **2016**, (2016).
156. Wu, S. *et al.* Electrochemically Reduced Single-Layer MoS<sub>2</sub> Nanosheets: Characterization, Properties, and Sensing Applications. 2264–2270 (2012). doi:10.1002/sml.201200044
157. Mos, D. N. A. Materials Chemistry B. 625–628 (2014). doi:10.1039/c3tb21570a
158. Lopez-Sanchez, O., Lembke, D., Kayci, M., Radenovic, A. & Kis, A. Ultrasensitive photodetectors based on monolayer MoS<sub>2</sub>. *Nat. Nanotechnol.* **8**, 497–501 (2013).
159. Biosensors, G. L. *et al.* MoS<sub>2</sub> Field-Effect Transistor for Next-. 3992–4003 (2014). doi:10.1021/nn5009148
160. Mos, T., Ghatak, S., Pal, A. N. & Ghosh, A. Nature of Electronic States in Atomically. 7707–7712 (2011). doi:10.1021/nn202852j
161. Yang, X. *et al.* Antibacterial activity of two-dimensional MoS<sub>2</sub> sheets. *Nanoscale* **6**, 10126–10133 (2014).
162. Liu, T. *et al.* Nanoscale Combined photothermal and photodynamic therapy delivered by PEGylated MoS<sub>2</sub> nanosheets †. 11219–11225 (2014). doi:10.1039/c4nr03753g
163. Xu, S., Li, D. & Wu, P. One-Pot, Facile, and Versatile Synthesis of Monolayer MoS<sub>2</sub> / WS<sub>2</sub> Quantum Dots as Bioimaging Probes and Efficient Electrocatalysts for Hydrogen Evolution Reaction. 1127–1136 (2015). doi:10.1002/adfm.201403863
164. Wang, N. *et al.* Synthesis of Strongly Fluorescent Molybdenum Disulfide Nanosheets for Cell-Targeted Labeling. (2014). doi:10.1021/am505305g
165. Cheng, L. *et al.* PEGylated WS<sub>2</sub> Nanosheets as a Multifunctional Theranostic Agent for in vivo Dual-Modal CT / Photoacoustic Imaging Guided Photothermal Therapy. 1886–1893 (2014). doi:10.1002/adma.201304497
166. Tan, C. & Zhang, H. Two-dimensional transition metal dichalcogenide nanosheet-based composites. *Chem. Soc. Rev.* **44**, 2713–2731 (2015).

167. Yuan, Y., Li, R. & Liu, Z. Establishing water-soluble layered WS<sub>2</sub> nanosheet as a platform for biosensing. *Anal. Chem.* **86**, 3610–3615 (2014).
168. Xie, X. *et al.* Low-Frequency Noise in Bilayer MoS<sub>2</sub>. 5633–5640 (2014). doi:10.1021/nm4066473
169. Xi, Q. *et al.* Highly Sensitive and Selective Strategy for MicroRNA Detection Based on WS<sub>2</sub> Nanosheet Mediated Fluorescence Quenching and Duplex-Specific Nuclease Signal Amplification. (2014). doi:10.1021/ac403944c
170. Tan, C. *et al.* Single-Layer Transition Metal Dichalcogenide Nanosheet-Assisted Assembly of Aggregation-Induced Emission Molecules to Form Organic Nanosheets with Enhanced Fluorescence. 1735–1739 (2014). doi:10.1002/adma.201304562
171. Wang, Q. H., Kalantar-zadeh, K., Kis, A., Coleman, J. N. & Strano, M. S. transition metal dichalcogenides. *Nat. Publ. Gr.* **7**, 699–712 (2012).
172. Huang, X. *et al.* Coating Two-Dimensional Nanomaterials with Metal–Organic Frameworks. 8695–8701 (2014). doi:10.1021/nm503834u
173. Yin, Z. *et al.* Angewandte Preparation of MoS<sub>2</sub>–MoO<sub>3</sub> Hybrid Nanomaterials for Light-Emitting Diodes \*\*. 12560–12565 (2014). doi:10.1002/anie.201402935
174. Osada, M. & Sasaki, T. Exfoliated oxide nanosheets : new solution to nanoelectronics †. 2503–2511 (2009). doi:10.1039/b820160a
175. Nos, S., Joensen, P., Frindt, R. F. & Morrison, S. R. 0025-5408 / 86 \$ 3 . 00 + . 00 C o p y r i g h t ( c ) 1986 P e r g a m o n P r e s s L t d . ( Received January by A . Wold ). **21**, 457–461 (1986).
176. Frindt, R. F. Single Crystals of MoS<sub>2</sub> Several Molecular Layers Thick. **1928**, 13–15 (1966).
177. Structures, B. OCTOBER 1973 Band Structures. **8**, (1973).
178. Py, A. Structural destabilization induced by lithium intercalation in MoS<sub>2</sub> and related compounds. (1982).

179. Weiss, K. & Phillips, J. M. Calculated specific surface energy of molybdenite (MoS<sub>2</sub>). *Phys. Rev. B* **14**, 5392–5395 (1976).
180. Downloaded, M., Studi, D. & Li, F. *Chem Soc Rev.* 6006–6018 (2013). doi:10.1039/c3cs60113g
181. Novoselov, K. S. *et al.* Two-dimensional atomic crystals. *Proc. Natl. Acad. Sci.* **102**, 10451–10453 (2005).
182. Ataca, C. & Ciraci, S. Stable, Single-Layer MX<sub>2</sub> Transition-Metal Oxides and Dichalcogenides in a Honeycomb-Like Structure. (2012). doi:10.1021/jp212558p
183. Agraït, N. & Agraït, N. Optical identification of atomically thin dichalcogenide crystals. **213116**, 94–97 (2010).
184. Castellanos-gomez, A. *et al.* Fast and reliable identification of atomically thin layers of TaSe<sub>2</sub> crystals. **6**, 191–199 (2013).
185. Yu Y, Jiang SL, Zhang GZ, Zhou WL, Miao XS, Zeng YK, et al. Universal ultrafast sandpaper assisting rubbing method for room temperature fabrication of two-dimensional nanosheets directly on flexible polymer substrate. App.pdf.
186. Liu, W. *et al.* Role of Metal Contacts in Designing High-Performance Monolayer n - Type WSe<sub>2</sub> Field Effect Transistors. (2013). doi:10.1021/nl304777e
187. Lee, H. S. *et al.* MoS<sub>2</sub> Nanosheet Phototransistors with Thickness-Modulated Optical Energy Gap. (2012). doi:10.1021/nl301485q
188. Radisavljevic, B., Whitwick, M. B. & Kis, A. Integrated Circuits and Logic Operations Based on Single-Layer MoS<sub>2</sub>. 9934–9938 (2011). doi:10.1021/nn203715c
189. Kim, S. *et al.* based on multilayer MoS<sub>2</sub> crystals. *Nat. Commun.* (2012). doi:10.1038/ncomms2018
190. Larentis, S. *et al.* Field-effect transistors and intrinsic mobility in ultra-thin MoSe<sub>2</sub> layers. **223104**, (2013).

191. Lee, H. S. *et al.* MoS<sub>2</sub> Nanosheets for Top-Gate Nonvolatile Memory Transistor Channel. 3111–3115 (2012). doi:10.1002/sml.201200752
192. Lembke, D. & Kis, A. Breakdown of High-Performance Monolayer MoS<sub>2</sub> Transistors. 10070–10075 (2012). doi:10.1021/nl303772b
193. Li, H. *et al.* Fabrication of single- and multilayer MoS<sub>2</sub> film-based field-effect transistors for sensing NO at room temperature. *Small* **8**, 63–67 (2012).
194. Qiu H, Pan L, Yao Z, Li J, Shi Y, Wang X. Electrical characterization of back-gated bilayer MoS<sub>2</sub> field-effect transistors and the effect of ambient on their performances. *Appl Phys Lett* 2012;100. 123104-3.pdf.
195. Buscema, M. *et al.* Large and Tunable Photothermoelectric Effect in Single-Layer MoS<sub>2</sub>. (2013). doi:10.1021/nl303321g
196. Castellanos-gomez, A., Rolda, R., Cappelluti, E. & Buscema, M. Local Strain Engineering in Atomically Thin MoS<sub>2</sub>. (2013). doi:10.1021/nl402875m
197. Novoselov, K. S. & Castro Neto, A. H. Two-dimensional crystals-based heterostructures: Materials with tailored properties. *Phys. Scr.* (2012). doi:10.1088/0031-8949/2012/T146/014006
198. Brent, J. R., Savjani, N. & Brien, P. O. Progress in Materials Science Synthetic approaches to two-dimensional transition metal dichalcogenide nanosheets. *Prog. Mater. Sci.* **89**, 411–478 (2017).
199. Chen, Z. *et al.* Core–shell MoO<sub>3</sub>–MoS<sub>2</sub> Nanowires for Hydrogen Evolution : 4168–4175 (2011). doi:10.1021/nl2020476
200. Whittingham, M. S. & Jr, F. R. G. No Title. **i**, (1975).
201. Wang, Y. *et al.* Electrochemical Control of Photoluminescence in Two-Dimensional MoS<sub>2</sub> Nanoflakes. 10083–10093 (2013). doi:10.1021/nl4041987
202. Cha, J. J. *et al.* Two-Dimensional Chalcogenide Nanoplates as Tunable Metamaterials via Chemical Intercalation. 5–10 (2013). doi:10.1021/nl402937g

203. Liu, H. *et al.* Self-Stacked, Small-Sized MoS<sub>2</sub> Nanosheets for High-Performance Lithium-Ion Batteries. *Energy Technol.* **5**, 2039–2045 (2017).
204. Whittingham, M. S. *CHEMISTRY OF INTERCALATION COMPOUNDS: METAL GUESTS IN CHALCOGENIDE HOSTS.* **12**, (1978).
205. Bang, G. S. *et al.* Effective Liquid-Phase Exfoliation and Sodium Ion Battery Application of MoS<sub>2</sub> Nanosheets. 2–7 (2014). doi:10.1021/am4060222
206. Dines, M. B. No Title. **I**, 87–91 (1975).
207. Yang, D. & Frindt, R. F. Li-INTERCALATION AND EXFOLIATION OF WS<sub>2</sub>. **57**, 1113–1116 (1996).
208. Gordon, R. A., Yang, D., Crozier, E. D., Jiang, D. T. & Frindt, R. F. Structures of exfoliated single layers of WS<sub>2</sub>, MoS<sub>2</sub>, and MoSe<sub>2</sub> in aqueous suspension. **65**, 1–9 (2002).
209. Golub AS, Protsenko GA, Gumileva LV, Buyanovskaya AG, Novikov YN. The formation of intercalation compounds of MoS<sub>2</sub> with cations of alkali metals and alkylammonium from monolayer dispersion of molybdenum disulfide. Russ Ch.pdf.
210. Golub AS, Protzenko GA, Yanovskaya IM, Lependina OL, Novikov YN. New intercalation compounds of molybdenum disulfide with transition metals, Az(H<sub>2</sub>O)<sub>y</sub>MoS<sub>2</sub> (A Fe, Co, Ni, Y, La, Er, Th). Mendeleev Commun 1993;3199–200.pdf.
211. Golub, A. S., Zubavichus, Y. V, Slovokhotov, Y. L. & Novikov, Y. N. Single-layer dispersions of transition metal dichalcogenides in the synthesis of intercalation compounds. **72**, (2003).
212. Miremadi, B. K., Morrison, S. R., Miremadi, B. K. & Morrison, S. R. The intercalation and exfoliation of tungsten disulfide. **4970**, (1988).
213. Murphy DW, Di Salvo FJ, Hull GW, Waszczak JV. Convenient preparation and physical properties of lithium intercalation compounds of Group 4B and 5B layered transition metal dichalcogenides. Inorg Chem 1976;1517–21].pdf.

214. Zeng, Z. *et al.* Single-layer semiconducting nanosheets: High-yield preparation and device fabrication. *Angew. Chemie - Int. Ed.* **50**, 11093–11097 (2011).
215. Tan, S. M., Luxa, J. & Pumera, M. Aromatic-Exfoliated Transition Metal Dichalcogenides: Implications for Inherent Electrochemistry and Hydrogen Evolution. (2016). doi:10.1021/acscatal.6b00761
216. Lukowski, M. A. *et al.* Enhanced Hydrogen Evolution Catalysis from Chemically Exfoliated Metallic MoS<sub>2</sub> Nanosheets. 1–4 (2013). doi:10.1021/ja404523s
217. Lukowski, M. A. *et al.* Environmental Science. 2608–2613 (2014). doi:10.1039/c4ee01329h
218. Yuwen, L. *et al.* ChemComm Rapid preparation of single-layer transition metal dichalcogenide nanosheets via ultrasonication enhanced lithium intercalation †‡. 529–532 (2016). doi:10.1039/c5cc07301d
219. Je, A. A., Nethravathi, C. & Rajamathi, M. Two-Dimensional Nanosheets and Layered Hybrids of MoS<sub>2</sub> and WS<sub>2</sub> through Exfoliation of Ammoniated MS<sub>2</sub> (M = Mo, W). **2**, (2014).
220. Rasamani, K. D., Alimohammadi, F. & Sun, Y. Interlayer-expanded MoS<sub>2</sub>. *Mater. Today* **20**, 83–91 (2017).
221. Hernandez, Y. *et al.* High-yield production of graphene by liquid-phase exfoliation of graphite. *Nat. Nanotechnol.* **3**, 563–568 (2008).
222. Chem, J. M., Cai, M., Thorpe, D., Adamson, H. & Schniepp, H. C. Methods of graphite exfoliation. 24992–25002 (2012). doi:10.1039/c2jm34517j
223. Jaber-ansari, L. & Hersam, M. C. Solution-processed graphene materials and composites. 1167–1176 (2020). doi:10.1557/mrs.2012.182
224. Coleman, J. N. Liquid Exfoliation of Defect-Free Graphene. **46**, (2013).
225. Du, W. & Zhu, L. exfoliation of graphite to produce single- and few-. 10592–10606 (2013). doi:10.1039/c3ta12212c

226. Ciesielski, A. & Samorì, P. *Chem Soc Rev.* 381–398 (2014). doi:10.1039/c3cs60217f
227. Texter, J. *Current Opinion in Colloid & Interface Science Graphene dispersions* ☆. *Curr. Opin. Colloid Interface Sci.* **19**, 163–174 (2014).
228. Wei, Y. & Sun, Z. *Current Opinion in Colloid & Interface Science Liquid-phase exfoliation of graphite for mass production of pristine few-layer graphene.* *Curr. Opin. Colloid Interface Sci.* **20**, 311–321 (2015).
229. Niu, L., Coleman, J. N., Zhang, H., Shin, H. & Chhowalla, M. *Production of Two-Dimensional Nanomaterials via Liquid-Based Direct Exfoliation.* 272–293 (2016). doi:10.1002/sml.201502207
230. Godwin, I., Rovetta, A., Lyons, M. E. G. & Duesberg, S. *Nanoscale.* 5737–5749 (2016). doi:10.1039/c5nr08553e
231. Two-dimensional, F. L. *et al.* *Functionalization of Liquid-Exfoliated Two-Dimensional 2H-MoS<sub>2</sub>* \*\*. 2638–2642 (2015). doi:10.1002/anie.201409412
232. Lei, Z., Zhou, Y. & Wu, P. *Simultaneous Exfoliation and Functionalization of MoSe<sub>2</sub> Nanosheets to Prepare ‘ Smart ’ Nanocomposite Hydrogels with Tunable Dual Stimuli-Responsive Behavior.* 3112–3118 (2016). doi:10.1002/sml.201600727
233. Shen, Z., Li, J., Yi, M. & Zhang, X. *Preparation of graphene by jet cavitation.* (2011). doi:10.1088/0957-4484/22/36/365306
234. Stoffel, B. & Sirok, B. *Development of a cavitation erosion model.* **261**, 642–655 (2006).
235. Lohse, D. & Wittenberg, C. *Cavitation hots up.* **434**, (2005).
236. Jinzhi, L. I. *et al.* *Experimental study on a designed jet cavitation device for producing two-dimensional nanosheets.* **55**, 2815–2819 (2012).
237. Yao, Y. *et al.* *Large-scale production of two-dimensional nanosheets.* *J. Mater. Chem.* **22**, 13494 (2012).
238. Khan, U. *et al.* *Solvent-Exfoliated Graphene at Extremely High Concentration.* 9077–

- 9082 (2011). doi:10.1021/la201797h
239. Online, V. A. Nanoscale Strongly luminescent monolayered MoS<sub>2</sub> prepared by effective ultrasound exfoliation. 3387–3394 (2013). doi:10.1039/c3nr00192j
240. Online, V. A. *et al.* Efficient liquid-exfoliation of MoS<sub>2</sub> nanosheets. 50981–50987 (2014). doi:10.1039/c4ra09001b
241. Zhang, S., Choi, H., Yue, H. & Yang, W. Controlled exfoliation of molybdenum disulfide for developing thin film humidity sensor. **14**, 264–268 (2014).
242. Hanlon, D. *et al.* Production of Molybdenum Trioxide Nanosheets by Liquid Exfoliation and Their Application in High-Performance Supercapacitors. (2014). doi:10.1021/cm500271u
243. Hanlon, D. *et al.* electronics. (2015). doi:10.1038/ncomms9563
244. Duclaux, L., Alvarez, L. & Hawełek, Ł. Cleavage and size reduction of graphite crystal using ultrasound radiation. **5**, (2012).
245. Varrla, E. *et al.* Large-scale production of size-controlled MoS<sub>2</sub> nanosheets by shear exfoliation. *Chem. Mater.* **27**, 1129–1139 (2015).
246. Cunningham, G. *et al.* Solvent exfoliation of transition metal dichalcogenides: Dispersibility of exfoliated nanosheets varies only weakly between compounds. *ACS Nano* **6**, 3468–3480 (2012).
247. Smith, R. J. *et al.* Large-scale exfoliation of inorganic layered compounds in aqueous surfactant solutions. *Adv. Mater.* **23**, 3944–3948 (2011).
248. Varrla, E. *et al.* Nanoscale using household detergent and a kitchen blender †. 11810–11819 (2014). doi:10.1039/c4nr03560g
249. Yi, M. Letter to the Editor Kitchen blender for producing high-quality few-layer graphene. *Carbon N. Y.* **78**, 622–626 (2014).
250. Boland, J. B. *et al.* Nanoscale Advances lithium ion battery applications †. 1560–1570

- (2019). doi:10.1039/c8na00241j
251. Hanlon, D. *et al.* Production of Molybdenum Trioxide Nanosheets by Liquid Exfoliation and their Application in High Performance Supercapacitors. 1–35
  252. Harvey, A.; Backes, C.; Gholamvand, Z.; Hanlon, D.; McAteer, D.; Nerl, H. C.; McGuire, E.; Seral-Ascaso, A.; Ramasse, Q. M.; McEvoy, N.; Winters, S.; Berner, N. C.; McCloskey, D.; Donegan, J. F.; Duesberg, G. S.; Nicolosi.pdf.
  253. E. Petroni, E. Lago, S. Bellani, D. W. Boukhvalov, A. Politano, B. Gürbulak, S. Duman, M. Prato, S. Gentiluomo, R. Oropesa-Nuñez, J.-K. Panda, P. S. Toth, A. E. Del Rio Castillo, V. Pellegrini, F. Bonaccorso, *Small* 2018, 1.pdf.
  254. Brent, J. R. *et al.* Tin(II) Sul fi de (SnS) Nanosheets by Liquid-Phase Exfoliation of Herzenbergite: IV – VI Main Group Two-Dimensional Atomic Crystals. (2015). doi:10.1021/jacs.5b08236
  255. Harvey, A. *et al.* Exploring the versatility of liquid phase exfoliation : producing 2D nanosheets from talcum powder , cat litter and beach sand Exploring the versatility of liquid phase exfoliation : producing 2D nanosheets from talcum powder , cat litter and beach sand. (2017).
  256. Harvey, A.; He, X.; Godwin, I. J.; Backes, C.; McAteer, D.; Berner, N. C.; McEvoy, N.; Ferguson, A.; Shmeliov, A.; Lyons, M. E. G.; Nicolosi, V.; Duesberg, G. S.; Donegan, J. F.; Coleman, J. N. Production of Ni(OH)<sub>2</sub> nanos.pdf.
  257. D. McAteer, I. J. Godwin, Z. Ling, A. Harvey, L. He, C. S. Boland, V. Vega- Mayoral, B. Szydłowska, A. A. Rovetta, C. Backes, J. B. Boland, X. Chen, M. E. G. Lyons, J. N. Coleman, *Adv. En. Mater.* 2018, 1702965.pdf.
  258. Finn, D. J. *et al.* MoS<sub>2</sub> nanosheets for printed device applications †. 925–932 (2014). doi:10.1039/c3tc31993h
  259. Torrisi, F. *et al.* Inkjet-Printed Graphene Electronics. 2992–3006 (2012). doi:10.1021/nn2044609

260. Mendoza-sánchez, B., Coelho, J., Pokle, A. & Nicolosi, V. Electrochimica Acta A 2D graphene-manganese oxide nanosheet hybrid synthesized by a single step liquid-phase co-exfoliation method for supercapacitor applications. *Electrochim. Acta* **174**, 696–705 (2015).
261. Chem, J. M. *et al.* Mechanically strong and highly conductive graphene aerogel and its use as electrodes for electrochemical power sources †. 6494–6497 (2011). doi:10.1039/c1jm10239g
262. Hu, G. *et al.* Chem Soc Rev. 3265–3300 (2018). doi:10.1039/c8cs00084k
263. Bonaccorso, F., Bartolotta, A., Coleman, J. N., Backes, C. & Vi, I. I. I. 2D-Crystal-Based Functional Inks. 6136–6166 (2016). doi:10.1002/adma.201506410
264. Bonaccorso, F. *et al.* energy conversion and storage. **347**, (2015).
265. Balaji, V., Lau, K., Hui, D. & Bhattacharyya, D. Graphene-based materials and their composites : A review on production , applications and product limitations. *Compos. Part B* **142**, 200–220 (2018).
266. Materials, G., Cravotto, G. & Cintas, P. Sonication-Assisted Fabrication and Post-Synthetic Modifications of. 5246–5259 (2010). doi:10.1002/chem.200903259
267. Han, J. T. *et al.* Extremely Efficient Liquid Exfoliation and Dispersion of Layered Materials by Unusual Acoustic Cavitation. 1–7 (2014). doi:10.1038/srep05133
268. Václav, Š., Slu, M. & Ecorchard, P. Ultrasound exfoliation of inorganic analogues of graphene. 1–14 (2014).
269. Villar-rodil, S., Mart, A. & Tasc, J. M. D. RSC Advances Production of aqueous dispersions of inorganic graphene analogues by exfoliation and stabilization with non-ionic surfactants †. 14115–14127 (2014). doi:10.1039/c4ra00212a
270. Zhao, G., Wu, Y., Shao, Y. & Hao, X. Nanoscale. 5407–5411 (2016). doi:10.1039/c5nr07950k
271. Jawaid, A. *et al.* Mechanism for Liquid Phase Exfoliation of MoS<sub>2</sub>. *Chem. Mater.* **28**,

- 337–348 (2016).
272. Muscuso, L., Cravanzola, S., Cesano, F., Scarano, D. & Zecchina, A. Optical , Vibrational , and Structural Properties of MoS<sub>2</sub> Nanoparticles Obtained by Exfoliation and Fragmentation via Ultrasound Cavitation in Isopropyl Alcohol. (2015). doi:10.1021/jp511973k
273. Jin, B., Bang, H. & Suslick, K. S. Applications of Ultrasound to the Synthesis of Nanostructured Materials. 1039–1059 (2010). doi:10.1002/adma.200904093
274. Xu, H., Zeiger, B. W. & Suslick, K. S. Chem Soc Rev. 2555–2567 (2013). doi:10.1039/c2cs35282f
275. Ashokkumar, M., Lee, J., Kentish, S. & Grieser, F. Bubbles in an acoustic field: An overview. **14**, 470–475 (2007).
276. Sutkar, V. S. & Gogate, P. R. Design aspects of sonochemical reactors : Techniques for understanding cavitation activity distribution and effect of operating parameters. **155**, 26–36 (2009).
277. Baranchikov, A. Y., Chem, R., Baranchikov, A. Y., Ivanov, V. K. & Tretyakov, Y. D. Related content Sonochemical synthesis of inorganic materials Sonochemical synthesis of inorganic materials. (2007). doi:10.1070/RC2007v076n02ABEH003644
278. Ma, H., Shen, Z. & Ben, S. Understanding the exfoliation and dispersion of MoS<sub>2</sub> nanosheets in pure water. *J. Colloid Interface Sci.* **517**, 204–212 (2018).
279. O'Neill, A., Khan, U. & Coleman, J. N. Preparation of high concentration dispersions of exfoliated MoS<sub>2</sub> with increased flake size. *Chem. Mater.* **24**, 2414–2421 (2012).
280. Hughes, J. M., Aherne, D. & Coleman, J. N. Generalizing Solubility Parameter Theory to Apply to One- and Two-Dimensional Solutes and to Incorporate Dipolar Interactions. 4483–4491 (2013). doi:10.1002/app.38051
281. Zhou, K. G., Mao, N. N., Wang, H. X., Peng, Y. & Zhang, H. L. A mixed-solvent strategy for efficient exfoliation of inorganic graphene analogues. *Angew. Chemie - Int. Ed.* **50**,

- 10839–10842 (2011).
282. Shen, J. *et al.* Surface Tension Components Based Selection of Cosolvents for Efficient Liquid Phase Exfoliation of 2D Materials. 2741–2749 (2016). doi:10.1002/sml.201503834
283. Shen, J. *et al.* Liquid Phase Exfoliation of Two-Dimensional Materials by Directly Probing and Matching Surface Tension Components. *Nano Lett.* **15**, 5449–5454 (2015).
284. Halim, U. *et al.* materials by directly probing liquid – solid interaction. *Nat. Commun.* 1–7 (2013). doi:10.1038/ncomms3213
285. Hernandez, Y., Lotya, M., Rickard, D., Bergin, S. D. & Coleman, J. N. Measurement of Multicomponent Solubility Parameters for Graphene Facilitates Solvent Discovery. **3**, 3208–3213 (2010).
286. Feng, J. *et al.* Giant Moisture Responsiveness of VS 2 Ultrathin Nanosheets for Novel Touchless Positioning Interface. 1969–1974 (2012). doi:10.1002/adma.201104681
287. Schilliger-musset, O. C. Inclusion of substances of very high concern in the Candidate List for eventual inclusion in Annex XIV ( Decision of the European Chemicals Agency ) Validity : Indefinite Quality Manager. **1**, 3–6 (2020).
288. Gambhir, S., Murray, E., Sayyar, S., Wallace, G. G. & Officer, D. L. Anhydrous organic dispersions of highly reduced chemically converted graphene. *Carbon N. Y.* **76**, 368–377 (2014).
289. Liu, G. *et al.* Hydrazine-Assisted Liquid Exfoliation of MoS 2 for Catalytic Hydrodeoxygenation of 4-Methylphenol. **430072**, 2910–2914 (2016).
290. Wang, B., Kalia, R. K., Nakano, A. & Vashishta, P. D. Dewetting of monolayer water and isopropanol between MoS 2 nanosheets. *Sci. Rep.* 1–6 (2018). doi:10.1038/s41598-018-35163-3
291. Castillo, A. E. D. R. *et al.* Materials Horizons. 890–904 (2018). doi:10.1039/c8mh00487k
292. Damm, C., Nacken, T. J. & Peukert, W. Quantitative evaluation of delamination of

- graphite by wet media milling. *Carbon N. Y.* **81**, 284–294 (2014).
293. Quintana, M., Herrero, M. A. & Fierro, J. L. G. ChemComm Few-layer graphenes from ball-milling of graphite with melamine w z. 10936–10938 (2011). doi:10.1039/c1cc14595a
294. Nacken, T. J., Damm, C., Xing, H., Rüger, A. & Peukert, W. Determination of quantitative structure – property and structure – process relationships for graphene production in water. **8**, 1865–1881 (2015).
295. Online, V. A. *et al.* Nanoscale nitride nanosheets and their application in improving composites †. 10660–10667 (2013). doi:10.1039/c3nr03714b
296. Liu, L., Shen, Z., Yi, M., Zhang, X. & Ma, S. RSC Advances. 36464–36470 (2014). doi:10.1039/c4ra05635c
297. Liang, S., Yi, M., Shen, Z., Liu, L. & Ma, S. by fluid-based method. 16127–16131 (2014). doi:10.1039/c4ra01250j
298. Li, Y., Yin, X. & Wu, W. Preparation of Few-Layer MoS<sub>2</sub>Nanosheets via an Efficient Shearing Exfoliation Method. *Ind. Eng. Chem. Res.* **57**, 2838–2846 (2018).
299. Backes, C. *et al.* Guidelines for Exfoliation, Characterization and Processing of Layered Materials Produced by Liquid Exfoliation. *Chem. Mater.* **29**, 243–255 (2017).
300. Lotya, M., King, P. J., Khan, U., De, S. & Coleman, J. N. High-Concentration, Surfactant-Stabilized Graphene Dispersions. **4**, 3155–3162 (2010).
301. Turner, P., Hodnett, M., Dorey, R. & Carey, J. D. Controlled Sonication as a Route to in-situ Graphene Flake Size Control. *Sci. Rep.* 1–8 (2019). doi:10.1038/s41598-019-45059-5
302. Liu, J. *et al.* Preparation of MoS<sub>2</sub>-Polyvinylpyrrolidone Nanocomposites for Flexible Nonvolatile Rewritable Memory Devices with Reduced Graphene Oxide Electrodes. 3517–3522 (2012). doi:10.1002/sml.201200999
303. Notley, S. M. Highly Concentrated Aqueous Suspensions of Graphene through Ultrasonic Exfoliation with Continuous Surfactant Addition. 14110–14113 (2012).

doi:10.1021/la302750e

304. Guardia, L. *et al.* High-throughput production of pristine graphene in an aqueous dispersion assisted by non-ionic surfactants. *Carbon N. Y.* **49**, 1653–1662 (2011).
305. Zu, S. & Han, B. Aqueous Dispersion of Graphene Sheets Stabilized by Pluronic Copolymers : Formation of. 13651–13657 (2009).
306. Chae, A. *et al.* Dielectric nanosheets made by liquid-phase exfoliation in water and their use in graphene- based electronics Dielectric nanosheets made by liquid-phase exfoliation in water and their use in graphene-based electronics. (2014). doi:10.1088/2053-1583/1/1/011012
307. Anbazhagan, R., Wang, H., Tsai, H. & Jeng, R. Highly concentrated MoS<sub>2</sub> nanosheets in water achieved by thioglycolic acid as stabilizer and used as biomarkers †. 42936–42941 (2014). doi:10.1039/c4ra07512a
308. Online, V. A., Sham, A. Y. W. & Notley, S. M. *Soft Matter*. 6645–6653 (2013). doi:10.1039/c3sm00092c
309. Ch, E. Preparation of Nanosheets by Ultrasonic Exfoliation with the Aid of Surfactant Poly(vinylpyrrolidone). 732–734 (2012). doi:10.1246/cl.2012.732
310. May, P., Khan, U., Hughes, J. M. & Coleman, J. N. Role of solubility parameters in understanding the steric stabilization of exfoliated two-dimensional nanosheets by adsorbed polymers. *J. Phys. Chem. C* **116**, 11393–11400 (2012).
311. Bissessur, R., Gallant, D. & Brüning, R. Novel nanocomposite material consisting of poly [oxymethylene- (oxyethylene)] and molybdenum disulfide. **82**, 316–320 (2003).
312. Zhou, K. *et al.* Facile preparation of poly (methyl methacrylate) / MoS<sub>2</sub> nanocomposites via in situ emulsion polymerization. *Mater. Lett.* **126**, 159–161 (2014).
313. Photocatalysis, V., Quinn, M. D. J., Ho, N. H. & Notley, S. M. Aqueous Dispersions of Exfoliated Molybdenum Disulfide for Use in Visible-Light Photocatalysis. (2013). doi:10.1021/am404161k

314. Backes, C. *et al.* Edge and confinement effects allow in situ measurement of size and thickness of liquid-exfoliated nanosheets. *Nat. Commun.* **5**, 1–10 (2014).
315. Torrisi, F. & Coleman, J. N. Electrifying inks with 2D materials Charging graphene for energy. *Nat. Publ. Gr.* **9**, 738–739 (2014).
316. Nanocatalysts, M. *et al.* Identification of Active Edge Sites for Electrochemical H<sub>2</sub> Evolution from. **317**, 100–103 (2007).
317. Chem, J. M., May, P., Khan, U., Neill, A. O. & Coleman, J. N. Approaching the theoretical limit for reinforcing polymers with graphene †. 1278–1282 (2012). doi:10.1039/c1jm15467b
318. Kang, J.; Seo, J.-W. T.; Alducin, D.; Ponce, A.; Yacaman, M. J.; Hersam, M. C. Thickness Sorting of Two-Dimensional Transition Metal Dichalcogenides via Copolymer-Assisted Density Gradient Ultracentrifugation. *Nat. Commun.*pdf.
319. Backes, C. *et al.* Production of highly monolayer enriched dispersions of liquid-exfoliated nanosheets by liquid cascade centrifugation. *ACS Nano* **10**, 1589–1601 (2016).
320. Backes, C.; Paton, K. R.; Hanlon, D.; Yuan, S.; Katsnelson, M. I.; Houston, J.; Smith, R. J.; McCloskey, D.; Donegan, J. F.; Coleman, J. N. Spectroscopic metrics allow in situ measurement of mean size and thickness of liq.pdf.



## **2.5. Characterization Tools**

### **2.5.1. Introduction**

For so many decades, the involvement of nanotechnology has given wonders to the society worldwide. The use of different nanomaterials or nanostructures have attracted a great attention in scientific and subsequently in commercial field. For the last twenty years or so, over dozens of Nobel Prize have been awarded for the significant discovery of different nanomaterials, characterization techniques and so on. On one hand, a wide number of fabrication protocols exist for the synthesis of different nanomaterials, there is an equal need to analyze those materials with novel characterization tools to understand their structure, morphology, elemental composition, chemical changes and a broad range of other physical properties in depth. A reliable characterization analysis of any fabricated nanomaterial will enhance the reproducibility in the fabrication process of nanomaterials for the intended application in focus. The increasing demand of novel nanomaterials worldwide demands a smooth and easily accessible characterization process to circumvent the inadequacy in analyzing different samples for various reasons such as the inherent difficulty of nanomaterials or nanostructures (too small size, too less concentration, less quantity and so on) to be examined appropriately<sup>[1]</sup>. So, material properties analyses, flaws in the fabrication procedure, optimization of characterization protocol depending on the type of nanomaterial or bulk to name a few, are important to get a deep insight into the multi-disciplinary field of nanoscience and nanotechnology.

Particularly, in this chapter I will explain the working principle of only those characterization tools which I have used to analyze my fabricated samples for this thesis. Irrespective of the

proposed applications of LPE exfoliated 2D nanosheets, spectroscopic and microscopic techniques are necessary to understand the size selection and thickness based distribution of the nanosheets. In the following sub-sections, UV-Visible spectroscopy and Raman spectroscopy will be discussed to get the very first confirmation of the successful exfoliation of the 2D nanosheets, zeta potential, to get insight into the surface charge and stability of dispersed 2D nanosheets in the given medium, scanning electron microscopy and transmission electron microscopy for morphological information and details and atomic force microscopy to get confirmation on morphology and thickness of exfoliated 2D nanosheets.

### **2.5.2. UV-Visible / Optical Absorption Spectroscopy**

Interaction of a light with the matter can be studied in different ways and it is actually a fundamental process which has been under exploration for centuries. This specific interaction of light with the matter is extremely useful in gaining insights into the material properties and significant involvement in various applications, especially biomedical science. Basically, the incident light after interaction with the matter can alter its path either by reflection or refraction and the interesting point is its behavior and propagation inside the medium. In the present work, absorption spectroscopy has been used to study the basic physical properties of exfoliated 2D MoS<sub>2</sub> nanosheets in de-ionized water. Generally, when a beam of incident light passes through any liquid medium, accounting for different densities from one medium to another, it is partially scattered or absorbed by the particles of the same medium. This, in result leads to decrease in the intensity of the incident light as shown in *Figure 2.15*. This variation in the intensity attributes to the measurement of the attenuation of incident beam light which is in actual is the sum of both

scattering and absorbance processes. Significant information on the particle size, electronic structure, and change in the concentration of the sample can be extracted from the UV data.

Generally, scattering can be defined as the change in the direction of incident photons upon interaction with the heterogeneous media inside the specific cuvette. It is categorized into two types:- elastic and inelastic scattering, where the former involves no energy exchange between the photons and the interacting medium and the latter exhibits the opposite nature. Absorption, on the other hand occurs when electronic transitions of the interacting medium matches with the frequency of the incident light or in other words, the photon energy matches that of rotational and vibrational energy modes inside the sample. Particularly, UV-Visible spectrophotometer measures the electronic properties of a given material over a wide range of wavelengths covering the electromagnetic spectrum UV (200-400 nm), visible (400-800 nm) and near infrared (800-2500 nm). The characteristic spectra obtained confirms a prior check of the successful fabrication of the material or dispersed nanomaterials with its inherent properties being tested, which further can be used for other characterization tools [2].

Mostly, for liquid based samples it is very quick and easy analysis to determine the sample concentration because the measurement of the attenuation in this case at a given wavelength increases with increase in the concentration of number of scattering/absorbed particles. This is generally explained by Beer-Lambert law [3]. The more common form of Beer-Lambert equation is:-

$$A = \alpha Cl \quad (2.1)$$

Where A = absorbance

$\alpha$  = extinction coefficient (in L.g.m<sup>-1</sup> units)

$C$  = concentration of the sample (to find)

$l$  = path length of the cuvette

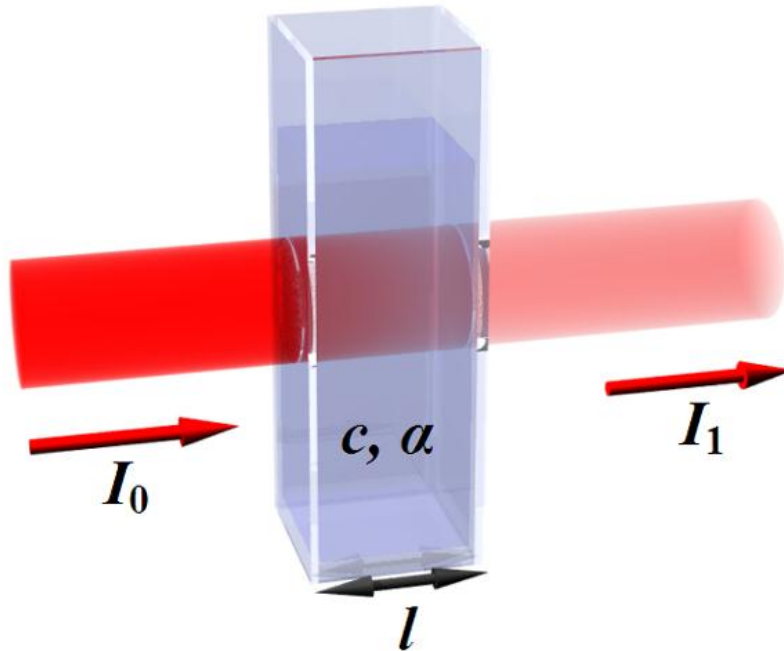


**Figure 2.15:** Schematic of Beer-Lambert law indicating an incident light with intensity  $I_0$ , length of the cuvette with  $l$  and the absorbed light with intensity  $I_1$ .

Extinction coefficient ( $\alpha$ ), is actually wavelength dependent and knowledge of its value at a given wavelength is pretty useful in determining the concentration of the layered 2D material, of course with known absorbance. Usually, the measured attenuation is the sum of both scattering and absorbance so; to analyze the characteristic spectra it is very crucial to both of the components. This can be done by extrapolating the scattering component from the redundant regions of the absorbance in a way, (absorption = extinction - scattering).

UV-Visible spectroscopy is the basic characterization to get insight into the optical and electrical features of layered 2D materials. The spectral region under study in this thesis is mainly UV-Visible (100-700 nm) for MoS<sub>2</sub> nanosheets, which measures the characteristic absorption peak at specific wavelengths in the spectra. Claudia Backes et al. have formulated some matrix to find out the correlation of extinction spectra with the concentration, thickness and lateral size of the MoS<sub>2</sub> and WS<sub>2</sub> exfoliated nanosheets in aqueous surfactant solution (sodium cholate (SC)), accounting it for edge and confinement effects because of strong exfoliation process [2,4]. So, basically UV-Visible spectroscopy is capable to investigate very useful information on the LPE exfoliated 2D MoS<sub>2</sub>/WS<sub>2</sub> and other layered materials, providing the structural integrity of the exfoliated nanosheets through the strong excitonic transitions upon the irradiation of the incident beam of light [5,6,7,8,9]. Then, concentration of the dispersed nanoflakes using the extinction coefficient which in result is size dependent and it contains both scattering and absorption components, after which the former one is subtracted to get the desired characteristic peak [2,4,8,10,11]. The change in the magnitude and position of the characteristic peak can be attributed to the edge and confinement effects introduced upon exfoliation. Moreover, the variation in the excitonic transitions and the subsequent alteration in the electronic band structure works as a function of thickness and lateral size of exfoliated 2D nanosheets [2,12,13]. It is because the absorption/extinction coefficients of the edges is different from the basal plane of the nanosheet which can be analyzed using ratio of different absorption intensities using UV-Visible spectroscopy [13]. Same authors then developed a matrix formula to calculate the mean nanosheet length using the peak intensity ratios for MoS<sub>2</sub> and WS<sub>2</sub> and this is valid for various other layered materials because of its robustness [2,4]. Following is the equation for mean nanosheet length calculation:-

$$\mathbf{L} = \frac{2.30 - \frac{Ext_{Max-HE}}{Ext_{Min}}}{0.02 \frac{Ext_{Max-HE}}{Ext_{Min}} - 0.0185} \quad (2.2)$$

Where,  $Ext_{max} - HE$  signifies the intensity at local maximum at high energy (270 nm for  $MoS_2$ ) and  $Ext_{min}$  signifies the intensity at local minimum (345 nm for  $MoS_2$ ).

Similarly, they also have formulated the spectral information on  $MoS_2$  nanosheet thickness from the absorbance spectra via the following equation:-

$$\mathbf{N} = 2.3 \times 10^{36} e^{\frac{-54888}{\lambda_A}} = 2.3 \times 10^{36} e^{-44.3E_A} \quad (2.3)$$

### 2.5.3. Equipment used for the measurement



*Figure 2.16: UV-Vis spectrophotometer of Jasco V-530 model with double beam slots for reference and sample used in this thesis.*

The UV-Visible spectrophotometer model used for the experiments in this work is the Jasco V-530 UV/VIS Spectrophotometer as shown in **Figure 2.16** with double beam slots for sample and reference respectively as shown in the schematic in **Figure 2.17**, which is designed to measure the absorption spectrum of a sample at wavelengths in the range 190 to 1100 nm. The light sources used in the V-530 are a deuterium (D2) lamp (190 to 350 nm) for the UV region and a halogen (WI) lamp (340 to 1100 nm) for the VIS/NIR region. Optical extinction spectra for the exfoliated samples were acquired on the same using 1 cm path length optics quartz cuvette. Initially, baseline was run for the given solvent placed in both of the cuvettes at a specific wavelength range and then spectra of the sample and the solvent at a time was acquired in the

range of 200 – 800 nm. Absorbance was measured by subtracting the baseline contribution taken initially. The extinction spectra of MoS<sub>2</sub> dispersion was analyzed to determine the in-situ Mean layer number ( $N$ ), Mean lateral size ( $L$ ) and Mean concentration ( $C$ ) of the nanosheets by metrics as explained by Backes et al [2,4].

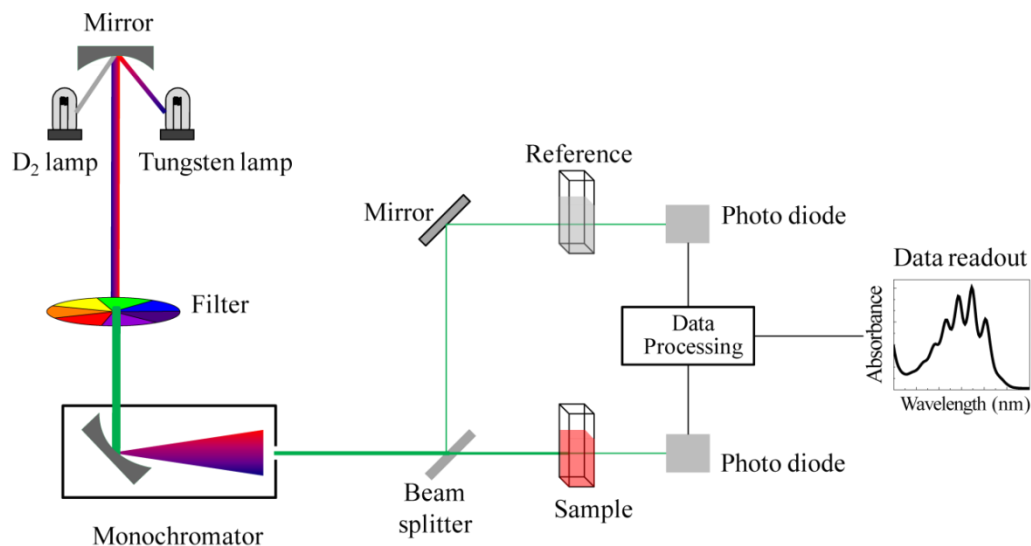


**Figure 2.17:** Schematic of double beam UV-Visible spectrophotometer<sup>5</sup>

### 2.5.4. Raman Spectroscopy

Generally, there are numerous forms of light-matter interactions such as fluorescence and phosphorescence where absorption and subsequent emission of light is measured. As mentioned in the previous section that interaction of an incident light beam with matter gives interesting information on the material properties and structure. In case of UV-Visible, attenuation in the light beam is measured as the sum of scattering and absorbance components. Scattering, in

<sup>5</sup> [<https://orgspectroscopyint.blogspot.com/p/basics-of-uv-visible-spectroscopy.html>]

general can be classified into two categories such as elastic scattering and inelastic scattering based on the change in wavelength of the light beam upon interaction with the matter/sample. The former one involves no change in the wavelength of incident light and can be signified as Rayleigh scattering by atoms or molecules and Mie/Tyndall scattering by dust particles, whereas the latter involves change in the wavelength of incident light and can be signified by Raman scattering by molecules and phonons, Compton scattering by charged particles [<sup>14</sup>] as shown in **Figure 2.18**. So, this section will highlight the basic principle and significance of Raman spectroscopy in probing optical phonons and to characterize different 2D materials by this fingerprint technique.

It is the most powerful analytical tool to characterize different materials and chemical species, serving as a fingerprint technique to identify a particular material via its vibrational/rotational modes and its implementation in broad range of applications such as pharmaceuticals, cosmetics, geology, mineralogy, carbon materials, semiconductors and extensive application in life science applications[<sup>15</sup>]. Sir C. V. Raman was the inventor who experimentally developed the basic principle of Raman spectroscopy in 1928 and two years after he was awarded with the Nobel Prize in Physics [<sup>16</sup>]. Basically, photon of a light interacts with the sample (liquid or powder or thin film) to produce scattering with different frequency.

# Raman Effect

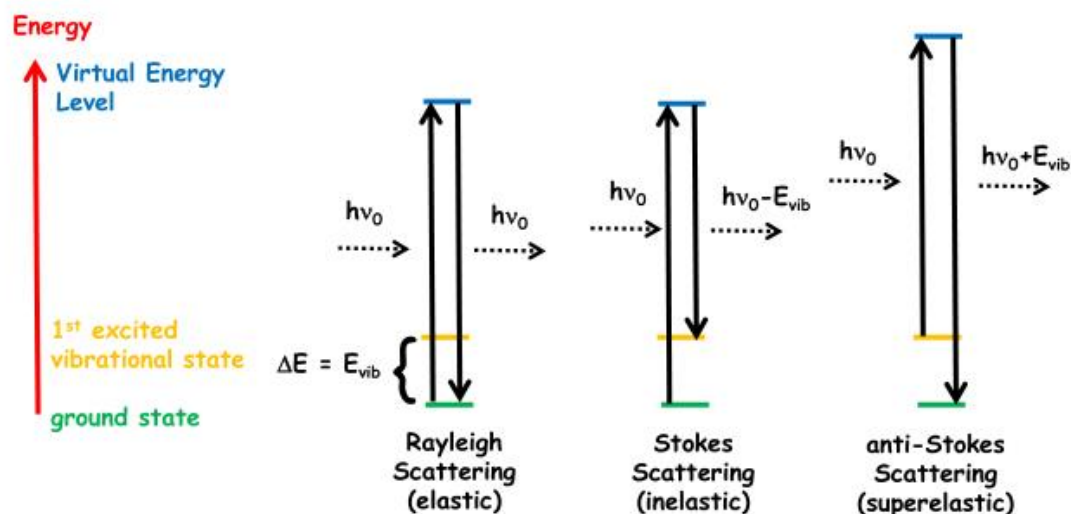


**Figure 2.18:** Represents the Energy level diagram of Raman scattering [<sup>17</sup>]

In principle, when a monochromatic source of light (laser light of known wavelength) interacts with the sample, some portion of the incident light gets scattered and subsequently it shows shift in the wavelength. This shift is the key parameter which makes this powerful technique to be eminent one in material science and which marks as a fingerprint technique to investigate and analyze that shift in wavelength in terms of the change in molecular vibrations and rotations of the sample being tested. The major difference between infrared absorption spectroscopy and Raman spectroscopy is that the former is a single photon process which shows resonance with the incident frequency of light and change in the vibrational spectra of the molecule, whereas the latter is a two photon process which apart from the vibrational spectra also involves polarization factor of the sample as well.

So, absorption of an incident photon results in excitation of that photon to a virtual energy state and emission of another photon to a different vibrational state with higher energy state than the starting one or with the lower energy state than the starting. The difference in these two energy states with the ground state is termed with Stokes and anti-Stokes Raman scattering process where the former is much more intense than the latter. On the other hand, resonant Raman scattering occurs when the frequency of incident photons matches with that of electronic transitions and subsequently it enhances the sensitivity of the measurement process [18].

Basically, a Raman spectrum is a plot or characteristic peak of Raman scattering intensity versus Raman shift  $\nu$ :-

$$\nu = \frac{1}{\lambda_i} - \frac{1}{\lambda_s} \quad (2.4)$$

Where,  $\lambda_i$  is the wavelength of incident light and  $\lambda_s$  is the wavelength of scattering light. To be Raman active, the polarisability of a bond of any specific molecule must change upon interaction with the incident light because the fingerprint concept of this technique is based on the Raman shift for that bond based on the change in the vibrational energy of the same. In such a case, external factors like temperature have a significant influence on the frequency of the incident light which brings some change in the vibrational energy of the molecule.

Raman spectroscopy has proven to be very prominent and powerful tool in characterizing different 2D materials such as graphene [19-21], 2D TMDs [22-24]] and the typical of this technique, measurement of phonon modes in crystals [14,25-27]. Specifically, for bulk 2H-MoS<sub>2</sub>, four Raman active modes exist; A<sub>1g</sub>, E<sub>1g</sub>, E<sub>1</sub> 2g and E<sub>2</sub> 2g. The two main characteristic features of MoS<sub>2</sub> nanosheets are E<sub>1</sub> 2g and A<sub>1g</sub> at 383 cm<sup>-1</sup> and 409 cm<sup>-1</sup> respectively [23,28]. E<sub>1</sub> 2g

corresponds to the in plane vibrations whereas A<sub>1g</sub> corresponds to out of plane vibrations. The shift in the characteristic Raman peak could be attributed to the difference in number of layers or thickness of exfoliated MoS<sub>2</sub> nanosheets and was first reported by Lee et al [23]. With decreasing number of layers, change in frequency of these *in plane* and *out of plane* modes is observed and this marks the robustness and quick means to explore and to find the thickness of MoS<sub>2</sub> nanosheets using Raman spectroscopy. Generally, Raman spectroscopy combined with photoluminescence measurement makes the analysis more comfortable in investigating the purity of exfoliated samples and functionalization of the same. Photoluminescence (PL), in general for 2D materials is preferable to explore the excitonic transitions in a specific region of the wavelength which differs for every 2D material. Any kind of surface modification or introduction of defects can be probed using PL spectroscopy [2,29-31]. Primarily, bulk 2H-MoS<sub>2</sub> as an indirect band gap material shows phonon assisted process and has negligible quantum yield but when the same material is exfoliated in to thin monolayer and few layer nanosheets a bright PL is detected which confirms its transition from indirect to direct band gap semiconductor [32-35].

### 2.5.5. Equipment used in the experiment



*Figure 2.19: Raman microscope used in this thesis*

A confocal Raman microscope (Jasco, NRS-3100) was used to obtain Raman spectra as shown in *Figure 2.19*. The 514 nm line of an air-cooled Ar<sup>+</sup> laser (Melles Griot, 35 LAP431 220), was injected into an integrated Olympus microscope and focused to a spot diameter of approximately 3  $\mu\text{m}$  by a 20x objective with a final 4 mW power at the sample. A holographic notch filter was used to reject the excitation laser line. The Raman backscattering was collected using a 0.1 mm slit and a diffraction lattice of 1200 grooves/mm, corresponding to an average spectral resolution

of  $8 \text{ cm}^{-1}$ . Solutions were left evaporating on Si substrates, and it took 60 s to collect a complete data set by a Peltier-cooled  $1024 \times 128$  pixel CCD photon detector (Andor DU401BVI). Raman measurements were at least triplicated for scope of reproducibility. Wavelength calibration was performed by using cyclohexane as a standard.

### **2.5.6. Zeta Potential**

Zeta potential ( $\zeta$  - potential), in general is the fundamental indicator of the stability of the particles in colloids. The surface charge of a nanoparticle dispersed in solution will explain the whole story of its stability in the same medium. In other words, it basically measures the effective electric charge on the nanoparticle's surface which further will indicate the role of a solvent or any surfactant or stabilizer in maintaining the colloidal stability of the nanoparticle. So, the magnitude of the surface charge basically indicates the degree of electrostatic repulsion between similarly charged and adjacent charged particles in the same medium. Normally, fabrication of a nanoparticle results in net surface charge on its surface and furthermore the screening of this net surface charge is done by the relative concentration of oppositely charged ions in the same medium. This creates an electric double layer of oppositely charged ions and generates an electric potential at the boundary of this layer. So, the measurement of this electric potential gives us the magnitude of surface charge or  $\zeta$  - potential. Usually the colloidal stability of a nanoparticle is governed by a certain value of  $\zeta$  - potential in the range of greater than +25 mV or less than -25 mV, whereas low value of  $\zeta$  - potential results in aggregation or flocculation of the colloidal particles in the solution.

So, in case of 2D nanosheets, role of a solvent or surfactant is mainly administered by the magnitude of surface charge on exfoliated 2D nanosheets. An electric field is applied to the dispersing solution containing nanosheets to confer their degree of movement in that medium. This process of applying an electric field is known as electrophoresis [36,37]. The following equation relates the particle mobility with the applied electric field which confers the magnitude of the surface charge on it:-

$$\mathbf{v} = \mu\mathbf{E} \quad (2.5)$$

Where,  $\mu$  corresponds to mobility of the particle,  $E$  corresponds to applied electric field and  $v$  corresponds to drift velocity of the particle in the dispersing medium. There is another equation which defines the relation between  $\zeta$  – potential and mobility of the particle in the following form:-

$$\zeta = \frac{3\eta\mu}{2\epsilon\epsilon_0 f(\kappa a)} \quad (2.6)$$

Here, zeta potential ( $\zeta$ ), depends upon the viscosity ( $\eta$ ), mobility ( $\mu$ ), permittivity ( $\epsilon\epsilon_0$ ), and Henry's function ( $f(\kappa a)$ ), where  $\kappa$  and  $a$  are the Debye length and the particle radius respectively [37]. The above equation also corresponds to Smoluchowski expression which holds for plate like morphology of particles [38]. Basically, to measure the zeta potential of any dispersion, velocity of the dispersed particles is calculated using the concept of Doppler velocimetry [39]. Under applied voltage, two beams are allowed to pass through the solution. In such a case, incident beam passes through the solution and the reference beam passes through the electrode containing

cell as shown in **Figure 2.20**. In such a way, the scattered laser light is analyzed through the cell which in result produces a signal, the frequency of which is proportional to the speed of the particles in the solution.

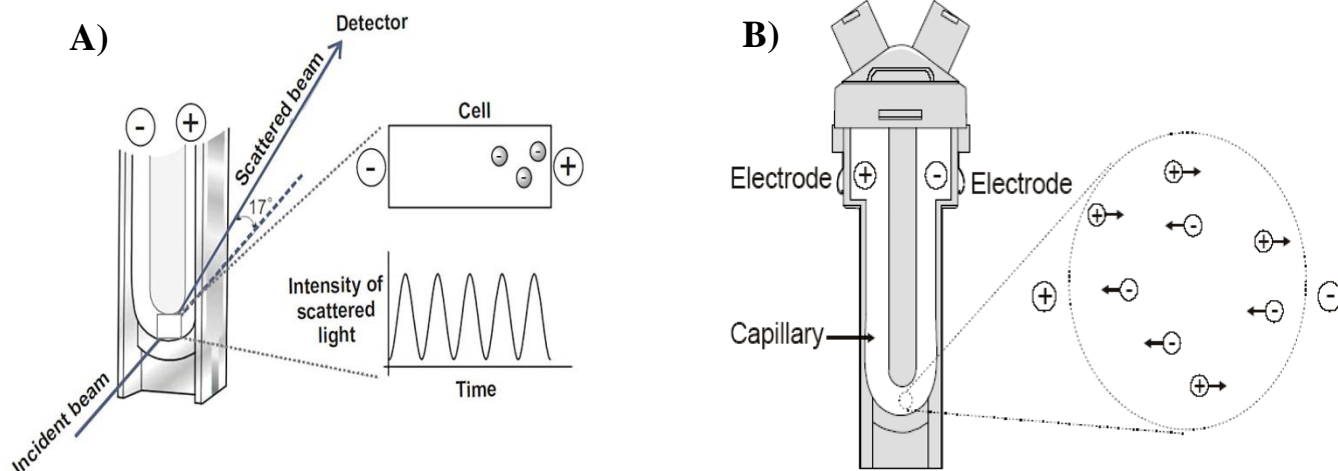


**Figure 2.20:** A) An electrophoretic mobility of the particles measured in a specific cuvette designed for zeta potential with two electrodes which works when an electric field is applied from outside. B) Represents the mobility of different ions in the designed capillary of the cuvette on applying an electric field from outside [<sup>38,40</sup>].

### 2.5.7. Equipment used in the experiments



*Figure 2.21: Malvern Zeta sizer nano used in this thesis*

Electrostatic stabilization is an important parameter to analyze the stability of the liquid exfoliated dispersions. The surface charges generated during the exfoliation can be attributed to electrophoretic mobility measurements ( $\mu$ ). So, these ( $\mu$ ) measurements were carried out on laser interferometric technique (Malvern Zetasizer Nano system) with irradiation from 633 nm He-Ne lasers shown in **Figure 2.21**. The samples were injected in folded capillary cells, and the electrophoretic mobility ( $\mu$ ) was measured using a combination of electrophoresis and laser Doppler velocimetry techniques [41]. The Henry's equation was used to estimate the zeta potential from the electrophoretic mobility data. For the possible upper and lower limits of the zeta potential values, Henry's equation was approximated to both the Huckel and Smoluchowsky limits. The reason for this approximation is due to the particular solvent-sample relationship;

Henry's equation is approximated to get an estimate of surface charge values of exfoliated nanosheets. All the measurements were carried out at 25 °C.

### **2.5.8. Electron Microscopy Tools**

In today's world we can imagine to look upon the smallest dimension of anything using advanced electron microscopy techniques whether it could be one single hair, tip of a pin, different pathogens such as bacteria, viruses, molecules or atoms in crystals. What we are looking today is actually not just a single technique but it is a multitude of different techniques which contributes specifically to investigate the deep dimensions of structural aspect, topology, morphology and composition of a material. It is actually one of the most broadly used techniques to explore the world of different nanomaterials. Informational prosperity achieved from different electron microscopic, imaging or spectroscopic techniques makes these characterization tools more demanding because they can be used in a wide range of applications such as biomedical science, mineralogy, geography, material science and pharmaceutical world to name a few. So, the basic interaction of electrons with the sample generates horde of signals which are responsible for creating the desired imaging of the given sample [<sup>42,43</sup>].

### **2.5.9. Basic parts of an Electron Microscope**

Basically, an ordinary microscope has four different and important parts such as a) source of light at the bottom which shines in the upward direction through a thin slice of specimen, b) specimen to be tested, c) lens to visualize magnified image of the specimen and d) magnified image itself by the bending or refraction of the incident light. Usually to investigate about the morphology or any other size related properties of nanomaterials, conventional optical

microscopes with very low resolutions were unsuitable for the desired purpose. Generally, resolution of any microscope can be formulated from the following equation:-

$$\delta = 0.6\lambda \quad (2.7)$$

$\lambda$  is the wavelength of the incident radiation and  $\delta$  corresponds to the resolution of the microscope [<sup>44</sup>].

Whereas, in an electron microscope a) instead of the source of light, a beam of fast moving electrons hits the specimen, b) a specific preparation of the sample is required and it has to be tested in vacuum chamber because of the beam of fast moving electrons, c) Instead of lenses, a series of coil-shaped electromagnets are utilized via which the electron beam travels and these electromagnets are responsible for the bending of moving electrons to produce a magnified image of the sample and d) image is directly produced as a photograph. It was in the late 1920s after de Broglie postulated that electrons have a dual character, wave and particle. So, this marked the beginning of the research was focused to develop imaging techniques working on the principle of high energy electrons rather than photons. De Broglie gave an equation explaining the relation between wavelength of electrons and their energy:-

$$\lambda = \frac{h}{mv} \quad (2.8)$$

Here,  $h$  is the planks constant,  $m$  and  $v$  corresponds to mass and velocity of the electrons respectively [<sup>44</sup>]. So, basically the electrons are the only component which segregates between the two main types of electron microscopies:- Scanning Electron Microscopy (SEM) and Transmission Electron Microscopy (TEM).

## 2.6. Scanning Electron Microscopy (SEM)

SEM is basically a surface sensitive technique in terms of a focused beam of electrons is scanned across the sample surface and then backscattered electrons are employed to work onto the image processing of the focused area as shown in *Figure 2.22*. Along with transmission electron microscopy tool, it is also a widely used versatile tool to image not only the nanomaterial's surface but even bulk crystals expanding its frontier in medical science, biological observations, semiconductors, ceramics, metals and in general revolutionizing the material science field. Basic principle is simple and similar to the above as explained that fast beam of electrons are accelerated through a voltage in the range between 2 and 10 eV and then to focus these electrons like in optical microscope (bending of light to image the specimen) coil shaped electromagnets are used for imaging purpose. The schematic of SEM is shown in *Figure 2.23*. The fast moving beam of electrons penetrates the sample surface resulting in a teardrop shaped interaction volume as shown in figure. After its interaction with the sample, backscattered electrons (BSE) and secondary electrons (SE) are employed upon raster scan of the surface to generate an image. BSE in general consist of high energy electrons scattered elastically from the sample surface making them less sensitive to the surface but they are pretty useful in investigating the composition of the sample surface being raster scanned with escape depth in microns. On the other hand, SE are scattered in-elastically from the sample surface and exhibit lower energy (3-5 eV) than the BSE making them more sensitive to the surface imaging process with micron depth in nanometers [42]. It is much easier with SEM sample preparation as it hardly takes 5 minutes to prepare the sample and then immediately scan it for the desired purpose. Specifically, in case of 2D materials, coating of some samples is required for the charge dissipation. In our case, MoS<sub>2</sub>

nanosheets thin film deposited onto either a glass substrate or silicon substrate is first gold coated to increase the contrast in imaging the sample.

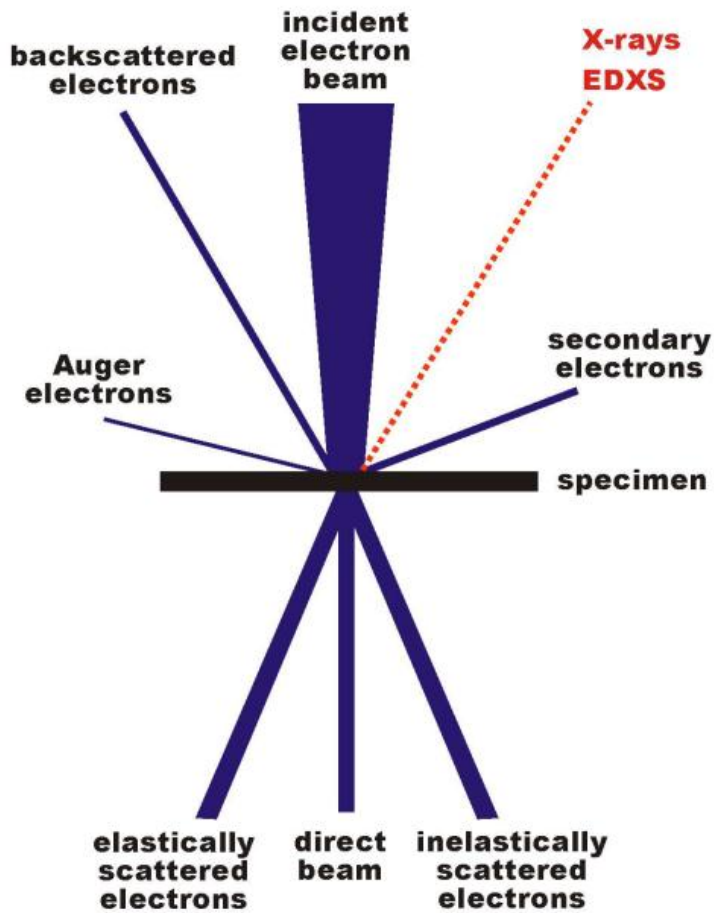


*Figure 2.22: Fundamental scheme of electron-matter interaction when an high energy electron beam hits the surface of the sample and subsequently different signals are received.*

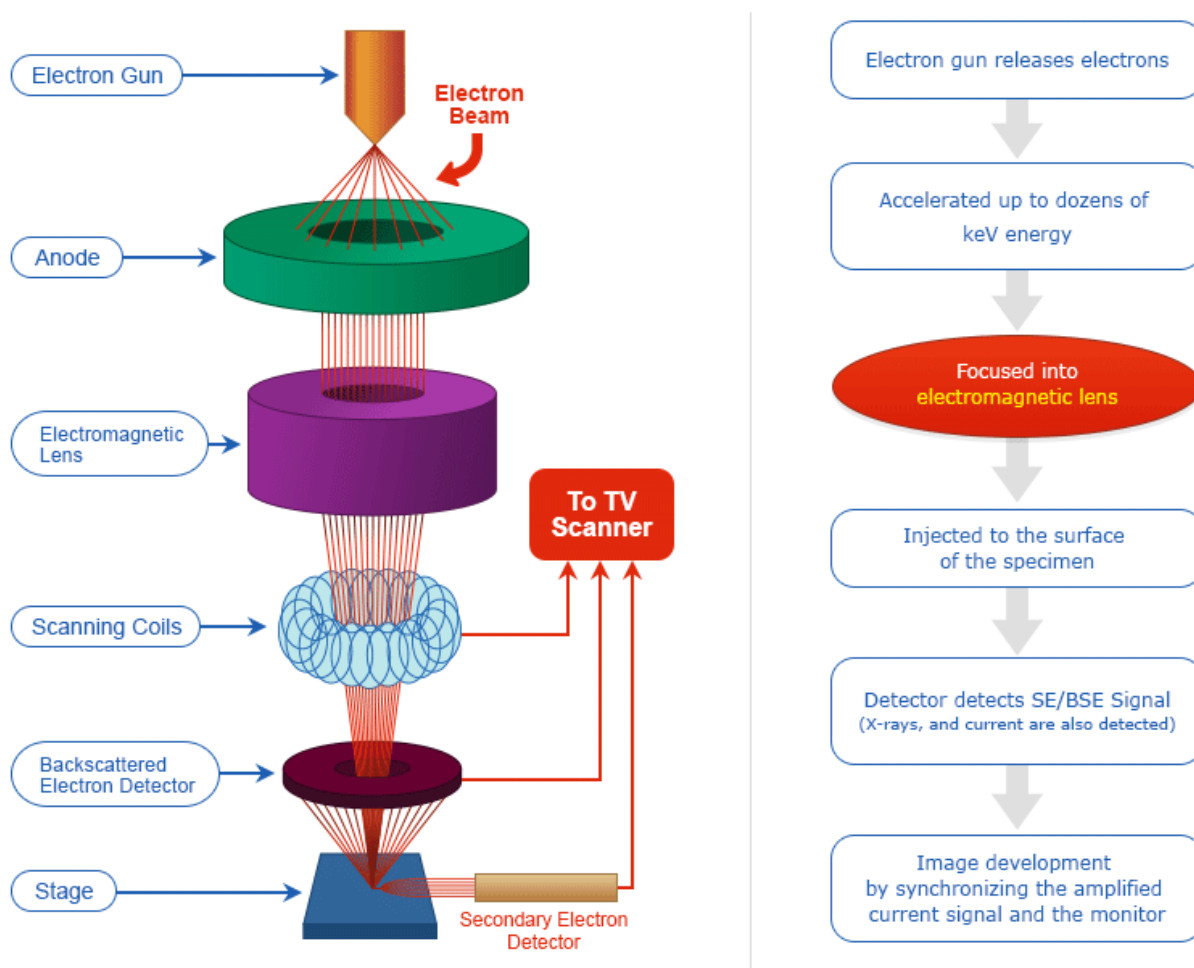


**Figure 2.23:** Schematic of scanning electron microscope <sup>6</sup>

### 2.6.1. Equipment used in the experiments

Morphological analyses of samples were performed with a scanning electron microscope (SEM) JEOL-JSM 5310 (CISAG laboratory, at University of Naples, Federico II). The SEM operating at 15 kV, is equipped with energy dispersive X-Ray spectroscopy (EDS); data were processed

<sup>6</sup> <https://www.springer.com/gp/book/9783319929545>

with INCA version 4.08 (Oxford Instruments, 2006). The samples were metalized with gold by using a sputter coater. Oxford Instruments (2006): INCA - The microanalysis suite issue 17a + SP1 - Version 4.08. Oxford Instr. Anal. Ltd., Oxfordshire, UK.

## Bibliography

1. Mourdikoudis, S., Pallares, R. M. & Thanh, N. T. K. Characterization techniques for nanoparticles: Comparison and complementarity upon studying nanoparticle properties. *Nanoscale* **10**, 12871–12934 (2018).
2. Backes, C. *et al.* Edge and confinement effects allow in situ measurement of size and thickness of liquid-exfoliated nanosheets. *Nat. Commun.* **5**, 1–10 (2014).
3. Swinehart, D. F. The Beer-Lambert law. *J. Chem. Educ.* **39**, 333–335 (1962).
4. Backes, C. *et al.* Production of highly monolayer enriched dispersions of liquid-exfoliated nanosheets by liquid cascade centrifugation. *ACS Nano* **10**, 1589–1601 (2016).
5. Weisbuch, C., Benisty, H. & Houdre, R. Overview of fundamentals and applications of electrons, excitons and photons in confined structures. *J. Lumin.* **85**, 271–293 (2000).
6. Taylor, P., Wilson, J. A. & Yoffe, A. D. Advances in Physics The transition metal dichalcogenides discussion and interpretation of the observed optical , electrical and structural properties. 37–41 (2006). doi:10.1080/00018736900101307
7. Wilson, J. A. & Yoffe, A. D. Advances in Physics The transition metal dichalcogenides discussion and interpretation of the observed optical , electrical and structural properties. **8732**, (2017).
8. Fan, X. *et al.* Controlled Exfoliation of MoS<sub>2</sub> Crystals into Trilayer Nanosheets. *J. Am. Chem. Soc.* **138**, 5143–5149 (2016).
9. Knirsch, K. C.; Berner, N. C.; Nerl, H. C.; Cucinotta, C. S.; Gholamvand, Z.; McEvoy, N.; Wang, Z.; Abramovic, I.; Vecera, P.; Halik, M.; Sanvito, S.; Duesberg, G. S.; Nicolosi, V.; Hauke, F.; Hirsch, A.; Coleman, J. N.;pdf.
10. Backes, C.; Paton, K. R.; Hanlon, D.; Yuan, S.; Katsnelson, M. I.; Houston, J.; Smith, R. J.; McCloskey, D.; Donegan, J. F.; Coleman, J. N. Spectroscopic metrics allow in situ measurement of mean size and thickness of liq.pdf.
11. Paton, K. R. & Coleman, J. N. Relating the optical absorption coefficient of nanosheet

- dispersions to the intrinsic monolayer absorption. *Carbon N. Y.* **107**, 733–738 (2016).
12. Backes, C. *et al.* Guidelines for Exfoliation, Characterization and Processing of Layered Materials Produced by Liquid Exfoliation. *Chem. Mater.* **29**, 243–255 (2017).
  13. Backes, C. *et al.* Preparation of liquid-exfoliated transition metal dichalcogenide nanosheets with controlled size and thickness: A state of the art protocol. *J. Vis. Exp.* **2016**, 10–13 (2016).
  14. Long, D. A. *The Raman effect: a unified treatment of the theory of Raman scattering by molecules.* 2002. West Sussex, England: John Wiley & Sons Ltd **8**, (2002).
  15. Vankeirsbilck, T. *et al.* Applications of Raman spectroscopy in pharmaceutical analysis. *TrAC - Trends Anal. Chem.* **21**, 869–877 (2002).
  16. Raman, C. V. A new radiation. *Proc. Indian Acad. Sci. - Sect. A* **37**, 333–341 (1953).
  17. Chaichi, A., Prasad, A. & Ranjan Gartia, M. Raman spectroscopy and microscopy applications in cardiovascular diseases: From molecules to organs. *Biosensors* **8**, 1–19 (2018).
  18. Edwards, H. G. M. *Modern Raman spectroscopy—a practical approach.* Ewen Smith and Geoffrey Dent. John Wiley and Sons Ltd, Chichester, 2005. Pp. 210. ISBN 0 471 49668 5 (cloth, hb); 0 471 49794 0 (pbk). *Journal of Raman Spectroscopy* **36**, (2005).
  19. Venezuela, P., Lazzeri, M. & Mauri, F. Theory of double-resonant Raman spectra in graphene: Intensity and line shape of defect-induced and two-phonon bands. *Phys. Rev. B - Condens. Matter Mater. Phys.* **84**, 1–25 (2011).
  20. Malard, L. M., Pimenta, M. A., Dresselhaus, G. & Dresselhaus, M. S. Raman spectroscopy in graphene. *Phys. Rep.* **473**, 51–87 (2009).
  21. Pimenta, M. A. *et al.* Studying disorder in graphite-based systems by Raman spectroscopy. *Phys. Chem. Chem. Phys.* **9**, 1276–1291 (2007).
  22. Yan, R. *et al.* Thermal conductivity of monolayer molybdenum disulfide obtained from temperature-dependent Raman spectroscopy. *ACS Nano* **8**, 986–993 (2014).

23. Lee, C. *et al.* Anomalous lattice vibrations of single-and few-layer MoS<sub>2</sub>. *ACS Nano* **4**, 2695–700 (2010).
24. Verble, J. L., Wietling, T. J. & Reed, P. R. Rigid-layer lattice vibrations and van der waals bonding in hexagonal MoS<sub>2</sub>. *Solid State Commun.* **11**, 941–944 (1972).
25. Establishment, R. R. & Malvern, G. The o r y o f t h e f i r s t - o r d e r R a m a n e f f e c t i n c r y s t a l s . 218–232 (1963).
26. Taylor, P. & Loudon, R. *Advances in Physics The Raman effect in crystals.* October (2010). doi:10.1080/00018736400101051
27. Knight, D. S. & White, W. B. Characterization of diamond films by Raman spectroscopy. *J. Mater. Res.* **4**, 385–393 (1989).
28. Molina-Sánchez, A. & Wirtz, L. Phonons in single-layer and few-layer MoS<sub>2</sub> and WS<sub>2</sub>. *Phys. Rev. B - Condens. Matter Mater. Phys.* **84**, 1–8 (2011).
29. Palummo, M., Bernardi, M. & Grossman, J. C. Exciton radiative lifetimes in two-dimensional transition metal dichalcogenides. *Nano Lett.* **15**, 2794–2800 (2015).
30. Lin, Y. *et al.* Dielectric screening of excitons and trions in single-layer MoS<sub>2</sub>. *Nano Lett.* **14**, 5569–5576 (2014).
31. Chow, P. K. *et al.* Defect-induced photoluminescence in monolayer semiconducting transition metal dichalcogenides. *ACS Nano* **9**, 1520–1527 (2015).
32. Ding, Q. *et al.* Basal-Plane Ligand Functionalization on Semiconducting 2H-MoS<sub>2</sub> Monolayers. *ACS Appl. Mater. Interfaces* **9**, 12734–12742 (2017).
33. Mak, K. F., Lee, C., Hone, J., Shan, J. & Heinz, T. F. Atomically thin MoS<sub>2</sub>: A new direct-gap semiconductor. *Phys. Rev. Lett.* **105**, 2–5 (2010).
34. Splendiani, A. *et al.* Emerging Photoluminescence in Monolayer. 1271–1275 (2010). doi:10.1021/nl903868w
35. Zhang, X. *et al.* Phonon and Raman scattering of two-dimensional transition metal

- dichalcogenides from monolayer, multilayer to bulk material. *Chem. Soc. Rev.* **44**, 2757–2785 (2015).
36. Musa, U. G., Cezan, S. D., Baytekin, B. & Baytekin, H. T. The Charging Events in Contact-Separation Electrification. *Sci. Rep.* **8**, 1–8 (2018).
  37. Tanager, B. Short Communications Short Communications. 2006–2007 (2011).
  38. Ohshima, H. Theory of electrostatics and electrokinetics of soft particles. *Sci. Technol. Adv. Mater.* **10**, (2009).
  39. Jackson, D. C. & Rouse, H. Hydraulics in the United States, 1776-1976. *Technol. Cult.* **18**, 693 (1977).
  40. Smith, R. J., Lotya, M. & Coleman, J. N. The importance of repulsive potential barriers for the dispersion of graphene using surfactants. *New J. Phys.* **12**, (2010).
  41. Lotya, M. *et al.* Liquid Phase Production of Graphene by Exfoliation of Graphite in Surfactant / Water Solutions. 3611–3620 (2009).
  42. Joy, D. C. The theory and practice of high-resolution scanning electron microscopy. *Ultramicroscopy* **37**, 216–233 (1991).
  43. Krumeich, B. F. Properties of Electrons, their Interactions with Matter. *ETH Zurich* 1–24 (2018).
  44. Williams, D. B. *et al.* *Methods in Cell Biology Methods in Cell Biology. Methods Biochem. Anal.* **44**, (2010).



## **2.7. Solubility Theories**

### **2.7.1. General Introduction on Solubility Theory**

The successful fabrication of nanoparticles and their subsequent stability in any medium is the key factor for their potential applications in various fields. Generally, the solubility of numerous pristine nanoparticles in water is very low due to their unfavorably surface chemistry. Apart from this, thermodynamics of the mixtures (solute and solvent parameters) and surface energies play an important role in stabilization of the dispersion.

Basically, there are a number of factors which govern the choice of a solvent for a particular experiment such as solution viscosity, evaporation rate, subsequently environmental and health concerns. The ability of a solvent to dissolve or colloiddally stabilize a material can be described in the framework of solution thermodynamics. For large and rigid objects such as nanomaterials, the entropic term to the Gibbs free energy of mixing can be neglected so that it is particularly important to minimize the enthalpy of mixing. This can be achieved by matching the solubility parameters of solvent and solute. There exists two main theories to describe solubility parameters which perhaps are the most widely applicable of all the systems, initially by Hildebrand and then by Hansen. So, Hildebrand developed a solubility parameter known by his name which is actually a numerical value which indicates the relative solvency behavior of a particular solvent. This solubility parameter has a strong relationship between heat of vaporization of the solvent, van der Waals forces and the subsequent solubility. So, in 1936, he proposed the solubility

theory which initially was known as solubility parameter but after a decade it was officially known by his name [1].

Then, after speculating various factors in the Hildebrand solubility parameter in 1966 Charles M. Hansen developed three parameter system which actually divides the obtained Hildebrand value ( $\delta_t^2$ ) into three categories such as a) dispersion component ( $\delta_d^2$ ), b) a hydrogen bonding component ( $\delta_h^2$ ) and a polar component ( $\delta_p^2$ ) and these can be represented as [2]:-

$$\delta_t^2 = \delta_d^2 + \delta_p^2 + \delta_h^2 \quad (2.9)$$

These solubility parameters can be used to screen the solvent stability, to investigate the solubility of nanomaterials in different solvents and to understand the chemistry of mixing and chemical resistance [3-6]. So, the correct matching of the surface energies of a given nanomaterial and solvent will give stable dispersion, whereas mismatchment in the solubility parameters will result in aggregation of the nanomaterial and subsequently it will sediment to the bottom. Similarly, to understand the interaction of 2D nanosheets and a suitable solvent for an excellent dispersion, it is important to consider the basic thermodynamics involved in solubility parameters which have been widely studied for various materials such as carbon nanotubes[3,7-9].

### **2.7.2. Thermodynamics of the solution by minimizing the enthalpy of mixing for a stable dispersion**

The fundamental concept of solubility thermodynamics is based on the Gibbs free energy of mixing ( $\Delta G_{\text{mix}}$ ). The energetics of the mixtures as governed by  $G_{\text{mix}}$  is a function of change in enthalpy ( $\Delta H_{\text{mix}}$ ) and change in entropy ( $\Delta TS_{\text{mix}}$ ) of the whole system with T as an absolute temperature. So, the solubility of two materials under isothermal conditions can be expressed by the following equation:-

$$\Delta G_{mix} = \Delta H_{mix} - T\Delta S_{mix} \quad (2.10)$$

Particularly for the liquid phase exfoliation process to occur spontaneously,  $\Delta H_{mix} < T\Delta S_{mix}$  which will result in negative value of  $G_{mix}$ . This condition implies that we will have a solution i.e. a spontaneous dissolution of the material up to a certain maximum concentration but if the other case happens where  $\Delta H_{mix} > T\Delta S_{mix}$ , the resulting product will be a metastable dispersion. The energy required for an exfoliation to occur is represented by  $\Delta H_{mix}$  per unit volume of the solvent. When this factor is minimized a well dispersed concentration of 2D nanosheets can be obtained which will confer that the surface energy of the solvent matches with that of the solute. This concept has been introduced as Hildebrandt Scatchard equation in the 1930s and adapted for carbon nanotubes in 2009 [7].

Basically, a number of authors have reported the successful stabilization of 2D materials such as for graphene and 2D TMDs in high boiling point solvents such as N-methyl pyrrolidone (NMP) and dimethylformamide (DMF) to achieve stable dispersions at high nanosheet concentration in the range of g/L. This has been rationalized on the basis of solubility theories considering the models relevant for 2D nanosheets as well [7,10-13]. Initially, a model was proposed by Bergin et al. to explain the solubility of single walled carbon nanotubes in some common solvents [3], which in 2008 was also validated by Hernandez et al. for exfoliation of graphite to achieve high yield production of graphene using LPE [14]. In this particular case, the authors have formulated  $H_{mix}$  from the following equation:-

$$\frac{\Delta H_{mix}}{V_{mix}} \approx \frac{2}{T_{flake}} (\sigma_{nanosheet} - \sigma_{solvent})^2 \phi \quad (2.11)$$

Where,  $V_{\text{mix}}$  denotes the mixture volume,  $t_{\text{nanoflake}}$  denotes the thickness of nanosheet,  $\delta_{\text{nanosheet}}$  and  $\delta_{\text{solvent}}$  represents the total surface energies of nanosheet and solvent, respectively. In addition,  $\phi$  represents the total volume fraction of the dispersed nanosheets. A general definition of the volume fraction of dispersed material can be expressed by,  $C = \rho_p \phi$ , where  $C$  is the dispersed concentration and  $\rho_p$  represents the density of nanosheets in that solvent. So, when the surface energy of the solute and solvent are well matched, this thermodynamically favors the mixing process and subsequently a colloidal stable dispersion with reasonable concentration is achieved after minimizing the net energy cost of the exfoliation. This approach was successful for only good and well suitable solvents but not for all.

On the same track, Hildebrand theory of solubility revolves around the same principle of minimizing the energy cost for exfoliation by reducing the energy for enthalpy of mixing to yield high dispersed concentrations of 2D layered materials. In this case, his theory takes into account all solute-solvent interactions by considering the cohesive energy density ( $E_T$ ) of the whole system, for solvent and for mixtures [<sup>10,12</sup>]:-

$$\delta_T = \sqrt{\frac{E}{V}} \quad (2.12)$$

Next step was taken by Charles M. Hansen in a way to cover the loopholes in Hildebrand solubility theory. Basically, he proposed the use of three different forms of cohesive energy in organic solvents to complement Hildebrand's theory of solubility. Hansen differentiates between polar ( $\delta_P$ ), dispersive ( $\delta_D$ ) and H-bonding interactions ( $\delta_H$ ) which add up to the Hildebrand parameter in the following way:-

$$\delta^2 = \delta_D^2 + \delta_P^2 + \delta_H^2 \quad (2.13)$$

So, the energy of exfoliation will be minimized when all the three parameters of the solvent must match with that of the solute and there must be an equilibrium among solvent-solvent, solvent-solute and solute-solute binding energies [8,10]. In such a case the enthalpy of mixing is related to Hansen solubility parameters by the following equation:-

$$\frac{H_{mix}}{V} = \frac{2}{t_p} [(\delta_{D_{solvent}} - \delta_{D_{nanoflake}})^2 + (\delta_{P_{solvent}} - \delta_{P_{nanoflake}})^2 + (\delta_{H_{solvent}} - \delta_{H_{nanoflake}})^2] \phi \quad (2.14)$$

### 2.7.3. Solubility theories applied to 2D nanosheets in water

Specifically, the present experimental work in this thesis has been carried out on the exfoliation of MoS<sub>2</sub> nanosheets in de-ionized water only with an aim to utilize those dispersions directly to understand the biological interactions of the dispersed nanosheets with the living matter such as different bacteria and human cells (normal and tumoral). It is true that all of the above mentioned solubility theories in the previous sections not hold true for MoS<sub>2</sub>/water based system because in this case the surface energy of the solute and solvent do not match. Different surface energy values for MoS<sub>2</sub> nanosheets has been reported such as 75 mJ m<sup>-2</sup> [13], 250 mJ m<sup>-2</sup> [15] and 45 mJ m<sup>-2</sup> [16]. On the other hand the surface tension value of water is 72 mJ m<sup>-2</sup> and Bergin et al. have reported the surface energy value of water near about 102 mJ m<sup>-2</sup>, which does not match the surface energy of MoS<sub>2</sub> nanosheets. This results poor dispersion quality of MoS<sub>2</sub> nanosheets. Generally, water is considered as a poor solvent to exfoliate 2D TMDs because of the mismatchment in the surface energy values of solute and solvent. So, the theories described above cannot be explained for the MoS<sub>2</sub>-water system [12].

Despite of that, we have employed water as our main solvent which comes under the category of green solvents. From the application point of view for my thesis work, it has proven to be an interesting solvent with significant results. Also, there is a room to scale up this protocol using water as a solvent because a number of authors have reported a significant exfoliation of 2D TMD nanosheets in water for different applications. Though, the dispersed concentration achieved in this thesis work is much lower than the one revealed in the exfoliation of MoS<sub>2</sub> nanosheets [<sup>17</sup>] in toxic and high boiling point solvents [<sup>10,18,17,19</sup>]. Experimental details are discussed in chapter-5 of this thesis.

## Bibliography

1. начальник отдела Л.В.Травин, Ленина», Ф. «Всероссийский электротехнический институт имени В. И. И., Л.В.Травин, начальник отдела & Ленина», Ф. «Всероссийский электротехнический институт имени В. И. И. No Title Основные направления развития электропередач постоянного тока (ЭПТ) Современный. 1–13 (2020).
2. Hansen, C. M. The Three Dimensional Solubility Parameter and Solvent Diffusion Coefficient. Their Importance in Surface Coating Formulation. *J. Paint Technol.* 104 (1967).
3. Bergin, S. D. *et al.* Towards solutions of single-walled carbon nanotubes in common solvents. *Adv. Mater.* **20**, 1876–1881 (2008).
4. Hernandez, Y. *et al.* High-yield production of graphene by liquid-phase exfoliation of graphite. 563–568 doi:10.1038/nnano.2008.215
5. Hughes, J. M., Aherne, D. & Coleman, J. N. Generalizing Solubility Parameter Theory to Apply to One- and Two-Dimensional Solutes and to Incorporate Dipolar Interactions. 4483–4491 (2013). doi:10.1002/app.38051
6. Detriche, S., Zorzini, G., Colomer, J. F., Fonseca, A. & Nagy, J. B. Application of the Hansen solubility parameters theory to carbon nanotubes. *J. Nanosci. Nanotechnol.* **8**, 6082–6092 (2008).
7. Bergin, S. D. *et al.* Multicomponent solubility parameters for single-walled carbon nanotube-solvent mixtures. *ACS Nano* **3**, 2340–2350 (2009).
8. Coleman, J. N. Liquid-phase exfoliation of nanotubes and graphene. *Adv. Funct. Mater.* **19**, 3680–3695 (2009).
9. Yi M, Shen ZG, Zhang XJ, Ma SL. Achieving concentrated graphene dispersions in wateracetone mixtures by the strategy of tailoring Hansen solubility parameters. *Journal of Physics D-Applied Physics* 46, (2013).pdf.

10. Coleman, J. N. *et al.* Two-Dimensional Nanosheets Produced by Liquid Exfoliation of Layered Materials. *Science (80-. )*. **331**, 568–571 (2011).
11. May, P., Khan, U., Hughes, J. M. & Coleman, J. N. Role of solubility parameters in understanding the steric stabilization of exfoliated two-dimensional nanosheets by adsorbed polymers. *J. Phys. Chem. C* **116**, 11393–11400 (2012).
12. Jenkins, S. *Hansen solubility parameters (HSP)*. *Chemical Engineering* **118**, (2011).
13. Cunningham, G. *et al.* Solvent Exfoliation of Transition Metal Dichalcogenides : Dispersibility of Exfoliated Nanosheets Varies Only Weakly between Compounds. *ACS Nano* **6**, 3468–3480 (2012).
14. Hernandez, Y. *et al.* High-yield production of graphene by liquid-phase exfoliation of graphite. *Nat. Nanotechnol.* **3**, 563–568 (2008).
15. Smith, R. J. *et al.* Large-scale exfoliation of inorganic layered compounds in aqueous surfactant solutions. *Adv. Mater.* **23**, 3944–3948 (2011).
16. Gaur, A. P. S. *et al.* Surface energy engineering for tunable wettability through controlled synthesis of MoS<sub>2</sub>. *Nano Lett.* **14**, 4314–4321 (2014).
17. Moore, C. *et al.* Industrial grade 2D molybdenum disulphide ( MoS<sub>2</sub> ): an in vitro exploration of the impact on cellular uptake , cytotoxicity , and inflammation Industrial grade 2D molybdenum disulphide ( MoS<sub>2</sub> ): an in vitro exploration of the impact on cellular uptake. *2D Mater.* **4** 025065 (2017)
18. Nicolosi, V., Chhowalla, M., Kanatzidis, M. G., Strano, M. S. & Coleman, J. N. Liquid Exfoliation of Layered Materials. *Science (80-. )*. **340**, 1226419–1226419 (2013).
19. Cunningham, G. *et al.* Solvent exfoliation of transition metal dichalcogenides: Dispersibility of exfoliated nanosheets varies only weakly between compounds. *ACS Nano* **6**, 3468–3480 (2012).

# Chapter-3 Results and Discussion

---

## 3.1. Introduction

Basically, the current chapter will put some light on the two dimensional (2D) MoS<sub>2</sub> nanosheets preparation by ultrasound mediated liquid phase exfoliation technique. A series of experimental procedures for the given sample preparation and further characterization of the fabricated samples will be discussed. Liquid phase exfoliation (LPE), which is one of the most versatile, scalable and cost effective methods has been adopted to exfoliate the bulk MoS<sub>2</sub> into 2D nanosheets by optimizing various pre-sonication and post-sonication parameters. It is worth to mention that several exfoliation parameters play a key role in producing high quality, stable dispersion 2D TMD nanosheets. Now, based on the Hansen solubility parameters water is considered as a poor solvent in exfoliating 2D TMD nanosheets and on the other hand, MoS<sub>2</sub> bulk powder or crystal itself is hydrophobic in nature. In such a case, a very careful optimization of the sonication parameters such as initial concentration of the dispersion, shape of the sonication vial, sonication time, amplitude of the sonicator signal and type of probe or tip used to exfoliate 2D TMD nanosheets (flat head, narrow head or tapered). Among these parameters, the

concept of ‘dead zones’ as explained by J. L. Capelo *et al.* is of paramount importance to have a minimum distance between the probe and the bottom of the tube used for exfoliation. The larger the contact area of the probe with the material the more effective the exfoliation and the transfer of acoustic energy and ultrasonic intensity through the probe [1]. Additionally, post exfoliation steps such as centrifugation speed, time, rotor angle, temperature during the centrifugation and filling height of the liquid are additional factors that need to be considered prior to studying the biological interactions of MoS<sub>2</sub> nanosheets with live matter.

To exfoliate MoS<sub>2</sub> bulk powder into thin 2D nanoflakes directly in de-ionized water, we have carefully chosen all of the above cited sonication parameters and performed a series of experiments to achieve an optimum value of the sonication parameters for a stable dispersion. Few years back, Long Pan et al reported a facile and water-borne exfoliation route for WS<sub>2</sub> nanosheets having number of layers in the range of one to five with stability maximum up to one week which was state-of-the art prior to our own work [2]. In our case as it will be shown in the results section below that we were able to exfoliate 2D MoS<sub>2</sub> nanosheets in de-ionized water with maximum stability up to 3 - 4 weeks which is non-trivial and holds a strong potential to be used for various biomedical applications.

Apart from this, a small review on the literature similar to the experimental work presented in this thesis will be outlined to focus our motive of adopting the present fabrication protocol. High energy tip/probe sonication is employed to isolate the bulk crystals into thin 2D nanosheets. After sonication and centrifugation, the decanted supernatants are subjected to various characterization tools such as UV-visible spectroscopy for the optical properties, zeta potential

for surface charge and stability analysis, Raman spectroscopy for thickness identification, Scanning electron microscopy (SEM) for morphological analysis, and transmission electron microscopy (TEM) for detailed morphological analysis.

### 3.1.1. Preparation of water based MoS<sub>2</sub> dispersions<sup>1</sup>

- Initially, the precursor commercialized bulk MoS<sub>2</sub> powder was purchased from Sigma Aldrich with the following powder details:-

*Product number – 69860 (Sigma Aldrich),*

*Particle size – 6 μm,*

*Density - 5.06 g mL<sup>-1</sup> at 25 °C*

- Exfoliation was carried out using a tip/probe sonicator with the following details:-

*Sonicator Model - Bandelin Ultrasound SONOPLUS HD3200*

*Maximum power – 200 W*

*Working frequency – 20 kHz*

*Tip model – KE- 76 (tapered tip, 6mm diameter) and MS-72 (micro tip, 2mm diameter).*

*Amplitude chosen for the experiments – 12% to 50 %*

- Centrifugation steps were performed using:-

*Eppendorf Bench top Centrifuge 5810 R, Rotor F-34-6-38.*

- Temperature for sample storage - 4°C

---

<sup>1</sup> The contents of this section 3.3.1. is based on our published article, Jasneet Kaur, **Manjot Singh** et al. “Biological interactions of biocompatible and water-dispersed MoS<sub>2</sub> nanosheets with bacteria and human cells”, *Scientific Reports*, **2018**, 8:16386 | DOI:10.1038/s41598-018-34679-y with major and equal contribution in all experimental and characterization analyses.

To optimize a relevant value for all sonication parameters, it was important to perform a series of exfoliation runs to achieve a stable dispersion, which then can be used to study the biological interactions with the human cells and different pathogens for various analyses. In a typical experiment, commercialized MoS<sub>2</sub> bulk powder was added into 12 mL or 15 mL (in some cases) of de-ionized / Elix water with the optimized initial concentration of 5 mg/mL (after trying different initial concentrations such as 2 mg/ml, 4 mg/ml, 8 mg/ml which gave very low final concentration) in a cylindrical glass tube (12 cm height and 2 cm diameter). The above system was sonicated for 3 hours using KE-76 tapered tip at amplitude of 12 % to 15 % under a controlled ice-water bath setup to avoid the over- heating caused during the exfoliation as can be seen from the *Figure 3.1* below. A regular check of the exfoliation energy {in kilo joules (kJ)} and the subsequent power output {in Watts (W)} after every 30 minutes of the sonication was maintained to have an idea about the homogeneity in the exfoliation for the whole duration. An error of  $\pm 2-3$  W was taken into account because of the change of ice-water bath after every 40 minutes. To have reproducibility in the results, we tried our best to use same parameters every time and moreover the distance of the tip was kept 1 cm above the bottom of the vial to generate homogeneously the high energy shock waves in the compression and rarefaction cycles.

Then, to select the obtained poly-disperse 2D nanosheets on the basis of their size and thickness, a successive step-wise controlled cascade centrifugation was applied as introduced by Backes et al. [3] using eppendorf Bench top Centrifuge 5810 R, Rotor F-34-6-38. Controlled centrifugation was performed at 40g, 160g, 620g and 1000g/ 1400g for 45 minutes each to analyze the supernatants. After optimizing a range of initial concentrations and various exfoliation constraints, a stable dispersion for up to three to four weeks was achieved. This was in good



**Figure 3.1:** Represents the proper setup of sonicator device with an ice-box.

consideration to utilize this material for biological applications without the use of any organic solvent or any stabilizer. Direct exfoliation of 2D TMDs ( $\text{MoS}_2$  and  $\text{WS}_2$  nanosheets) in water is itself a big challenge because the surface tension of water is too high as compared to the surface tension of  $\text{MoS}_2$  nanosheets. This, in result makes very difficult to exfoliate the bulk crystal into thin nanoflakes with a considerable amount of stability and concentration. Though, the concentration we achieved in our experiments is not too high as that of in organic solvents such as N-methyl 2-pyrrolidone (NMP), dimethyl sulfoxide (DMSO) etc. But depending on our need, the obtained dispersion was sufficiently good and it gave very interesting results on the interaction pathways of  $\text{MoS}_2$  nanosheets with live-matter. The biological experiments were performed at different  $\text{MoS}_2$  dispersion concentration achieved in the range of 10  $\mu\text{g/mL}$  to 50  $\mu\text{g/mL}$ .

### 3.1.2. Characterization Results

Building on literature, we first centrifuged the stock dispersion at very low centrifugal force (40g) for 45 minutes to remove the un-exfoliated 2D MoS<sub>2</sub> nanosheets. Then, the supernatant was subjected to higher centrifugal speed (160g) for 45 minutes. In almost all cases we discarded the sediment obtained at 160g and began collecting the material for analyses above this threshold. The obtained supernatant was subjected to higher centrifugal speed (620 g). Now, the sediment was separated obtained at 620g and re-dispersed into fresh solvent of volume 3-5 mL. At this step, we separated half part of the dispersion for basic characterization of the material and the remaining was centrifuged at further higher centrifugal force at 1000 g for 45 minutes. The cascade was completed by repeated centrifugation in the same way at 1400g, 2700g and 3500g for the same duration. **Figure 3.2.** shows the supernatants of water exfoliated MoS<sub>2</sub> nanosheets dispersion centrifuged at different speeds. As we can see from the **Figure 3.2.**, the color of MoS<sub>2</sub> nanoflakes dispersion starts to diminish from dark green to light green. Moreover, as the centrifuge speed increases, thinner flakes are obtained which remains in the supernatant. **Figure 3.3** in G) shows the un-exfoliated MoS<sub>2</sub> powder after the sonication which did not completely mixed up during the sonication. In such a case, we have observed in our experiments that the subsequent centrifuged supernatant samples produces very low final concentration of the dispersed 2D MoS<sub>2</sub> nanosheets. Though, the basic hydrophobic nature of MoS<sub>2</sub> bulk powder is one of the reasons for the remaining un-exfoliated powder after the sonication but apart from that heterogeneity in the sonication parameters also lead to poor exfoliation when de-ionized/elix water is used as pure solvent. **Figure 3.4** shows the UV visible extinction spectra of MoS<sub>2</sub> nanosheets at 620 g, 2700 g and 3500 g after the immediate preparation and up to three weeks of storage. Higher centrifuged dispersions revealed much improved stability which was achieved by

optimizing various parameters after a number of experimental trials. The produced water exfoliated dispersions of MoS<sub>2</sub> nanosheets, which are highly stable in pure water, are biocompatible and thus can be useful for various biomedical and biotechnological applications.

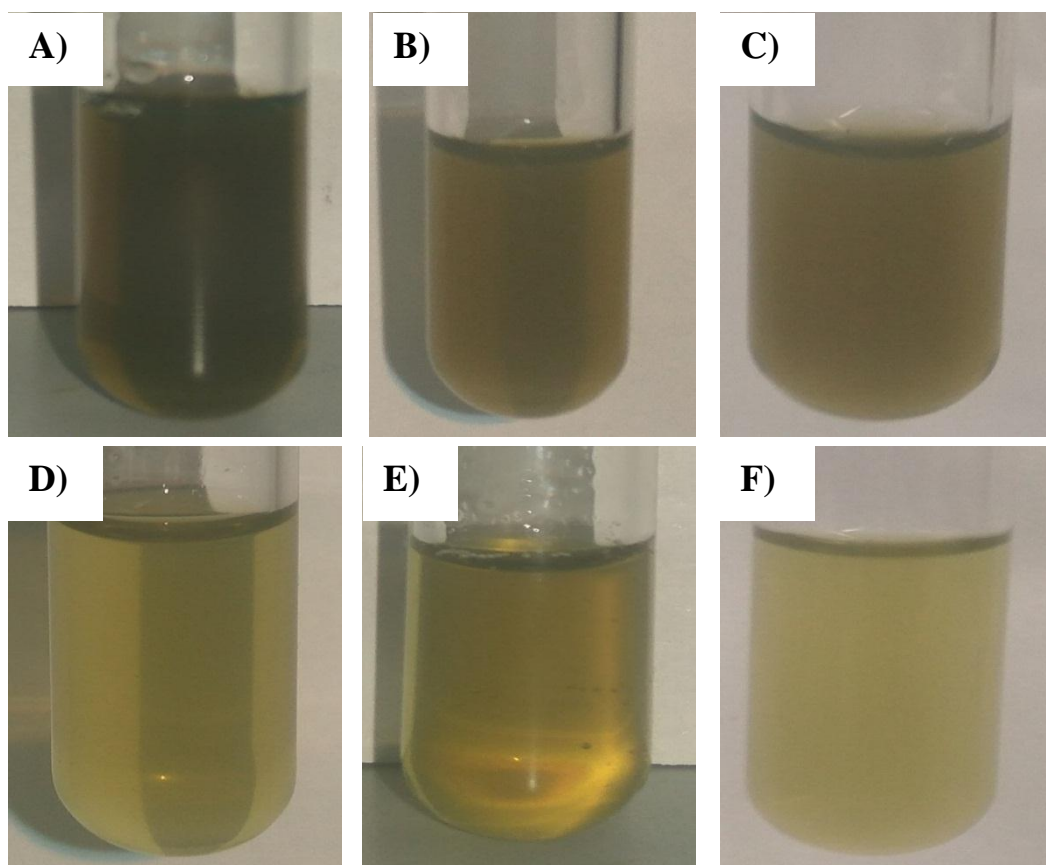


**Figure 3.2:** Panel (A-F) represents water-dispersed 2D MoS<sub>2</sub> samples centrifuged at A) 160 g, B) 620g, C) 1000g, D) 1400g, E) 2700g and F) 3300g. As the centrifuge speed increases, the color of the supernatant starts to diminish from dark green to light green (A-F).



**Figure 3.3:** Represents the tapered tip (KE-76, 6mm diameter) used for the exfoliation. Particularly, it shows the remaining and un-exfoliated MoS<sub>2</sub> powder cum semi-paste after the exfoliation.

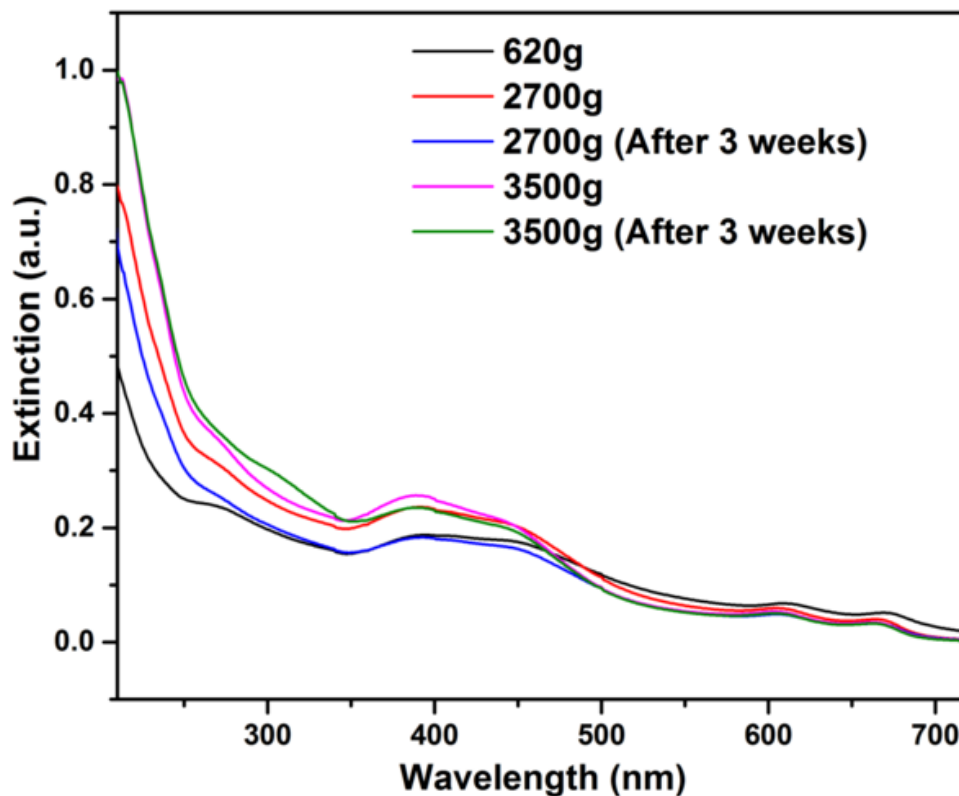


*Figure 3.4: UV-Visible absorbance spectra of water-dispersed MoS<sub>2</sub> nanosheets at centrifuged at different speeds, 620g, 2700g and 3500g for 45 minutes each. Higher centrifuged sample were kept under gravitational storage and at 4°C for three weeks just after the exfoliation. The above graph represents a good stability of water exfoliated samples which is crucial for further studies.*

### 3.1.3. Yield estimation

After exfoliation and size selection as described above, we let the samples dry by vacuum evaporation overnight to obtain a powder. Then, we weighed the obtained powder and used the following formula<sup>4</sup> to estimate the final yield:

$$\alpha = \frac{c_1}{c_0} \times 100\% \quad (3.1)$$

where  $\alpha$  is the overall yield and  $c_1$  and  $c_0$  are the final and initial concentrations of MoS<sub>2</sub> nanosheets dispersion, respectively.

The final estimated yield for  $c_0=5$  mg/mL of MoS<sub>2</sub> nanosheets is  $\approx 0.6\%$ . This value is lower than typically obtained in organic solvents and their mixtures, where it is possible to achieve  $\approx 2-5\%$  [5]. This is due to the solubility of MoS<sub>2</sub> nanosheets in pure water that is poorer than in organic solvents. However, by adding some biosurfactants or biomolecules such as hydrophobins, more concentrated and more stable MoS<sub>2</sub> based dispersions can be produced in eco-friendly and biocompatible solvents, which can be useful for multiple applications.

#### 3.1.4. UV-Visible Extinction Spectroscopy

Even though, UV-Visible spectroscopy is a very basic measurement technique, in general useful information can be extracted from such colloidal dispersions. The extinction spectra in the UV-visible region of MoS<sub>2</sub> samples contain the contribution from both absorbance and scattering components. Both of these components are size dependent. In our experiment protocol, at lower centrifugal forces 40 g and 160 g, scattering component was more dominant with high extinction peaks at 750–800 nm (See **Figure 3.4** confirming the presence of large particles). Whereas, at higher centrifugal forces 620 g and 1000 g, the characteristic excitonic transitions are observed and the scattering background is reduced. In addition, the A-exciton peak shifted towards the lower wavelength region which is related to decreasing layer number. With the increase in centrifugal force, number of layers per flake decreases which results in few layered enriched dispersions. The extinction spectra of MoS<sub>2</sub> after the final steps of centrifugation at 620 g and 1000 g are shown in **Figure 3.5 A**). Extinction parameters based on the formulation [6–8] as

shown in *equations 3.2 and 3.3* obtained immediately after the exfoliation of MoS<sub>2</sub> nanosheets and after three weeks of storage are shown in *Table 1*. The physical parameters of MoS<sub>2</sub> dispersion at different centrifugal forces are shown in *Table 2*.

$$N = 2.3 \times 10^{36} e^{\frac{-54888}{\lambda_A}} = 2.3 \times 10^{36} e^{-44.3E_A} \quad (3.2)$$

$$L (\mu m) = \frac{3.5Ext_B / Ext_{345} - 0.14}{11.5 - Ext_B / Ext_{345}} \quad (3.3)$$

<i>Parameters achieved after the exfoliation</i>	<i>Values of the parameters after the exfoliation</i>	<i>Values of the parameters after three weeks of storage</i>
A - exciton value	662 nm	662 nm
Number of layers ( $\bar{N}$ )	2	2
Concentration ( $\mu\text{g/mL}$ ) ( $\bar{C}$ )	10 $\mu\text{g/ml}$	10 $\mu\text{g/ml}$
Lateral size ( $\bar{L}$ )	76 nm	71 nm

**Table 1:** Mean value of dispersion concentration, number of layers, lateral size and A-exciton wavelength obtained from the optical extinction spectra just after the exfoliation and kept for three weeks of storage based on the metrics [<sup>3</sup>].

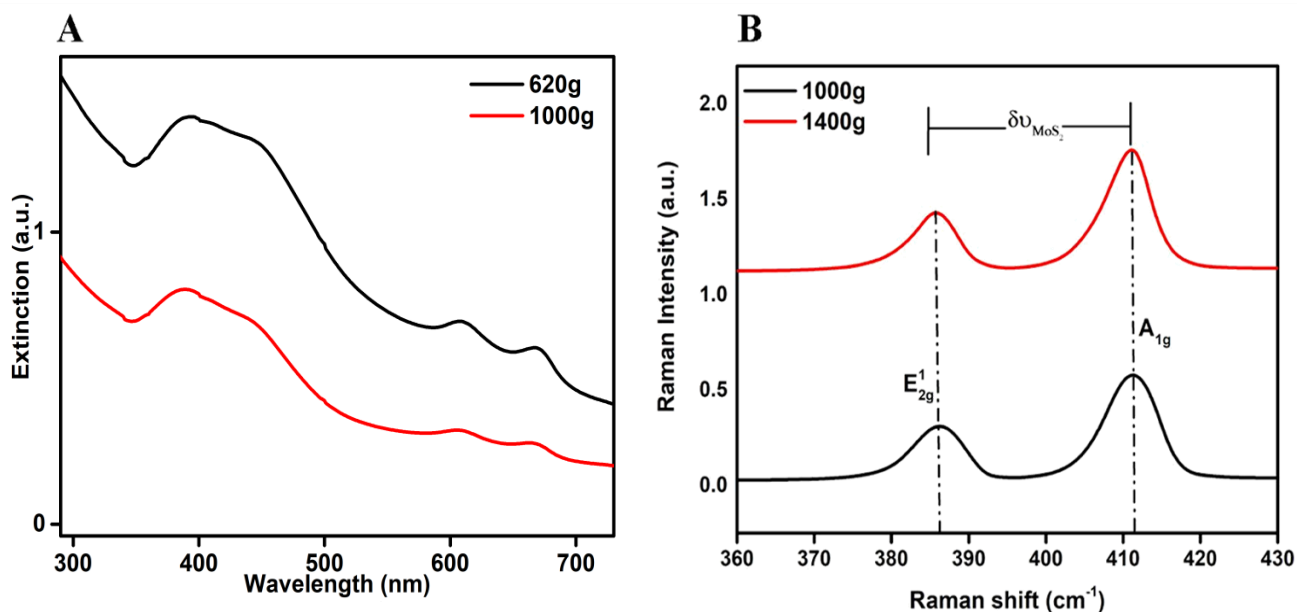


**Figure 3.5:** A) UV-Visible extinction spectra of 2D MoS<sub>2</sub> nanosheets dispersion at 620g and 1000g. B) Raman spectra of the two main vibrational modes E<sub>2g</sub><sup>1</sup> and A<sub>1g</sub> of MoS<sub>2</sub> nanosheets centrifuged at 1000g and 1400g. Raman shift in the region from 380 - 412 cm<sup>-1</sup> range represents MoS<sub>2</sub> nanoflakes in the range from 2-4 layers.

<i>S. No.</i>	<i>Centrifugal Force (C.F)</i>	<i>Mean Layer Number &lt;N&gt;</i>	<i>Mean Lateral Size &lt;L&gt;</i>
1.	620g	5	220 nm
2.	1000g	2-3	160 nm
3.	1400g	2	100 nm
4.	2700g	3	90 nm
5.	3500g	2	70 nm

**Table 2:** Mean value of number of layers and lateral size at the given centrifugal speeds. The given values are obtained from the UV-Visible optical extinction spectra using the metrics as reported by Backes et al. [3].

### 3.1.5. $\zeta$ - Potential Measurements

Generation of surface charges over the surface of 2D nanosheets plays a crucial role to understand the stability of liquid exfoliated dispersions. To identify these surface charges, electrophoretic mobility measurements ( $\mu$ ) are performed in general. These ( $\mu$ ) measurement works as a quantifying tool to understand the electrostatic stabilization between the nanosheets by estimating the zeta potential ( $\zeta$ ). In case of 2DMs, dynamic interactions among the nanosheets and their electrostatic stabilization play a fundamental role to anticipate the stability of liquid dispersions. It was observed that after the exfoliation, the MoS<sub>2</sub> flakes exhibit high surface charge density depending upon the different centrifugal forces applied as seen from the **Table 3**. Generally, defect free MoS<sub>2</sub> nanosheets are neutral and nanomaterial with no surface charge will

precipitate in the end. Exfoliation of MoS<sub>2</sub> nanosheets in water might have generated charged edges which were responsible for the stabilization of dispersed nanoflakes in pure water.

<i>Centrifugal Force (g)</i>	<i>Zeta Potential (<math>\zeta</math>) mV</i>	<i>Electrophoretic mobility (<math>\mu</math>)</i>
620g	-23.9 ± 0.6	- 1.88 ± 0.04
1000g	-29.2 ± 1.3	-2.9 ± 0.1
1400g	-25.6 ± 0.700	-2.008 ± 0.05736
2700g	-23.4 ± 0.346	-1.835 ± 0.02536
3500g	-16.5 ± 1.51	-1.294 ± 0.1174

**Table 3.**  $\zeta$ - Potential values of MoS<sub>2</sub> nanosheets dispersion at different centrifugal forces.

### 3.1.6. Raman Micro-spectroscopy of MoS<sub>2</sub> nanosheets in absence of cells

Raman spectroscopy is a widely employed tool to estimate the thickness of TMD nanoflakes [9-12]. The Raman spectrum of MoS<sub>2</sub> shows two characteristic bands at  $E_{2g}^1$  and  $A_{1g}$ , which corresponds to the in-plane and out-of-plane vibrational modes, that for bulk fall at about 380

$cm^{-1}$  and  $403\text{ cm}^{-1}$  respectively [10]. MoS<sub>2</sub> nano-structuring modifies the Raman features of the bulk with an increase for the  $E_{2g}^1$  frequency and a corresponding decrease of the  $A_{1g}$ .

$$\Delta\vartheta_{MoS_2} = \vartheta_{A_{1g}} - \vartheta_{2g}^1 \quad (3.4)$$

The frequency shift allows for an identification of the number of layers in the nanoflakes [10,11]. In **Figure 3.5 B**), the Raman spectra of MoS<sub>2</sub> nanoflakes in absence of cells centrifuged at 1000 g and 1400 g are shown, with laser excitation at 514.5 nm. We observed similar modification in the Raman spectrum compared to bulk for both centrifugal protocols, with a common range of frequency shift  $\Delta\vartheta_{MoS_2}$  of peaks ranging in the 23–24.6  $cm^{-1}$  window. The  $\Delta\vartheta_{MoS_2}$  range observed via Raman micro-spectroscopy corresponds to a nano-structuring spanning from 4 to 2 layers. These micro-Raman spectroscopy results look consistent with the range of nano-structuring indicated by UV-Vis extinction spectroscopy. For more Raman spectra please refer to the *Appendix section* of this thesis.

### **3.1.7. Scanning Electron Microscopy (SEM) Images of water dispersed MoS<sub>2</sub> nanosheets**

The following SEM images displayed in **Figures 3.6 and 3.7** have been obtained from the water-dispersed 2D MoS<sub>2</sub> nanosheets centrifuged at 3000g for 45 minutes. For the SEM sample preparation, the dispersion was drop-casted onto the silicon substrate and was put under vacuum to dry for 15 minutes and the following day SEM measurement was performed.

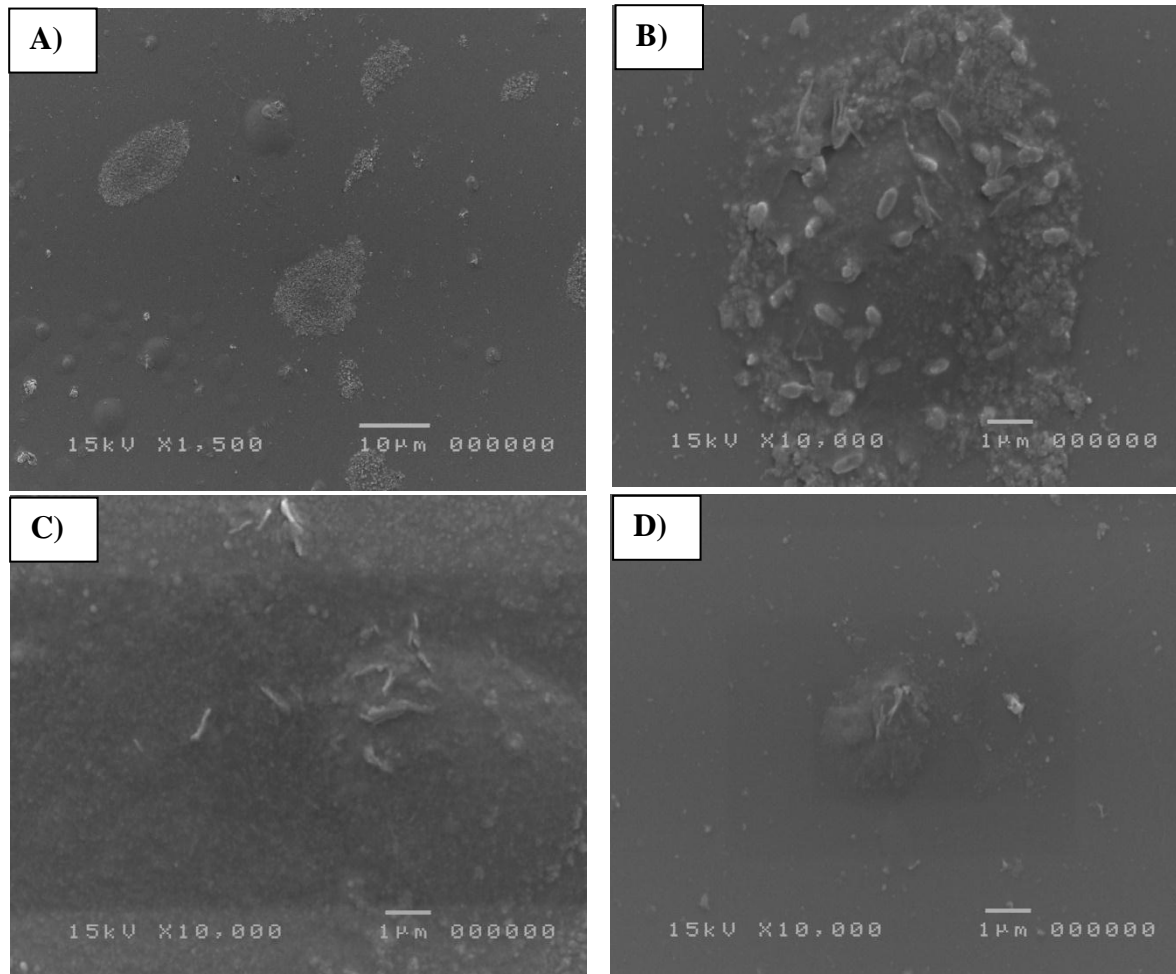


**Figure 3.6:** Pannel (A-D) represents two different scales of SEM obtained for water-exfoliated 2D MoS<sub>2</sub> nanosheets dried under vacuum for 15 minutes and centrifuged dispersion at 2000g. (A) Shows small islands of an ensemble of 2D nanosheets which aggregated on drying. (B-D) shows large and small chunks of 2D MoS<sub>2</sub> nanosheets at 1 μm scale which clearly signifies the ability of water to act as a considerable solvent to exfoliate 2D TMDs for some specific applications where few layer and multi-layer nanosheets are required.

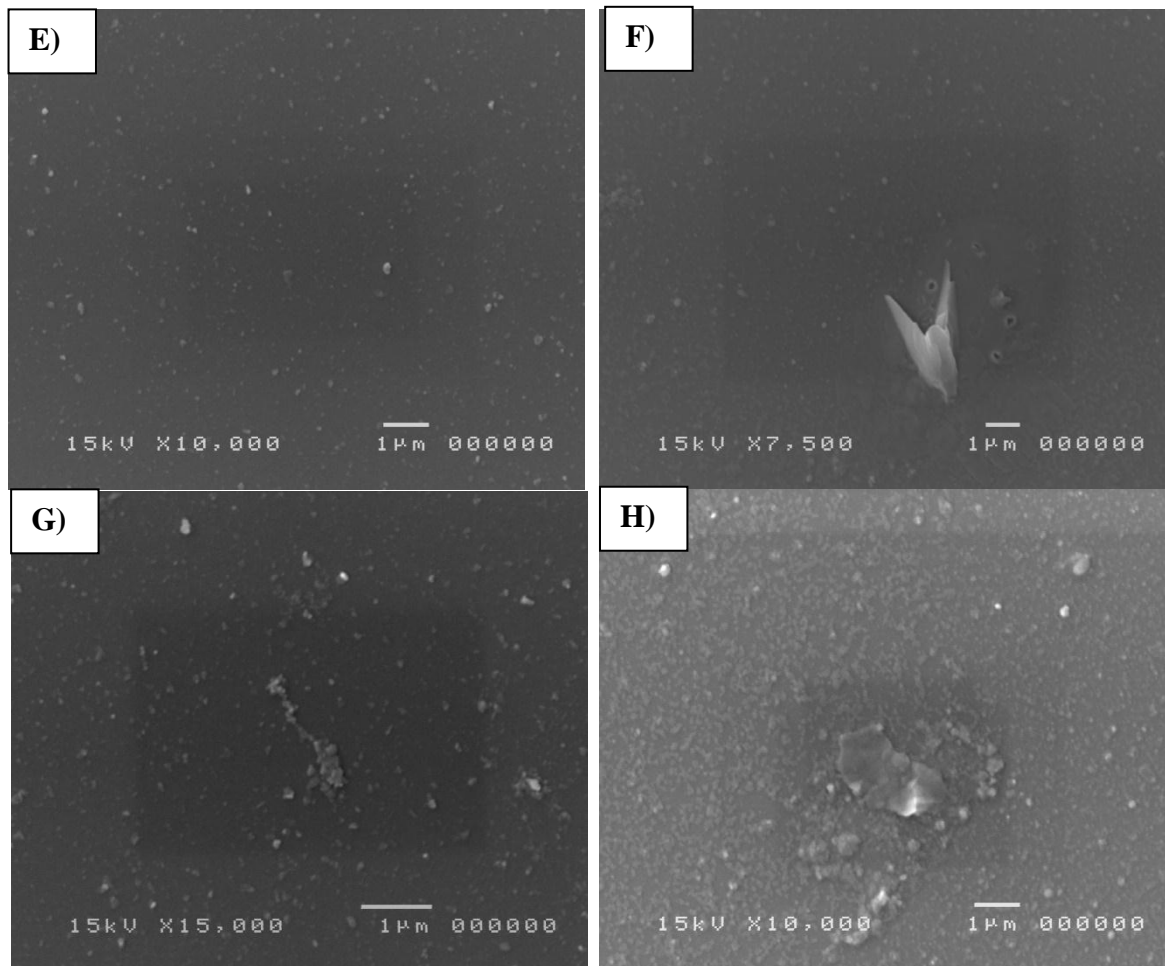


**Figure 3.7:** Pannel (E-H) represents another panel of SEM images at 1  $\mu\text{m}$  scale dried under vacuum for 15 minutes and centrifuged dispersion at 3000g. E) Shows a homogenous distribution of water exfoliated MoS<sub>2</sub> nanosheets over the silicon substrate. F) Shows a peculiar kind of sharp knife type morphology of MoS<sub>2</sub> nanosheets and the surrounding homogenous distribution of small lateral size 2D nanflakes. (G-F) Represents small and large chunks of water exfoliated few layer 2D MoS<sub>2</sub> nanosheets.

### 3.1.8. Transmission Electron Microscopy (TEM) Images

Particularly, we collected the TEM images of water exfoliated 2D MoS<sub>2</sub> nanosheets based on their centrifugal speeds at which we have achieved a significant amount of stability on the exfoliated dispersion as explained in section 5.6.2. (UV-Visible Extinction Spectroscopy) The obtained TEM images revealed the fabrication of very thin few layer MoS<sub>2</sub> nanosheets at different centrifugal speeds such as 620g, 1400g and 3500g. **Figure 3.8(I)** shows large few layer ultrathin MoS<sub>2</sub> nanoflakes with a wrinkled surface. **Figure 3.8 (II)** shows the magnified image of a particular portion over the copper grid where MoS<sub>2</sub> dispersion is deposited. The intensity of the flakes deposited in this particular region is not very high, whereas some other regions of the MoS<sub>2</sub> nanoflakes deposited copper grid shows a considerable amount of 2D nanoflakes with some aggregation. **In Figure 3.9 (I)**, magnified view of few layer MoS<sub>2</sub> nanosheets is visible stacked diagonally upon each other, whereas the rest of the portion shows the aggregated flakes. **In Figure 3.9 (II)**, a high population of single layer and few layer thin 2D MoS<sub>2</sub> nanoflakes can be seen which due to increase in centrifugal force decreases the thickness of exfoliated nanoflakes.

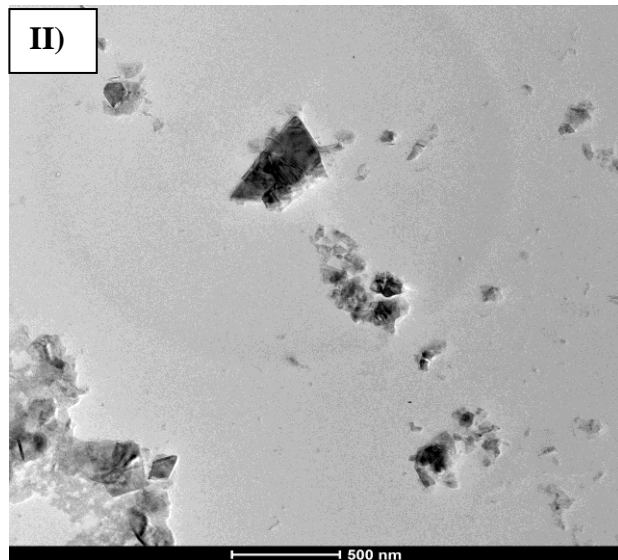
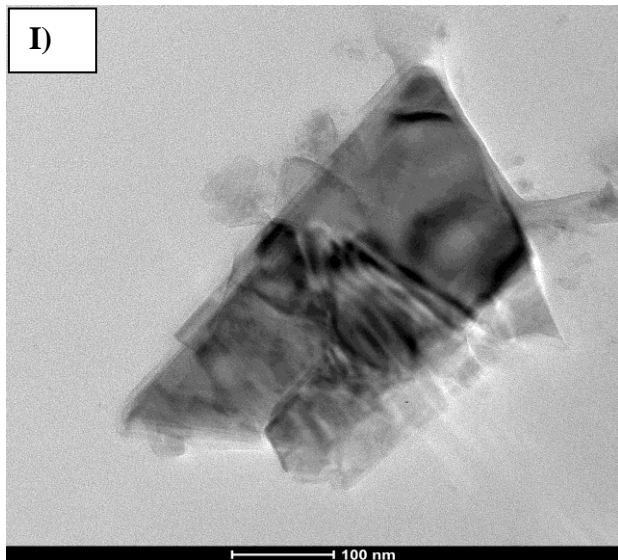


**Figure 3.8:** Represents the TEM image of water exfoliated 2D MoS<sub>2</sub> nanosheets at 620 g.

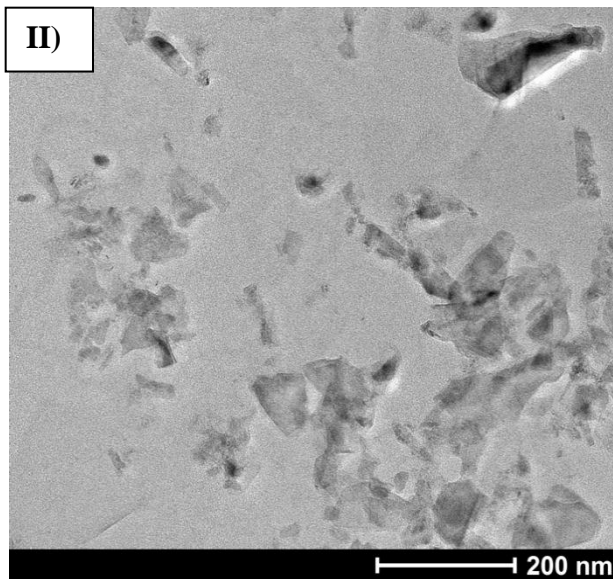
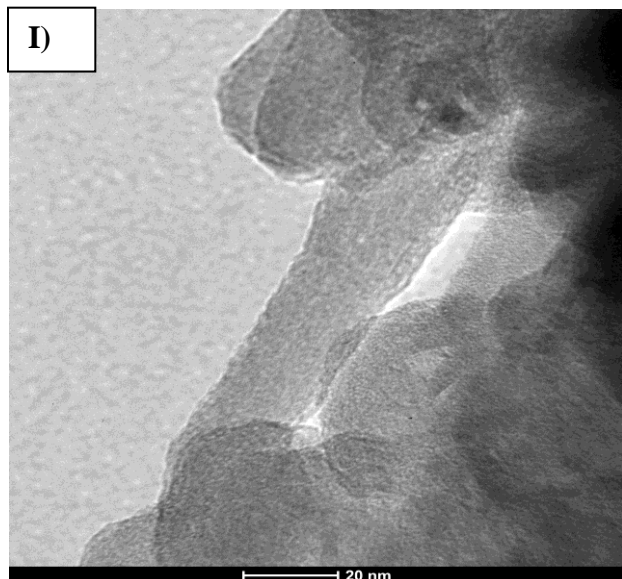


**Figure 3.9:** Represents the TEM image of water exfoliated 2D MoS<sub>2</sub> nanosheets at 1400 g.

## **3.2. Experimental Details**

### **3.2.1. Ultra-sonication Technique**

Ultra-sonication is a term which refers to the transfer of sound energy to mechanical energy for various applications such as membrane cell disruption, nanoparticles dissolution, production of biofuels, polymer processing, de-agglomeration of nanomaterials and exfoliation of layered crystals to name a few. It has been considered as one of the green fabrication technology to synthesize different nanoparticles in a wide range of solvents which in result provide control over their size, morphology, concentration and other physical parameters. The generation of intense ultrasonic waves in a given liquid is configured by two different routes:- ultrasonic bath and probe/tip sonicator. Basically, in an ultrasonic bath, rectangular shaped metal liquid container with a free surface over the top is attached with several transducer elements which produces plane standing wave pattern in a given liquid (usually de-ionized water). On the other hand, probe/tip sonicator consists of a metal tip with different diameters which in the end are dipped into the given medium with specified amplitude to be run for a given amount of time. Generally, the passage of ultrasonic waves produces high pressure and low pressure waves in a given medium which results in the formation and collapse of large number of microbubbles for a very short time say for about few microseconds. The formation, growth and collapse of the microbubbles creates cavities in those regions and furthermore high speed jets and thermal shock waves which acts as a driving force for peeling out or de-agglomeration of various nanomaterials. Both kinds of ultra-sonication are material dependent and furthermore, physical parameters of the fabricated nanomaterial can be tuned/controlled by varying the operating parameters of the ultra-sonicator device such as final output power, amplitude of the probe sonicator, pulse modes with tunable time selection, sonication time and sonication vial.

The basic principle behind the exfoliation of bulk layered crystals using LPE is to overcome the weak van der Waals forces of attraction and to break the strong covalent bonding between the layers so as to separate them into thin nanosheets. Subsequently, this step is aided by adding suitable solvents/surfactants to avoid the aggregation of exfoliated 2D nanosheets.

Though, there are different other routes as well to achieve the desired 2D nanosheets but ultrasonication is the most versatile route to separate the bulk layers via physical/mechanical vibration as a result of the conversion of electrical signal to mechanical energy by exciting the piezoelectric crystals. This in results generates a vibration/motion travelling through the tip/horn/probe of the sonicator device to produce high energy pressure waves in the given dispersing liquid. Due to this vibration, micro-cavities or millions of bubbles are introduced into the liquid which implode violently and generates high energy jets or shock waves to peel out the bulk crystal very efficiently. This in general is known as compression and rarefaction cycles because of the generation of millions of shock waves in the given medium. As a result, the local pressure and temperature of the medium elevates substantially at the imploding sites which in result is able to overcome the weak van der Waals forces of attraction to cleave the individual layers from the bulk crystal. A range of materials have been successfully isolated into ultrathin 2D nanosheets such as graphene [<sup>13-16,17-19,20</sup>], 2D TMDs [<sup>21-23</sup>] and carbon nanotubes [<sup>13,24-28</sup>].

Now, two different devices can be employed for this purpose, one is ultrasonic bath which operates with a power output of 40 W or more. On the other hand, tip/probe sonicator is a high energy device with an output power of up to 750W. In view of this, the latter processes the material efficiently in much shorter time. Apart from this, reproducibility using ultrasonic bath is very hard to achieve because the position of the sample vial should be at the same position every

time, whereas in tip sonication the mechanical vibration is transferred longitudinally to the sample dipped into the liquid medium. An important point in both cases is to provide either continuous supply of circulating cooled water or performing the exfoliation in a covered ice box so as to avoid the over-heating of the sample which in result can degrade the quality of exfoliated nanosheets.

### **3.2.2. Liquid Phase Exfoliation (LPE) of MoS<sub>2</sub> nanosheets in pure water**

To unravel the full potential of 2D TMDs nanosheets, it is very crucial to have proper control over their production route. To accomplish this, a more versatile and scalable technique is apparent. In view of this, one of the most versatile ultra-sonication method to exfoliate various 2DMs in a wide range of solvents is liquid phase exfoliation technique which from the application point of view is much flexible and scalable technique. [<sup>29,30</sup>]. Recently, Han Ma et al. have reported the cavitation induced thinning and fragmentation of MoS<sub>2</sub> nanoflakes directly exfoliated in water. In this work, it is mentioned that the smaller lateral size nanosheets induce stability to the dispersion due to enhanced edge effects on the basis of Hemi-wicking model [<sup>31</sup>]. Mohammad Heiranian et al have reported a theoretical study to develop the force field parameters for MoS<sub>2</sub> nanosheets – water interaction studies which the authors proposed could be extremely useful in DNA/RNA interaction, drug delivery and other biomedical applications [<sup>32</sup>].

The appealing biocompatibility and bio-interactions of MoS<sub>2</sub> nanosheets embraces its potential in terms of environmental impact and toxicity to the cell world. The main objective of my thesis project is to study the biological interactions of water dispersed 2D MoS<sub>2</sub> nanosheets with live-matter such as human cells and different pathogens. So, to execute this aim, it was very

important to fabricate a good quality of MoS<sub>2</sub> nanosheets in a green and biocompatible solvent which can be directly used in the physiological medium, which in my case is de-ionized water which serves as an ideal solvent other than the toxic organic solvents for the given application. Additionally, a concrete optimization of the sonication parameters such as, choice of green solvents, initial concentration of the solution, exfoliation time and controlled centrifugation for size and thickness selection of 2D nanosheets is required to achieve the desired results and to understand the fate of LPE exfoliated 2D nanosheets in biological media [<sup>33-35</sup>].

Therefore, water dispersed, defect free and biocompatible 2D MoS<sub>2</sub> nanosheets are an appealing and demanding option to study different biological interactions and their behavior with the living cells, tissues and different pathogens to name a few. Moreover, to the best of our knowledge, a thorough study on the different interaction pathways of naked MoS<sub>2</sub> nanosheets with different human cell lines and various pathogens is highly needed and still missing in the most important case, namely for nanosheets produced by eco-friendly methods and dispersed into water based media that is the native surrounding of biological matter.

### **3.2.3. Research attempts on direct LPE of 2D TMDs in pure water**

Considering the significance of MoS<sub>2</sub> nanosheets in biomedical field, it is very important to understand its behavior, toxicology, biocompatibility and environmental impact in that surrounding [<sup>36,37</sup>]. Achieving a considerable understanding on these issues will finally open some doors to use MoS<sub>2</sub> and other 2D TMDs for various in-vivo and clinical trial studies. To accomplish this goal, green and scalable fabrication of MoS<sub>2</sub> nanosheets is extremely important. In view of this, there have been several attempts made to stabilize MoS<sub>2</sub> and other 2D TMDs

using different biomolecules such as, proteins [38-40], polysaccharides [41,42] and DNA/RNA nucleotides [42,43] to name a few. The above cited biomolecules acts as a stabilizer or surfactants to minimize the net exfoliation cost to make the dispersion stable for a long time. On the other hand, when the exfoliated 2D TMD nanosheets are dispersed in water for their actual purpose, the remaining impurities from these cited compounds inevitably bring adverse effects to the ultimate performance of 2D TMDs in bio applications. Though, there are different biomedical paths where 2D TMDs are employed such as drug delivery, tissue engineering, biosensors and biocompatible scaffolds for cancer treatment to name a few [44-49,50]. But to understand the cellular level interactions and the impact of MoS<sub>2</sub> nanosheets on the outer membrane of various live-matters such as human cells and different pathogens, bacteria and viruses, it is crucial to fabricate the 2D nanosheets without the use of additives.

Very few studies have been reported so far on the direct exfoliation of MoS<sub>2</sub> and other 2D TMD nanosheets in pure water, which on the other hand do not focus on the cellular level interaction of MoS<sub>2</sub> nanosheets, rather on energy storage, catalysis and other applications [2,51-54]. Few years back, Forsberg et al reported a combination of mechanical and liquid exfoliation of MoS<sub>2</sub> nanosheets in pure water with a final concentration of 0.14 mg ml<sup>-1</sup> [54]. The authors have explained the reason for the stabilization of 2D nanosheets because of generation of electrical charges upon electrophoretic mobility measurements. In another study, authors made an attempt to exfoliate MoS<sub>2</sub> nanosheets in pure water by using lab made MoS<sub>2</sub> as a parent material. Though, the exfoliation was successful but the major loophole in their attempt was that it did not work for commercial samples and moreover, their produced 2D TMD nanosheets were highly defective [55]. In one of the studies, authors have reported the successful exfoliation of MoS<sub>2</sub> nanosheets in water by generating additional shear forces apart from the ultra-sonication by

using magnetic stirring [56]. Kim et al have reported a detailed study of the exfoliation of MoS<sub>2</sub>, WS<sub>2</sub>, MoSe<sub>2</sub> and other 2D layered compounds in pure water without any functionalization [34]. Control over the storage and preparation temperature played a key role in stable dispersions of these layered materials. In another study, authors made an attempt to exfoliate MoS<sub>2</sub> nanosheets in alkaline environment and the stability of the produced 2D nanosheets was much better than in alkali-free medium because of the intercalation of K<sup>+</sup> ions into the interlayer spaces of MoS<sub>2</sub> bulk material which assists in exfoliation and reduces the net exfoliation cost [57,58].

### **3.2.4. Sonicator equipment details for this thesis**

Basically, for all sonication experiments employed in this thesis have been performed by a tip sonicator (Bandelin Ultrasound SONOPLUS HD3200) which has a fixed frequency output of 20 kHz and maximum power of 200W as shown in the *Figure 3.1*. To exfoliate bulk MoS<sub>2</sub> powder into thin nanosheets, two different probes/tips (MS-72, a micro tip with 2mm diameter and KE-76, a tapered tip with 6mm diameter) are employed, depending on the volume of the sample to be exfoliated. Certain values of amplitudes have been chosen for different time durations to optimize the sonication parameters and subsequently the exfoliation efficiency of MoS<sub>2</sub> nanosheets. Each exfoliation experiment was accompanied by a chilled ice bath to avoid the over-heating of the samples. As suggested by Paton et al. [1] that larger diameter of the tip can process larger volumes and hence higher yield but the relation is not proportional because increasing the volume and subsequently the parameters of the sonicator will saturate at a certain point and no more separation/isolation of the bulk crystal will occur. The following equation (1) gives an idea on the production rate and concentration of the exfoliated nanosheets:-

$$P_R = \frac{CV}{t} \quad (3.5)$$

Where  $P_R$  is the production/exfoliation rate,  $C$  is the final concentration of the dispersed nanosheets,  $V$  is the volume of the liquid and  $t$  is the sonication time. So, this production rate is also dependent on the sonicator parameters chosen such as amplitude and the final output power of the device. Operating at low amplitude will give low intense exfoliation and vice versa. To get higher reproducibility in results using tip sonicator certain parameters such as, amplitude setting, volume of the liquid, sonication vial, viscosity of the medium and temperature must remain constant [<sup>59,60</sup>]. After the sonication, the most important step is the centrifugation of the as exfoliated poly-disperse 2D nanosheets so as to select them on the basis of their size and thickness for the desired application.

### 3.2.5. Centrifugation

The fundamental disadvantage of LPE of 2DMs is that it gives poly disperse nature of exfoliated 2D nanosheets in the given medium. These consist of un-exfoliated material, unstable dispersed nanosheets and of course separated and exfoliated nanoflakes which are poly-disperse in nature of various dimensions depending upon the wisely chosen solvent for exfoliation and the corresponding matching of surface tension with that of the solute material. The larger dense particles tend to sediment faster than the less dense under the earth's gravitational field. Basically, for a spherical particle certain important parameters account for its sedimentation in a given medium such as viscosity of the liquid ( $\eta$ ), gravitational force ( $g$ ), density of the particle ( $\rho_p$ ) and given medium ( $\rho_m$ ), velocity of the particle to sediment ( $V$ ) and diameter of the particle ( $d$ ). These parameters can be represented in a following equation which is known as Stokes Equation:-

$$V = \frac{d^2}{18n} (\rho_p - \rho_m)g \quad (3.6)$$

Depending on the density of the particle and medium, in some cases natural sedimentation to the bottom of the vial would not occur. So, in such as case, to enhance the magnitude of gravitation force artificially to improve the sedimentation of un-exfoliated or unstable particles in the medium, centrifugation is extremely important. Three different forces are balanced in the given environment during centrifugation such as force due to gravity ( $F_g$ ), force due to buoyancy ( $F_b$ ) and force due to viscous drag ( $F_d$ ) as shown in the *Figure 3.10*.

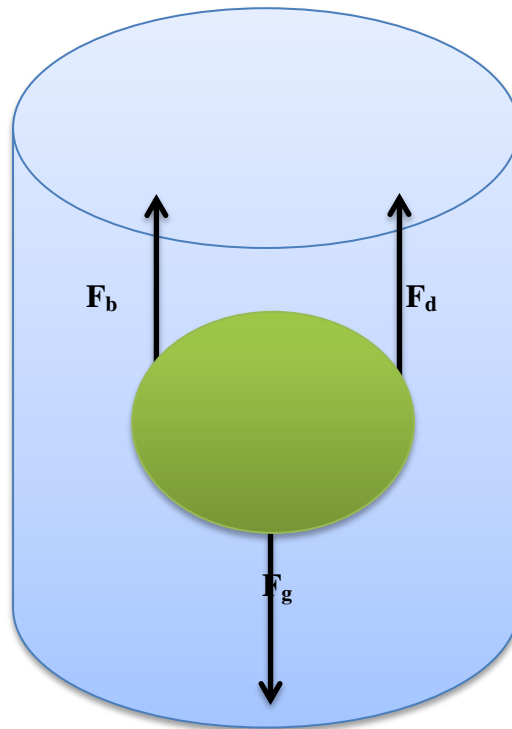


*Figure 3.10: Different forces acting on a particle in the given medium.*

Basically, when the dispersed particle will have higher density than that of the medium, it will move towards the bottom of the vial and subsequently the viscosity of the medium will decide the time it takes to reach at the bottom [61,62]. Though, the above equation is applicable only to spherical particles but several authors have explained the sedimentation of 2D nanosheets using the first approximation of the Stokes Equation even though an advanced theory to completely understand the sedimentation of anisotropically shaped nanosheets has not been developed yet. It is because during the centrifugation buoyancy and friction of nanosheets with the medium are morphology dependent. So, the concept of centrifugation for 2D nanosheets has been explicitly explained by several authors based on its mass [63–68], even though the concept has been described in a very simple way.

Being inspired by the work done on liquid cascade centrifugation (LCC) of aqueous surfactant exfoliated various 2D nanoflakes by Backes et al. [3], and thanks to the flexibility to tune any cascade step according to the desired application, we have adopted LCC to achieve thin and few layer MoS<sub>2</sub> nanoflakes to understand the interaction of different lateral size selected 2D nanosheets with the live matter in de-ionized water.

### **3.2.6. Centrifugation equipment details for this thesis**

In our experiments, eppendorf bench top centrifuge with a specific rotor FA-45-6-30 (6x50 mL) with *QuickLock* lid is employed as shown in the **Figure 3.11**. This fixed motor has the capacity to hold 6 samples at a time with the ability to tune the angle of rotor up to 45°. There is also a provision to choose a particular temperature at which the samples have to be centrifuged with flexible acceleration and de-acceleration values from 1-9. Maximum speed 20,130 × g (12,100

rpm) in Centrifuge 5810 R or  $16,639 \times g$  (11,000 rpm) in 5804/5804R/5810. Basically, we have employed controlled centrifugation steps inspired by Backes et al. [3]. Particularly, the as exfoliated poly disperse sample was centrifuged at different speeds such as 40g, 160g, 620g, 1000g, 1400g and in some cases 2000g – 3500g as well, shifting the supernatant which is de-ionized water in this case, to next cascade step at each step and re-dispersing the sediment after the second step to reuse the dispersion for further characterization analyses.

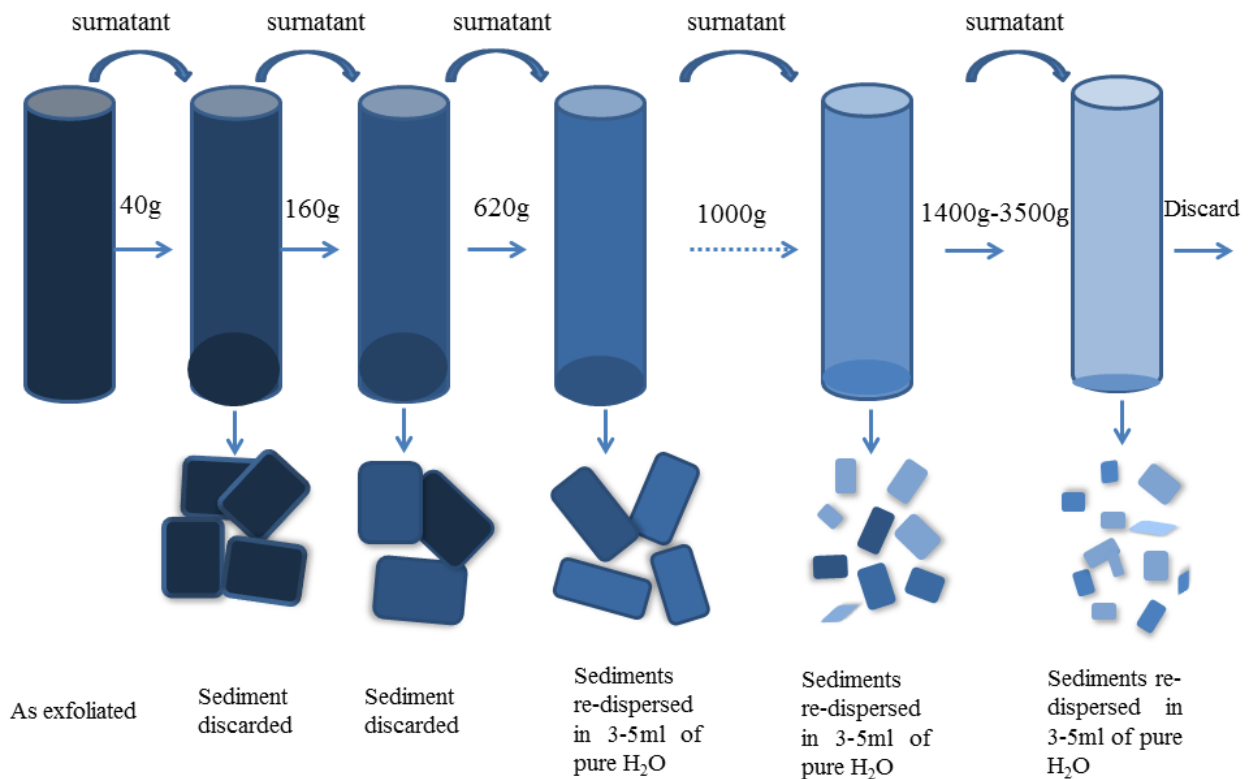


**Figure 3.11:** Liquid Cascade centrifugation scheme applied in our experiments

### 3.2.7. Technical characterization details

Subsequently, the supernatants obtained after the controlled centrifugation steps at different gravitational speeds (g-force) were subjected to microscopic and optical spectroscopic characterization measurements such as UV-Visible absorbance spectroscopy for optical extinction spectra generation for dispersion concentration, lateral size and number of layers of exfoliated 2D nanosheets. *Optical extinction spectra* were acquired on Jasco V-530 UV-Vis spectrophotometer using 1 cm optics quartz cuvette. Basically, for all experiments performed in this thesis, have relied on optical extinction spectra to obtain the values for MoS<sub>2</sub> dispersion concentration  $\langle C \rangle$ , mean lateral size  $\langle L \rangle$  and number of layers  $\langle N \rangle$  at the given centrifugal speeds mentioned as above. The metrics to obtain  $\langle C \rangle$ ,  $\langle L \rangle$ ,  $\langle N \rangle$  have been introduced by Backes et al. [3] which we have followed in our work. Then, to obtain some information on the surface charge of exfoliated 2D MoS<sub>2</sub> nanosheets, we have employed the use of zeta potential which measures the electrophoretic mobility of the 2D nanoflakes in the given medium by applying an external potential.

*Raman microscopy* was used to analyze the number of layers of exfoliated and bulk MoS<sub>2</sub> nanosheets. The samples for Raman spectroscopy measurements were prepared by evaporating the dispersion under vacuum and this resulted in characteristic, yet not very pronounced changes in the two main peaks of MoS<sub>2</sub> nanosheets which are  $E_{2g}^1$  and  $A_{1g}$ . A *confocal Raman microscope* (Jasco, NRS-3100) was used to obtain Raman and photoluminescence spectra. The 514 nm line of an air-cooled Ar<sup>+</sup> laser (Melles Griot, 35 LAP431 220), was injected into an integrated Olympus microscope and focused to a spot diameter of approximately 3 μm by a 20x objective with a final 4 mW power at the sample. A holographic notch filter was used to reject the

excitation laser line. The Raman backscattering was collected using a 0.1 mm slit and a diffraction lattice of 1200 grooves/mm, corresponding to an average spectral resolution of 8 cm<sup>-1</sup>. Solutions were left evaporating on Si substrates, and it took 60 s to collect a complete data set by a Peltier-cooled 1024 x 128 pixel CCD photon detector (Andor DU401BVI). Raman measurements were at least triplicated for scope of reproducibility. Wavelength calibration was performed by using cyclohexane as a standard.

*Electrostatic stabilization* is an important parameter to analyze the stability of the liquid exfoliated dispersions. The surface charges generated during the exfoliation can be attributed to electrophoretic mobility measurements ( $\mu$ ). So, these ( $\mu$ ) measurements were carried out on laser interferometric technique (Malvern Zetasizer Nano system) with irradiation from 633 nm He-Ne laser. The samples were injected in folded capillary cells, and the electrophoretic mobility ( $\mu$ ) was measured using a combination of electrophoresis and laser Doppler velocimetry techniques [69]. The Henry's equation was used to estimate the zeta potential from the electrophoretic mobility data. For the possible upper and lower limits of the zeta potential values, Henry's equation was approximated to both the Huckel and Smoluchowsky limits. The reason for this approximation is due to the particular solvent-sample relationship; Henry's equation is approximated to get an estimate of surface charge values of exfoliated nanosheets. All the measurements were carried out at 25 °C.

Morphological analyses of samples were performed with a *scanning electron microscope (SEM)* JEOL-JSM 5310 (CISAG laboratory, at University of Naples, Federico II). The SEM operating at 15 kV, is equipped with energy dispersive X-Ray spectroscopy (EDS); data were processed with INCA version 4.08 (Oxford Instruments, 2006). The samples were metalized with gold by

using a sputter coater. Oxford Instruments (2006): INCA - The microanalysis suite issue 17a + SP1 - Version 4.08. Oxford Instr. Anal. Ltd., Oxfordshire, UK.

Thanks to our new collaboration, to further investigate the nanosheet morphology, *transmission electron microscopy* was carried out recently. TEM micrographs were collected using a FEI TECNAI G2 S-twin 200kV apparatus operating at 120kV (LaB6 source). A drop (5uL) of flakes (suspension in water) was transferred on carbon-coated copper grids and then left at room temperature until the solvent was completely evaporated we have obtained MoS<sub>2</sub> nanosheets images from transmission electron microscopy (TEM) showing few layers and in some portions aggregated morphology of 2D MoS<sub>2</sub> nanosheets.

## Bibliography

1. Santos, H. M., Lodeiro, C. & Capelo-Martínez, J. L. The Power of Ultrasound. *Ultrasound Chem. Anal. Appl.* 1–16 (2009).
2. Pan, L., Liu, Y. T., Xie, X. M. & Ye, X. Y. Facile and Green Production of Impurity-Free Aqueous Solutions of WS<sub>2</sub> Nanosheets by Direct Exfoliation in Water. *Small* **12**, 6703–6713 (2016).
3. Backes, C. *et al.* Production of highly monolayer enriched dispersions of liquid-exfoliated nanosheets by liquid cascade centrifugation. *ACS Nano* **10**, 1589–1601 (2016).
4. Dong, H., Chen, D., Wang, K. & Zhang, R. High-Yield Preparation and Electrochemical Properties of Few-Layer MoS<sub>2</sub> Nanosheets by Exfoliating Natural Molybdenite Powders Directly via a Coupled Ultrasonication-Milling Process. *Nanoscale Res. Lett.* **11**, (2016).
5. Li, Y., Yin, X. & Wu, W. Preparation of Few-Layer MoS<sub>2</sub> Nanosheets via an Efficient Shearing Exfoliation Method. *Ind. Eng. Chem. Res.* **57**, 2838–2846 (2018).
6. Backes, C. *et al.* Production of Highly Monolayer Enriched dispersions of liquid-exfoliated nanosheets by liquid cascade centrifugation. *ACS Nano* **10**, 1589–1601 (2016).
7. Backes, C. *et al.* Edge and confinement effects allow in situ measurement of size and thickness of liquid-exfoliated nanosheets. *Nat. Commun.* **5**, 1–10 (2014).
8. Backes, C. *et al.* Preparation of liquid-exfoliated transition metal dichalcogenide nanosheets with controlled size and thickness: A state of the art protocol. *J. Vis. Exp.* **2016**, 10–13 (2016).

9. Kaur, J. *et al.* Green synthesis of luminescent and defect-free bio-nanosheets of MoS<sub>2</sub> : interfacing two-dimensional crystals with hydrophobins. *RSC Adv.* **7**, 22400–22408 (2017).
10. Lee, C. *et al.* Anomalous lattice vibrations of single-and few-layer MoS<sub>2</sub>. *ACS Nano* **4**, 2695–700 (2010).
11. Zhang, X. *et al.* Phonon and Raman scattering of two-dimensional transition metal dichalcogenides from monolayer, multilayer to bulk material. *Chem. Soc. Rev.* **44**, 2757–2785 (2015).
12. Kaur, J. *et al.* Electrostatically driven scalable synthesis of MoS<sub>2</sub>–graphene hybrid films assisted by hydrophobins. *RSC Adv.* **7**, 50166–50175 (2017).
13. Coleman, J. N. Liquid-phase exfoliation of nanotubes and graphene. *Adv. Funct. Mater.* **19**, 3680–3695 (2009).
14. Hernandez, Y. *et al.* High-yield production of graphene by liquid-phase exfoliation of graphite. *Nature Nanotechnology* **3** 563–568 (2008)
15. Bourlinos, A. B. *et al.* Aqueous-phase exfoliation of graphite in the presence of polyvinylpyrrolidone for the production of water-soluble graphenes. *Solid State Commun.* **149**, 2172–2176 (2009).
16. Du, W. & Zhu, L. From graphite to graphene: direct liquid-phase exfoliation of graphite to produce single- and few-layered pristine graphene. *J. Mater. Chem. A*, **1**, 10592–10606 (2013).
17. Geim, A. K. Graphene : Status and Prospects. **324**, 1530–1535 (2009).

18. Barwich, S., Khan, U. & Coleman, J. N. A technique to pretreat graphite which allows the rapid dispersion of defect-free graphene in solvents at high concentration. *J. Phys. Chem. C* **117**, 19212–19218 (2013).
19. Cui, X., Zhang, C., Hao, R. & Hou, Y. Liquid-phase exfoliation, functionalization and applications of graphene. *Nanoscale* **3**, 2118–2126 (2011).
20. Green, A. A. & Hersam, M. C. Solution phase production of graphene with controlled thickness via density differentiation. *Nano Lett.* **9**, 4031–4036 (2009).
21. Chhowalla, M. *et al.* The chemistry of two-dimensional layered transition metal dichalcogenide nanosheets. *Nat. Chem.* **5**, 263–275 (2013).
22. Cunningham, G. *et al.* Solvent exfoliation of transition metal dichalcogenides: Dispersibility of exfoliated nanosheets varies only weakly between compounds. *ACS Nano* **6**, 3468–3480 (2012).
23. Varrla, E. *et al.* Large-scale production of size-controlled MoS<sub>2</sub> nanosheets by shear exfoliation. *Chem. Mater.* **27**, 1129–1139 (2015).
24. Bergin, S. D. *et al.* Towards solutions of single-walled carbon nanotubes in common solvents. *Adv. Mater.* **20**, 1876–1881 (2008).
25. Furtado, C. A. *et al.* Debundling and Dissolution of Single-Walled Carbon Nanotubes in Amide Solvents. *J. Am. Chem. Soc.* **126**, 6095–6105 (2004).
26. Bergin, S. D., Sun, Z., Streich, P., Hamilton, J. & Coleman, J. N. New solvents for nanotubes: Approaching the dispersibility of surfactants. *J. Phys. Chem. C* **114**, 231–237 (2010).

27. Detriche, S., Zorzini, G., Colomer, J. F., Fonseca, A. & Nagy, J. B. Application of the Hansen solubility parameters theory to carbon nanotubes. *J. Nanosci. Nanotechnol.* **8**, 6082–6092 (2008).
28. Cheng, Q., Debnath, S., Gregan, E. & Byrne, H. J. Effect of solvent solubility parameters on the dispersion of single-walled carbon nanotubes. *J. Phys. Chem. C* **112**, 20154–20158 (2008).
29. Coleman, J. N. *et al.* Two-Dimensional Nanosheets Produced by Liquid Exfoliation of Layered Materials. *Science (80-. )*. **331**, 568–571 (2011).
30. Nicolosi, V., Chhowalla, M., Kanatzidis, M. G., Strano, M. S. & Coleman, J. N. Liquid Exfoliation of Layered Materials. *Science (80-. )*. **340**, 1226419–1226419 (2013).
31. Ma, H., Shen, Z. & Ben, S. Understanding the exfoliation and dispersion of MoS<sub>2</sub> nanosheets in pure water. *J. Colloid Interface Sci.* **517**, 204–212 (2018).
32. Heiranian, M., Wu, Y. & Aluru, N. R. Molybdenum disulfide and water interaction parameters. *J. Chem. Phys.* **147**, (2017).
33. Shen, J. *et al.* Liquid Phase Exfoliation of Two-Dimensional Materials by Directly Probing and Matching Surface Tension Components. *Nano Lett.* **15**, 5449–5454 (2015).
34. Kim, J. *et al.* Direct exfoliation and dispersion of two-dimensional materials in pure water via temperature control. *Nat. Commun.* **6**, 1–9 (2015).
35. Choi, J., Zhang, H., Du, H. & Choi, J. H. Understanding Solvent Effects on the Properties of Two-Dimensional Transition Metal Dichalcogenides. *ACS Appl. Mater. Interfaces* **8**, 8864–8869 (2016).

36. Li, X. *et al.* Recent Advances in Synthesis and Biomedical Applications of Two-Dimensional Transition Metal Dichalcogenide Nanosheets. *Small* **13**, 1–28 (2017).
37. Lim, C., Garaj, S. & Leong, D. T. Directing Assembly and Disassembly of 2D MoS<sub>2</sub> Nanosheets with DNA for Drug Delivery. *ACS Appl. Mater. Interfaces* **9**, 18, 15286–15296 (2017).
38. Bang, G. S. *et al.* DNA-Assisted Exfoliation of Tungsten Dichalcogenides and Their Antibacterial Effect. *ACS Appl. Mater. Interfaces* **8**, 1943–1950 (2016).
39. Guan, G. *et al.* Protein induces layer-by-layer exfoliation of transition metal dichalcogenides. *J. Am. Chem. Soc.* **137**, 6152–6155 (2015).
40. Ge, Y., Wang, J., Shi, Z. & Yin, J. Gelatin-assisted fabrication of water-dispersible graphene and its inorganic analogues. *J. Mater. Chem.* **22**, 17619 (2012).
41. Li, Y. *et al.* Nanocellulose as green dispersant for two-dimensional energy materials. *Nano Energy* **13**, 346–354 (2015).
42. Zong, L., Li, M. & Li, C. Bioinspired Coupling of Inorganic Layered Nanomaterials with Marine Polysaccharides for Efficient Aqueous Exfoliation and Smart Actuating Hybrids. *Adv. Mater.* **29**, 1–8 (2017).
43. Ayán-Varela, M. *et al.* Aqueous exfoliation of transition metal dichalcogenides assisted by DNA/RNA nucleotides: Catalytically active and biocompatible nanosheets stabilized by acid-base interactions. *ACS Appl. Mater. Interfaces* **9**, 2835–2845 (2017).
44. Paredes, J. I. & Villar-Rodil, S. Biomolecule-assisted exfoliation and dispersion of graphene and other two-dimensional materials: A review of recent progress and

- applications. *Nanoscale* **8**, 15389–15413 (2016).
45. Zhang, L., Shen, S., Liu, Z. & Ji, M. Label-Free, Quantitative Imaging of MoS<sub>2</sub> - Nanosheets in Live Cells with Simultaneous Stimulated Raman Scattering and Transient Absorption Microscopy. *Adv. Biosyst.* **1**, 1700013 (2017).
  46. Liu, Y. *et al.* Molybdenum disulfide/graphene oxide nanocomposites show favorable lung targeting and enhanced drug loading/tumor-killing efficacy with improved biocompatibility. *NPG Asia Mater.* **10**, e458 (2018).
  47. Teo, W. Z., Chng, E. L. K., Sofer, Z. & Pumera, M. Cytotoxicity of exfoliated transition-metal dichalcogenides (MoS<sub>2</sub>, WS<sub>2</sub>, and WSe<sub>2</sub>) is lower than that of graphene and its analogues. *Chem. - A Eur. J.* **20**, 9627–9632 (2014).
  48. Moore, C. *et al.* Industrial grade 2D molybdenum disulphide (MoS<sub>2</sub>): an *in vitro* exploration of the impact on cellular uptake, cytotoxicity, and inflammation. *2D Mater.* **4**, 25065 (2017).
  49. Siepi, M. *et al.* Production of biofunctionalized MoS<sub>2</sub> flakes with rationally modified lysozyme: a biocompatible 2D hybrid material. *2D Mater.* **4**, 35007 (2017).
  50. Appel, J. H. *et al.* Low Cytotoxicity and Genotoxicity of Two-Dimensional MoS<sub>2</sub> and WS<sub>2</sub>. *ACS Biomater. Sci. Eng.*, **2**, 3, 361-367 (2016).
  51. Gutiérrez, M. & Henglein, A. Preparation of colloidal semiconductor solutions of MoS<sub>2</sub> and WSe<sub>2</sub> via sonication. *Ultrasonics* **27**, 259–261 (1989).
  52. Yao, Y. *et al.* High-concentration aqueous dispersions of MoS<sub>2</sub>. *Adv. Funct. Mater.* **23**, 3577–3583 (2013).

53. Liu, Y.-T., Zhu, X.-D. & Xie, X.-M. Direct Exfoliation of High-Quality, Atomically Thin MoSe<sub>2</sub> Layers in Water. *Adv. Sustain. Syst.* **1700107**, 1700107 (2017).
54. Forsberg, V. *et al.* Exfoliated MoS<sub>2</sub> in Water without Additives. *PLoS One* **11**, e0154522 (2016).
55. Li, Y. *et al.* MoS<sub>2</sub> nanoparticles grown on graphene: An advanced catalyst for the hydrogen evolution reaction. *J. Am. Chem. Soc.* **133**, 7296–7299 (2011).
56. Zhao, G., Wu, Y., Shao, Y. & Hao, X. Large quantity and continuous preparation of two dimensional nanosheets *Nanoscale*, **8**, 5407–5411 (2016).
57. Ma, H., Shen, Z. & Ben, S. Surfactant-free exfoliation of multilayer molybdenum disulfide nanosheets in water. *J. Colloid Interface Sci.* **537**, 28–33 (2019).
58. Van Thanh, D., Pan, C. C., Chu, C. W. & Wei, K. H. Production of few-layer MoS<sub>2</sub> nanosheets through exfoliation of liquid N<sub>2</sub>-quenched bulk MoS<sub>2</sub>. *RSC Adv.* **4**, 15586–15589 (2014).
59. Verhaagen, B. & Fernández, D. Ultrasonics Sonochemistry Measuring cavitation and its cleaning effect. *Ultrason. - Sonochemistry* **29**, 619–628 (2016).
60. Lee, J. *et al.* Ultrasonics Sonochemistry Development and optimization of acoustic bubble structures at high frequencies. *Ultrason. - Sonochemistry* **18**, 92–98 (2011).
61. Bonaccorso, F. *et al.* Production and processing of graphene and 2d crystals. *Mater. Today* **15**, 564–589 (2012).
62. Carney, R. P. *et al.* Determination of nanoparticle size distribution together with density

- or molecular weight by 2D analytical ultracentrifugation. *Nat. Commun.* **2**, (2011).
63. Kynch, G. J. A theory of sedimentation. *Trans. Faraday Soc.* **48**, 166–176 (1952).
64. Akbulut, O. *et al.* Separation of nanoparticles in aqueous multiphase systems through centrifugation. *Nano Lett.* **12**, 4060–4064 (2012).
65. Nicolosi, V. *et al.* Solubility of MoS<sub>2</sub> nanowires in common solvents: A sedimentation study. *J. Phys. Chem. B* **109**, 7124–7133 (2005).
66. Atkins, P., Paula, J. De & Keeler, J. Atkins & Keeler's Physical Chemistry Eleventh Edition  
Author Information : Table of Contents Reviews & Awards :
67. Basson, D. K., Berres, S. & Bürger, R. On models of polydisperse sedimentation with particle-size-specific hindered-settling factors. *Appl. Math. Model.* **33**, 1815–1835 (2009).
68. Zimmels, Y. Theory of hindered sedimentation of polydisperse mixtures. *AIChE J.* **29**, 669–676 (1983).
69. Lotya, M. *et al.* Liquid Phase Production of Graphene by Exfoliation of Graphite in Surfactant / Water Solutions. *J AM Chem Soc.* **131** (10) 3611–3620 (2009).

## Chapter-4

# Biological interaction results analyses of 2D MoS<sub>2</sub> nanosheets with human cells and pathogens

*The content of this chapter is based on our published article, Jasneet Kaur, Manjot Singh et al. “Biological interactions of biocompatible and water-dispersed MoS<sub>2</sub> nanosheets with bacteria and human cells”, Scientific Reports, 2018, 8:16386, with major and equal contribution in all experiments and results analyses.*

---

### 4.1. Introduction

Before transferring any nanomaterial from laboratory experiments to clinical trials in biomedicine and biotechnological applications, it is extremely important to deeply study its biological safety. Graphene and its analogues have been explored in depth for various biomedical studies such as bio-sensing [1-6], antibacterial activity [7-9], drug delivery [10] etc. Particularly, 2D TMDs such as MoS<sub>2</sub> nanosheets largely used in my case have attracted a significant attention from the scientists worldwide in biomedical applications. Thanks to its peculiar chemical and physical properties [11-21] which highlights its potential and promising results in various

biomedical applications such as drug delivery, bio-sensing, *in-vivo* and *in-vitro* antibacterial studies, tissue regeneration, cancer treatment and medical imaging to name a few [22–28]. Therefore, it is very crucial to understand the biological behavior of 2D MoS<sub>2</sub> nanosheets in different biological systems and contexts. To this aim, very few reports have been published which discuss the behavior of 2D MoS<sub>2</sub> nanosheets with different human cell lines, particularly their internalization and toxicity pathways into cells [29,30]. Keeping in mind the biocompatibility and biosafety issues of MoS<sub>2</sub> nanosheets, we have directly exfoliated bulk MoS<sub>2</sub> powder in de-ionized water to produce good quality few-layer 2D nanosheets which can be readily used in various biological tests to understand different interaction pathways with the given human cell lines such as MCF-7 (breast cancer), U937 (leukemia) and HaCaT (normal epithelium).

#### **4.1.1. General information on the tested human cell lines in this thesis**

##### **4.1.1.1. MCF-7 Cell Line**

Breast cancer, in general is the highest occurring and most frequent malignancy in women and it holds second place among all other types of cancer in terms of its deadly growth. Many north European countries have the highest breast cancer occurring rate due to which it represents a critical public health problem. Many research groups and doctors have been working on the diagnosis and specific treatment of this particular kind of menace. To accomplish this task, basic and fundamental research at molecular level is required which involves the usage of specific cell lines as an *in-vitro* cancer cell model for laboratory experiments. MCF-7 is a commonly used cancer cell line which has been under investigation for more than 40 years by various research groups for estrogen receptor (ER)-positive breast cancer cell experiments [31,32].

It basically represents some important growth receptors on its surface which helps in proliferation of these tumor cells. Estrogen (ER), Progesterone (PR) and some growth receptors could be very helpful in inhibiting the growth of breast cancer cells and more importantly it grows in adhesion.

MCF-7 cell line is well characterized in terms of the number of reports published on its structure, cell culture preparations and its interaction with different nanoparticles. Such a strong experience with this cell line actually helps various research groups to put their extensive efforts into cancer pathogenesis and treatment protocols using steadfast *in vitro* assays.

#### **4.1.1.2. U937 Cell Line**

The basic origin of U937 cell line is from the human Caucasian histiocytic lymphoma of a 37 year old male. It is one of the cell lines which actually express many of the monocytic like characteristics from its origin for tumorigenicity studies. So, this human myeloid leukemia cell line exhibits a range of characteristics of monocytes relatively with uniform number and ease in use [33]. The basic role of this leukemia cell line model is to explicate the mechanism behind monocyte and macrophage differentiation. Along with this it also exhibit translocation of genes which enhances the tumor growth proteins [34]. U937 cells grow in suspension in the relevant medium for its growth.

#### **4.1.1.3. HaCaT Cell Line**

HaCaT cell line is basically the normal epithelium cell model extracted from the human skin and widely used for research investigations. It is also known as a spontaneously immortal keratinocyte cell model to study the differentiation and gene delivery in to the same. They have

the high potential to proliferate *in-vitro* and the advantage of using this cell line is that it can be easily propagated into the culture medium [35]. Our basic purpose to use this cell line was to study the interaction of 2D MoS<sub>2</sub> nanosheets with these adherent cells upon incubation into the respective medium for its growth in comparison with the other two tumor cell lines.

## 4.2. Cytotoxicity study on different cell lines

### 4.2.1. Introduction

Toxicity, environmental impact and biocompatibility of MoS<sub>2</sub> onto different human cell lines is very important to investigate, in view of the more and more massive use of these 2D materials in a number of practical applications and their increased presence in the human day-to-day life. Morphology, size and thickness of 2D nanosheets are some key parameters to induce and potentially control the surface interactions of MoS<sub>2</sub> nanosheets onto live matter. Functionalized MoS<sub>2</sub> nanosheets have been studied with different human cell lines to tap the potential of 2D nanosheets in various biomedical applications such as drug delivery, cancer diagnosis and cell imaging [26,36,37]. For instance, Coleman and co-workers reported the size and concentration dependent toxicity of MoS<sub>2</sub> nanosheets on three different established cell lines [38]. Siepi *et al.* reported on the biocompatible lysozyme-functionalized exfoliated MoS<sub>2</sub> nanosheets. They incubated MoS<sub>2</sub> nanosheets on two different cell lines (HeLa and HaCaT) with no cytotoxicity evidence at higher concentrations [39]. J. H. Appel *et al.* reported on the interactions of naked MoS<sub>2</sub> nanosheets, obtained by mechanical exfoliation and chemical vapor deposition, with human epithelial kidney cells (HEK293f) observing low cytotoxicity and genotoxicity in their experimental conditions [40]. P. Shah *et al.* probed the effect of MoS<sub>2</sub> nanosheets produced by liquid exfoliation onto rat cells finding a relatively good biocompatibility at high 2D material concentration [20]. Therefore a thorough study on the different interaction pathways of naked

MoS<sub>2</sub> nanosheets with different human cell lines and various pathogens is highly needed and still missing in the most important case, namely for nanosheets produced by eco-friendly methods and dispersed into water based media that is the native context of biological matter.

### **4.3. Effects of 2D MoS<sub>2</sub> nanosheets on cellular growth**

Cytotoxicity experiments were performed using two cancer cell lines (U937 and MCF-7) and one non-cancer cell line (HaCaT).

#### **4.3.1. Cell cycle analysis**

Cytotoxicity experiments were performed in two different cell culture conditions: in suspension and in adhesion. This approach allowed to examine the interaction between MoS<sub>2</sub> nanosheets and cells under the condition in which bona fide either the entire cell surface - in case of suspension cultures - or part of it - cell monolayer of adherent cultures - resulted exposed to 2D nanomaterial. The impact of different concentrations  $\langle C \rangle$ , mean number of layers  $\langle N \rangle$  and mean lateral size  $\langle L \rangle$  of MoS<sub>2</sub> nanosheets dispersion was investigated upon their incubation with two tumoral cell lines (U937 and MCF-7) and one normal cell line (HaCaT), *as shown in Table 4.1*. It is worth noting that for cells the effective concentration of the nanomaterial is lowered by about a factor of four as compared to the concentration value of the initial preparation. The reason is, to avoid an excessive dilution of the culture media and nutrients therein. The dispersion was drop cast into the cell medium and the incubation was carried out for 24, 48 and 72 h. At the end of the incubation, the cell cycle progression was determined by flow cytometer or fluorescence activated cell sorting (FACS), a technique that discriminates the cells at different phases of cell cycle for their content in DNA (*Figure 4.1*). The cytometer processes

the fluorescence intensity of a group of cells labeled with fluorescent dye (PI) that is able to bind to DNA. The data is displayed as number of cells versus fluorescence intensity, a number proportional to cell DNA content. The cell scattering shows two peaks: G1 (gap 1), the gap between mitosis (nuclear division) and DNA replication, corresponding to cells metabolically active but that do not replicate their DNA and G2 (gap 2) corresponding to cells that grow and synthesize the proteins for mitosis. Between G1 and G2 there is the S phase in which the cells replicate their DNA. The cell death is revealed as percentage of cells in pre-G1 phase, corresponding to a pick of fragmented DNA [<sup>41,42</sup>]. Our data of **Figure 4.1** revealed that MoS<sub>2</sub> dispersion did not affect the MCF-7 distribution along cell cycle phases within 48 hours even at the highest concentration. Only the longest incubation time was able to induce a decrease of S phase in dose-independent manner and increase in the progression to G2/M phase (**Figure 4.1a**). Conversely, the cell cycle distribution of U937 cell was strongly affected in time dependent manner (**Figure 4.1b**). At 48 h, MoS<sub>2</sub> dispersion at three different concentrations was able to induce a block in S phase and an increase of cell death percentage. Notably, the lowest used concentration of MoS<sub>2</sub> dispersion (0.5 µg/mL) induced the strongest effect on cell death after 48 h. However, the cell death (pre-G1) was attenuated at 72 h probably because of sedimentation of 2D MoS<sub>2</sub> dispersion. Similar trends were found in HaCaT cells as shown in **Figure 4.1c**. In human keratinocyte cell line, the induction of both S-phase block and cell death were observed at 72 h. Delayed response on cell cycle progression accounted for the slower proliferation rate of this normal cellular model.

<i>Concentration of MoS<sub>2</sub> dispersion</i>	<i>Layer Number (N)</i>	<i>Lateral Size (L)</i>
5 µg/mL	9	220 nm
2 µg/mL	6	180 nm
0.5 µg/mL	5	160 nm

**Table 4.1** Properties of exfoliated MoS<sub>2</sub> nanosheets used in cell cycle progression experiments.

The final parameters shown in the above table corresponds to the samples prepared for cytotoxicity experiments. The final concentrations shown above also correspond to the obtained dispersions at 620g, 1000g and 2500g, whereas the dispersion parameters shown in the *chapter - 3* are related to the obtained and optimized values after number of exfoliation runs. Though, exfoliation in water is a challenging task and to have the reproducibility in the final parameters is again a hard nut to crack but we have tried to utilize the same initial parameters to achieve good reproducibility in the final samples.

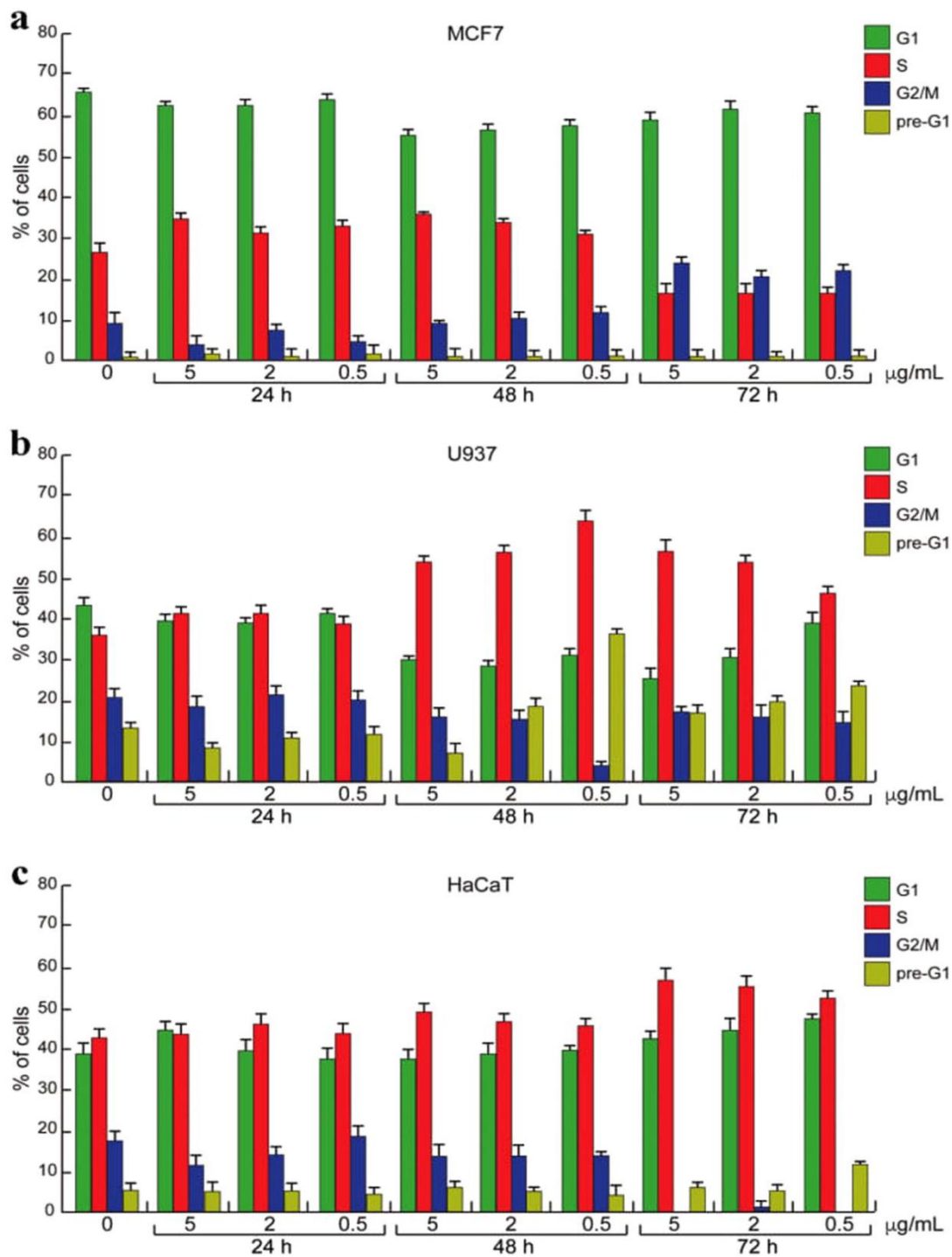


**Figure 4.1:** Cell cycle analysis. (a) MCF-7, (b) U937 and (c) HaCaT cell lines at different final concentrations of 2D MoS<sub>2</sub> dispersion after 24 h, 48 h and 72 hours from the beginning of the treatment. The cell scattering shows two peaks: G1 (gap 1), the gap between mitosis (nuclear

division) and DNA replication, corresponding to cells metabolically active but that do not replicate their DNA and G2 (gap 2) corresponding to cells that grows and synthesize the proteins for mitosis. Between G1 and G2 there is the S phase in which the cells replicate their DNA. The cell death is revealed as percentage of cells in pre-G1 phase; corresponding to a pick of fragmented DNA Error bars indicate standard deviation of triplicate analysis.

## **4.4. Effects of 2D MoS<sub>2</sub> nanosheets on cellular viability**

### **4.4.1. Cell line culture, conditions and preparations**

To better investigate the cytotoxicity, viability of the above mentioned three human cell lines was investigated after 24 and 48 h of exposure to MoS<sub>2</sub> dispersion. MTT experiments were performed by growing cells onto plates coated with 50 and 100  $\mu$ L drops of MoS<sub>2</sub> nanosheets.

The exfoliation of MoS<sub>2</sub> dispersion exhibit 14  $\mu$ g/mL (C) with 6 number of layers (N) and Lateral size (L) of 220 nm. The viability of U937 highest cell density (**Figure 4.2 b**). In fact, differently from what we observed for U937 cells, MTT analysis performed on the adherent MCF-7 cells showed an interesting interference effect induced by 2D nanosheets as shown in **Figure 4.2 (c,d)** The presence of MoS<sub>2</sub> nanosheets coating on the plate mainly affected the viability (and/or adhesive properties) of the cells. After 24 h more than 50% of cell death was already observed (**Figure 4.2 c**). No significant effect of both the quantity of MoS<sub>2</sub> nanosheets and cellular concentration was noted. In **Figure 4.2 d**, taking twice the number of MCF-7 cells present in **Figure 4.2 c** the cell viability in this case was much less affected than in **Figure 4.2 c**. We ascribe this finding to the specific type of interaction between the adhered MCF-7 cells and the nanoflakes. In fact, in case of adhered cells the interaction always takes place through the interface surface between the cell medium and the nanoflakes. This interface, constituted by the

most external cell layer, is approximately keeping the same size and involving the same number of cells regardless the actual entire volume of the growth cells below the separation surface. Therefore, simply increasing the number of cells while keeping the same interface results in minimizing the interaction between adhered cells and MoS<sub>2</sub> nanosheets. Similar effects were observed in HaCaT cells incubated with MoS<sub>2</sub> nanosheets coated onto the plates (Properties of Exfoliated MoS<sub>2</sub> nanosheets dispersion are shown in **Table 4.2**). Like MCF-7, HaCaT cell line viability was strongly affected by the presence of MoS<sub>2</sub> nanosheets coated over the plates. Here we can also see that in the case of 14  $\mu\text{g/mL}$  *C*, but with two different *N*, 6 and 10, the induced evident reduction of cell viability is not changing, suggesting that no major role is played in such a case by the *C*. The above findings corroborated the idea that a prolonged physical proximity between 2D nanosheets and cells is required to induce the cell death. In fact, while this is certainly the case for MCF-7 and HaCaT that grow up in adhesion, for U937 that grow up in suspension MoS<sub>2</sub> nanosheets can be much more diluted in the entire volume of the solution so to interact much more weakly with cells. Normally the interaction of nanomaterials with cells is studied with the latter being placed at the bottom of a culture plate.

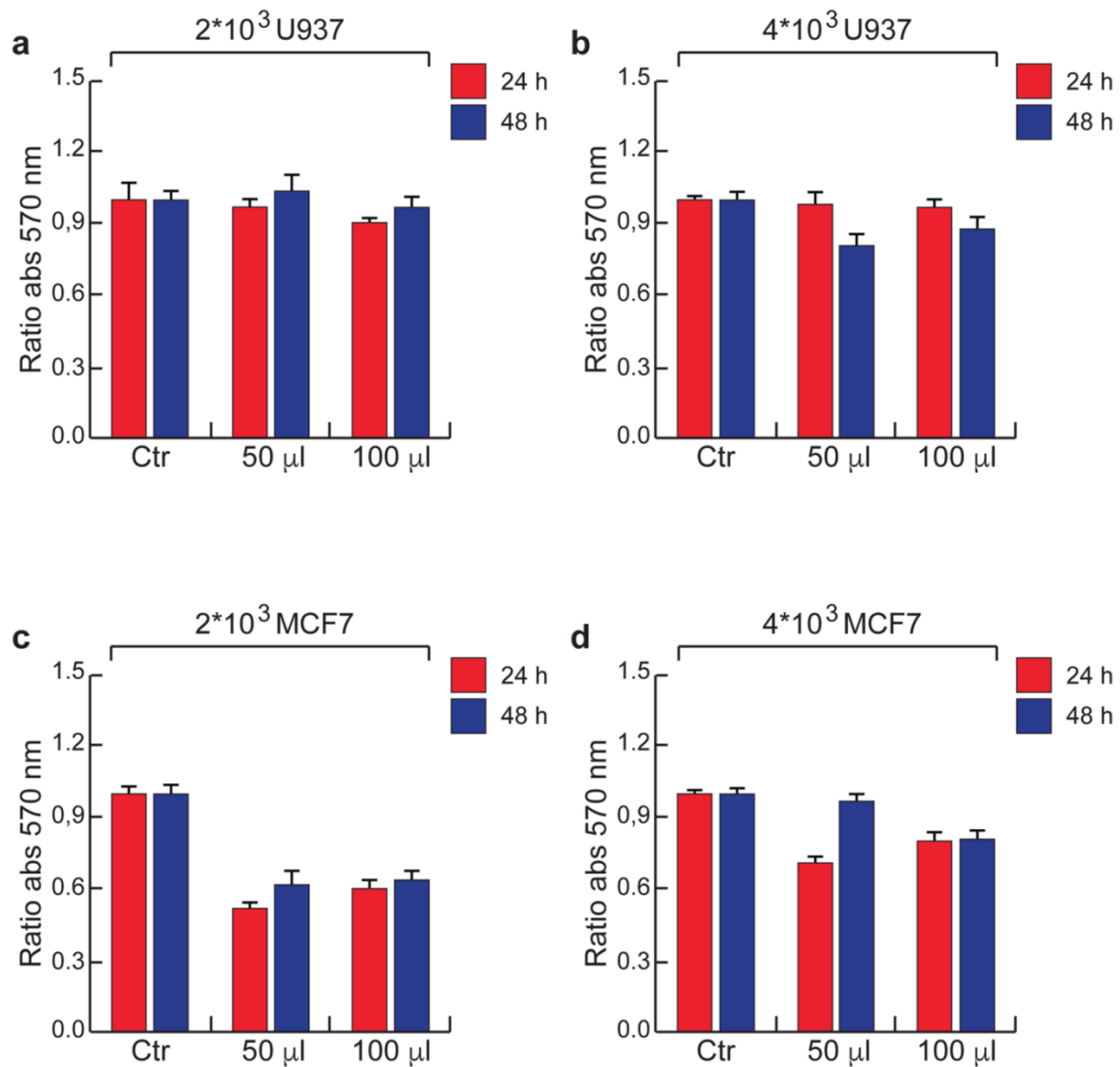


**Figure 4.2:** MTT analysis. (a,b) MTT assay performed on U937 cell line with (a) 2000 and (b) 4000 cells at 570 nm absorbance for 24 h and 48 h. (c,d) MTT assay performed on MCF-7 cell line with (c) 2000 and (d) 4000 cells at 570 nm absorbance for 24 h and 48 h. Error bars indicate three independent experiments in (a–d).

<b>Concentration of MoS<sub>2</sub> dispersion (µg/mL)</b>	<b>Layer Number (N)</b>	<b>Lateral Size (L)</b>	<b>Absorbance after 24 h (570 nm)</b>	<b>Absorbance after 48 h (570 nm)</b>
10	2	145 nm	0.55 ± 0.02	0.57 ± 0.06
14	10	250 nm	0.54 ± 0.02	0.45 ± 0.02
14	6	220 nm	0.63 ± 0.02	0.57 ± 0.01
22	5	200 nm	0.61 ± 0.01	0.53 ± 0.01
36	12	300 nm	0.64 ± 0.01	0.49 ± 0.01

**Table 4.2** Concentration, mean layer number and mean lateral size of exfoliated MoS<sub>2</sub> nanosheets pre-incubated with 3000 HaCaT cells for 24 h and 48 h. Absorbance values at 570 nm after 24 h and 48 h of incubation with nanosheets. Negative control is normalized to absorbance equal to 1

*In vitro*, cellular response to nanoflakes can also be evidently influenced by the altered diffusion and sedimentation velocities of the nanostructured flakes [43], as well as by electrostatic forces arising from the interaction between exfoliated MoS<sub>2</sub> nanosheets that are negatively charged (**Table 3.1** of Chapter-3 (Zeta Potential) and cell membrane which is typically positively charged on the external side, thus generating a negative transmembrane potential [44]. Within the electrostatic forces that may play a role in the interactions between cells and MoS<sub>2</sub> nanosheets it is worth, as in case of potassium ion, that might be affected by the presence of 2DM nanosheets [45]. Cell adhesion is an important aspect in cell proliferation, and can play a role in the

interaction of cells incubated with nanomaterials. Typically, cells are prepared so to adhere before the addition of the nanomaterial solution to the preparation [46]. In our case, cells are adhered onto the plates coated with two MoS<sub>2</sub> dispersion drops having different volumes. Since U937 cells by nature grow up in suspension, typically tend to a minor surface-like interactions resulting in a poor adhesion and thus a weaker interaction with the nanoflakes. Therefore, the cell viability was not affected as in the case of the other cell lines. On the other hand, both MCF-7 and HaCaT cells grow up in adhesion to a surface. This property makes them more appropriate for surface-like interactions, there including those ones with the nanomaterial. This leads MCF-7 and HaCaT cells to exhibit a strong decrease in cell viability when incubated with 2D MoS<sub>2</sub> nanosheets, in the range of ≈0–50% in our experimental conditions.

## **4.5. MTT assay on HaCaT and MCF-7 cells pre-incubated with MoS<sub>2</sub> nanosheets**

### **4.5.1. MTT- Cell proliferation assay**

Walking on this line, we exploited another interaction pathway of pre-incubation and rotation of 2D nanosheets with cells, so to increase their direct contact of interaction in the medium. So, basically this was our third interaction pathway which we have studied on HaCaT cells. After performing cell cytotoxicity studies on all three used cell lines and subsequently MTT assay on U937 and MCF-7 cells, it was important to study the effect of MoS<sub>2</sub> nanosheets on normal cells via pre-incubation and rotation of 2D nanosheets with the given cells. In this setting, adherent HaCaT cell line was pre-incubated for 1 h in gentle rotation with the indicated quantities of MoS<sub>2</sub> nanosheets and then cultured for next 24 and 48 h in standard growing conditions. In this condition, cells viability was profoundly impaired in the presence of MoS<sub>2</sub> nanosheets as shown

in **Table 4.2**. Our data also revealed that cellular response was somehow dependent on  $C$  and  $N$  of MoS<sub>2</sub> nanosheets, though the mechanism for interplay between  $N$  and  $C$  on the induced biological effects in this peculiar geometry of interaction still needs to be more deeply investigated. The general behavior here indicates that adding MoS<sub>2</sub> nanosheets in the preparation as described above leads always to a strong cell viability decrease, even larger than 65%, and suggests to some extent that the lower the concentration the higher the cell viability decrease. **In Table 4.3**, we report the viability of MCF-7 cells via MTT assay, pre-incubated with 2D MoS<sub>2</sub> nanosheets having different  $C$  and  $L$ . Even in this case there is a strong impact of the nanosheets over the cell viability, even stronger than in HaCaT, in the same conditions. The sample absorbance decreases in this case from 1 (negative control) to a value in the 0.1–0.35 range, when checked at 24 h and 48 h after treatment. No clear dependence is observed in this case on the  $C$  and on the parameters characterizing the nanosheets such as  $N$  and  $L$ .

<b>Concentration of MoS<sub>2</sub> dispersion (μg/mL)</b>	<b>Layer Number (N)</b>	<b>Lateral Size (L)</b>	<b>Absorbance after 24 h (570 nm)</b>	<b>Absorbance after 48 h(570 nm)</b>
10	2	145 nm	0.163 ± 0.012	0.194 ± 0.002
14	10	250 nm	0.118 ± 0.002	0.136± 0.001
14	6	220 nm	0.120 ± 0.002	0.107± 0.001
22	5	200 nm	0.299 ± 0.003	0.358± 0.003
36	12	300 nm	0.209 ± 0.012	0.221 ± 0.012

**Table 4.3:** Concentration, mean layer number and mean lateral size of exfoliated MoS<sub>2</sub> nanosheets pre-incubated with 3000 MCF7 cells for 24 h and 48 h. Absorbance values at 570 nm after 24 h and 48 h of incubation with nanosheets. Negative control is normalized to absorbance equal to 1.

## 4.6. Cell morphology by scanning electron microscope (SEM)

### 4.6.1. Visualization of cell morphology

To better characterize the microscopic structural features of the interaction between cells and MoS<sub>2</sub> nanosheets, SEM experiments were performed. After the pre-incubation for 1 h with MoS<sub>2</sub> dispersion, the three cell lines used were conventionally cultured on cover-glasses. Then, cells were observed by SEM after 24 h of incubation with two dispersions of MoS<sub>2</sub> nanosheets (having 10 µg/mL C with 6 N, and 14 µg/mL C with 3 N). SEM images clearly revealed the deposition of some MoS<sub>2</sub> flakes over the cell surface. **Figure 4.3** shows the interaction of MoS<sub>2</sub> nanoflakes with MCF-7, U937 and HaCaT cell lines, the flakes having *L* in the 0.5–10 µm range. MCF-7 line of **Figure 4.3 a** represents the negative control case (absence of MoS<sub>2</sub> dispersion) with two MCF-7 cells exhibiting their typical epithelial morphology. MoS<sub>2</sub> flakes from the two samples (10 µg/mL and 14 µg/mL) were added, **Figure 4.3 b** showing the typical structural aspect of a flake. The addition of the MoS<sub>2</sub> nanoflakes resulted in an alteration of the cell structure that appears seriously damaged as in **Figure 4.3 c**. In the second line of **Figure 4.3 (d-f)**, a strong cytotoxic effect of MoS<sub>2</sub> nanosheets is revealed on U937 cells, resulting in a massive cell death of this hematological cellular system. **Figure 4.3 d** shows the typical appearance of a control U937 cell (in absence of MoS<sub>2</sub> dispersion). The cell death is associated to deposition of sodium chloride crystals appearing both as little cubes and massive aggregates. In **Figure 4.3 e**, treated

U937 cells are heavily damaged as compared to the control. The presence of 2D nanosheets induced a complete distortion of the U937 cell structure upon their interaction, leading to complete cell death. Both sodium chloride types of crystals are visible as typical final product of cell decomposition induced by the stress due to MoS<sub>2</sub> nanoflakes reported in **Figure 4.3 f**. In this case a fragment of decomposed U937 cell is shown, surrounded by the sodium chloride crystals that probably coat also the smaller MoS<sub>2</sub> flakes. In the last line of **Figure 4.3 (g,h)**, untreated HaCaT cells represent a mesh-like structure with several filaments over the periphery of its cell membrane in **Figure 4.3 g**. MoS<sub>2</sub> nanosheets treatment at 10  $\mu\text{g/mL}$  caused a disruption of the cell structure with separation of the mesh into two parts. The presence of 2D flakes, highlighted in the figure by red arrows, resulted in destruction of the HaCaT cell membrane in **Figure 4.3 h**. MoS<sub>2</sub> dispersion at 14  $\mu\text{g/mL}$  shows the presence of 2D multilayer flakes over the cell surface, where craters also appear in the membrane as a result of the mechanical damage induced by the MoS<sub>2</sub> nanosheets to HaCaT cells in **Figure 4.3 i**. Taken together, these results provide evidences of the capability of MoS<sub>2</sub> nanosheets to interact with the cellular surface and to trigger changes in cell morphology that likely evidence a strong mechanical damage.

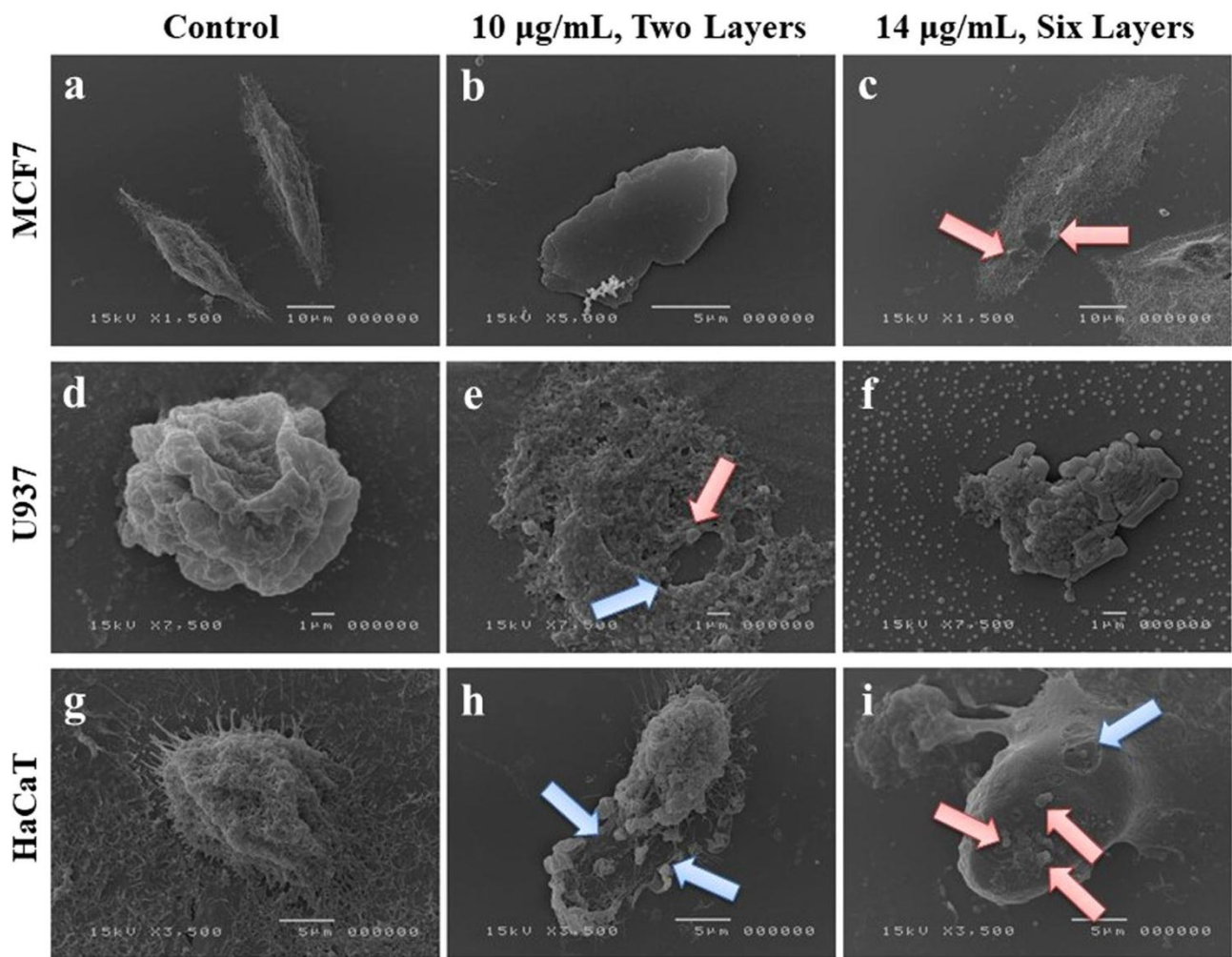


**Figure 4.3.** SEM analysis of human cell lines. (a–c) MCF-7 (top, the red arrows indicating the nanoflakes onto the cell), (d–f) U937 (middle, the blue arrows indicating the damaged areas and the red the nanoflakes) and (g–i) HaCaT cells (bottom, the blue arrows indicating the damaged areas and the red the nanoflakes) untreated and treated with  $\text{MoS}_2$  dispersion at the indicated concentrations. The  $N$  was two at 10  $\mu\text{g/mL}$  and six at 14  $\mu\text{g/mL}$ .

## 4.7. MoS<sub>2</sub> nanosheets and cells interaction pathway

*Figure 4.4* explains a simple scheme of three different interaction pathways of 2D MoS<sub>2</sub> nanosheets with adhesion and suspension human cells. *Figure 4.4 a* shows the adhesion interaction of MoS<sub>2</sub> nanosheets over the cell surface. In such a case, MCF-7 cells (adherent) were coated over the cell plate and then MoS<sub>2</sub> dispersion was added for 72 h incubation. The cell viability was not affected even after 48 h of exposure with nanosheets. We observed a change in S phase of cells after 72 h of incubation because of slow sedimentation velocity of MoS<sub>2</sub> nanosheets in cell medium (*Figure 4.1*). A Similar effect was observed in case of HaCaT cells (again adherent). In *Figure 4.4 b*, the interaction scheme of MoS<sub>2</sub> nanosheets with suspension cells (U937) is represented. After 48 h incubation with nanosheets, time dependent cell death was observed together with a high decrease in cell viability even at the lowest concentration of the MoS<sub>2</sub> dispersion (in *Figure 4.1*). In *Figure 4.4 c*, MoS<sub>2</sub> nanosheets dispersion was coated over the plates and then cells were exposed to the nanosheets surface. In case of adhesion cells (MCF-7), after 24 h incubation, more than 50% cell death was observed at the lowest cell density because a better contact between flakes and cells takes place resulting in maximum damage (*Figure 4.2*). In *Figure 4.4 d*, suspension cells exhibit less damage because of the smaller chance to interact with the coated plated surface treated with MoS<sub>2</sub> nanosheets (*Figure 4.2*). In *Figure 4.4 e*, MoS<sub>2</sub> dispersion and cells were pre-incubated and rotated for 1 h to have better mixing and maximum interaction in the dispersion. In this respect, we observed the exciting result of maximum damage to both the tumoral cell lines and negligible effect to the normal one. This interaction between cells and MoS<sub>2</sub> nanosheets resulted in the more virulent nature for the cells already in suspension (U937). While in case of adhesion cells, as they adhere slowly to the

bottom of the plate, their interaction resulted in a minor less damage for HaCaT cells (normal) compared to tumor MCF-7 in *Figure 4.5 a*.

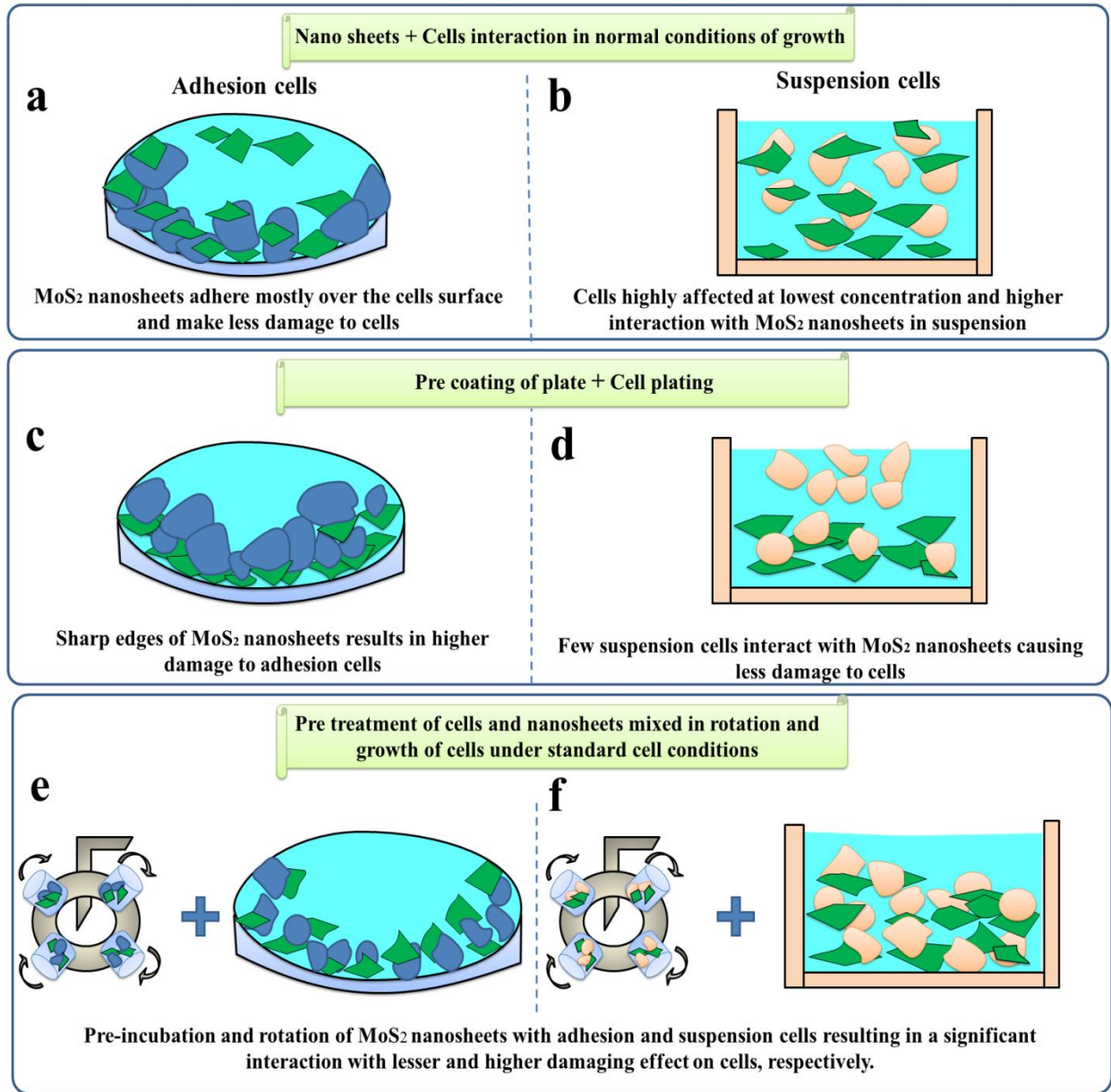


**Figure 4.4.** Interaction pathway for adhesion (MCF-7 and HaCaT cells) and suspension cells (U937) with 2D MoS<sub>2</sub> nanosheets.

## 4.8. MoS<sub>2</sub> mediated cell death evaluation

### 4.8.1. Propidium iodide staining: cell death evaluation

We integrated the qualitative morphological analysis of the MoS<sub>2</sub> nanosheets impact onto the above mentioned three cell lines, carried out by SEM images, by evaluating the cell death based on FACS. Then, a quantitative estimate of the induced cell death after 24 h is obtained as percentage of cells positive to the Propidium Iodide test, as shown in *Figure 4.5 a*. The result is very surprising and somewhat striking: while MoS<sub>2</sub> nanosheets were able to induce cell death in both of the cancer cell lines, they essentially did not in normal cell line, as shown in *Figure 4.5*, where the Propidium Iodide positive cell level is even lower than the untreated control indicating no induction of cell death. In fact, in breast cancer MCF-7 cell line, MoS<sub>2</sub> dispersion incubated in both quantities induced a two fold increase of cell death. Acute myeloid leukemia U937 cell line appeared the most sensitive to 2D nanomaterial treatment, with an increase of cell death of 8–12 folds as compared to the untreated cells. Negligible effect was instead observed in HaCaT cell line even when these cells were exposed to MoS<sub>2</sub> nanosheets for longer duration of observation up to 96 h after treatment: a difference in favor of the untreated cells was observed here, demonstrating the inefficacy of MoS<sub>2</sub> nanosheets in such cell system in *Figure 4.5 b*. Interestingly, the anti-proliferative effect is obtained both in hematological and solid cancer cell lines, appearing at this stage to be a cell-type-independent cancer response, restricted to the only tumor cells. HaCaT cells in fact, here utilized as a model for non-cancer cells, are unaffected in each scheme of treatment (*Figure 4.4*) but the case where MoS<sub>2</sub> nanosheets dispersion was coated over the plates and then cells were exposed to the nanosheets surface in *Figure 4.4 c*, which resulted in a weaker effect as compared to the analog for tumor cells see *Table 4.2* and *Figure 4.2 (a–d)*. Whether this feature is a general finding characterizing cancer cells regardless

their type or is cell-type-dependent, for instance because of the interaction between the negatively charged nanosheets and the cell membrane having an electrostatic potential varying from type to type, is a very intriguing question, whose response to is out of the scope of this thesis and will be addressed in future investigations some of which we have summarized in the *Chapter-7* of this thesis. This finding indicates MoS<sub>2</sub> nanosheets as a possible promising atoxic tool in cancer therapy. If confirmed, this preliminary observation would be of extreme importance, and would open the route to concrete applications of MoS<sub>2</sub> nanosheet treatment in living systems as possible targeted anti-cancer system. It is worth pointing out that this result is not at odd with morphological analysis based on SEM investigation of the treated cells, that indicated possible mechanical damage in all the three cell lines, since morphological analysis is not quantitative and basically enlightens only mechanical stresses.

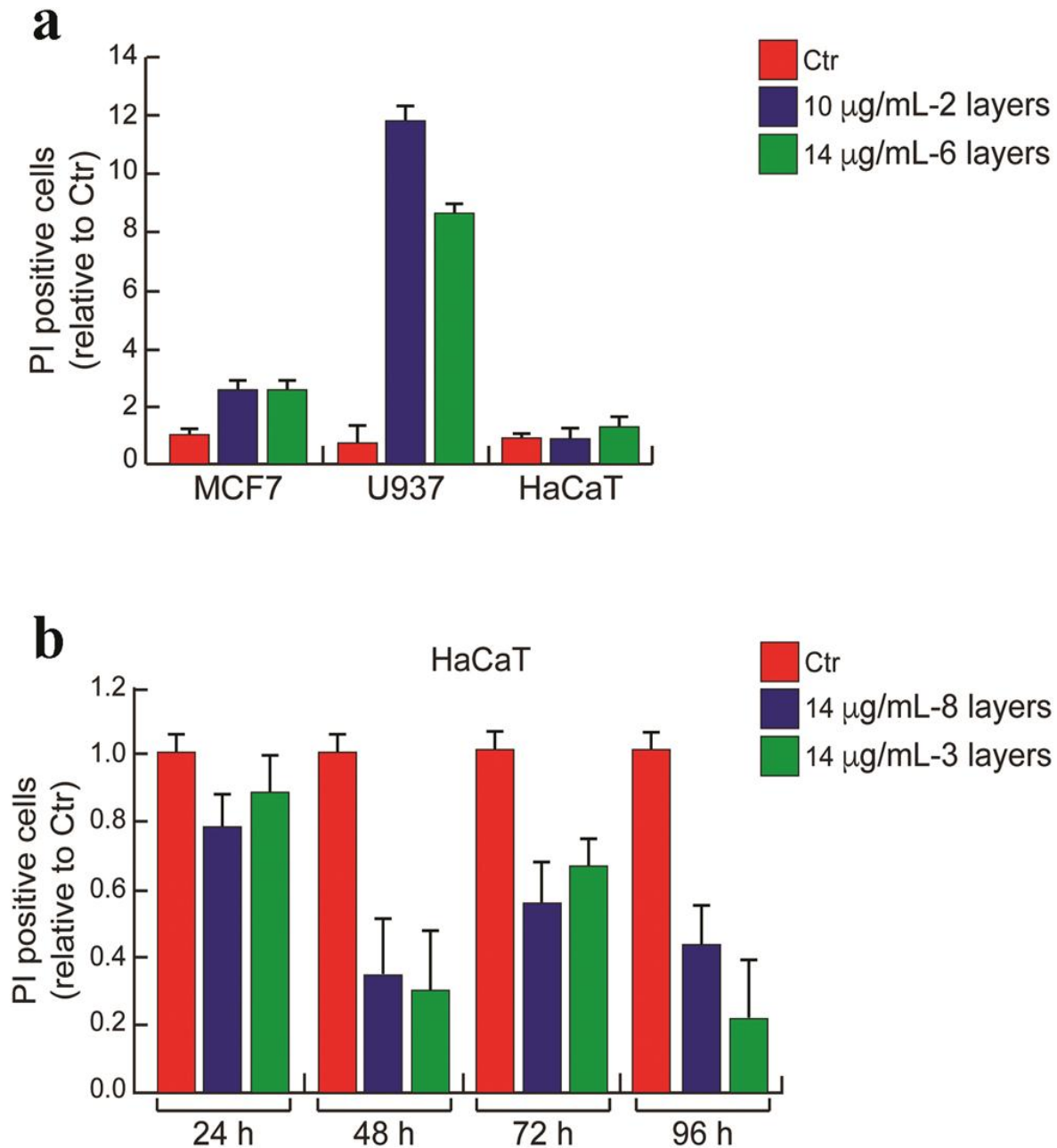


**Figure 4.5.** Cell death analysis for long duration. (a) Cell Death induced by MoS<sub>2</sub> nanosheets treatment in the same experimental setting of SEM experiment. (b) Cell Death induced by MoS<sub>2</sub> nanosheets treatment with HaCaT cells checked at 24, 48, 72 and 96 h after treatment, in the same experimental conditions of SEM experiment. Error bars report standard deviation after three independent experiments in (a,b).

#### **4.9. Antibacterial effect by naked MoS<sub>2</sub> nanosheets**

Graphene and its derivatives have been explored a lot for their antibacterial activities, but there are few studies which reflect the antibacterial mechanism of TMDs. Liu. X. *et al.* studied time and concentration dependent antibacterial activity of WS<sub>2</sub> nanosheets on gram negative *E. coli* and gram positive *Staphylococcus aureus* bacteria [47]. Shinde and co-workers demonstrated the inhibitory effects of WS<sub>2</sub> and WS<sub>2</sub>-rGO composite nanosheets on gram negative (*E. coli*) and *Salmonella typhimurium* (*S. typhimurium*), and Gram positive *Bacillus subtilis* (*B. subtilis*) and *Staphylococcus epidermidis* (*S. epidermidis*) bacterial strains [48]. Na Wu *et al.* studied the toxicity of MoS<sub>2</sub> on *E. coli* with its increasing concentration by utilizing metabolomics technology [49]. Studies on *Salmonella* bacteria using TMDs have generally been explored very little. Zhang X. *et al.* studied chitosan functionalized and antibiotic loaded MoS<sub>2</sub> nanosheets to combat the *S. aureus* and gram negative *Salmonella* bacteria against the bacterial resistance and biofilm formation [50]. To utilize 2D TMDs in various antibacterial applications, it is important to study first the interaction of 2D nanosheets with the bacterial target. In this aspect, we have chosen *S. typhimurium* which is well known to be a pathogen causing nosocomial infections, often contaminating water or food [51]. The latter case is very much timely: a number of applications are currently investigated one of the most interesting examples being the possibility to make new food packaging systems to avoid or to reduce *Salmonella* contamination of food.

#### **4.10. General Information of Salmonella Typhimurium**

*Salmonella typhimurium* is basically a gram negative bacterium which is responsible for gastroenteritis and a systemic typhoid fever [52]. Approximately, 1.3 billion cases of non-typhoid fever and subsequently 2-3 million deaths have been reported worldwide [53,54]. Basically,

entering via bloodstream and then penetrating through small intestinal epithelial cells to various other organs of the body such as liver, spleen and bone marrow makes it more viable to increase in number and in consequence it causes high fever [55]. By this way, infection throughout the body is initiated and it basically controls the doom of human cells by invading enterocytes and it results in a specific kind of secretion system to enhance the pathogenic effect inside the host cells with its cylindrical structure [56]. Various antibiotics have been reported to use against the infection caused by *S. typhimurium* but over usage of these antibiotics have helped *Salmonella* to acquire strong resistance against these antibiotics [57]. So, keeping in mind regarding an excellent antibacterial activity of MoS<sub>2</sub> nanosheets towards other Gram-negative and Gram-positive bacterium and the deadly symptoms caused due to salmonella provoked us to study the effect of water-dispersed 2D MoS<sub>2</sub> nanosheets on this food pathogen.

The two different categories of *Salmonella* bacteria (ATCC 14028 and wild-type (WT) *Salmonella*) were used to interact with liquid exfoliated MoS<sub>2</sub> nanosheets. A clear antibacterial action of MoS<sub>2</sub> nanosheets was observed in SEM images where MoS<sub>2</sub> nanosheets acted as a sharp knife and cuts the outer membrane of *Salmonella*. Then MTT assay was performed to study the bacterial viability after the interaction with MoS<sub>2</sub> nanosheets.

## **4.11. Antibacterial activity: proliferation test**

### **4.11.1. Microbial strains, culture conditions and preparations**

Incubation of *S. typhimurium* bacterial models was performed at two different concentrations of 2D MoS<sub>2</sub> nanosheets dispersion (11.2 and 20 µg/mL) for 24 h. Bacterial viability was studied via a proliferation test. Samples incubated with MoS<sub>2</sub> nanosheets dispersion (properties of MoS<sub>2</sub> nanosheets dispersion mentioned in **Table 4.1**) were checked after the first four hours from the

treatment, and then re-checked after 24 h to investigate the bacterial death (**Figure 4.6**). Incubation of the bacterial models under the same conditions were used as a positive control for the experiment, without MoS<sub>2</sub> nanosheets dispersion. From the colony counting images (**Figure 4.6**) we can clearly see an antibacterial effect in all cases. The antibacterial action of MoS<sub>2</sub> nanosheets is due to both membranes mechanical injury, as imaged in **Figure 4.7 (i-l)** by SEM, and oxidative stress [<sup>58</sup>]. From **Figure 4.6 (a-f)**, we observed a clear antibacterial effect of 2D MoS<sub>2</sub> nanosheets on *S. typhimurium*. In **Figure 4.6 a**, SA+ denotes the control wild-type *Salmonella* with no incubation with 2D nanosheets. The bactericidal action is very clear and similar in **Figure 4.6 b** at 11.2 µg/mL with  $N = 2$  and in **Figure 4.6 c** at 20 µg/mL with  $N = 4$ . From **Figure 4.6 (d-f)**, we observed an even more evident bactericidal effect on the ATCC 14028 *Salmonella*, which resulted in complete death of bacterial cells upon incubation with sharp edged 2D MoS<sub>2</sub> nanosheets. In **Figure 4.6 d**, SATCC+ denotes the positive control ATCC 14028 lab *Salmonella typhimurium* other than the wild-type. Bactericide effect in ATCC 14028 *Salmonella* is much stronger than the corresponding case in wild-type, as somewhat expected. Moreover, differences between the two concentrations of the nanoflakes as shown in **Figure 4.6 e** and **Figure 4.6 f** can be considered negligible, being the number of counted colonies in the range of some units in both cases. We interpret our finding as, the MoS<sub>2</sub> flakes could act as nano-knives or nano-blades on the *Salmonella* bacteria, being capable to cut the bacterial external cell wall since the flake has a smaller or approximately the same thickness as the wall, this latter being 10–12 nm [<sup>59</sup>]. Alternatively, sheets can wrap around the cell surface (wrapping) without penetrating it. In a further mechanism, called trapping, a net of MoS<sub>2</sub> flakes traps bacteria. This will be strikingly clear from SEM images of the bacteria treated with MoS<sub>2</sub> nanosheets in the forthcoming section.

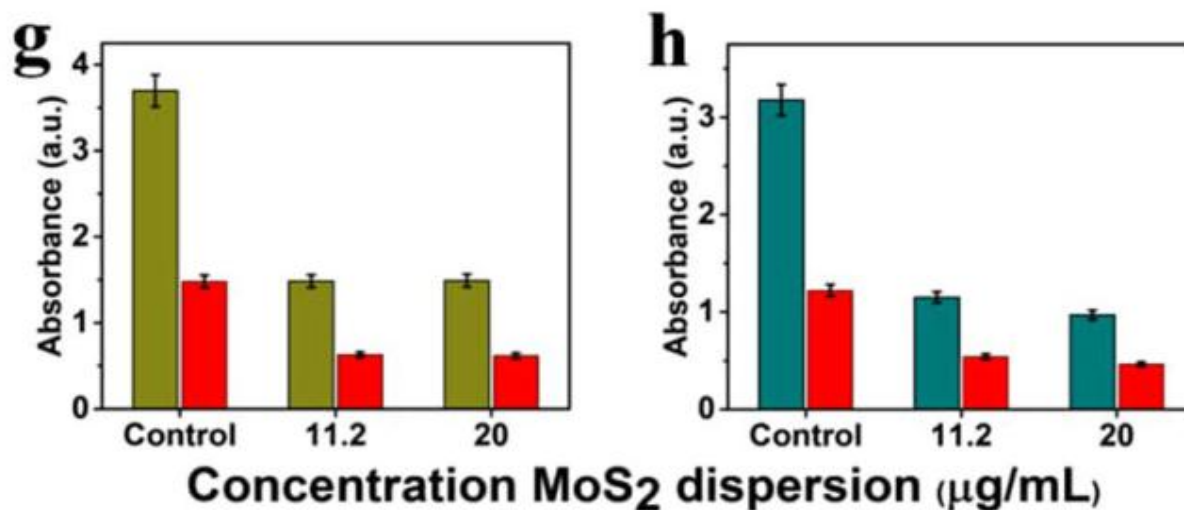
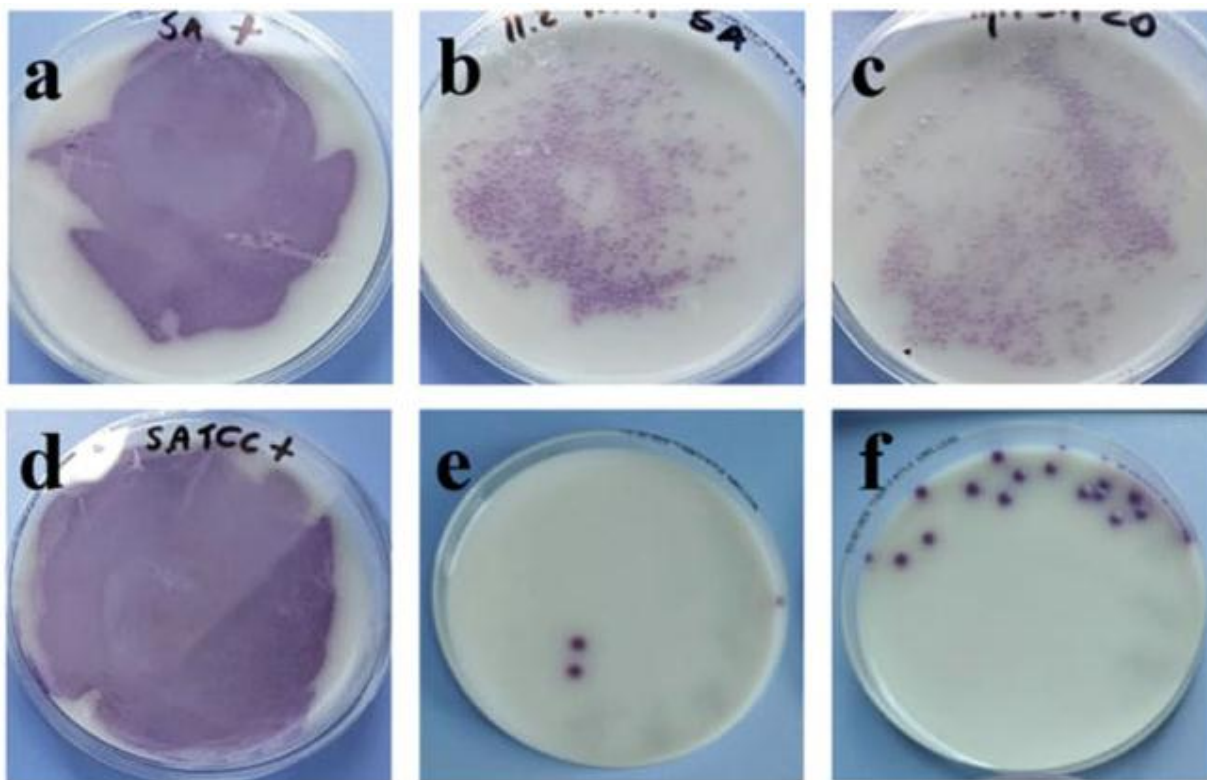


**Figure 4.6.** Proliferation test. Two different concentrations of 2D MoS<sub>2</sub> dispersion interacted with *S. typhimurium* represented as (a–f). (a) Positive control of wild-type *Salmonella* without 2D MoS<sub>2</sub>, (b) incubation at 11.2 µg/mL and (c) at 20 µg/mL; (d–f) *Salmonella* bacteria grown in the lab (ATCC 14028), (d) positive control without 2D MoS<sub>2</sub>, (e) incubation at 11.2 µg/mL and

(f) at 20  $\mu\text{g/mL}$ . All the samples treated with  $\text{MoS}_2$  nanoflakes were checked after 4 h from the treatment. (g) MTT plots of 2D  $\text{MoS}_2$  dispersion incubated with ATCC 14028 Laboratory *Salmonella* and (h) wild-type *Salmonella* at 11.2  $\mu\text{g/mL}$  and 20  $\mu\text{g/mL}$ . The absorbance of the incubation is presented at 450 nm (green) and 490 nm (red) wavelengths. Interaction of 2D  $\text{MoS}_2$  nanosheets at 20  $\mu\text{g/mL}$  with average thickness of  $N = 4$ .

## **4.12. MTT assay - MTT plots of lab prepared *Salmonella* incubation with 2D $\text{MoS}_2$ dispersion**

### **4.12.1. Determination of bacterial viability**

Basically, In **Figure 4.6 (g,h)**, we have demonstrated the effect of incubation of two different *C* of 2D  $\text{MoS}_2$  nanosheets with ATCC 14028 and wildtype *S. typhimurium*. MTT analysis reveals the oxidative stress generated upon incubation of  $\text{MoS}_2$  nanosheets with bacteria. From **Figure 4.6 g,h** we can see that for both *Salmonella* types a relevant oxidative stress was induced, reducing the absorbance to about 40% of the untreated sample. *Salmonella* Chromogen Agar plates. After incubation overnight at 37 °C for *S. typhimurium*, colonies on the plates were counted and compared with those on the control plates (without any  $\text{MoS}_2$  nanosheets) to calculate the loss of viability caused by the  $\text{MoS}_2$  nanosheets samples.

## 4.13. Scanning Electron Microscopy measurement (SEM)

### 4.13.1. Antibacterial activity: the action mechanisms of MoS<sub>2</sub> nanosheets.

Strikingly, in *Figure 47 (a-d)*, we observe the role of direct contact of 2D MoS<sub>2</sub> nanosheets, having sharp edges, with the bacterial membrane. In *Figure 47 a*, under the control experiment we can clearly see the normal rod shaped morphology with smooth and intact membranes of ATCC 14028 *S. typhimurium*. After incubating with 2D MoS<sub>2</sub> dispersion, a stress in the membrane is visible, that causes bacteria fragmentation as in *Figure 47 b* and/or cuts in the bacteria membrane as in *Figure 47 c*, where we can figure out the action of the 2D MoS<sub>2</sub> nanosheets sharp edges as they acted as a sharp nano-knife. In *Figure 47 d*, leakage of the intracellular components results in complete distortion of the bacterial membrane caused by mechanical stress induced by the nanoflakes lying nearby.

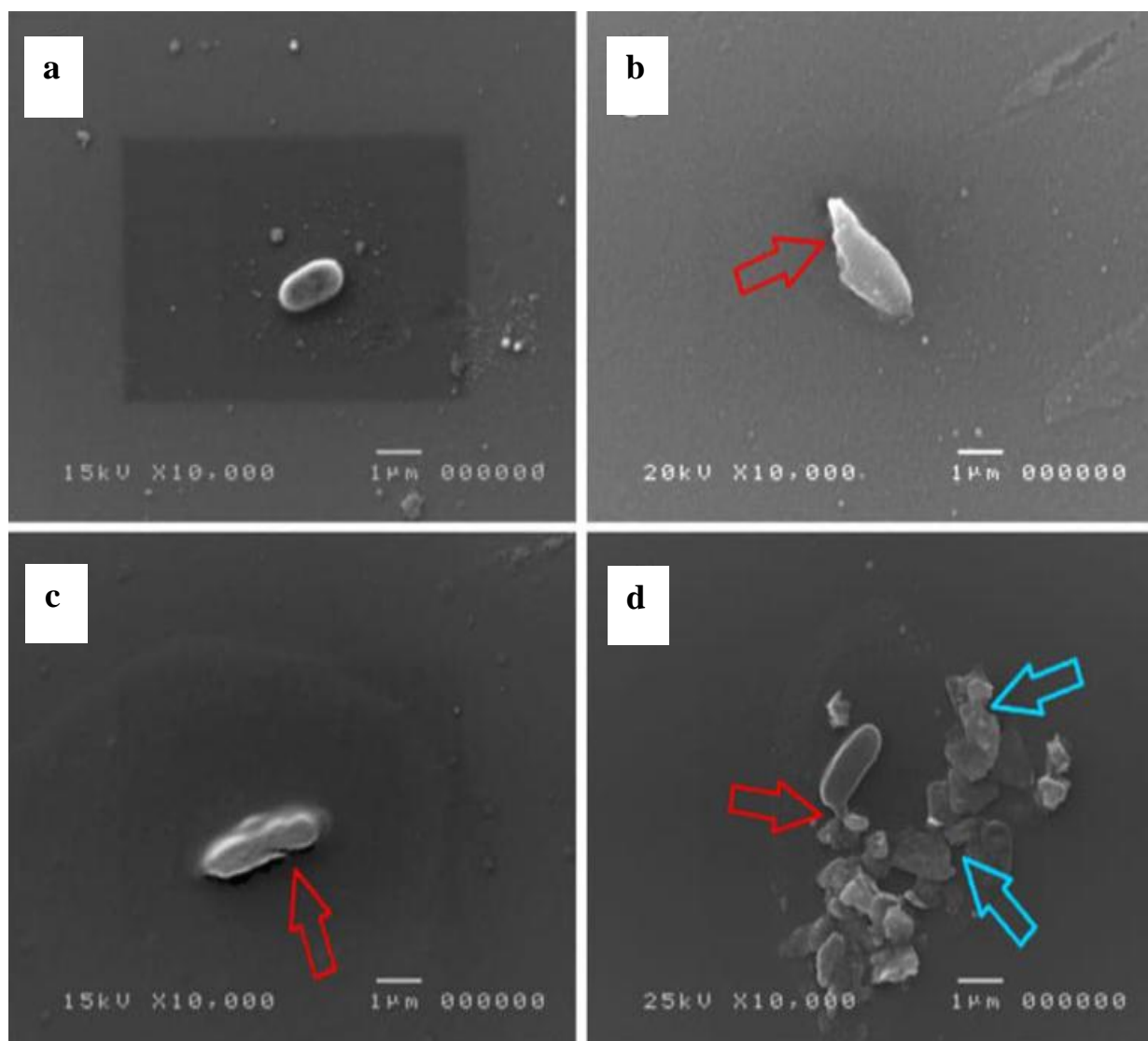


**Figure 4.7:** (a) Control rod shaped *ATCC 14028S. typhimurium* (b) fragment of a bacterium cut by a nanosheet evidenced by the red arrow, (c) slight cut at the outer bacterial membrane as shown by red arrow, and (d) leakage of intracellular components of *Salmonella* bacteria (red arrow) upon interaction with the sharp edges of the 2D  $\text{MoS}_2$  nanosheets present nearby (blue arrows).

## **4.1.4 Experimental details**

### **4.14.1. Cell cycle analysis**

Cells were collected by centrifugation at 1200 rpm for 5 minutes and then re-suspended in 500  $\mu\text{L}$  of a hypotonic buffer composed of 0.1% NP-40, 0.1% sodium citrate, 50  $\mu\text{g}/\text{mL}$  propidium iodide (Sigma Aldrich), RNase A. The samples were then incubated in the dark for 30 minutes. Analysis was performed by FACS-Calibur (Becton Dickinson) using Cell Quest Pro software (Becton Dickinson) and ModFit LT version 3 software (Verity). Experiments were performed in triplicate.

### **4.14.2. Cell line culture, conditions and preparations**

U937 (acute myeloid leukemia cell line) cells were grown in RPMI 1640 medium (EuroClone) supplemented with 10% heat-inactivated FBS (Sigma Aldrich), 1% glutamine (EuroClone), 1% penicillin/streptomycin (EuroClone) and 0.1% gentamycin (EuroClone), at 37 °C in air containing 5% CO<sub>2</sub>. MCF-7 (human breast adenocarcinoma cell line) and HaCaT (immortalized non tumorigenic human keratinocytes) cells were grown DMEM medium supplemented with the same components described above and in the same incubation conditions.

### **4.14.3. MTT- Cell proliferation assay**

The MoS<sub>2</sub> nanosheets were dispersed in Elix water at different concentrations (8, 14 and 20  $\mu\text{g}/\text{mL}$ ). Dilutions by a factor of about four as compared to the concentration value of the initial preparation were performed. The cell viability was evaluated using 3-[4, 5-dimethyltriazol-2-yl]-2, 5-diphenyl tetrazolium bromide (MTT) as substrate. MTT assay (Sigma Aldrich) was performed according to the protocol provided by the Supplier. The absorbance was measured

with microplate reader (Tecan EVO M1000 PRO) at the wavelength of 570 nm and using 630 nm as reference wavelength. Experiments were performed in triplicate.

#### **4.14.4. Visualization of cell morphology**

The HaCaT and MCF-7 cells were cultured directly on coverslips. U937 cells were coated on polyisined coverlips before the SEM procedures. The cells were fixed with 2.5% glutaraldehyde in 0.2 M PBS at pH 7.2–7.4 for 2–4 h at 4 °C. The cells were then washed three times with PBS 0.2 M for 10 minutes. Additional fixing was performed by OsO<sub>4</sub> 1–2% in PBS 0.2 M at pH 7.4 for 2 h at 4 °C in dark. The cells were then washed with PBS 0.2 M (3% for 10 minutes) at 4 °C. The samples were dehydrated by ethanol 30%; 50%; 70%; 80%; 95% for 10 minutes and 100% for 1 h at 4 °C. Morphological analyses of samples were performed with a scanning electron microscope (SEM) JEOL-JSM 5310 (CISAG laboratory, at University of Naples, Federico II). The SEM operating at 15 kV, is equipped with energy dispersive X-Ray spectroscopy (EDS); data were processed with INCA version 4.08 (Oxford Instruments, 2006). The samples were metalized with gold by using a sputter coater. Oxford Instruments (2006): INCA - The microanalysis suite issue 17a + SP1 - Version 4.08. Oxford Instr. Anal. Ltd., Oxfordshire, UK.

#### **4.14.5. Propidium iodide staining: cell death evaluation**

After the induction with MoS<sub>2</sub> for different times and at different concentrations, cells were collected and centrifuged at 1200 rpm and then washed with cold PBS. Cell pellets were re-suspended in PI staining solution (0.2 µg/mL). PI positive cells were counted by flow cytometry (FACS). Experiments were performed in triplicate.

#### 4.14.6. Bacterial cell growth

Bacteria were diluted up to  $10^6$  CFU/mL and exposed to MoS<sub>2</sub> nanosheets at different concentrations in a final volume of 100  $\mu$ L. Experiments were made in duplicates. Different final concentrations of MoS<sub>2</sub> were tested at 11.2  $\mu$ g/mL and 20  $\mu$ g/mL. Aliquots were collected after four hours, conveniently diluted by serial dilutions 1:10 and plated in *Salmonella* Chromogen Agar plates. The plates were incubated overnight at 37 °C. CFU were counted the following day.

#### 4.14.7. Microbial strains, culture conditions and preparations

We used (*S. typhimurium*) ATCC 14028 and wild-type *S. typhimurium* as a model bacterium to evaluate the antibacterial activity of MoS<sub>2</sub> nanosheets. Also all the bacterial samples without the incubation of nanosheets were used as a positive control in nuclease free water. The bacterial cell suspension was diluted in isotonic saline solution to obtain cell samples containing 150 colony forming units (CFU). Cell growth was determined by measuring the optical density at 600 nm (Lambda-25 spectrophotometer, Perkin-Elmer, USA) in six parallel measurements for each time-point. *S. typhimurium* ATCC 14028 and wild-type *S. typhimurium* were maintained on buffered peptone water (BPW) at 37 °C under constant orbital shaking at 220 rpm for up to 24 h. The MoS<sub>2</sub> nanosheets dispersion was diluted at two different concentrations 11.2  $\mu$ g/mL and 20  $\mu$ g/mL, respectively, using culture medium with a final concentration of bacteria of  $1 \times 10^6$  CFU mL<sup>-1</sup>. Both categories of *S. typhimurium* were cultured at the condition of 37 °C for up to 6 h. Antibacterial effect was evaluated by the colony counting method. In brief, the incubation bacterial solutions were initially diluted to  $1 \times 10^5$  CFU mL<sup>-1</sup>. Later, 100  $\mu$ L of the diluted bacterial cells were spread respectively on the *Salmonella* Chromogen Agar plates. After

incubation overnight at 37 °C for *S. typhimurium*, colonies on the plates were counted and compared with those on the control plates (without any MoS<sub>2</sub> nanosheets) to calculate the loss of viability caused by the MoS<sub>2</sub> nanosheets samples.

#### **4.14.8. Determination of bacterial viability**

Methylthiazolyldiphenyl-tetrazolium bromide (MTT) reagent (Sigma-Aldrich,USA) was used for bacterial viability measurements. Two different categories of *Salmonella* bacteria were exposed to 20 µg/mL and 11.2 µg/mL of MoS<sub>2</sub> nanosheets in PBS. 10 µL of the 12 mM MTT stock solution was added to each well. A negative control of 10 µL of the MTT stock solution was added to 100 µL of medium alone. Then this solution was incubated at 37 °C for 4 h. At high cell densities the incubation time can be shortened to 2 h. Then, 100 µL of the SDS-HCl solution was added to each well and thoroughly mixed using the pipette. Then, the microplate was incubated at 37 °C for 4 h in a humidified chamber. Longer incubations generally decrease the sensitivity of the assay so short incubation time was more preferred in this experiment. After mixing each sample again using a pipette the absorbance was observed at 450 and 490 nm.

#### **4.14.9. Antibacterial activity: the action mechanisms of MoS<sub>2</sub> nanosheets.**

Changes in the morphology of salmonella bacteria were studied using scanning electron microscopy (SEM). Obtaining acceptable SEM images with good ultrastructural preservation requires careful application of the SEM sample preparation methods. The concentration of 2D MoS<sub>2</sub> dispersion and its incubation with *Salmonella* for SEM analysis was chosen at 20 µg/mL).

After incubation overnight at 37 °C for *S. typhimurium* with/without MoS<sub>2</sub> nanosheets in buffered peptone water (BPW) for 24 h, preparation for SEM was carried out according to the following protocol:

1. Bacterial broth was centrifuged.
2. Pellet was washed with saline phosphate buffer for 3 times.
3. 0.25% gluteraldehyde was added in sodium phosphate at pH- 7.2.
4. Then this mixture was incubated at room temperature for 30 minutes.
5. Then the overnight incubation was performed.
6. Sodium phosphate buffer was washed for 3 times.
7. After centrifugation, the pellet was collected.
8. The sample was dehydrolysed by different ethanol volumes starting from 30%, 50%, 70%, 80%, 90% and 100%.
9. For each ethanol volume the sample was incubated for 10 minutes.
10. Additionally, incubation of the sample was performed in 100% ethanol volume for 1 h.
11. Sample preparation for SEM was performed by applying adhesive tape and then the bacterial sample was added over the adhesive tape.

## Bibliography

1. Gravagnuolo, A. M. *et al.* In situ production of biofunctionalized few-layer defect-free microsheets of graphene. *Adv. Funct. Mater.* **25**, 2771–2779 (2015).
2. Hassan, A. H. A., Bergua, J. F., Morales-Narváez, E. & Merkoçi, A. Validity of a single antibody-based lateral flow immunoassay depending on graphene oxide for highly sensitive determination of *E. coli* O157:H7 in minced beef and river water. *Food Chem.* **297**, 124965 (2019).
3. Morales-Narváez, E., Naghdi, T., Zor, E. & Merkoçi, A. Photoluminescent Lateral-Flow Immunoassay Revealed by Graphene Oxide: Highly Sensitive Paper-Based Pathogen Detection. *Anal. Chem.* **87**, 8573–8577 (2015).
4. Morales-Narváez, E., Baptista-Pires, L., Zamora-Gálvez, A. & Merkoçi, A. Graphene-Based Biosensors: Going Simple. *Adv. Mater.* **29**, (2017).
5. Cheeveewattanagul, N. *et al.* Straightforward Immunosensing Platform Based on Graphene Oxide-Decorated Nanopaper: A Highly Sensitive and Fast Biosensing Approach. *Adv. Funct. Mater.* **27**, 1–8 (2017).
6. Morales-Narváez, E. & Merkoçi, A. Graphene Oxide as an Optical Biosensing Platform: A Progress Report. *Adv. Mater.* **31**, 1–12 (2019).
7. Liu, S. *et al.* Lateral Dimension Dependent Antibacterial Activity of Graphene Oxide Sheets. *Langmuir* **28**, 12364–12372 (2012).
8. Szunerits, S. & Boukherroub, R. Antibacterial activity of graphene-based materials. *J. Mater. Chem. B* **4**, 6892–6912 (2016).

9. Liu, S. *et al.* Antibacterial activity of graphite, graphite oxide, graphene oxide, and reduced graphene oxide: Membrane and oxidative stress. *ACS Nano* **5**, 6971–6980 (2011).
10. Roy, H., Bhanja, S., Panigrahy, U. P. & Theendra, V. K. *Graphene-Based Nanovehicles for Drug Delivery. Characterization and Biology of Nanomaterials for Drug Delivery* (Elsevier Inc., 2019). doi:10.1016/b978-0-12-814031-4.00004-0
11. Chhowalla, M. *et al.* The chemistry of two-dimensional layered transition metal dichalcogenide nanosheets. *Nat. Chem.* **5**, 263–275 (2013).
12. Salmeron, M., Somorjai, G. A. & Chianelli, R. R. A leed-aes study of the structure of sulfur monolayers on the Mo(100) crystal face. *Surf. Sci.* **127**, 526–540 (1983).
13. Wilson, J. M. LEED and AES study of the interaction of H<sub>2</sub>S and Mo (100). *Surf. Sci.* **53**, 330–340 (1975).
14. Niu, L., Coleman, J. N., Zhang, H., Shin, H. & Chhowalla, M. Production of Two-Dimensional Nanomaterials via Liquid-Based Direct Exfoliation, *small*, 272–293 (2016).
15. Cao, T. *et al.* Valley-selective circular dichroism of monolayer molybdenum disulphide. *Nat. Commun.* **3**, (2012).
16. Chhowalla, M., Liu, Z. & Zhang, H. Two-dimensional transition metal dichalcogenide (TMD) nanosheets. *Chem. Soc. Rev.* **44**, 2584–2586 (2015).
17. Li, H., Wu, J., Yin, Z. & Zhang, H. Preparation and applications of mechanically exfoliated single-layer and multilayer MoS<sub>2</sub> and WSe<sub>2</sub> nanosheets. *Acc. Chem. Res.* **47**, 1067–1075 (2014).

18. Radisavljevic, B., Radenovic, A., Brivio, J., Giacometti, V. & Kis, A. Single-layer MoS<sub>2</sub> transistors. *Nat. Nanotechnol.* **6**, 147–150 (2011).
19. Splendiani, A. *et al.* Emerging photoluminescence in monolayer MoS<sub>2</sub>. *Nano Lett.* **10**, 1271–1275 (2010).
20. Shah, P., Narayanan, T. N., Li, C.-Z. & Alwarappan, S. Probing the biocompatibility of MoS<sub>2</sub> nanosheets by cytotoxicity assay and electrical impedance spectroscopy. *Nanotechnology* **26**, 315102 (2015).
21. Chou, S. S. *et al.* Chemically Exfoliated MoS<sub>2</sub> as Near-Infrared Photothermal Agents *Angew. Chemie-Int Ed.*, **22904**, 1–6 (2013).
22. Cheng, L. *et al.* Ultrathin WS<sub>2</sub> nanoflakes as a high-performance electrocatalyst for the hydrogen evolution reaction. *Angew. Chemie - Int. Ed.* **53**, 7860–7863 (2014).
23. Qian, X., Shen, S., Liu, T., Cheng, L. & Liu, Z., Two dimensional TiS<sub>2</sub> nanosheets for in-vivo photoacoustic imaging and photothermal cancer therapy, *Nanoscale*, 6380–6387 (2015).
24. Gong, L. *et al.* Two-dimensional transition metal dichalcogenide nanomaterials for combination cancer therapy. *J. Mater. Chem. B* **5**, 1873–1895 (2017).
25. Yin, W. *et al.* Functionalized Nano-MoS<sub>2</sub> with Peroxidase Catalytic and Near-Infrared Photothermal Activities for Safe and Synergetic Wound Antibacterial Applications. *ACS Nano* **10**, 11000–11011 (2016).
26. Liu, Y. *et al.* Molybdenum disulfide/graphene oxide nanocomposites show favorable lung targeting and enhanced drug loading/tumor-killing efficacy with improved

- biocompatibility. *NPG Asia Mater.* **10**, e458 (2018).
27. Gong, H. *et al.* Engineering of multifunctional nano-micelles for combined photothermal and photodynamic therapy under the guidance of multimodal imaging. *Adv. Funct. Mater.* **24**, 6492–6502 (2014).
  28. Guan, G. *et al.* Protein induces layer-by-layer exfoliation of transition metal dichalcogenides. *J. Am. Chem. Soc.* **137**, 6152–6155 (2015).
  29. Kurapati, R., Kostarelos, K., Prato, M. & Bianco, A. Biomedical Uses for 2D Materials Beyond Graphene: Current Advances and Challenges Ahead. *Adv. Mater.* 6052–6074 (2016).
  30. Kurapati, R. *et al.* Enzymatic Biodegradability of Pristine and Functionalized Transition Metal Dichalcogenide MoS<sub>2</sub> Nanosheets. *Adv. Funct. Mater.* **27**, (2017).
  31. COMŞA, Ş., CÎMPEAN, A. M. & RAICA, M. The Story of MCF-7: Anticancer research. *Anticancer Res.* **35**, 3147–3154 (1981).
  32. Sweeney, E. E., McDaniel, R. E., Maximov, P. Y., Fan, P. & Craig Jordan, V. Models and mechanisms of acquired antihormone resistance in breast cancer: Significant clinical progress despite limitations. *Horm. Mol. Biol. Clin. Investig.* **9**, 143–163 (2012).
  33. Smith, S. D. & Rosen, D. Establishment and characterization of a human null-cell lymphoblastic lymphoma cell line (K-LL-3). *Int. J. Cancer* **23**, 494–503 (1979).
  34. Strefford, J. C. *et al.* The characterisation of the lymphoma cell line U937, using comparative genomic hybridisation and multi-plex FISH. *Cytogenet. Cell Genet.* **94**, 9–14 (2001).

35. Boukamp, P. *et al.* Normal keratinization in a spontaneously immortalized aneuploid human keratinocyte cell line. *J. Cell Biol.* **106**, 761–771 (1988).
36. Zhang, L., Shen, S., Liu, Z. & Ji, M. Label-Free, Quantitative Imaging of MoS<sub>2</sub> - Nanosheets in Live Cells with Simultaneous Stimulated Raman Scattering and Transient Absorption Microscopy. *Adv. Biosyst.* **1**, 1700013 (2017).
37. Teo, W. Z., Chng, E. L. K., Sofer, Z. & Pumera, M. Cytotoxicity of exfoliated transition-metal dichalcogenides (MoS<sub>2</sub>, WS<sub>2</sub>, and WSe<sub>2</sub>) is lower than that of graphene and its analogues. *Chem. - A Eur. J.* **20**, 9627–9632 (2014).
38. Moore, C. *et al.* Industrial grade 2D molybdenum disulphide (MoS<sub>2</sub>): an *in vitro* exploration of the impact on cellular uptake, cytotoxicity, and inflammation. *2D Mater.* **4**, 25065 (2017).
39. Siepi, M. *et al.* Production of biofunctionalized MoS<sub>2</sub> flakes with rationally modified lysozyme: a biocompatible 2D hybrid material. *2D Mater.* **4**, 35007 (2017).
40. Appel, J. H. *et al.* Low Cytotoxicity and Genotoxicity of Two-Dimensional MoS<sub>2</sub> and WS<sub>2</sub>. *ACS Biomater. Sci. Eng.* **2**, 3, 361-367 (2016).
41. Harashima, H., Dissmeyer, N. & Schnittger, A. Cell cycle control across the eukaryotic kingdom. *Trends Cell Biol.* **23**, 345–356 (2013).
42. Hunt, T., Nasmyth, K. & Novak, B. The cell cycle. *Philos. Trans. R. Soc. B Biol. Sci.* **366**, 3494–3497 (2011).
43. Cho, E. C., Zhang, Q. & Xia, Y. The effect of sedimentation and diffusion on cellular uptake of gold nanoparticles. *Nat. Nanotechnol.* **6**, 385–391 (2011).

44. Fraser, J. A. & Huang, C. L. H. A quantitative analysis of cell volume and resting potential determination and regulation in excitable cells. *J. Physiol.* **559**, 459–478 (2004).
45. Gu, Z. *et al.* Exploring the Nanotoxicology of MoS<sub>2</sub>: A Study on the Interaction of MoS<sub>2</sub> Nanoflakes and K<sup>+</sup> Channels. *ACS Nano* acsnano.7b07871 (2017).
46. Senapati, S. *et al.* Engineered Cellular Uptake and Controlled Drug Delivery Using Two Dimensional Nanoparticle and Polymer for Cancer Treatment. *Mol. Pharm.* **15**, 679–694 (2018).
47. Liu, X., Duan, G., Li, W., Zhou, Z. & Zhou, R. Membrane destruction-mediated antibacterial activity of tungsten disulfide (WS<sub>2</sub>). *RSC Adv.* **7**, 37873–37880 (2017).
48. Navale, G. R. *et al.* Oxidative and membrane stress-mediated antibacterial activity of WS<sub>2</sub> and rGO<sub>2</sub> nanosheets. *RSC Adv.* **5**, 74726–74733 (2015).
49. Wu, N. *et al.* Investigating the influence of MoS<sub>2</sub> nanosheets on E. coli from metabolomics level. *PLoS One* **11**, 1–18 (2016).
50. Palmieri, V. *et al.* Antibiotic-loaded MoS<sub>2</sub> nanosheets to combat bacterial resistance via biofilm inhibition. *Nanotechnology*, **28**, 225101 (2017).
51. Pham, R., Virnelson, R. C., Sankaran, R. M. & Lacks, D. J. Contact charging between surfaces of identical insulating materials in asymmetric geometries. *J. Electrostat.* **69**, 456–460 (2011).
52. Hurley, D., McCusker, M. P., Fanning, S. & Martins, M. Salmonella-host interactions - modulation of the host innate immune system. *Front. Immunol.* **5**, 1–11 (2014).

53. Chimalizeni, Y., Kawaza, K. & Molyneux, E. The epidemiology and management of non typhoidal salmonella infections. *Adv. Exp. Med. Biol.* **659**, 33–46 (2010).
54. Azmatullah, A., Qamar, F. N., Thaver, D., Zaidi, A. K. M. & Bhutta, Z. A. Systematic review of the global epidemiology, clinical and laboratory profile of enteric fever. *J. Glob. Health* **5**, (2015).
55. Everest, P., Wain, J., Roberts, M., Rook, G. & Dougan, G. The molecular mechanisms of severe typhoid fever. *Trends Microbiol.* **9**, 316–320 (2001).
56. Haraga, A., Ohlson, M. B. & Miller, S. I. Salmonellae interplay with host cells. *Nat. Rev. Microbiol.* **6**, 53–66 (2008).
57. Kalra, E. K. Nutraceutical - Definition and introduction. *AAPS J.* **5**, 1–2 (2003).
58. Pandit, S., Karunakaran, S., Boda, S. K., Basu, B. & De, M. High antibacterial activity of functionalized chemically exfoliated MoS<sub>2</sub>. *ACS Appl. Mater. Interfaces* **8**, 31567–31573 (2016).
59. Palmieri, V. *et al.* The graphene oxide contradictory effects against human pathogens. *Nanotechnology* **28**, 152001 (2017).
60. Chen, Y., Tan, C., Zhang, H. & Wang, L. Two-dimensional graphene analogues for biomedical applications. *Chemical Society Reviews* **44**, 2681–2701 (2015).
61. Liu, T. & Liu, Z. 2D MoS<sub>2</sub> Nanostructures for Biomedical Applications. *Adv. Healthc. Mater.* **1701158**, 1701158 (2017).

# Chapter-5 Conclusions and Future prospects

---

## 5.1. Conclusions

We have reported a novel green route for scalable production of defect-free and few-layered MoS<sub>2</sub> nanosheets by direct exfoliation in pure water. Exfoliation of MoS<sub>2</sub> nanosheets using water as a solvent via LPE is a big challenge itself. Therefore, after optimizing the most relevant parameters for exfoliation, we achieved a stable dispersion for up to three weeks. Additionally, by using different centrifugal forces we attained size and thickness selection of nanosheets possibly restricting our production in the 2–5 layer band. Samples were characterized by extinction measurements which revealed the final mean concentration of the dispersion, mean lateral size and mean thickness of MoS<sub>2</sub> nanoflakes.  $\zeta$ - potential measurements estimated the negative surface potential of MoS<sub>2</sub> nanosheets. Interactions of few-layered MoS<sub>2</sub> nanosheets on live human cells and bacteria were also investigated. Here, we found a very interesting and novel result: the impact of MoS<sub>2</sub> nanoflakes was found to be quite different in normal from cancer cell lines in the investigated range of nanoflakes concentration. While the latter cells revealed a significant cytotoxic effect based on a very large increase of cell death, the former were essentially unaffected in this respect and only showed some mechanical damage when morphologically analyzed by SEM microscopy. This cytotoxic effect was also found to depend

on the concentration and layer number of 2D nanoflakes. In the near future, this preliminary analysis might open up new routes for significant applications of MoS<sub>2</sub> nanosheets as targeted anti-cancer systems. This analysis was further extended to bacteria. SEM images of *S. typhimurium* treated with 2D nanosheets revealed that the sharp edges of the nanoflakes can cut and/or damage bacterial membrane leading to an evident bactericidal effect.

Bacterial viability was studied by colony counting images and MTT assay that probed possible oxidative stresses induced by treatment with the nanoflakes. The results obtained by treating *Salmonella* bacteria with MoS<sub>2</sub> nanosheets are interesting and will be further extended to higher concentrations of 2D MoS<sub>2</sub> dispersions. One might see whether the interaction with nanoflakes in such condition leads to an increase of intra-cellular metabolites or might investigate the effects on amino acids and pyruvate metabolism. This could help in clarifying the mechanism of the antimicrobial effect of MoS<sub>2</sub> nanosheets. The results obtained in studying the impact of water-based preparation of MoS<sub>2</sub> few-layered nanoflakes with live matter represent an important step to unveil the scenario of the interactions of these novel materials with bacteria, viruses and human cells. Moreover, further optimization of a number of parameters in the exfoliation can additionally improve the quality of the nano-samples in terms of biocompatibility and stability of the water-based dispersion. This is essential from a practical point of view aiming at designing and realizing applications of this innovative 2DMs to biomedical sciences and food packaging. This innovative preparation technique is versatile and can be easily extended to other 2DMs at large scale production.

## 5.2. Some key challenges to overcome

Basically, the novel fabrication route of water-dispersed 2D MoS<sub>2</sub> nanosheets and that can certainly be extended to other TMDs as well could be highly effective not only in understanding the different interaction pathways but also the intriguing mechanism behind these biological interactions. A deep comprehension of these key issues will open some doors to targeted drug delivery and other relevant biomedical applications [60,61]. The present work in this thesis represents a very preliminary results of a very specific action of water-dispersed MoS<sub>2</sub> nanosheets on tumor cells, whereas very less or negligible effect on normal human cell line. Now to confirm our presented hypothesis, we are investigating the effect of water-dispersed MoS<sub>2</sub> nanosheets on the same cell lines as presented in this thesis by advanced Raman microscopy technique. Subsequently, we are also investigating the mechanism of action of water-dispersed MoS<sub>2</sub> nanosheets by studying the role of different ion channels on the given cell membrane type. Preliminary results from these advances are exciting and very promising, despite these topics are still under investigation. In view of the above goals, still there are some key challenges which need to be overcome so as to focus the current research activity to the frontiers of biomedicine and biotechnology. These challenges are:-

- a) Taking into consideration the green and scalable fabrication protocol used in this thesis, there still remain a lot of work to be done to improve the protocol to produce the desired 2D nanoflakes with homogenous structure and the required lateral size. Special dedication should be dedicated to controlling the thickness of exfoliated 2D nanosheets that plays a key role in their interactions with live matter.
- b) Also, negative surface zeta potential of water-dispersed MoS<sub>2</sub> nanosheets was surprising because the exfoliated 2D nanosheets should be neutral. It will therefore be important to

find out the source of negative zeta potential for water exfoliated MoS<sub>2</sub> nanosheets (for example defects at edges or basal planes).

- c) Though, 2D TMDs and other family members of 2D materials, such as 2D metal oxides, carbides etc., have proven to be biocompatible and exhibit very low toxicity, direct exfoliation of 2D MoS<sub>2</sub> nanosheets in water will however provide naked encounter with biological matter and depending on the cell -/ tissue type, the effect of toxicity might increase. So, these questions need to be studied while extending the knowledge on the basic interactions and behavior of water-dispersed 2D MoS<sub>2</sub> nanosheets.
- d) Results out coming from points a) and b) can push the research activity towards proper biosafety assessment measures for future clinical trial applications.
- e) Although, some of the research groups have already tested the long term bio-distribution and excretion route of exfoliated 2D TMDs (functionalized) , an appropriate assessment of cellular uptake and bio-distribution of only water-dispersed MoS<sub>2</sub> and other 2D TMDs nanosheets is still missing and urgently required.
- f) Results out coming from points a) – d) can enhance the fabrication techniques of novel 2D TMDs so to produce the flakes directly into the physiological medium together with a suitable optimization of fabrication parameters which in itself is a big challenge!

Moreover, the extension of our research activities is not only limited to understand the intriguing interaction of 2D MoS<sub>2</sub> nanosheets with human cells but we are also investigating their potential as an antibacterial agent in *Escherichia. coli* and *Staphylococcus Aureus* with a range of final dispersed MoS<sub>2</sub> concentrations, which results in a very intriguing mechanical damage to bacteria. Additionally, a very interesting antiviral activity of water-dispersed MoS<sub>2</sub> nanosheets is also

under investigation which, on the other hand, has not been reported so far in the literature to the best of our knowledge. The first- phase results of these experiments have shown substantial amount of good antiviral activity. All these activities related to ongoing projects have been briefly explained in Chapter-6 (Indeed called Ongoing Projects) of this thesis.

# Chapter-6 Ongoing Projects/ Future Directions

---

## (I) First Project

### 6.1. Detailed mechanism analysis of different interaction pathways of water-dispersed 2D MoS<sub>2</sub> nanosheets

Just to summarize, our previously published study [1] gave very intriguing results indicating that MoS<sub>2</sub> nanosheets exfoliated in de-ionized water only showed cytotoxic effects on the given two tumor cell lines (MCF-7 and U937) whereas, very little or negligible effect was found on normal cell line (HaCaT). We showed a perceptible progress in the green and scalable fabrication of MoS<sub>2</sub> nanosheets directly exfoliated in water as a pure solvent, having stability up to three-four weeks. The LPE technique is also flexible: in fact one can play in the fabrication steps with the sonication parameters to obtain 2D nanoflakes with the desired features for the applications of interest. In our case, it was extremely important to have biocompatible and eco-friendly 2D TMD dispersion to analyze its impact on the live matter in its instinctive milieu. In view of this issue, we tried a number of experiments with a substantial optimization of exfoliation parameters to achieve a stable dispersion. Subsequently, we opted to utilize this dispersion to study three different interaction pathways with the reported human cell lines which furthermore showed very

interesting results based on the nature of the cell type and its interaction route. Additionally, we extended our study to analyze the impact of water exfoliated 2D MoS<sub>2</sub> nanosheets on a two different kinds of the same bacteria which is considered as a food pathogen and is responsible for gastroenteritis, *Salmonella Typhimurium*. MTT assays and SEM morphological measurements showed that water-dispersed MoS<sub>2</sub> nanosheets acted as a sharp knife interacting with bacteria with the induction of severe cuts and mechanical damage to their membrane structure.

Enthralled by these results, we further continued our experiments to understand the specificity in the puzzling mechanism of action of water dispersed 2D MoS<sub>2</sub> nanosheets on tumor and normal cell lines. In view of this, currently we have been investigating a similar kind of 2D MoS<sub>2</sub> preparation and its interaction with the given human cell lines using advanced Raman microscopy techniques. Particularly, we are looking for some specific regions on cell membrane which upon interaction with MoS<sub>2</sub> nanosheets are affected. Till date, we have been pretty successful in confirming our already published hypothesis of three different interaction pathways of water dispersed 2D MoS<sub>2</sub> nanosheets with the live-matter, as briefly can be seen from **Figure 6.1**. Additionally, we obtained other interesting results (still under investigation) which clearly confirms our proposed hypothesis and paves a way to understand the mechanism of action of water dispersed 2D MoS<sub>2</sub> nanosheets on live-matter.

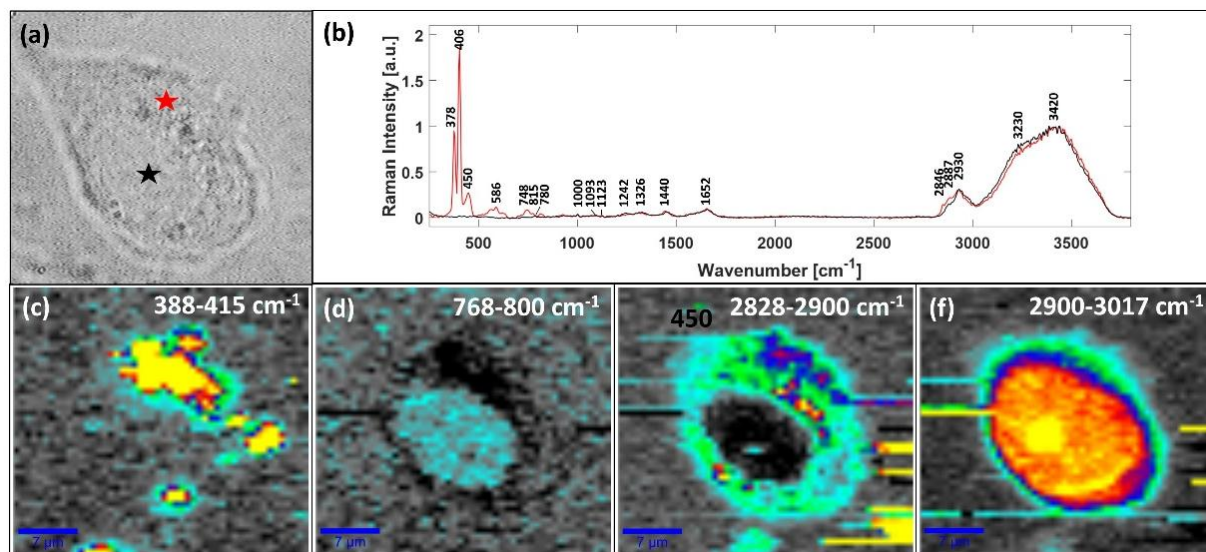


**Figure 6.1:** Raman imaging of a MCF7 cell exposed to MoS<sub>2</sub> flakes: (a) Bright field image, (b) Comparing of the Raman spectra corresponding to the points indicated in (a), Raman mapping corresponding to the spectral range of (c) 388-415 cm<sup>-1</sup>, (d) 768-800 cm<sup>-1</sup>, (e) 2828-2900 cm<sup>-1</sup> and (f) 2900-3017 cm<sup>-1</sup>. The scale bar is 7 μm.

## 6.1.1. Experimental Procedure

### 6.1.1.1. Methods

Samples were prepared by liquid phase exfoliation [2] using a Bandelin Ultrasound SONOPLUS HD3200 (200 W) tip sonicator using KE- 76 (tapered tip, 6mm diameter) and MS-72 (micro tip, 2mm diameter). Initial precursor bulk MoS<sub>2</sub> powder was purchased from Sigma-Aldrich (Particle size – 6 μm, Density - 5.06 g mL<sup>-1</sup> at 25 °C). 150 mg of starting material was dispersed in 30 mL of de-ionized water (Ci = 5 mg/ml) and sonicated (1h, pulse: 10 s on and 10 s off, 50% amplitude and with a provision of completely filled ice box to avoid the degradation of exfoliated 2D nanosheets because of overheating during the sonication). After centrifugation at

1500g for 1.5 h, the resulting sediment was re-dispersed in the same volume of de-ionized water and tip sonicated again (2.5 h, pulse 10 s on and 10 s off, 60% amplitude and with the provision of completely filled ice box).

The stock dispersion of exfoliated MoS<sub>2</sub> nanosheets dispersion was size selected via liquid cascade centrifugation [3] in an Eppendorf bench top centrifuge 5810 R with a fixed angle rotor F-34-6-38 at 15°C. The as exfoliated dispersion was centrifuged at 40g and the sediment discarded. The supernatant was centrifuged again at 620g. The sediment was collected in fresh de-ionized water at reduced volume (5 mL) and labelled as 40g-620g. The successive centrifugation steps were performed at 1400g and 2000g in a similar way. All centrifugation steps were run for 45 minutes and labelled as demonstrated above. The obtained sediment and supernatant dispersions were used for further characterization analyses and subsequently based on the results were further employed for biological tests.

Raman measurements were carried out using a confocal Raman microscope (WiTec Alpha 300) provided with a Nd-YAG laser at 532 nm as Raman excitation source. Raman mapping of MCF7 cell was obtained by recording 50 points for line and 50 points for scan with a total of 2500 spectra and using an integration time of 3 s per spectrum. The **Figure 6.1(b)** shows the comparison of two Raman spectra extracted in two different points of the cell as indicated in **Figure 6.1**. Both the spectra exhibit the typical peaks ascribable to the vibrational bands of nucleic acids (780, 1093 cm<sup>-1</sup>), proteins (1000, 1242, 1326, 1652, 2930 cm<sup>-1</sup>), lipids (1123, 1440, 2846, 2887 cm<sup>-1</sup>) and water (broad band at 3400 cm<sup>-1</sup>) present in the cells [4-7]. The main difference is highlighted by the peaks in the region 370-820 cm<sup>-1</sup> assigned to first- and second-order Raman active modes in MoS<sub>2</sub> [8,9]. Indeed, the Raman intensity map of the band centred at the most prominent peak 406 cm<sup>-1</sup> shown in **Figure 6.1(c)** clearly reproduces the spatial

distribution of MoS<sub>2</sub> flakes attached to the cell membrane. The **Figure 6.1**(d), (e) and (f) shows the Raman intensity maps corresponding to the nucleic, lipidic and proteic parts of the cell, respectively.

### **6.1.2. Improvement in Fabrication Protocol by two step exfoliation method**

Simultaneously, we are working to improve our current fabrication protocol in view of specific applications. Being inspired by Backes et al. [<sup>10,11</sup>] we have adopted a two-step exfoliation route to avoid the presence of impurities and to enhance the final dispersed concentration of 2D nanoflakes. The changed protocol has shown a significant improvement in the concentration and lateral size obtained after size selection of water exfoliated 2D MoS<sub>2</sub> nanosheets upon cascade centrifugation. Along with these improvements, we are also investigating the impact of different centrifugal forces on the final concentration and zeta potential to optimize sonication parameters accordingly. It is because, along with the different interaction pathway studies of 2D MoS<sub>2</sub> nanosheets, we are now going to investigate the cellular uptake and internalization of not only MoS<sub>2</sub> but also WS<sub>2</sub> nanosheets which will explain the mechanism of action on the basis of peculiar characteristics of these exfoliated 2D TMDs. Simultaneously, detailed analysis of the water-dispersed 2D TMDs will be carried out using AFM and TEM measurements to get a clear picture of number of layers, lateral size and shape. Subsequently, the impact on the interaction of 2D nanosheets with cell membrane and cytoplasm in the aqueous environment will also be studied.

## (II) Second Project

### 6.2. Antibacterial and Antiviral action of 2D TMDs (MoS<sub>2</sub> & WS<sub>2</sub>), Graphene and its Analogues

In our previously published article [<sup>12</sup>], we saw very severe and significant antibacterial action of water dispersed 2D MoS<sub>2</sub> nanosheets on two different kinds of *Salmonella typhimurium* (ATCC 14028 & Wild type). In this particular case, low concentration of dispersed MoS<sub>2</sub> nanosheets acted as a sharp knife that resulted in mechanical damage to the bacterial membrane and leakage of its essential components.

This motivated us to further extend these experiments to other kinds of bacteria such as *Escherichia. coli* and *Staphylococcus. aureus* to analyze in a general prospect the antibacterial impact of water-dispersed MoS<sub>2</sub> nanosheets. Interestingly, after following the two-step exfoliation process and the subsequent improvement in the physical parameters of dispersed 2D nanosheets, we have achieved very intriguing results with severe mechanical damage to both the bacterial types at low and high concentrations in the 0.1 - 0.2 mg/mL range as it can be briefly seen in **Figure 6.2**. Simultaneously, we have also investigated antiviral action of water-dispersed MoS<sub>2</sub> nanosheets on Herpes Simplex Virus (HSV-1) which so far has not been studied in the literature. The novel interaction of water-dispersed MoS<sub>2</sub> nanosheets with this specific kind of virus in its preliminary stage has shown a prominent inhibition of virus growth which is still under investigation. Experiments on the co-treatment and virus pre-treatment of the exfoliated 2D MoS<sub>2</sub> nanosheets with the given virus are being carried out. The preliminary results obtained reveal that 2D MoS<sub>2</sub> was effective in reducing HSV-1 titer in the virus pre-treatment assay: in details, 2D MoS<sub>2</sub> nanosheets was able to halve HSV-1 infectivity at 100 µg/mL with respect to

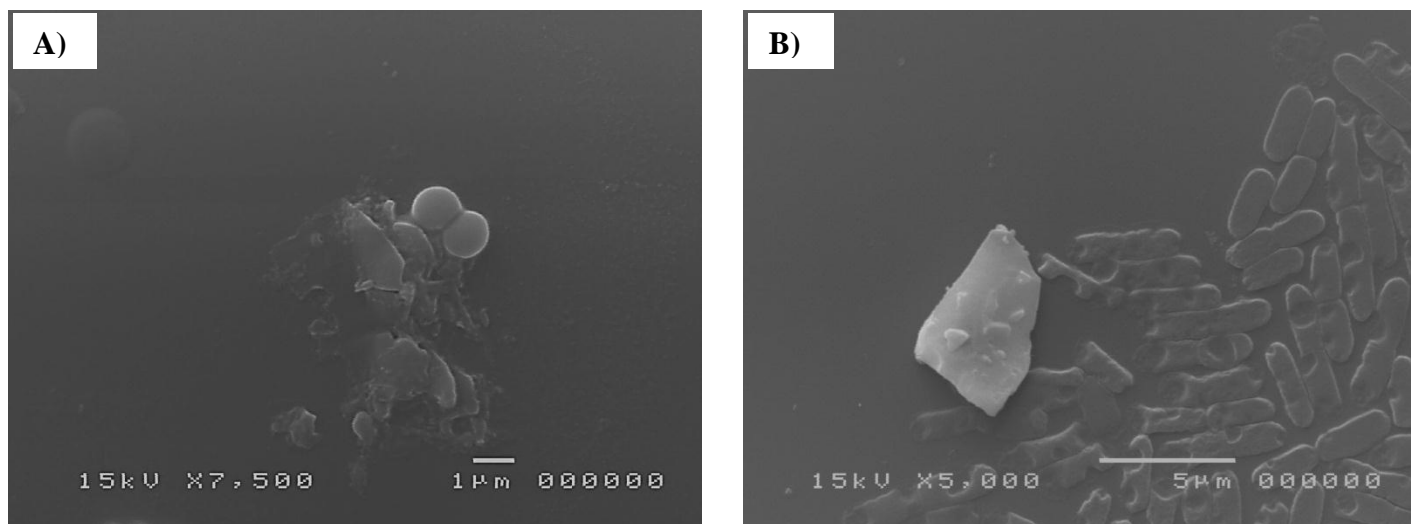


**Figure 6.2:** (A-B) represents the mechanical damage to the tested bacterium. (A) Shows a clear damage to the circular morphology of *Staphylococcus Aureus* at 100 μg/mL, whereas in B) a clear mechanical cut on the morphology of *E. Coli* upon interaction is shown with a large MoS<sub>2</sub> nanoflake at 100 μg/mL.

untreated infected cells. These data indicated that 2D MoS<sub>2</sub> nanosheets function directly on the viral particles. HSV-1 infection was monitored also through fluorescence microscopy using an engineered HSV-1 strain able to express the tegument protein vp22 gene recombinant with Green Fluorescence Protein (GFP). We observe a slight decrease in the GFP signal, and in the HSV-1 infectivity, only at the higher concentration of 100 μg/mL. The novel interaction of water-dispersed MoS<sub>2</sub> nanosheets with this specific kind of virus in its initial stage has shown a prominent inhibition of virus growth which is still under investigation.

### **(III) Third Project**

#### **6.3. Femtosecond laser surface irradiation of silicon substrate in air with special focus on laser pulse repetition rates**

The main aim of this project is: Firstly, to create different surface patterns using femtosecond laser sources with optimization of the pulse repetition rates to obtain the desired pattern of nanostructures on the machined substrate. Basically, the laser surface irradiation using femtosecond laser opens a wide range of applications in surface texturing [13-15], drilling and cutting [16], tribology and control over the wettability of machined substrate [17-19]. Particularly, the study of the formation of grooves and ripples during the laser irradiation shows that tuning the laser pulse repetition rate allows one to trigger the formation of different nanostructure on the machined surface. The mechanism for this effect is believed to basically rely in the back deposition of respective nanoparticles over the machined substrate. These studies are still ongoing with various research groups involved [20-27].

Captivated by the chance to pattern a substrate with nanometric control using femtosecond laser sources, where the role played in the mechanism by the laser pulse repetition rates has been investigated in our recent article [28], we are now investigating the homogenous deposition of liquid phase exfoliated 2D MoS<sub>2</sub> nanosheets onto the machined substrates. Furthermore, we are investigating the relevant fabrication procedure steps to obtain homogenous deposition of exfoliated 2D MoS<sub>2</sub> nanosheets over the grooves and ripples of the realized nano-pattern. We are also studying the non-linear optical response of these nanomachined samples having 2D MoS<sub>2</sub>

nanosheets depositions with particular attention to the role played by the layer number. To summarize, we have three different motives to pursue this project:-

- a) To study the high harmonics generation of the nano-patterened surfaces/substrates (which will largely be dependent on the femtosecond laser pulse repetition rates) in attosecond temporal regime ( $10^{-17} - 10^{-16}$ ) and to analyze the structure of the obtained signal in spatial (nanometer and sub-nanometer) as well as temporal resolution using advanced characterization tools.
- b) In continuation with point a), we are also investigating the random but homogenous deposition of liquid phase exfoliated 2D nanoflakes of various types onto the machined/patterned substrates which will act as nano-antennas to analyze HHG signal in the same temporal regime as in point a).
- c) Following points a) and b), we are also investigating an ordered deposition of a monolayer of 2D nanoflakes with lateral size in the range of the few hundreds of nanometers which will be in the size range of produced grooves or ripples on the machined surface.

The very preliminary step to accomplish the above summarized points have already been given a green signal and point a) has partially been fulfilled in our recent article [<sup>28</sup>] in which very intriguing and novel machining of silicon substrate with control over the femtosecond laser pulse repetition rate is discussed.

To accomplish point b) we have made a first attempt to analyze the random deposition of liquid phase exfoliated 2D MoS<sub>2</sub> nanosheets onto the machined silicon substrate. **Figure 6.3** shows low magnification optical microscope images of only the machined silicon substrate in different regions. Whereas, **Figure 6.4** shows SEM images of both the formation of nano-

patterned grooves and ripples on the machined surface and random deposition of liquid phase exfoliated few layer 2D MoS<sub>2</sub> nanosheets with very few are deposited onto the grooves, whereas rest are randomly distributed over the machined substrate.

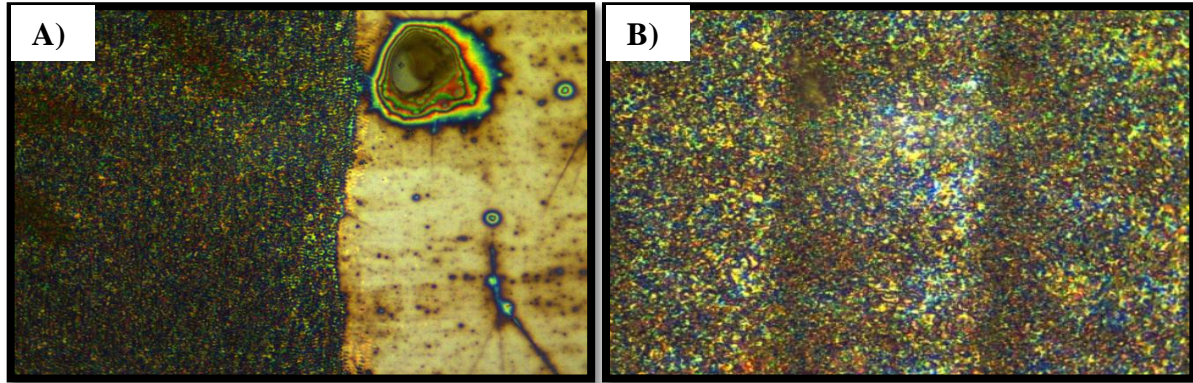


**Figure 6.3:** Pannel (A-B) shows a low magnification optical microscope images of only machined silicon substrate at different regions. A) Represents both machined and non-machined surface of the same silicon substrate with dark and light regions, respectively; B) shows a different regions of the patterned silicon substrate with groves and ripples.

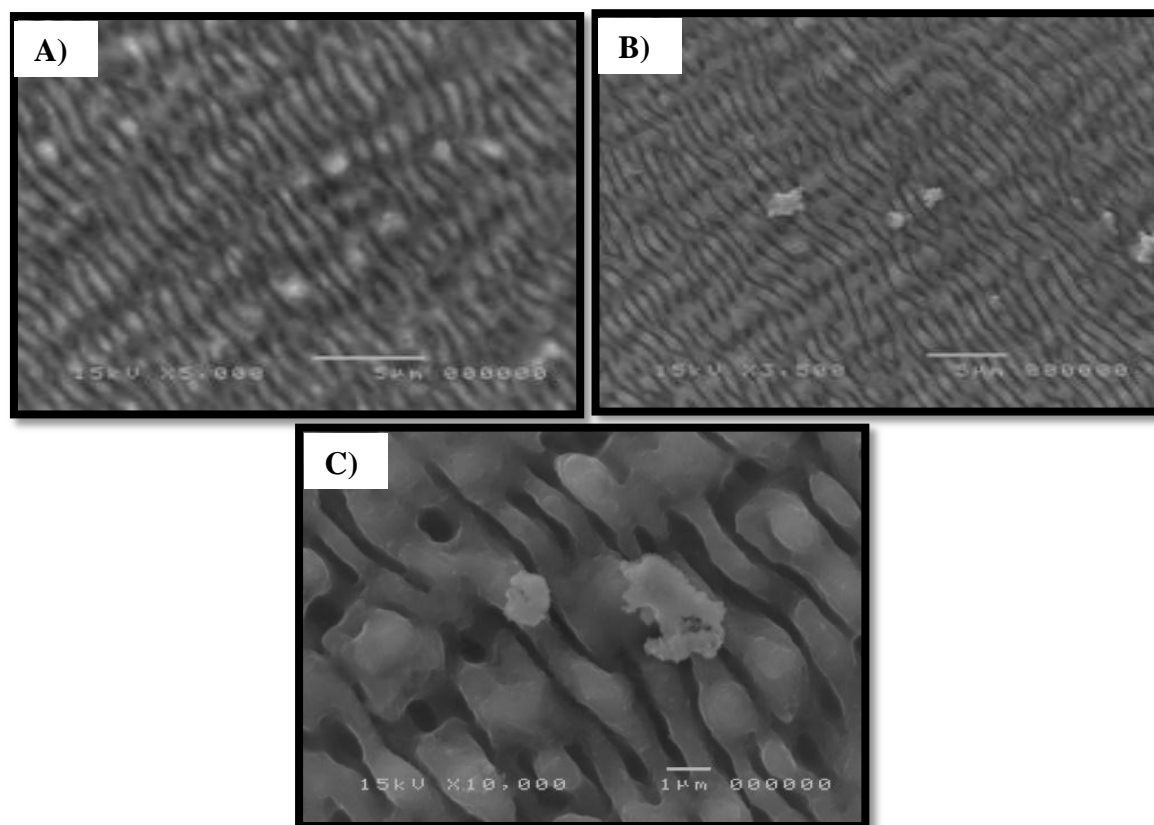


**Figure 6.4:** Panel (A-C) shows SEM images of both the machined grooves and ripples on the machined surface and liquid phase exfoliated few layer 2D MoS<sub>2</sub> nanosheets. A) Low resolution microscopic image exhibiting distribution of 2D MoS<sub>2</sub> nanoflakes onto the machined substrate; B) Random distribution of very-few and few layer MoS<sub>2</sub> nanosheets on the patterned silicon substrate and C) shows enlarged at high resolution microscopic image of deposited 2D MoS<sub>2</sub> nanoflakes in between the grooves with irregular morphology and large lateral size of few microns.

## 6.4. Conclusions and Future Prospective

Captivated by our first report on the tumor cell selective cytotoxic effect of water-dispersed MoS<sub>2</sub> nanosheets motivated us to study in detail their mechanism of action on live-matter such as human cells and different pathogens. Though, it is very challenging to exfoliate 2D MoS<sub>2</sub>/WS<sub>2</sub> nanosheets in water with a good amount of stability and concentration but several other groups worldwide are struggling to prepare high quality 2D TMD nanosheets well suitable for various biological applications. Inspired by Backes et al. [10,29], we have observed a significant improvement in the final concentration, lateral size and thickness of LPE MoS<sub>2</sub>. To understand their mechanism of action on the given tumor and normal cells, we are investigating their presence and the subsequent role of water in contact with different cellular components such as DNA, lipids and proteins using advanced Raman microscopy technique. Further extending our study to utilize the given dispersions, we are investigating the interaction of exfoliated MoS<sub>2</sub> and other 2D nanosheets on different pathogens such as *E. coli* and *S. aureus* at different concentrations resulting in a strong bactericidal impact. Additionally, we are also investigating the novel antiviral effect of water-dispersed MoS<sub>2</sub> and other 2D nanosheets on Herpes Simplex Virus (HSV-1) which is still in infancy to be studied so far in the literature. On the other hand, we are investigating the homogenous deposition of LPE 2D TMD nanosheets onto a machined substrate to study the high harmonics generation of the nano-patterened substrate in attosecond temporal regime ( $10^{-17} - 10^{-16}$ ). The study of non-linear optical response of the nanomachined samples having 2D MoS<sub>2</sub> nanosheets depositions with particular attention to the role played by number of layers will give intriguing results in the given temporal and spatial resolution.

## Bibliography

1. Kaur, J. *et al.* Biological interactions of biocompatible and water-dispersed MoS<sub>2</sub> nanosheets with bacteria and human cells. *Sci. Rep.* **8**, 1–15 (2018).
2. Coleman, Jonathan N Lotya, M. *et al.* Two-Dimensional Nanosheets Produced by Liquid Exfoliation of Layered Materials. *Science (80-. ).* **331**, 568--571 (2011).
3. Backes, C. *et al.* Production of highly monolayer enriched dispersions of liquid-exfoliated nanosheets by liquid cascade centrifugation. *ACS Nano* **10**, 1589–1601 (2016).
4. Notingher, I. *et al.* In situ characterisation of living cells by Raman spectroscopy. *Spectroscopy* **16**, 43–51 (2002).
5. Howell, N. K., Arteaga, G., Nakai, S. & Li-Chan, E. C. Y. Raman spectral analysis in the C - H stretching region of proteins and amino acids for investigation of hydrophobic interactions. *J. Agric. Food Chem.* **47**, 924–933 (1999).
6. Gniadecka, M., Nielsen, O. F., Christensen, D. H. & Wulf, H. C. Structure of water, proteins, and lipids in intact human skin, hair, and nail. *J. Invest. Dermatol.* **110**, 393–398 (1998).
7. Heraud, P. *et al.* Label-free in vivo Raman microspectroscopic imaging of the macromolecular architecture of oocytes. *Sci. Rep.* **7**, 31–34 (2017).
8. Chen, J. M. & Wang, C. S. Second order Raman spectrum of MoS<sub>2</sub>. *Solid State Commun.* **14**, 857–860 (1974).
9. Placidi, M. *et al.* Multiwavelength excitation Raman scattering analysis of bulk and two-dimensional MoS<sub>2</sub>: Vibrational properties of atomically thin MoS<sub>2</sub> layers. *2D Mater.* **2**,

- (2015).
10. Backes, C. *et al.* Preparation of liquid-exfoliated transition metal dichalcogenide nanosheets with controlled size and thickness: A state of the art protocol. *J. Vis. Exp.* **2016**, 10–13 (2016).
  11. Castagnola, V. *et al.* Biological recognition of graphene nanoflakes. *Nat. Commun.* **9**, 1–9 (2018).
  12. Kaur, J. *et al.* Biological interactions of biocompatible and water-dispersed MoS<sub>2</sub> nanosheets with bacteria and human cells. 1–15 (2018). doi:10.1038/s41598-018-34679-y
  13. Dusser, B. *et al.* Controlled nanostructures formation by ultra fast laser pulses for color marking. *Opt. Express* **18**, 2913 (2010).
  14. Vorobyev, A. Y. & Guo, C. Direct femtosecond laser surface nano/microstructuring and its applications. *Laser Photonics Rev.* **7**, 385–407 (2013).
  15. Vorobyev, A. Y. & Guo, C. Colorizing metals with femtosecond laser pulses. *Appl. Phys. Lett.* **92**, 1–4 (2008).
  16. Kamlage, G., Bauer, T., Ostendorf, A. & Chichkov, B. N. Deep drilling of metals by femtosecond laser pulses. *Appl. Phys. A Mater. Sci. Process.* **77**, 307–310 (2003).
  17. Kirner, S. V. *et al.* Mimicking bug-like surface structures and their fluid transport produced by ultrashort laser pulse irradiation of steel. *Appl. Phys. A Mater. Sci. Process.* **123**, 1–13 (2017).
  18. Hermens, U. *et al.* Mimicking lizard-like surface structures upon ultrashort laser pulse

- irradiation of inorganic materials. *Appl. Surf. Sci.* **418**, 499–507 (2017).
19. Bonse, J., Kirner, S. V., Griepentrog, M., Spaltmann, D. & Krüger, J. Femtosecond laser texturing of surfaces for tribological applications. *Materials (Basel)*. **11**, 1–19 (2018).
  20. Zhang, H. *et al.* Coherence in ultrafast laser-induced periodic surface structures. *Phys. Rev. B - Condens. Matter Mater. Phys.* **92**, 1–14 (2015).
  21. Bonse, J., Munz, M. & Sturm, H. Structure formation on the surface of indium phosphide irradiated by femtosecond laser pulses. *J. Appl. Phys.* **97**, (2005).
  22. Tsibidis, G. D., Fotakis, C. & Stratakis, E. From ripples to spikes: A hydrodynamical mechanism to interpret femtosecond laser-induced self-assembled structures. *Phys. Rev. B - Condens. Matter Mater. Phys.* **92**, 1–6 (2015).
  23. Tsibidis, G. D. *et al.* Modelling periodic structure formation on 100Cr6 steel after irradiation with femtosecond-pulsed laser beams. *Appl. Phys. A Mater. Sci. Process.* **124**, 1–13 (2018).
  24. Tsibidis, G. D., Skoulas, E., Papadopoulos, A. & Stratakis, E. Convection roll-driven generation of supra-wavelength periodic surface structures on dielectrics upon irradiation with femtosecond pulsed lasers. *Phys. Rev. B* **94**, 2–6 (2016).
  25. He, S. *et al.* Surface structures induced by ultrashort laser pulses: Formation mechanisms of ripples and grooves. *Appl. Surf. Sci.* **353**, 1214–1222 (2015).
  26. He, S., Nivas, J. J., Vecchione, A., Hu, M. & Amoroso, S. On the generation of grooves on crystalline silicon irradiated by femtosecond laser pulses. *Opt. Express* **24**, 3238 (2016).

27. Nivas, J. J. J. *et al.* Influence of ambient pressure on surface structures generated by ultrashort laser pulse irradiation. *Appl. Phys. A Mater. Sci. Process.* **124**, 2710–2713 (2018).
28. Allahyari, E. *et al.* Femtosecond laser surface irradiation of silicon in air: pulse repetition rate influence on removal efficiency and surface texture. *Submitted* **126**, 106073 (2020).
29. Backes, C. *et al.* Guidelines for Exfoliation, Characterization and Processing of Layered Materials Produced by Liquid Exfoliation. *Chem. Mater.* **29**, 243–255 (2017).